

UNIVERSITY OF KWAZULU-NATAL

**VAPOUR-LIQUID EQUILIBRIUM OF
CARBOXYLIC ACIDS**

662 672 662, 672

A.P. HWENGWERE

[B.Eng (Hons)]
National University of Science & Technology

May, 2005

VLE data is essential for the design and optimisation of industrial separation processes. Carboxylic acids are of significant interest because of their importance in both industrial and biological processes. Carboxylic acids are used as raw materials for a wide range of products, which include soaps, detergents, nylon, biodegradable plastics, medical drugs and food additives. They are also used both as solvents and as additives and co solvents under a wide range of conditions.

Carboxylic acids exhibit strong self and cross-association through hydrogen bonds in both liquid and vapour phases. A thorough understanding of how these molecules interact both with themselves and with other solvents becomes necessary if existing processes may be optimised and new processes developed.

Vapour-liquid equilibrium (VLE) data were measured for carboxylic acid systems ranging from C_3 to C_6 . New vapour-liquid equilibrium data were measured for the following binary carboxylic acid systems:

- Propionic acid + Hexanoic acid at 20 kPa, 403.15 K, 408.15 K and 413.15 K.
- Isobutyric acid + Hexanoic acids at 20 kPa, 413.15 K and 423.15 K.
- Valeric acid + Hexanoic acid at 15 kPa, 423.15 K and 433.15 K.
- Hexanoic acid + Heptanoic acid at 10 kPa and 443.15 K.

A highly refined dynamic VLE Still by Raal (Raal and Mühlbauer [1998]) was used to undertake the VLE measurements. The still was operated either isothermally or isobarically using a computer control scheme. The isobaric and isothermal control was measured to be ± 0.03 kPa and ± 0.02 K respectively. The experimental procedure was verified with the highly volatile cyclohexane (1) + ethanol (2) system. The cyclohexane (1) + ethanol (2) measured VLE data was found to be in good agreement with that of Joseph (2001) and passed both the direct test and point test for thermodynamic consistency. A high degree of confidence was then placed on the equipment set-up and experimental procedure, as well as the new carboxylic acids VLE data.

The VLE data for all the systems measured were modelled. Two data reduction methods were used:

- i. The combined ($\gamma - \phi$) method
- ii. The direct method ($\phi - \phi$) method.

In the combined method, the vapour phase non-ideality was corrected using the Pitzer-Curl (1957) correlation and the Hayden and O'Connell (1975) chemical theory approach. Three liquid phase activity coefficient models were used namely the Wilson, NRTL, and UNIQUAC equations. The Peng-Robinson equation of state (Peng and Robinson [1976]) in combination with the Twu and Coon mixing rule was used in the direct method. Thermodynamic consistency tests were done on all the systems measured. The point test (Van Ness et al. [1973]) and the direct test Van Ness ([1995]) were used for consistency tests. The direct test could not be carried out on the carboxylic acids data because of the model's inability to adequately characterise the experimental activity coefficients. Generally the models fitted the data well but failed to accurately predict the "S" shape of the carboxylic acids phase diagrams.

Considerable work still exists for further investigation into carboxylic acids. Currently, many experimentalists are working in this area. Peng et al. (2004) presented their progress on developing an equation of state incorporating chemical theory to specifically handle carboxylic acids at the ICCT conference in Beijing, 2004. Raal and Clifford (University of Kwa-Zulu Natal, Thermodynamics Research Unit) are currently developing activity coefficient models incorporating chemical theory for a binary mixture of carboxylic acids. This work is part of the continuing research to understand the phase behaviour of carboxylic acids.

BRN 441449
HC 05/05732

VAPOUR-LIQUID EQUILIBRIUM OF CARBOXYLIC ACIDS

Alex P Hwengwere

A thesis submitted in fulfillment
of the academic requirements for the
degree of Master of Science in Engineering at the
School of Chemical Engineering,
University of KwaZulu-Natal,
Durban



(All work performed in the
School of Chemical Engineering,
University of KwaZulu-Natal,
Durban, South Africa)

T
660.2992.
HWE

May, 2005

"There are only two ways to live your life. One is as though nothing is a miracle. The other is as though everything is a miracle." Albert Einstein (1879-1955)

PREFACE

The work presented in this thesis was performed at the University of KwaZulu-Natal (formerly University of Natal until January 2004) from January 2003 to December 2004. The work was supervised by Professor D. Ramjugernath and Professor J.D. Raal.

This thesis is presented as the full requirement for the degree of M.Sc. in Chemical Engineering. All the work in this thesis is original unless otherwise stated and has not (in whole or part) been submitted previously to any tertiary institute as part of a degree.

A.P. Hwengwere

As the candidate's supervisor I have/have not approved this thesis for submission.

D. Ramjugernath

Date _____

ACKNOWLEDGEMENTS

I would like to acknowledge the following people for their contribution to this work:

- Firstly, my supervisors, Professors D. Ramjugernath and J.D. Raal, for their advice and assistance during this work. Without their knowledge, help and ideas this project could not have been completed. *“If we take people as we find them, we may make them worse, but if we treat them as though they are what they should be, we help them become what they are capable of becoming”* Johan Wolfgang von Goethe. Thank you Deresh.
- NRF (Thutuka programme) and Thrip for financial support during my degree
- My colleagues, Nhlanganiso, Tyrone, Minal, Ranjeetha, Ildephose, Myriam, Denny, Mkhokeli, Gambarenyika, Allen, Viran, Jason and Etienne for their ideas and friendship. Thanks for the laughter, fun and work. *“Without friends no one can choose to live, though he had all other good”* Aristotle.
- A special thanks to my colleague, Scott who has done similar work for assisting me in this work.
- The School of Chemical Engineering staff at the University of Kwa-Zulu Natal, both administrative and workshop.
- On a personal note to my family, Baba naAmai Hwengwere, Enetty, Allen, Albert and Eldinah for their love and support over the years.
- Thanks to God for strength and prayers answered.

TABLE OF CONTENTS

Abstract	ii
Preface	vi
Acknowledgements	vii
Nomenclature	xvi
CHAPTER ONE: INTRODUCTION	1
CHAPTER TWO: CARBOXYLIC ACIDS	3
2.1 Introduction	3
2.2 Nomenclature	4
2.3 Geometry and Structure	4
2.4 Chemical Forces	5
2.4.1 Dimerisation	5
2.4.1.1 Hydrogen Bonds	5
2.4.1.2 Chemical Complex	5
2.4.1.3 Electron Donor – Electron Acceptor Interaction	5
2.4.1.4 Acidic – Basic Complex Formation	5
2.5 Chemical Properties of Carboxylic Acids	6
CHAPTER THREE: PHASE EQUILIBRIUM	7
3.1 Introduction	7
3.2 Equilibrium	7
3.3 Fugacity and Fugacity Coefficient	8
3.4 Activity Coefficients	10
3.4.1 Activity Coefficients and Gibbs Free Energy	12
3.4.1.1 Margules Equation	12
3.4.1.2 Van Laar Equation	13
3.4.1.3 Wilson Equation	14
3.4.1.4 T-K Wilson Equation	15
3.4.1.5 NRTL Equation	16
	viii

3.4.1.6 UNIQUAC Equation	17
3.4.1.7 UNIFAC	19
3.4.2 Activity Coefficient Models Incorporation Chemical Theory	20
3.4.2.1 Non-polar and an Associating Component	20
3.4.2.2 Activity Coefficient Model for Cross Association	22
3.4.3 Activity Coefficients at Infinite Dilution	24
3.5 Gas Phase Non-ideality	25
3.5.1 Chemical Theory	25
3.5.2 Hayden and O'Connell (1975) Correlation	27
3.5.3 Pitzer Curl Correlation	28
3.6 Equations of State	30
3.6.1 Virial Equation Of State	31
3.6.2 Van der Waals Equation (1873)	32
3.6.3 Redlich Kwong (1949) Equation	33
3.6.4 Peng-Robinson (1976) Equation	34
3.6.5 Equation Of State for Carboxylic Acids (Twu & Coon, [1993])	36
3.7 Mixing Rules for Equations Of State	39
3.7.1 Quadratic Mixing Rule	39
3.7.2 Panagiotopoulos- Reid Mixing Rule	39
3.7.3 Stryjek-Vera (1986) Mixing Rule	40
3.7.4 Mathias-Klotz-Prausnitz (1991) Mixing Rule	40
3.8 Gibbs-Duhem Equation	40
3.9 Thermodynamic Consistency Tests	41
3.9.1 Slope Test	41
3.9.2 Area Test	42
3.9.3 Point/ Residual Test	43
3.9.4 Direct Test	43
CHAPTER FOUR: VAPOUR-LIQUID EQUILIBRIUM EQUIPMENT	45
4.1 Introduction	45
4.2 Low Pressure Vapour-Liquid Equilibrium Measurements	45
4.2.1 Dynamic Method	46
4.2.2 Static Methods	46
4.2.3 Semi-Micro Techniques	46
4.2.4 Dew Point and Bubble Point Methods	47

4.3 Raal Dynamic VLE Still	47
4.4 Temperature Measurement and Control	49
4.5 Pressure Measurement and Control	50
4.6 Sampling and Composition Analysis	50
CHAPTER FIVE: EXPERIMENTAL PROCEDURE	51
5.1 Introduction	51
5.2 Cleaning the VLE Still	51
5.3 Pressure Calibration	52
5.4 Temperature Calibration	52
5.5 Gas Chromatograph Calibration	52
5.6 Procedure for Isobaric and Isothermal VLE measurements	54
5.6.1 Measurement of Isobaric VLE	55
5.6.2 Measurement of Isothermal VLE	56
5.7 Plateau Region	56
CHAPTER SIX: RESULTS	58
6.1 Introduction	58
6.2 Chemical Purity	58
6.3 Cyclohexane + Ethanol systems	59
6.4 Propionic Acid + Hexanoic Acid Systems	63
6.5 Isobutyric Acid + Hexanoic Acid Systems	70
6.6 Valeric acid + Hexanoic acid Systems	75
6.7 Hexanoic acid + Heptanoic acid Systems	80
CHAPTER SEVEN: DISCUSSION	84
7.1 Introduction	84
7.2 Pure Component Properties	84
7.3 VLE Data Reduction	85
7.4 Cyclohexane (1) + ethanol (2) system	85
7.5 Carboxylic Acid Systems	88
7.5.1 Alpha Functions	89
7.5.2 Activity Coefficients	90

7.6 Propionic Acid + Hexanoic Acid Systems	91
7.7 Isobutyric Acid + Hexanoic Acid system	105
7.8 Valeric acid + Hexanoic Acid System	116
7.9 Hexanoic Acid + Heptanoic Acid System	127
CHAPTER EIGHT: CONCLUSIONS	135
CHAPTER NINE: RECOMMENDECTIONS	138
REFERENCES:	140
APPENDIX A: CARBOXYLIC ACIDS	148
A.1 Chemical Properties of Carboxylic Acids	150
A.1.1 Acidity	150
A.1.2 Carboxylic Acid Reactions	151
A.1.2.1 Reactions involving cleavage of the <i>O-H</i> bond	151
A.1.2.2 Reaction at the carbonyl carbon	151
A.1.2.3 Decarboxylation	152
A.1.2.4 Reaction of the α carbon	152
A.2 Phase Equilibria	152
A.3 Evaluation of Infinite Dilution Activity Coefficient	155
A.4 VLE Data Regression algorithms	156
APPENDIX B: PURE COMPONENT PROPERTIES	160
B.1 Carboxylic Acids Dimerisation Equilibrium Constants	161
B.2 Acentric Factor	162
B.3 Mean Radius of Gyration	162
B.4 Cyclohexane + Ethanol Pure Component properties	163
B.5 Carboxylic acids Pure Component properties	163

APPENDIX C: CYCLOHEXANE + ETHANOL REGRESSION RESULTS	165
C.1 Regression Results for Cyclohexane + Ethanol at 40 kPa	165
C.2 Thermodynamic Consistency Results for Cyclohexane (1) + Ethanol (2) System 323.15 K	168
APPENDIX D: EQUIPMENT PHOTO	171

LIST OF FIGURES

CHAPTER TWO

Figure 2-1: Hydrogen bonding of acetic acid to form a dimer 3

CHAPTER FOUR

Figure 4-1: Schematic diagram of the VLE Still (Raal) 48

Figure 4-2: Schematic diagram of equipment setup 49

CHAPTER FIVE

Figure 5-1: The plateau region in the temperature vs. energy input plot for boiling mixtures. 56

CHAPTER SIX

Figure 6-1: GC Calibration for Cyclohexane(1) + Ethanol(2) – Ethanol rich region 59

Figure 6-2: GC Calibration for Cyclohexane (1) + Ethanol (2) – Cyclohexane rich region 60

Figure 6-3: x-y Diagram for Cyclohexane (1) + Ethanol (2) System at 40 kPa 61

Figure 6-4: T-x-y Phase diagram for Cyclohexane (1) + Ethanol (2) system at 40 kPa. 61

Figure 6-5: x-y Diagram for Cyclohexane (1) + Ethanol (2) System at 323.15 K 62

Figure 6-6: P-x-y Phase diagram for Cyclohexane (1) + Ethanol (2) system at 323.15 K. 62

Figure 6-7: GC Calibration for Propionic acid (1) + Hexanoic acid (2) system – Hexanoic acid rich region 63

Figure 6-8: GC Calibration for Propionic acid (1) + Hexanoic acid (2) system – Propionic acid rich region 63

Figure 6-9: x-y Phase diagram for Propionic Acid (1) + Hexanoic Acid (2) at 20 kPa 66

Figure 6-10: T-x-y Phase diagram for Propionic Acid (1) + Hexanoic Acid (2) at 20 kPa 66

Figure 6-11: x-y Phase diagram for Propionic Acid (1) + Hexanoic Acid (2) at 403.15 K 67

Figure 6-12: P-x-y Phase diagram for Propionic Acid (1) + Hexanoic Acid (2) at 403.15 K 67

Figure 6-13: x-y Phase diagram for Propionic Acid (1) + Hexanoic Acid (2) at 408.15 K 68

Figure 6-14: P-x-y Phase diagram for Propionic Acid (1) + Hexanoic Acid (2) at 408.15 K 68

Figure 6-15: x-y Phase diagram for Propionic Acid (1) + Hexanoic Acid (2) at 413.15 K 69

Figure 6-16: P-x-y Phase diagram for Propionic Acid (1) + Hexanoic Acid (2) at 413.15 K 69

Figure 6-17: GC Calibration for Isobutyric acid (1) + Hexanoic acid (2) system – Hexanoic acid rich region	70
Figure 6-18: GC Calibration for Isobutyric acid (1) + Hexanoic acid (2) system – Isobutyric acid rich region	70
Figure 6-19: x-y Phase diagram for Isobutyric Acid (1) + Hexanoic Acid (2) at 20 kPa	72
Figure 6-20: T-x-y Phase diagram for Isobutyric Acid (1) + Hexanoic Acid (2) at 20 kPa	72
Figure 6-21: x-y Phase diagram for Isobutyric Acid (1) + Hexanoic Acid (2) at 408.15 K	73
Figure 6-22: P-x-y Phase diagram for Isobutyric Acid (1) + Hexanoic Acid (2) at 408.15 K	73
Figure 6-23: x-y Phase diagram for Isobutyric Acid (1) + Hexanoic Acid (2) at 423.15 K	74
Figure 6-24: P-x-y Phase diagram for Isobutyric Acid (1) + Hexanoic Acid (2) at 423.15 K	74
Figure 6-25: GC Calibration for Valeric acid (1) + Hexanoic acid (2) system – Hexanoic acid rich region	75
Figure 6-26: GC Calibration for Valeric acid (1) + Hexanoic acid (2) system – Valeric acid rich region	75
Figure 6-27: x-y Phase diagram for Valeric Acid (1) + Hexanoic Acid (2) at 15 kPa	77
Figure 6-28: T-x-y Phase diagram for Valeric Acid (1) + Hexanoic Acid (2) at 15 kPa	77
Figure 6-29: x-y Phase diagram for Valeric Acid (1) + Hexanoic Acid (2) at 423.15 K	78
Figure 6-30: P-x-y Phase diagram for Valeric Acid (1) + Hexanoic Acid (2) at 423.15 K	78
Figure 6-31: x-y Phase diagram for Valeric Acid (1) + Hexanoic Acid (2) at 433.15 K	79
Figure 6-32: P-x-y Phase diagram for Valeric Acid (1) + Hexanoic Acid (2) at 433.15 K	79
Figure 6-33: GC Calibration for Hexanoic acid (1) + Heptanoic acid (2) system – Heptanoic acid rich region	80
Figure 6-34: GC Calibration for Hexanoic acid (1) + Heptanoic acid (2) system – Hexanoic acid rich region	80
Figure 6-35: x-y Phase diagram for Hexanoic Acid (1) + Heptanoic Acid (2) at 10 kPa	82
Figure 6-36: T-x-y Phase diagram for Hexanoic Acid (1) + Heptanoic Acid (2) at 10 kPa	82
Figure 6-37: x-y Phase diagram for Hexanoic Acid (1) + Heptanoic Acid (2) at 443.15 K	83
Figure 6-38: P-x-y Phase diagram for Hexanoic Acid (1) + Heptanoic Acid (2) at 443.15 K	83

CHAPTER SEVEN

Figure 7-1: Fit of Wilson, NRTL and Uniquac model to x-y diagram of cyclohexane (1) + ethanol (2) system at 323.15 K	87
Figure 7-2: Fit of Wilson, NRTL and Uniquac model to P-x-y diagram of cyclohexane (1) + ethanol (2) system at 323.15 K	87
Figure 7-3: Comparison between the experimental activity coefficients and those calculated from the Wilson, NRTL and Uniquac model for the cyclohexane (1) + ethanol (2) system at 323.15 K	88

Figure 7-4: Experimental liquid-phase activity coefficients for propionic acid (1) + hexanoic acid (2) system at 408.15 K	91
Figure 7-5: Fit of Peng-Robinson EOS to x-y data using the Twu-Coon mixing rule for the propionic acid (1) + Hexanoic acid (2) system at 403.15 K	94
Figure 7-6: Fit of Peng-Robinson EOS to P-x-y data using the Twu-Coon mixing rule for the propionic acid (1) + Hexanoic acid (2) system at 403.15 K	94
Figure 7-7: Fit of Wilson and Uniquac model to x-y data using chemical theory for the propionic acid (1) + Hexanoic acid (2) system at 403.15 K	95
Figure 7-8: Fit of Wilson and Uniquac model to P-x-y data using chemical theory for the propionic acid (1) + Hexanoic acid (2) system at 403.15 K	95
Figure 7-9: Fit of Wilson, Uniquac and NRTL model to x-y data using the Pitzer-Curl correlation for the propionic acid (1) + Hexanoic acid (2) system at 403.15 K	96
Figure 7-10: Fit of Wilson, Uniquac and NRTL model to P-x-y data using the Pitzer-Curl correlation for the propionic acid (1) + Hexanoic acid (2) system at 403.15 K	96
Figure 7-11: Fit of Peng-Robinson EOS to x-y data using the Twu-Coon mixing rule for the propionic acid (1) + Hexanoic acid (2) system at 408.15 K	97
Figure 7-12: Fit of Peng-Robinson EOS to P-x-y data using the Twu-Coon mixing rule for the propionic acid (1) + Hexanoic acid (2) system at 408.15 K	97
Figure 7-13: Fit of Wilson and Uniquac model to x-y data using chemical theory for the propionic acid (1) + Hexanoic acid (2) system at 408.15 K	98
Figure 7-14: Fit of Wilson and Uniquac model to P-x-y data using chemical theory for the propionic acid (1) + Hexanoic acid (2) system at 408.15 K	98
Figure 7-15: Fit of Wilson, Uniquac and NRTL model to x-y data using the Pitzer-Curl correlation for the propionic acid (1) + Hexanoic acid (2) system at 408.15 K	99
Figure 7-16: Fit of Wilson, Uniquac and NRTL model to P-x-y data using the Pitzer-Curl correlation for the propionic acid (1) + Hexanoic acid (2) system at 408.15 K	99
Figure 7-17: Fit of Peng-Robinson EOS to x-y data using the Twu-Coon mixing rule for the propionic acid (1) + Hexanoic acid (2) system at 413.15 K	100
Figure 7-18: Fit of Peng-Robinson EOS to P-x-y data using the Twu-Coon mixing rule for the propionic acid (1) + Hexanoic acid (2) system at 413.15 K	100
Figure 7-19: Fit of Wilson and Uniquac model to x-y data using chemical theory for the propionic acid (1) + Hexanoic acid (2) system at 413.15 K	101
Figure 7-20: Fit of Wilson and Uniquac model to P-x-y data using chemical theory for the propionic acid (1) + Hexanoic acid (2) system at 413.15 K	101
Figure 7-21: Fit of Wilson, Uniquac and NRTL model to x-y data using the Pitzer-Curl correlation for the propionic acid (1) + Hexanoic acid (2) system at 413.15 K	102

Figure 7-22: Fit of Wilson, Uniquac and NRTL model to P-x-y data using the Pitzer-Curl correlation for the propionic acid (1) + Hexanoic acid (2) system at 413.15 K	102
Figure 7-23: Fit of Peng-Robinson EOS to x-y data using the Twu-Coon mixing rule for the propionic acid (1) + Hexanoic acid (2) system at 20 kPa	103
Figure 7-24: Fit of Peng-Robinson EOS to T-x-y data using the Twu-Coon mixing rule for the propionic acid (1) + Hexanoic acid (2) system at 20 kPa	103
Figure 7-25: Fit of NRTL model to x-y data using the Pitzer-Curl correlation for the propionic acid (1) + Hexanoic acid (2) system at 20 kPa	104
Figure 7-26: Fit of NRTL model to T-x-y data using the Pitzer-Curl correlation for the propionic acid (1) + Hexanoic acid (2) system at 20 kPa	104
Figure 7-27: Fit of Peng-Robinson EOS to x-y data using the Twu-Coon mixing rule for the Isobutyric acid (1) + Hexanoic acid (2) system at 408.15 K	108
Figure 7-28: Fit of Peng-Robinson EOS to P-x-y data using the Twu-Coon mixing rule for the Isobutyric acid (1) + Hexanoic acid (2) system at 408.15 K	108
Figure 7-29: Fit of Wilson and Uniquac model to x-y data using chemical theory for the Isobutyric acid (1) + Hexanoic acid (2) system at 408.15 K	109
Figure 7-30: Fit of Wilson and Uniquac model to P-x-y data using chemical theory for the Isobutyric acid (1) + Hexanoic acid (2) system at 408.15 K	109
Figure 7-31: Fit of Wilson, Uniquac and NRTL model to x-y data using the Pitzer-Curl correlation for the Isobutyric acid (1) + Hexanoic acid (2) system at 408.15 K	110
Figure 7-32: Fit of Wilson, Uniquac and NRTL model to P-x-y data using the Pitzer-Curl correlation for the Isobutyric acid (1) + Hexanoic acid (2) system at 408.15 K	110
Figure 7-33: Fit of Peng-Robinson EOS to x-y data using the Twu-Coon mixing rule for the Isobutyric acid (1) + Hexanoic acid (2) system at 423.15 K	111
Figure 7-34: Fit of Peng-Robinson EOS to P-x-y data using the Twu-Coon mixing rule for the Isobutyric acid (1) + Hexanoic acid (2) system at 423.15 K	111
Figure 7-35: Fit of Wilson and Uniquac model to x-y data using chemical theory for the Isobutyric acid (1) + Hexanoic acid (2) system at 423.15 K	112
Figure 7-36: Fit of Wilson and Uniquac model to P-x-y data using chemical theory for the Isobutyric acid (1) + Hexanoic acid (2) system at 423.15 K	112
Figure 7-37: Fit of Wilson, Uniquac and NRTL model to x-y data using the Pitzer-Curl correlation for the Isobutyric acid (1) + Hexanoic acid (2) system at 423.15 K	113
Figure 7-38: Fit of Wilson, Uniquac and NRTL model to P-x-y data using the Pitzer-Curl correlation for the Isobutyric acid (1) + Hexanoic acid (2) system at 423.15 K	113
Figure 7-39: Fit of Peng-Robinson EOS to x-y data using the Twu-Coon mixing rule for the Isobutyric acid (1) + Hexanoic acid (2) system at 20 kPa	114

Figure 7-40: Fit of Peng-Robinson EOS to T-x-y data using the Twu-Coon mixing rule for the Isobutyric acid (1) + Hexanoic acid (2) system at 20 kPa	114
Figure 7-41: Fit of NRTL model to x-y data using the Pitzer-Curl correlation for the Isobutyric acid (1) + Hexanoic acid (2) system at 20 kPa	115
Figure 7-42: Fit of NRTL model to T-x-y data using the Pitzer-Curl correlation for the Isobutyric acid (1) + Hexanoic acid (2) system at 20 kPa	115
Figure 7-43: Fit of Peng-Robinson EOS to x-y data using the Twu-Coon mixing rule for the Valeric acid (1) + Hexanoic acid (2) system at 423.15 K	119
Figure 7-44: Fit of Peng-Robinson EOS to P-x-y data using the Twu-Coon mixing rule for the Valeric acid (1) + Hexanoic acid (2) system at 423.15 K	119
Figure 7-45: Fit of Wilson and Uniquac model to x-y data using chemical theory for the Valeric acid (1) + Hexanoic acid (2) system at 423.15 K	120
Figure 7-46: Fit of Wilson and Uniquac model to P-x-y data using chemical theory for the Valeric acid (1) + Hexanoic acid (2) system at 423.15 K	120
Figure 7-47: Fit of Wilson, Uniquac and NRTL model to x-y data using the Pitzer-Curl correlation for the Valeric acid (1) + Hexanoic acid (2) system at 423.15 K	121
Figure 7-48: Fit of Wilson, Uniquac and NRTL model to P-x-y data using the Pitzer-Curl correlation for the Valeric acid (1) + Hexanoic acid (2) system at 423.15 K	121
Figure 7-49: Fit of Peng-Robinson EOS to x-y data using the Twu-Coon mixing rule for the Valeric acid (1) + Hexanoic acid (2) system at 433.15 K	122
Figure 7-50: Fit of Peng-Robinson EOS to P-x-y data using the Twu-Coon mixing rule for the Valeric acid (1) + Hexanoic acid (2) system at 433.15 K	122
Figure 7-51: Fit of Wilson and Uniquac model to x-y data using chemical theory for the Valeric acid (1) + Hexanoic acid (2) system at 433.15 K	123
Figure 7-52: Fit of Wilson and Uniquac model to P-x-y data using chemical theory for the Valeric acid (1) + Hexanoic acid (2) system at 433.15 K	123
Figure 7-53: Fit of Wilson, Uniquac and NRTL model to x-y data using the Pitzer-Curl correlation for the Valeric acid (1) + Hexanoic acid (2) system at 433.15 K	124
Figure 7-54: Fit of Wilson, Uniquac and NRTL model to P-x-y data using the Pitzer-Curl correlation for the Valeric acid (1) + Hexanoic acid (2) system at 433.15 K	124
Figure 7-55: Fit of Peng-Robinson EOS to x-y data using the Twu-Coon mixing rule for the Valeric acid (1) + Hexanoic acid (2) system at 15 kPa	125
Figure 7-56: Fit of Peng-Robinson EOS to T-x-y data using the Twu-Coon mixing rule for the Valeric acid (1) + Hexanoic acid (2) system at 15 kPa	125
Figure 7-57: Fit of NRTL model to x-y data using the Pitzer-Curl correlation for the Valeric acid (1) + Hexanoic acid (2) system at 15 kPa	126

Figure 7-58: Fit of NRTL model to T-x-y data using the Pitzer-Curl correlation for the Valeric acid (1) + Hexanoic acid (2) system at 15 kPa	126
Figure 7-59: Fit of Peng-Robinson EOS to x-y data using the Twu-Coon mixing rule for the Hexanoic acid (1) + Heptanoic acid (2) system at 443.15 K	130
Figure 7-60: Fit of Peng-Robinson EOS to P-x-y data using the Twu-Coon mixing rule for the Hexanoic acid (1) + Heptanoic acid (2) system at 443.15 K	130
Figure 7-61: Fit of Wilson and Uniquac model to x-y data using chemical theory for the Hexanoic acid (1) + Heptanoic acid (2) system at 443.15 K	131
Figure 7-62: Fit of Wilson and Uniquac model to P-x-y data using chemical theory for Hexanoic acid (1) + Heptanoic acid (2) system at 443.15 K	131
Figure 7-63: Fit of Wilson, Uniquac and NRTL model to x-y data using the Pitzer-Curl correlation for Hexanoic acid (1) + Heptanoic acid (2) system at 443.15 K	132
Figure 7-64: Fit of Wilson, Uniquac and NRTL model to P-x-y data using the Pitzer-Curl correlation for Hexanoic acid (1) + Heptanoic acid (2) system at 443.15 K	132
Figure 7-65: Fit of Peng-Robinson EOS to x-y data using the Twu-Coon mixing rule for the Hexanoic acid (1) + Heptanoic acid (2) system at 10 kPa	133
Figure 7-66: Fit of Peng-Robinson EOS to T-x-y data using the Twu-Coon mixing rule for the Hexanoic acid (1) + Heptanoic acid (2) system at 10 kPa	133
Figure 7-67: Fit of NRTL model to x-y data using the Pitzer-Curl correlation for Hexanoic acid (1) + Heptanoic acid (2) system at 10 kPa.	134
Figure 7-68: Fit of NRTL model to T-x-y data using the Pitzer-Curl correlation for Hexanoic acid (1) + Heptanoic acid (2) system at 10 kPa.	134

APPENDIX A

Figure A-1: Ionisation of acetic acid in water	150
Figure A-2: Cleavage of the <i>O</i> – <i>H</i> bond.	151
Figure A-3: Reaction at the carbonyl carbon	151
Figure A-4: Decarboxylation reaction	152
Figure A-5: Reaction of the α carbon	152

APPENDIX B

Figure B-1: Pressure Transducer calibration	160
Figure B-2: Low Temperature Calibration of Pt-100 Bulb.	160
Figure B- 3: High Temperature Calibration of Pt-100 Bulb.	161

APPENDIX C

Figure C-1: Fit of Wilson model to x-y diagram of cyclohexane (1) + ethanol (2) system at 40 kPa	165
Figure C-2: Fit of Wilson model to P-x-y diagram of cyclohexane (1) + ethanol (2) system at 40 kPa	165
Figure C-3: Fit of NRTL model to x-y diagram of cyclohexane (1) + ethanol (2) system at 40 kPa	166
Figure C-4: Fit of NRTL model to P-x-y diagram of cyclohexane (1) + ethanol (2) system at 40 kPa	166
Figure C-5: Fit of UNIQUAC model to x-y diagram of cyclohexane (1) + ethanol (2) system at 40 kPa	167
Figure C-6: Fit of UNIQUAC model to P-x-y diagram of cyclohexane (1) + ethanol (2) system at 40 kPa	167
Figure C-7: Graph showing the deviation of the activity coefficients calculated using the Wilson model from the experimental activity coefficients for the cyclohexane (1) + ethanol (2) system at 323.15 K	168
Figure C-8: Graph showing the deviation of the vapour compositions calculated using the Wilson model from the experimental activity coefficients for the cyclohexane (1) + ethanol (2) system at 323.15 K	168
Figure C-9: Graph showing the deviation of the activity coefficients calculated using the NRTL model from the experimental activity coefficients for the cyclohexane (1) + ethanol (2) system at 323.15 K	169
Figure C-10: Graph showing the deviation of the vapour compositions calculated using the NRTL model from the experimental activity coefficients for the cyclohexane (1) + ethanol (2) system at 323.15 K	169
Figure C-11: Graph showing the deviation of the activity coefficients calculated using the UNIQUAC model from the experimental activity coefficients for the cyclohexane (1) + ethanol (2) system at 323.15 K	170
Figure C-12: Graph showing the deviation of the vapour compositions calculated using the UNIQUAC model from the experimental activity coefficients for the cyclohexane (1) + ethanol (2) system at 323.15 K	170

APPENDIX D

Figure D-1: Photograph of the experimental used in this project	171
---	-----

LIST OF TABLES

CHAPTER TWO

Table 2-1: Bond lengths and bond angles for short chain carboxylic acids (Patai [1979])	4
---	---

CHAPTER THREE

Table 3- 1: Direct test index for thermodynamic consistency, Van Ness (1995)	44
--	----

CHAPTER FIVE

Table 5-1: Operating conditions for the Varian 3300 gas chromatograph	54
---	----

CHAPTER SIX

Table 6-1: Purity of Chemical reagents	59
--	----

Table 6-2: Vapour-Liquid Equilibrium Data for Cyclohexane (1) + Ethanol (2) at 40 kPa	60
---	----

Table 6-3: Vapour-Liquid Equilibrium Data for Cyclohexane (1) + Ethanol (2) at 323.15 K	60
---	----

Table 6-4: Vapour-Liquid Equilibrium Data for Propionic Acid (1) + Hexanoic Acid (2) at 20 kPa	64
--	----

Table 6-5: Vapour-Liquid Equilibrium Data for Propionic Acid (1) + Hexanoic Acid (2) at 403.15 K	64
--	----

Table 6-6: Vapour-Liquid Equilibrium Data for Propionic Acid (1) + Hexanoic Acid (2) at 408.15 K	65
--	----

Table 6-7: Vapour-Liquid Equilibrium Data for Propionic Acid (1) + Hexanoic Acid (2) at 413.15 K	65
--	----

Table 6-8: Vapour-Liquid Equilibrium Data for Isobutyric Acid (1) + Hexanoic Acid (2) at 20 kPa	71
---	----

Table 6-9: Vapour-Liquid Equilibrium Data for Isobutyric Acid (1) + Hexanoic Acid (2) at 408.15 K	71
---	----

Table 6-10: Vapour-Liquid Equilibrium Data for Isobutyric Acid (1) + Hexanoic Acid (2) at 423.15 K	71
--	----

Table 6-11: Vapour-Liquid Equilibrium Data for Valeric Acid (1) + Hexanoic Acid (2) at 15kPa	76
--	----

Table 6-12: Vapour-Liquid Equilibrium Data for Valeric Acid (1) + Hexanoic Acid (2) at 423.15 K	76
Table 6-13: Vapour-Liquid Equilibrium Data for Valeric Acid (1) + Hexanoic Acid (2) at 433.15 K	76
Table 6-14: Vapour-Liquid Equilibrium Data for Hexanoic Acid (1) + Heptanoic Acid (2) at 10 kPa	81
Table 6-15: Vapour-Liquid Equilibrium Data for Hexanoic Acid (1) + Heptanoic Acid (2) at 443.15 K	81

CHAPTER SEVEN

Table 7-1: Model parameters and deviations between calculated and experimental vapour phase, pressure and temperature for cyclohexane (1) + ethanol (2) system	86
Table 7-2: Best fit models for the propionic acid + hexanoic acid system	92
Table 7-3: Model parameters and deviations between calculated and experimental vapour phase and pressure/ temperature using the Peng-Robinson EOS and the Twu & Coon mixing rule for the Propionic acid + Hexanoic acid system.	92
Table 7-4: Model parameters and deviations between calculated and experimental vapour phase and pressure/ temperature using the Pitzer-Curl correlation for the Propionic acid + Hexanoic acid system.	93
Table 7-5: Model parameters and deviations between calculated and experimental vapour phase and pressure/ temperature using chemical theory for the Propionic acid + Hexanoic acid system.	93
Table 7-6: Best fit models for the isobutyric acid + hexanoic acid system	105
Table 7-7: Model parameters and deviations between calculated and experimental vapour phase and pressure/ temperature using the Peng-Robinson EOS and the Twu & Coon mixing rule for the Isobutyric acid + Hexanoic acid system.	106
Table 7-8: Model parameters and deviations between calculated and experimental vapour phase and pressure/ temperature using the Pitzer-Curl correlation for the Isobutyric acid + Hexanoic acid system.	106
Table 7-9: Model parameters and deviations between calculated and experimental vapour phase and pressure/ temperature using chemical theory for the Isobutyric acid + Hexanoic acid system.	107
Table 7-10: Best fit models for the valeric acid + hexanoic acid system	116
Table 7-11: Model parameters and deviations between calculated and experimental vapour phase and pressure/ temperature using the Peng-Robinson EOS and the Twu & Coon mixing rule for the Valeric acid + Hexanoic acid system.	117

Table 7-12: Model parameters and deviations between calculated and experimental vapour phase and pressure/ temperature using the Pitzer-Curl correlation for the Valeric acid + Hexanoic acid system.	117
Table 7-13: Model parameters and deviations between calculated and experimental vapour phase and pressure/ temperature using chemical theory for the Valeric acid + Hexanoic acid system.	118
Table 7-14: Best fit models for the hexanoic acid + heptanoic acid system	127
Table 7-15: Model parameters and deviations between calculated and experimental vapour phase and pressure/ temperature using the Peng-Robinson EOS and the Twu & Coon mixing rule for the Hexanoic acid + Heptanoic acid system.	128
Table 7-16: Model parameters and deviations between calculated and experimental vapour phase and pressure/ temperature using the Pitzer-Curl correlation for the Hexanoic acid + Heptanoic acid system.	128
Table 7-17: Model parameters and deviations between calculated and experimental vapour phase and pressure/ temperature using chemical theory for the Hexanoic acid + Heptanoic acid system.	129

APPENDIX A

Table A-1 : Carboxylic Acids Binary Vapour-Liquid Equilibrium Data Currently Available	148
Table A-2: Common names, IUPAC names, Melting point, Boiling point and Solubility of Carboxylic acids, Patai (1979)	149

APPENDIX B

Table B-1: Carboxylic Acids Dimerisation Equilibrium Constants	161
Table B- 2: Carboxylic Acids L, M And N Parameters For The Twu-Coon Mixing Rule.	162
Table B- 3: Pure Component Properties for Cyclohexane and Ethanol.	163
Table B- 4: Pure Component Properties for Carboxylic Acids.	163
Table B-5: Second Virial Coefficients for the Propionic acid + Hexanoic acid system	163
Table B-6: Second Virial Coefficients for the Isobutyric acid + Hexanoic acid system	164
Table B- 7: Second Virial Coefficients for the Valeric acid + Hexanoic acid system	164
Table B- 8: Second Virial Coefficients for the Hexanoic acid + Heptanoic acid system	164

NOMENCLATURE

List of Symbols

a	Intermolecular attraction force parameter in Peng-Robinson [1976] equation of state
B^0	Parameter in the Pitzer-Curl [1957] correlation
B^i	Parameter in the Pitzer-Curl [1957] correlation
B_{ii}	Second virial coefficient of pure component i [cm^3/mol]
B_{ij}	Second virial coefficient for species i - species j interaction [cm^3/mol]
b	Molecular size parameter in Peng-Robinson [1976] equation of state
f	Fugacity [kPa]
\hat{f}	Fugacity in solution [kPa]
G	Molar or specific Gibbs energy [J/mol]
G_{12}	Parameter in the NRTL [1968] model
G_{21}	Parameter in the NRTL [1968] model
\bar{G}	Partial molar Gibbs energy [J/mol]
g_{ij} - g_{ii}	Parameter representing energy interactions between species in the NRTL [1968] model
H	Enthalpy [J/mol]
ΔH_{vap}	Enthalpy of vapourization [J/mol]
K	Equilibrium constant
k	Mixing rule parameter
k_B	The Boltzmann constant [1.381×10^{-23} J/mol.K]
k_{ij}	Binary interaction parameter
L'	Parameter in the Twu et al. [1991] alpha correlation
l_i	Parameter in the UNIQUAC [1975] model (Section 3.4.1.6)
l_{ij}	Binary interaction parameter for mixing rules
M	General thermodynamic property
M'	Parameter in the Twu et al. [1991] alpha correlation
N'	Parameter in the Twu et al. [1991] alpha correlation
n	Number of moles
n_i	Number of moles of dimer or monomer in Twu et al. [1993] equation of state
n_T	Total number of moles of monomer and dimer in Twu et al. [1993] equation of state

n_0	Number of moles that would exist if no association was occurring (Section 3.6.5)
P	System pressure [kPa]
P'	Parachor
q_i	Pure component area parameter in the UNIQUAC [1975] model (Section 3.4.1.6)
R	Universal gas constant [J/mol.K]
R_d	Mean radius of gyration [\AA]
r_i	Pure component volume parameter in the UNIQUAC [1975] model (Section 3.4.1.6)
S	Molar or specific entropy [cm^3/mol]
T	System temperature [$^{\circ}\text{C}$ or K]
u	Constant integer value in Twu et al. [1993] equation of state
V	Molar or specific volume [cm^3/mol]
w	Constant integer value in Twu et al. [1993] equation of state
x	Liquid phase mole fraction (or composition)
y	Vapour phase mole fraction (or composition)
Z	Compressibility factor
z	Coordination number in the UNIQUAC equation (Section 3.4.1.6)
z_i	True mole fraction of species i

Greek Letters

α	Scaling factor in Peng-Robinson [1976] equation of state
α_{12}	Parameter in NRTL [1968] model representing solution non-randomness
δ	Denotes a residual (e.g. δP)
δ_{ij}	Term relating the second virial coefficients (Equations (3-116))
ϵ_A	Tolerance in the flow diagrams for the bubblepoint iterations
ϵ_B	Tolerance in the flow diagrams for the bubblepoint iterations
ϵ_C	Tolerance in the flow diagrams for the bubblepoint iterations
ϵ_{PR}	Constant in the Peng-Robinson [1976] equation of state
Φ	Ratio of fugacity coefficients, with the Poynting correction factor (Equation 3-116))
Φ_1	Segment fraction in the UNIQUAC [1975] model (Section 3.4.1.6)
Φ_2	Segment fraction in the UNIQUAC [1975] model (Section 3.4.1.6)
ϕ	Fugacity coefficient

$\hat{\phi}$	Fugacity coefficient in solution
ϕ^*	True species fugacity coefficient
γ	Activity coefficient
γ_i^∞	Infinite dilution activity coefficient
η	Solvation (unlike species) and association (pure species) parameters
κ	Characteristic constant in Peng-Robinson[1976] equation of state
Λ_{12}	Parameter in the Wilson [1964] model
Λ_{21}	Parameter in the Wilson [1964] model
$\lambda_{ij}-\lambda_{ii}$	Parameter representing molar interactions between species in the Wilson [1964] model
μ	Dipole moment [debye]
μ_i	Chemical potential of component i
μ_i^m	Molecular dipole
θ_1	Area fraction in the UNIQUAC [1975] model (section 3.4.1.6))
θ_2	Area fraction in the UNIQUAC [1975] model (section 3.4.1.6))
σ_{PR}	Constant in the Peng-Robinson [1976] equation of state
τ_{12}	Parameter in the NRTL [1968] model
τ_{21}	Parameter in the NRTL [1968] model
ω	Acentric factor

Subscript

1	Denotes component 1
2	Denotes component 2
avg	Denotes an average value
c	Denotes a critical property
$calc$	Denotes a calculated value
ex	Denotes an experimental value
i	Denotes component i
lit	Denotes a literature value
m	Denotes a mixture property
vdw	Denotes a “van der Waals” property

Superscript

<i>D</i>	Denotes the “dimerized” contribution to the second virial coefficient in the Hayden and O’Connell method [1975]
<i>E</i>	Denotes an excess property
<i>F</i>	Denotes the “free” contribution to the second virial coefficient in the Hayden and O’Connell method [1975]
<i>l</i>	Denotes the liquid phase
<i>sat</i>	Denotes a saturated value
<i>v</i>	Denotes the vapour phase

Abbreviations

EOS	Equation of State
GC	Gas Chromatograph
P-R	Peng-Robinson
VLE	Vapour-Liquid Equilibrium

INTRODUCTION

This project is a continuation of research initiated by Sewnarain (2002) and Clifford (2004) at the University of KwaZulu-Natal (then University of Natal). The aim of this project is to measure new vapour-liquid equilibrium (VLE) data for binary carboxylic acid + carboxylic acid systems which are currently unavailable in open literature. This project arose out of SASOL (South African Coal & Oil Limited) looking at the feasibility of developing a separation plant for the purification of the acids, instead of incinerating them. There are very few carboxylic acid + carboxylic acid binary systems that have been measured experimentally. This is evident from the lack of published data in excellent compilations like the Dortmund Data Bank (DDB) and the Korean Data Base (KDB). Table A-1 in Appendix A, shows the published binary carboxylic acid + carboxylic acid systems found in open literature and available databanks.

Recent years have seen the phrase “Sustainable Development” becoming a frequent topic of debate. Much legislation has been put in place in developed countries. Third world countries are difficult to legislate because of their development status. Developed countries have progressed significantly putting in place legislation that advocates compliance with strict set environmental standards. Industrial waste disposal standards have been reviewed making them stringent with stiff penalties and action being levelled against the lawbreaker. Globalisation is becoming a reality in every country. This has seen the opening up of world markets forcing companies to be efficient in their operations to retain their competitive edge. Industries are now employing state of the art technologies with their main focus being that of maximising products output from raw materials at the lowest cost. What once was considered waste is being processed to extract valuable components. The above two reasons, among others, have resulted in process

modifications and design research as industry strives to meet environmental standards and maintain competitiveness in the new unfolding global markets.

The design of such separation and purification plant requires VLE data for the components in the stream to be purified. VLE data can be obtained by experimental techniques or by predictive methods such as molecular simulation. Research has advanced considerably over the last 10 years in the area of molecular simulation, which allows the prediction of VLE data using atomic models. However, there is still a great reliance on experimental VLE data in the design of separation and purification plants. It must be stated though that experimental measurement of VLE data is costly and time-consuming; factors that have resulted in the advancement of research in the area of molecular simulations.

The dynamic VLE still developed by Raal, (Raal and Mühlbauer [1998]) was used to undertake the VLE measurements. New vapour-liquid equilibrium data were measured for the following binary carboxylic acid systems:

- Propionic acid + Hexanoic acid at 20 kPa, 403.15 K, 408.15 K and 413.15 K.
- Isobutyric acid + Hexanoic acids at 20 kPa, 413.15 K and 423.15 K.
- Valeric acid + Hexanoic acid at 15 kPa, 423.15 K and 433.15 K.
- Hexanoic acid + Heptanoic acid at 10 kPa and 443.15 K.

Carboxylic acids are known for their strong association due to the ability of the molecules to form hydrogen bonds with like molecules. The measured data were regressed using two methods namely the “gamma - phi” method and the “phi - phi” method. The “gamma - phi” method relates pressure, temperature, vapour composition and liquid composition at equilibrium. The virial coefficients to calculate the vapour phase non-ideality were computed using two different methods namely Pitzer-Curl (Pitzer and Curl [1957]) and chemical theory. The “phi - phi” method also known as the direct method, which uses cubic equations of state was used to regress the experimental data. Thermodynamic consistency tests were done using the point test, (VanNess et al. [1973]).

The need to find correlations that accurately model carboxylic acid mixtures is still on going. Many experimentalists who include Nan et al. (2003), Peng and coworkers (2004) and Raal and Clifford (University of Kwa-Zulu Natal) are working on developing models that accurately characterize the phase behavior of carboxylic acid mixtures.

CARBOXYLIC ACIDS

2.1 Introduction

Carboxylic acids fall into the carbonyl group ($C = O$). Carboxylic acids that have long (12 to 24 carbon atoms) un-branched aliphatic groups are called fatty acids. The carboxyl group ($COOH$) is one of the most interesting organic molecules especially from a physiochemical point of view (Patai [1979]). Interesting features of carboxylic acids emerge from their geometry. There are two carbon-oxygen bonds, with different lengths. The group is planar and the hydrogen atom might be in the *cis* or the *trans* position with respect to the carbonyl group. The group participates in hydrogen bonding, acting as a hydrogen donor or acceptor. Carboxylic acids have a tendency to dimerise through the formation of two hydrogen bonds as shown in Figure 2-1. These chemical forces are significant and have major importance in determining the thermodynamic properties of a solution. Cyclic dimers and polymolecular chains are often found in acid crystals. Dimerisation equilibria in liquid solutions and in the gas phase have been a subject of thermodynamic investigation dating back to the work by Dolezalek (1908).

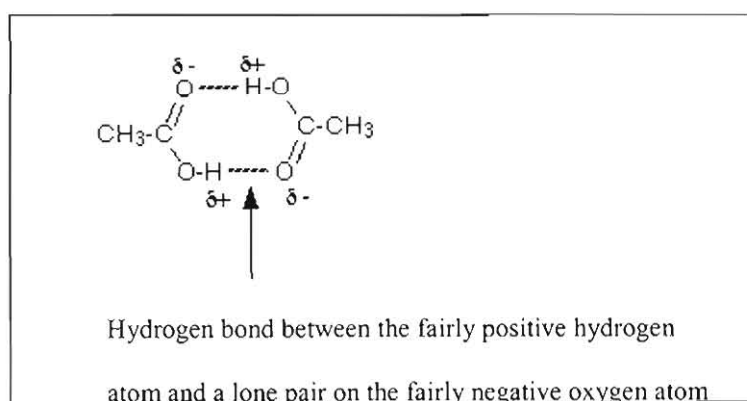


Figure 2-1: Hydrogen bonding of acetic acid to form a dimer

2.2 Nomenclature

The common names of carboxylic acids reflect an old format of naming compounds after their natural source. The IUPAC names for carboxylic acids are formed by dropping the -e from the IUPAC name of the corresponding parent alkane and replacing it by -oic. However, older common names that end in -ic are still used. The -oic acid naming scheme is superior because it unambiguously identifies the material as a carboxylic acid. In cases where another functional group takes naming precedence, "carboxy" is used as a prefix, although in certain cases the suffix "carboxylic acid" may also be used. Table A-2 in appendix A gives the common name, IUPAC name, melting point, boiling point and solubility in water of low chain carboxylic acids.

2.3 Geometry and Structure

The geometry and structure of carboxylic acids contribute significantly to the strength of the hydrogen bonds formed in dimers. The crystalline structures of carboxylic acids have been investigated by many authors in an effort to comprehend the physiochemical properties of these compounds. Table 2-1, adapted from Patai (1979), shows selected low chain carboxyl group principal data of C - O, C = O bond lengths and the COO bond angles.

Table 2-1: Bond lengths and bond angles for short chain carboxylic acids (Patai [1979])

Acid	C - O (Å)	C = O (Å)	Bond angle degrees	OH --- O (Å)	C - C (Å)
Formic	1.23	1.26	123	2.58	-
Acetic	1.24	1.29	122	2.61	1.54
Propionic	1.23	1.32	122	2.64	1.50
Butyric	1.22	1.35	123	2.62	1.54
Valeric	1.26	1.35	118	2.63	1.53
Dodecanedioic	1.244	1.294	122	2.65	1.497
Benzoic	1.24	1.29	122	2.64	1.48

The range of the C - O bond length is 1.22 – 1.26 Å with an average of 1.238 Å over the seven acids selected above. The corresponding values of the C = O bond are 1.26 – 1.35 Å with an average of 1.31 Å. As can be seen from Table 2-1, one of the C - O bond lengths is considerably shorter. This has a remarkable effect of increasing the hydrogen bond strength in the cyclic dimers increasing the association and dissociation energy. An exception is formic acid whose C - O bond length is 1.23 ± 0.03 Å and C=O bond length is 1.26 ± 0.03 Å. The molecules are

linked by hydrogen bonds at both ends to form long polymeric chains. Liquid formic acid consists of chain-like associates connected by hydrogen bonds 2.7 Å long.

2.4 Chemical Forces

2.4.1 Dimerisation

As stated in Chapter 1, there are specific forces of attraction that lead to the formation of new molecular species. Such forces are called chemical forces. There are quite a number of specific chemical forces, which are important in the thermodynamics of solutions. The chemical forces that affect the thermodynamic behaviour of carboxylic acids are hydrogen bonds. The chemical forces that affect solutions include:

2.4.1.1 Hydrogen Bonds

Hydrogen bonds are a relatively strong form of intermolecular attraction. The hydrogen atom is attached directly to one of the most electronegative elements, in this case oxygen, causing the hydrogen to acquire a significant amount of positive charge. Each of the elements to which the hydrogen is attached is not only significantly negative, but also has two "active" lone pairs of electrons. Lone pairs at the second level have the electrons contained in a relatively small volume of space, which therefore has a high density of negative charge. Lone pairs at higher levels are more diffuse and not so attractive to positive charges. Atkins et al. (2001) and Patai (1979) discuss hydrogen bonds in detail.

2.4.1.2 Chemical Complex

Chemical complexes are similar to hydrogen bonds. Different molecules are attracted to each other because of their polarity forming chemical complexes.

2.4.1.3 Electron Donor- Electron Acceptor Interaction

These are molecular interactions where a molecular entity transfers an electron to another molecular entity.

2.4.1.4 Acidic-Basic Complex Formation

This is based on the definition of a Lewis acid and base. An example is that of Al^{3+} ion which acts as an acid, accepting electron pairs from water, which acts as a base, an electron-pair donor. The two combine to form $\text{Al}(\text{H}_2\text{O})_6^{3+}$, an acid-base complex

The main difference between chemical and physical forces lies in the criterion of saturation. Chemical forces are saturated and physical forces are not. Saturation is connected with the theory of covalent bonding and the law of multiple proportion which states that the ratio of atoms in a molecule is a small, integral number (Proust [1794]). With chemical forces, once the bond is formed, the molecule has no appreciable tendency to further form another bond enlarging the molecule. The attractive forces in the bond would have been satisfied or saturated. Physical forces on the other hand know no such satisfaction. A good example is that of argon. Two argon atoms, which are attracted to form a doublet, still have a tendency to form a triplet and further on. Chemical forces in solution are classified in terms of association or solvation. Malanowski (1992), defines these as follows:

- **Association** – The tendency of molecules to form polymers.
- **Solvation** – The tendency of molecules of different species to form complexes.

The extent of association is a strong function of composition, especially in the range that is dilute with respect to the associating component. Pure acetic acid exists primarily as a dimer, but when acetic acid is dissolved in excess hexane, it exists as a monomer. As the acetic acid concentration increases, more polymers are formed. As a result the fugacity (a concept discussed in Section 3.2) of acetic acid is a highly non-linear function of its mole fraction.

2.5 Chemical Properties of Carboxylic Acids

The chemical properties of carboxylic acids will not be discussed here. A brief discussion is given in Appendix A.

PHASE EQUILIBRIUM

3.1 Introduction

The design and operation of fluid-phase separation processes depends fundamentally on the knowledge of phase equilibria. VLE data need always to be interpreted and interpolated correctly at any temperature and pressure. The primary thermodynamic value from VLE data taken at relatively low temperature is that one can calculate values for the excess Gibbs function. This chapter deals with the thermodynamic treatment of VLE data, especially that relevant to carboxylic acids.

3.2 Equilibrium

Equilibrium denotes static conditions, the absence of change (Smith & Van Ness [1996]). In thermodynamics it is taken to also mean the absence of any tendency towards change on a macroscopic scale. For a system that has different phases, the following criteria are essential for equilibrium. The equality of temperature of the phases in contact is required for thermal equilibrium and equality of pressure for hydrostatic equilibrium. The chemical potential needs to be uniform for diffusive equilibrium. The chemical potential is denoted by μ . For a two-phase system one can conclude that:

$$\mu_i^\alpha = \mu_i^\beta \quad (i = 1, 2, \dots, N) \quad (3-1)$$

where N is the number of species present in the system. In other words the chemical potential of species i in phase α should be equal to the chemical potential of i in phase β for the system to be in equilibrium. This concept can be generalised to systems that have more than two phases; the results for π phases is:

$$\mu_i^\alpha = \mu_i^\beta = \dots = \mu_i^\pi \quad (i = 1, 2, \dots, N) \quad (3-2)$$

3.3 Fugacity and Fugacity Coefficient

We have already seen that the fundamental condition for equilibrium in phase equilibria is the equality of the chemical potential as given by Equation (3-1). The more useful concept though is fugacity, which has the units of pressure.

$$f_i^\alpha = f_i^\beta \quad (i = 1, 2, \dots, N) \quad (3-3)$$

In this case we are mainly concerned about the vapour and liquid equilibria and so one can write:

$$f_i^v = f_i^l \quad (i = 1, 2, \dots, N) \quad (3-4)$$

The solution to this equation for the equilibrium phase compositions depends on the pressure of the system in question. At pressures up to about 10-20 bar, the non-ideality of the liquid phase is reasonably well represented by the activity coefficients (γ) determined around 1 bar; the effect of pressure on the liquid phase far from the critical region is mild enough to permit this (Winnick [1996]). The vapour phase fugacities are well represented in this region with expressions developed from the virial equation of state. Owing to the small convergence radius of the virial expansion for carboxylic acids, it is not possible to express the deviations from ideal behaviour in the vapour phase of these substances directly from the virial equation of state truncated after the second term as it is common in the vicinity of normal pressure for non associating or weakly associating systems (Malijevska et al. [1984]). At higher pressures, activity coefficients determined at 1 bar are not applicable for non-associating systems. At low pressure the vapour phase is within a few percent of ideal gas behaviour. This however, is not true for associating substances like carboxylic acids. The liquid phase behaves far from a Raoult's law mixture. Strong chemical interaction, as well as size and shape differences between component molecules lead to non-ideal mixing.

Several thermodynamic correlations have been proposed for data reduction of strongly associated substances of which some are reviewed and used in this work. Walas (1985), Malanowski (1992) review thermodynamic models correlating vapour phase non-idealities and fugacity coefficient models for associating substances. At low to moderate pressures, the fugacity of the phases in equilibrium are represented for the vapour by:

$$f_i^v = y_i \hat{\phi}_i P \quad (3-5)$$

and for the liquid by:

$$f_i^l = x_i \gamma_i \hat{\phi}_i^{sat} P_i^{sat} \exp\left[\frac{V_i(P - P_i^{sat})}{RT}\right] \quad (3-6)$$

One can equate Equations (3-5) and (3-6) in conditions of equilibrium to get:

$$y_i \hat{\phi}_i P = x_i \gamma_i \hat{\phi}_i^{sat} P_i^{sat} \exp\left[\frac{V_i(P - P_i^{sat})}{RT}\right] \quad (3-7)$$

or

$$y_i \Phi_i P = x_i \gamma_i P_i^{sat} \quad (3-8)$$

where

$$\Phi_i = \frac{\hat{\phi}_i}{\hat{\phi}_i^{sat}} \exp\left[\frac{-V_i(P - P_i^{sat})}{RT}\right] \quad (3-9)$$

The exponential term in Equation (3-6) is known as the Poynting correction factor; $\hat{\phi}_i$ and $\hat{\phi}_i^{sat}$ are the vapour fugacity and saturated vapour fugacity coefficient respectively; P_i^{sat} is the saturated pressure of the pure component and V_i is the liquid molar volume. In the pressure range (0 to ~20 bar) it is reasonable to assume constant molar volume. The Poynting correction factor and the saturated vapour fugacity can be treated as unity at low pressure (Prausnitz et al. [1986]). One can also see that by setting Φ_i and γ_i equal to unity, the equation reverts to Raoult's law, which assumes ideal behaviour of both the vapour and liquid phases.

3.4 Activity Coefficients

An activity coefficient, γ , is the correction factor that measures the departure of a solution from ideal solution behaviour. It is defined in different ways with respect to various composition parameters and is always the empirical ratio of activity to that of the composition parameter. It is defined as:

$$\gamma_i = \frac{a_i}{x_i} = \frac{f_i'}{f_i^{sat} x_i} \quad (3-10)$$

The excess Gibbs energy, G^E , is one of the most useful thermodynamic concepts for expressing non-ideality of a liquid mixture. Excess properties express the difference between actual property values of a solution and the values that would be exhibited by an ideal solution at the same temperature, pressure and composition. Van Ness (1959) derived the fundamental excess property relation showing the inter-relation of these properties:

$$d \left[\frac{nG^E}{RT} \right] = \frac{nV^E}{RT} dP - \frac{nH^E}{RT^2} dT + \sum \ln \gamma_i dn_i \quad (3-11)$$

where G^E is the molar excess Gibbs Energy, V^E is the molar excess volume and H^E is the molar excess enthalpy. Taking the partial derivatives of the fundamental excess property relation yields:

$$\left[\frac{\partial G^E / RT}{\partial P} \right]_{T,x} = \frac{V^E}{RT} \quad (3-12)$$

$$-T \left[\frac{\partial G^E / RT}{\partial T} \right]_{P,x} = \frac{H^E}{RT} \quad (3-13)$$

$$\left[\frac{\partial (nG^E / RT)}{\partial n_i} \right]_{T,P,n_j} = \ln \gamma_i \quad (3-14)$$

where n_i is the number of moles of component i , the liquid mole fraction, $x_i = \frac{n_i}{\sum_i n_i}$. The

excess Gibbs energy and the activity coefficient can be expressed as:

$$\frac{G^E}{RT} = \sum x_i \ln \gamma_i \quad (3-15)$$

Equation (3-15) can be written in terms of the activity coefficient for a binary mixture:

$$\gamma_1 = \exp \left[\frac{G^E}{RT} + x_2 \frac{d(G^E / RT)}{dx_1} \right] \quad (3-16)$$

$$\gamma_2 = \exp \left[\frac{G^E}{RT} + x_1 \frac{d(G^E / RT)}{dx_1} \right] \quad (3-17)$$

Activity coefficients can be calculated from vapour-liquid equilibrium data since the molar excess Gibbs energy is a function of temperature, pressure and composition. The effect of temperature on the activity coefficient is expressed by the relationship:

$$\left[\frac{\partial(\ln \gamma_i)}{\partial T} \right]_{P, x_j} = -\frac{\bar{H}_i^E}{RT^2} \quad (3-18)$$

where \bar{H}_i^E and \bar{V}_i^E are the mixture partial molar excess enthalpy and excess volume respectively. The effect of pressure on activity coefficients is given by:

$$\left[\frac{\partial(\ln \gamma_i)}{\partial P} \right]_{T, x_j} = -\frac{\bar{V}_i^E}{RT} \quad (3-19)$$

The effect of pressure on activity coefficients is very small at low pressures since \bar{V}_i^E is small.

3.4.1 Activity Coefficients and Gibbs Free Energy

It can be seen that from a full experimental data set of P-T-x-y, both the activity coefficients and the Gibbs free energy can be immediately calculated by Equation (3-8). However, some VLE measurement devices like static cells give only P-T-x data, hence activity coefficients cannot be determined by Equation (3-8). Fortunately, activity coefficients can be calculated from activity coefficient models. Many functional forms of the activity coefficient models and the excess Gibbs energy, G^E , have been developed over the years because none have been able to accurately represent all the type of systems and all types of conditions. The complexity of the equation will depend primarily on the complexity of the system behaviour. Any form of the excess Gibbs energy and activity coefficient model can be used as long as it is accurate and it has the correct pure component limits. For a binary mixture as x_1 and x_2 approach zero, G^E must approach zero, and as x_1 and x_2 approach one, γ_1 and γ_2 should equal one. There are eight well-known correlations of G^E and activity coefficients namely the Margules, van Laar, Wilson, T-K Wilson, NRTL (Non-Random Two Liquid), UNIQUAC (UNiversal QUAsi-Chemical), Scathard-Hildebrand method, and finally the predictive method UNIFAC (UNiquac Functional group Activity Coefficients). These models find extensive use in summarising voluminous VLE data and can be used to extrapolate and interpolate beyond regions in which the data were measured. In this work the Wilson, NRTL and UNIQUAC equations were used to correlate the experimental data of the carboxylic acids. The Scatchard-Hilderbrand, ASOG and UNIFAC methods are used for the prediction of low pressure VLE and will not be further discussed in this work. The reader is referred to Walas (1985), Malanowski and Anderko (1992), and Raal and Mühlbauer (1998) for detailed reviews on these topics.

3.4.1.1 Margules Equation

The Margules equations were originally proposed in 1895. They can be derived from the Redlich-Kister expansion. They still find considerable use, as they are able to correlate VLE data well. The molar Gibbs energy is given by:

$$\frac{G^E}{RT} = x_1 x_2 [A_{12} x_2 + A_{21} x_1] \quad (3-20)$$

The activity coefficients are calculated by:

$$\ln \gamma_1 = [A_{12} + 2(A_{21} - A_{12})x_1]x_2^2 \quad (3-21)$$

$$\ln \gamma_2 = [A_{21} + 2(A_{12} - A_{21})x_2]x_1^2 \quad (3-22)$$

where A_{12} and A_{21} are normally temperature independent constants. The temperature dependence of constants A_{12} and A_{21} can be found by reduction of isothermal data at two or more temperatures. It is suitable for systems with a linear dependence of the G^E/RTx_1x_2 to x_1 plot.

If another term is included it becomes the “four-suffix” Margules equation:

$$\frac{G^E}{RT} = x_1x_2 [A_{12}x_2 + A_{21}x_1 - Cx_1x_2] \quad (3-23)$$

$$\ln \gamma_1 = [A_{12} + 2(A_{21} - A_{12} - C)x_1 + 3Cx_1^2]x_2^2 \quad (3-24)$$

$$\ln \gamma_2 = [A_{21} + 2(A_{12} - A_{21} - C)x_2 + 3Cx_2^2]x_1^2 \quad (3-25)$$

The Margules “four-suffix” equation is superior to its predecessors. This is not surprising as it is a three parameter model unlike the former.

3.4.1.2 Van Laar Equation

Van Laar (1910) proposed the following equations.

$$\frac{G^E}{RT} = x_1x_2 \frac{A_{12}A_{21}}{A_{12}x_1 + A_{21}x_2} \quad (3-26)$$

The activity coefficients implied by this equation are:

$$\ln \gamma_1 = A_{12} \left[1 + \frac{A_{12}x_1}{A_{21}x_2} \right]^{-2} \quad (3-27)$$

$$\ln \gamma_2 = A_{21} \left[1 + \frac{A_{21}x_2}{A_{12}x_1} \right]^{-2} \quad (3-28)$$

The Van Laar equation takes into account the size difference between molecules. It does not however, do well in representing highly non-ideal systems. As a result no attempt was made to use it in this work to correlate the strongly associating carboxylic acids. Its poor performance means that interactions between molecules are not properly characterised. Prausnitz et al. (1986) recommend the use of the Van Laar equation for relatively simple non-polar solutions. The Margules and the Van Laar equations, though quite flexible in composition and widely used in the past, have no sound theoretical basis and are not readily extended to multi-component mixtures (Raal and Mühlbauer [1998]). As mentioned earlier they do not incorporate the explicit temperature dependence of the parameters. They have the merit of simplicity and provide flexibility in fitting VLE data for simple binary systems.

3.4.1.3 Wilson Equation

In 1964, Wilson published a new model, which was based on the concept of local composition. Within a liquid solution, local compositions different from the overall mixture compositions are presumed to account for the short-range order and non-random molecular orientation that results from differences in molecular size and inter molecular forces (Smith and Van Ness [1996]). Wilson (1964) expressed the local composition as volume fractions. The compositions are defined in probabilistic terms by the Boltzmann distribution of energies. This led to the following equations for a binary mixture:

$$\frac{G^E}{RT} = -x_1 \ln[x_1 + x_2 \Lambda_{12}] - x_2 \ln[x_2 + x_1 \Lambda_{21}] \quad (3-29)$$

The corresponding activity coefficient equations are:

$$\ln \gamma_1 = -\ln[x_1 + x_2 \Lambda_{12}] + x_2 \left[\frac{\Lambda_{12}}{x_1 + x_2 \Lambda_{12}} - \frac{\Lambda_{21}}{x_2 + x_1 \Lambda_{21}} \right] \quad (3-30)$$

$$\ln \gamma_2 = -\ln[x_2 + x_1 \Lambda_{21}] - x_1 \left[\frac{\Lambda_{12}}{x_1 + x_2 \Lambda_{12}} - \frac{\Lambda_{21}}{x_2 + x_1 \Lambda_{21}} \right] \quad (3-31)$$

The two adjustable parameters Λ_{12} and Λ_{21} are related to the pure liquid molar volume by:

$$\Lambda_{12} = \frac{V_2}{V_1} \exp \left[-\frac{\lambda_{12} - \lambda_{11}}{RT} \right] \quad (3-32)$$

$$\Lambda_{21} = \frac{V_1}{V_2} \exp \left[-\frac{\lambda_{21} - \lambda_{22}}{RT} \right] \quad (3-33)$$

The parameters $(\lambda_{12} - \lambda_{11})$ and $(\lambda_{21} - \lambda_{22})$ characterise the molecular interactions of the components. The difference between the interaction parameters $(\lambda_{ij} - \lambda_{ji})$, can be found experimentally and no specific values can be assigned to the quantities based on the behaviour of components in a mixture. The Wilson equation often represents VLE data more accurately than the Van Laar and Margules equations. Unlike the Margules and the Van Laar models, the temperature dependence of the Wilson equation is clearly seen. The Wilson equation works well when applied to non-ideal systems. This means that the contributions of local composition is significant and should be accounted to produce accurate forms of the excess Gibbs energy. Raal and Mühlbauer (1998) report that the equation is appreciably superior particularly for polar / non-polar mixtures. Orye and Prausnitz (1965) show the superiority of the Wilson equation over other activity coefficient models for approximately one hundred miscible mixtures of various chemical types. The Wilson equation can be readily generalised to multi-component mixtures without introducing parameters other than for the constituent binaries. The equation has some disadvantages, which are not serious for most applications.

- The equation cannot be used for systems exhibiting a maximum or minimum in the $\ln \gamma$ versus x_1 curves (such as methanol/ cyclohexane). Very few mixtures exhibit this phenomenon.
- The Wilson equation cannot predict liquid immiscibility.

Many modifications of the Wilson equation have been proposed over the years. A well-accepted modification is that given by Tsuboka and Katamaya (1975).

3.4.1.4 T-K Wilson Equation

Tsuboka and Katamaya (1975) proposed a modification of the Wilson (1964) equation. The excess Gibbs energy function and activity coefficient models are:

$$\frac{G^E}{RT} = x_1 \ln \left[\frac{x_1 + V_{12}x_2}{x_1 + \Lambda_{12}x_2} \right] + x_2 \ln \left[\frac{x_2 + V_{21}x_1}{x_2 + x_1\Lambda_{21}} \right] \quad (3-34)$$

$$\ln \gamma_1 = \ln \left[\frac{x_1 + V_{12}x_2}{x_1 + \Lambda_{12}x_2} \right] + [\beta - \beta_v]x_2 \quad (3-35)$$

$$\ln \gamma_2 = \ln \left[\frac{x_2 + V_{21}x_1}{x_2 + \Lambda_{21}x_1} \right] - [\beta - \beta_v]x_1 \quad (3-36)$$

$$\text{where } \beta = \frac{\Lambda_{12}}{x_1 + \Lambda_{12}x_2} - \frac{\Lambda_{21}}{x_2 + \Lambda_{21}x_1}$$

$$\beta_v = \frac{V_{12}}{x_1 + V_{12}x_2} - \frac{V_{21}}{x_2 + V_{21}x_1}$$

$$V_{12} = \frac{V_2}{V_1}$$

$$V_{21} = \frac{V_1}{V_2}$$

V_{ij} are the ratios of the molal volumes. It is interesting to note that when they are unity the Wilson equation results. The parameter Λ_{12} and Λ_{21} are as in the Wilson equation. The modification permits handling of systems with partial liquid miscibility i.e. it can be used for liquid-liquid equilibria or vapour-liquid-liquid equilibria.

3.4.1.5 NRTL (NonRandom Two Liquid) Equation

Renon and Prausnitz (1968) published an improved local composition model, in much the same way as the Wilson equation, but added an additional term to account for non-randomness in the solution. The NRTL equation is applicable to both partially miscible and completely miscible systems. The equation is suitable for highly non-ideal and multi-component systems and hence was used to correlate the carboxylic acids VLE data in this project. It contains limited explicit temperature dependence. The equation has become one of the most useful and widely used equations in phase equilibrium studies (Raal and Mühlbauer [1998]). The Equation for the excess Gibbs energy is:

$$\frac{G^E}{RT} = x_1x_2 \left[\frac{\tau_{21}G_{21}}{x_1 + x_2G_{21}} + \frac{\tau_{12}G_{12}}{x_2 + x_1G_{12}} \right] \quad (3-37)$$

The activity coefficients are given by:

$$\ln \gamma_1 = x_2^2 \left[\tau_{21} \left(\frac{G_{21}}{x_1 + x_2 G_{21}} \right)^2 + \left(\frac{\tau_{12} G_{12}}{(x_2 + x_1 G_{12})^2} \right) \right] \quad (3-38)$$

$$\ln \gamma_2 = x_1^2 \left[\tau_{12} \left(\frac{G_{12}}{x_2 + x_1 G_{12}} \right)^2 + \left(\frac{\tau_{21} G_{21}}{(x_1 + x_2 G_{21})^2} \right) \right] \quad (3-39)$$

$$G_{12} = \exp(-\alpha_{12} \tau_{12})$$

$$G_{21} = \exp(-\alpha_{12} \tau_{21})$$

$$\tau_{12} = \frac{g_{12} - g_{22}}{RT}$$

$$\tau_{21} = \frac{g_{21} - g_{11}}{RT}$$

The parameter $\alpha_{12} = \alpha_{21}$ and is related to the non-randomness of the mixture. Suitable values of α_{12} have been found to range from -1 to 0.5 and a value is often fixed arbitrarily. Walas (1985) recommends values of 0.30 for non-aqueous and 0.40 for aqueous organic mixtures. Gmehling and Onken (1977-1982) have found values greater than unity when they fitted the NRTL parameters. The parameter g_{ji} is an energy parameter, which is characteristic of the interaction between component j and i . The NRTL equation can be extended to handle multi-component mixtures. Some of the disadvantages of the model include increased computer times encountered with the addition of a third parameter and the interdependence of the parameters.

3.4.1.6 UNIQUAC (UNIversal QUAsi-Chemical) Equation

Abrams and Prausnitz (1975) published a model for the excess Gibbs energy, which extended the quasi-chemical lattice theory of Guggenheim. The basis of the model is that a liquid can be represented by a three dimensional lattice, with each lattice site occupied by a segment of a molecule. Abrams and Prausnitz used local surface area fraction in the derivation of the UNIQUAC model. The Wilson and NRTL models use a local volume fraction in the development of their expressions for the excess Gibbs energy. In the UNIQUAC equation, the excess Gibbs energy is considered to be made of two parts, a combinatorial part due to

molecular size and shape, G_{Comb}^E , and a residual part primarily for intermolecular energy interactions, G_{Res}^R .

$$G^E = G_{comb}^E + G_{res}^E \quad (3-40)$$

$$\frac{G_{comb}^E}{RT} = x_1 \ln \frac{\Phi_1}{x_1} + x_2 \ln \frac{\Phi_2}{x_2} + \frac{z}{2} \left[q_1 x_1 \ln \frac{\theta_1}{\Phi_1} + q_2 x_2 \ln \frac{\theta_2}{\Phi_2} \right] \quad (3-41)$$

$$\frac{G_{res}^E}{RT} = -q_1' x_1 \ln [\theta_1' + \theta_2' \tau_{21}] - q_2' x_2 \ln [\theta_2' + \theta_1' \tau_{12}] \quad (3-42)$$

The co-ordination number, z , is set equal to 10. The segment fraction, Φ_i and the area fraction θ_i and θ_i' are given by:

$$\Phi_1 = \frac{x_1 r_1}{x_1 r_1 + x_2 r_2} \quad \Phi_2 = \frac{x_2 r_2}{x_1 r_1 + x_2 r_2} \quad (3-43)$$

$$\theta_1 = \frac{x_1 q_1}{x_1 q_1 + x_2 q_2} \quad \theta_2 = \frac{x_2 q_2}{x_1 q_1 + x_2 q_2} \quad (3-44)$$

$$\theta_1' = \frac{x_1 q_1'}{x_1 q_1' + x_2 q_2'} \quad \theta_2' = \frac{x_2 q_2'}{x_1 q_1' + x_2 q_2'} \quad (3-45)$$

The parameters, r , q and q' are pure component molecular constants with r being a size parameter and q , an area parameter. As can be seen θ' is a function of q' whereas θ is a function of function of q . The parameter q' has special values for water and alcohols. Tabulation of some of these r and q values can be found in Raal and Mühlbauer (1998). Abrams and Prausnitz (1975) defined these area and size parameters as:

$$r_i = \frac{V_{wi}}{1.517 * 10^{-2}} \quad (3-46)$$

$$q_i = \frac{A_{wi}}{2.5 * 10^8} \quad (3-47)$$

where V_{wi} (m^3/kmol) and A_{wi} (m^2/kmol) are the van der Waals volume and area as calculated by the method of Bondi (1968). V_{wi} and A_{wi} values for some molecules are available in the data compilation by Daubert and Danner (1989). Fortunately, r and q values for a large number of compounds were available from DECHEMA.

$$\tau_{12} = \exp\left[\frac{-u_{12} - u_{22}}{RT}\right] \quad (3-48)$$

$$\tau_{21} = \exp\left[\frac{-u_{21} - u_{11}}{RT}\right] \quad (3-49)$$

The two adjustable parameters τ_{12} and τ_{21} are expressed in terms of the characteristic energies ($u_{12} - u_{22}$) and ($u_{21} - u_{11}$). The activity coefficients are given by:

$$\ln \hat{\gamma}_i = \ln \gamma_i^{comb} + \ln \gamma_i^{res} \quad (3-50)$$

$$\ln \gamma_i^{comb} = \ln \frac{\Phi_i}{x_i} + \frac{z}{2} q_i \ln \frac{\theta_i}{\Phi_i} + \Phi_j \left[l_i - \frac{r_i}{r_j} l_j \right] \quad (3-51)$$

$$\ln \gamma_i^{res} = -q_i \ln \left[\theta_i + \theta_j \tau_{ji} \right] + \theta_i q_i \left[\frac{\tau_{ji}}{\theta_i + \theta_j \tau_{ji}} - \frac{\tau_{ij}}{\theta_j + \theta_i \tau_{ij}} \right] \quad (3-52)$$

$$l_i = \frac{z}{2} [r_i - q_i] - [r_i - 1] \quad (3-53)$$

This equation finds great use and is able to characterise many systems (Prausnitz [1986]). It can be applied to multi-component mixtures. Its main draw back is its complexity and the need for r and q values.

3.4.1.7 UNIFAC

The UNIFAC method is a further development based on the UNIQUAC equation. Activity coefficients are calculated from group contributions of the various groups making up the molecules of a solution. For a detailed review on the method, the reader is referred to Fredenslund et al. (1975) Smith and van Ness (1986) and Raal and Mühlbauer (1998).

3.4.2 Activity Coefficients Models Incorporating Chemical Theory

3.4.2.1 Non-polar and an Associating Component

Chemical theory of solution behaviour was first developed by Dolezalek (1903). At about the same time Van Laar was progressively working on developing his work on solutions. The following treatment, proposed by Prausnitz (1969) can be used to calculate the activity coefficient of a binary mixture of non-polar and polar associating components. In the treatment A is the non-polar substance and B is the polar associating substance, in our case the acid that dimerises. The correlation cannot be used for a binary mixture of two associating substances such as those measured in this project. The equation describing the chemical equilibrium relationship of the associating substance is:



The equilibrium constant for the dimerisation is given by:

$$K = \frac{a_{B_2}}{a_B^2} \quad (3-55)$$

where a_B is the activity of monomer B molecules and a_{B_2} is the activity of dimer B_2 molecules. The system is assumed to be in equilibrium and that the three species A, B, and B_2 are in equilibrium with one another. For an ideal solution the activity can be replaced by the mole fractions. The equilibrium constant becomes:

$$K = \frac{z_{B_2}}{z_B^2} \quad (3-56)$$

where z stands for the "true" mole fraction. If there are n_1 moles of A and n_2 moles of B then

$$n_1 = n_A \quad (3-57)$$

$$n_2 = n_B + 2n_{B_2} \quad (3-58)$$

where n_B is the number of moles of monomer B and n_{B_2} is the number of moles of dimer B_2 .

The "true" total number of moles is:

$$n_A + n_B + n_{B_2} \quad (3-59)$$

$$= n_1 + n_2 - n_{B_2} \quad (3-60)$$

$$z_A = \frac{n_1}{n_1 + n_2 - n_{B_2}} \quad (3-61)$$

$$z_B = \frac{n_B}{n_1 + n_2 - n_{B_2}} = \frac{n_2 - 2n_{B_2}}{n_1 + n_2 - n_{B_2}} \quad (3-62)$$

$$z_{B_2} = \frac{n_{B_2}}{n_1 + n_2 - n_{B_2}} \quad (3-63)$$

The equilibrium constant K , is related to α by (Prausnitz et al. [1980]):

$$K = \frac{(\alpha/2)[1-(\alpha/2)]}{(1-\alpha)^2 P} \quad (3-64)$$

α is the fraction of moles that dimerise and is a function of the component that associates as discussed in Section 3.5.1. By combining Equation (3-64) with Equations (3-62) and (3-63) and eliminating n_{B_2} with Equation (3-61) an expression to solve for z_A is obtained and from this we can obtain the activity coefficient of component A .

$$x_1 = \frac{n_1}{n_1 + n_2} \quad (3-65)$$

$$x_2 = \frac{n_2}{n_1 + n_2} \quad (3-66)$$

$$\gamma_1 = \frac{a_1}{x_1} = \frac{2k}{(2k-1)x_1 + kx_2 + (x_1^2 + 2kx_1x_2 + kx_2^2)^{1/2}} \quad (3-67)$$

where $k \equiv 4K + 1$. By similar stoichiometric considerations the activity coefficient for the dimerised component can be shown to be:

$$\gamma_2 = \frac{a_2}{x_2} = \left(\frac{k^{1/2} + 1}{x_2}\right) \left[\frac{-x_1 + (x_1^2 + 2kx_1x_2 + kx_2^2)^{1/2}}{(2k-1)x_1 + kx_2 + (x_1^2 + 2kx_1x_2 + kx_2^2)^{1/2}}\right] \quad (3-68)$$

It can be seen that it is a property of both equations for all $K > 0$, positive deviation from Raoult's law results: thus $\gamma_A \geq 1$ and $\gamma_B \geq 1$. For $K = \infty$, all molecules of component B are dimerised and in that limiting case we have:

$$\lim_{K \rightarrow \infty} \gamma_A = \frac{1}{x_1 + (x_2/2)} \quad (3-69)$$

$$\lim_{K \rightarrow \infty} \gamma_B = \frac{1}{(2x_1x_2 + x_2^2)^{1/2}} \quad (3-70)$$

and at infinite dilution:

$$\lim_{K \rightarrow \infty, x_1 \rightarrow 0} \gamma_A = 2$$

$$\lim_{K \rightarrow \infty, x_2 \rightarrow 0} \gamma_B = \infty$$

The treatment of polar organic components that form high chains (trimers, tetramers etc.) will not be dealt with here. Prausnitz (1969) and Malanowski (1992) devote part of their chemical theory chapters to these high chain polymers. It must be noted though that treatment for higher chain oligomers results in many equilibrium constants forming many equations, which become complex to solve.

3.4.2.2 Activity Coefficient Model for Cross-Association

The chemical theory describing the association between two different species of associating substances is as detailed below. This model does not assume self-association of the species in the solution. This is not true for carboxylic acids. However many authors (Malijevska et al. [1984] Prausnitz et al. [1980], Kato et al. [1989], and Klekers et al. [1968]) concur that mainly cross association dimers are formed in the binary mixtures of carboxylic acids. We shall include this chemical treatment on that basis. The equation describing the chemical equilibrium relationship is:



The equilibrium constant K , is related to the activities of the species by:

$$K = \frac{a_{AB}}{a_A a_B} \quad (3-72)$$

If the solution is formed from N_1 moles and N_2 moles of A and B respectively and at equilibrium there are N_{AB} of the dimer complexes then the "true" mole fraction z of A , B & AB are:

$$z_A = \frac{N_1 - N_{AB}}{N_1 + N_2 - N_{AB}} \quad (3-73)$$

$$z_B = \frac{N_2 - N_{AB}}{N_1 + N_2 - N_{AB}} \quad (3-74)$$

$$z_{AB} = \frac{N_{AB}}{N_1 + N_2 - N_{AB}} \quad (3-75)$$

Taking the Dolezalek assumption that the true species form an ideal solution, therefore the activity of each species is equal to its true mole fraction. The apparent mole fractions of the two components x_1 and x_2 are given by:

$$x_1 = \frac{N_1}{N_1 + N_2} \quad (3-76)$$

$$x_2 = \frac{N_2}{N_1 + N_2} \quad (3-77)$$

The activity coefficient is given by:

$$\gamma_1 = \frac{a_A}{x_1} = \frac{kx_1 - 2 + 2(1 - kx_1x_2)^{1/2}}{kx_1^2} \quad (3-78)$$

$$\gamma_2 = \frac{a_B}{x_2} = \frac{kx_2 - 2 + 2(1 - kx_1x_2)^{1/2}}{kx_2^2} \quad (3-79)$$

where $k = \frac{4K}{K+1}$

3.4.3 Activity Coefficients at Infinite Dilution

The derivative of the Gibbs excess energy, Equation (3-15), with respect to x_1 is:

$$\frac{d\left(G^E/RT\right)}{dx_1} = x_1 \frac{d \ln \gamma_1}{dx_1} + \ln \gamma_1 + x_2 \frac{d \ln \gamma_2}{dx_2} - \ln \gamma_2 \quad (3-80)$$

Combining Equation (3-80) and the Gibbs-Duhem equation (Section 3.8) gives:

$$\frac{d\left(G^E/RT\right)}{dx_1} = \ln \frac{\gamma_1}{\gamma_2} \quad (3-81)$$

In the limit as $x_1 \rightarrow 0$ ($x_2 \rightarrow 1$) this becomes:

$$\lim_{x_1 \rightarrow 0} \frac{d\left(G^E/RT\right)}{dx_1} = \lim_{x_1 \rightarrow 0} \ln \frac{\gamma_1}{\gamma_2} = \ln \gamma_1^\infty \quad (3-82)$$

where γ_1^∞ is the activity coefficient at infinite dilution for component (1). Similarly as $x_1 \rightarrow 1$ ($x_2 \rightarrow 0$)

$$\lim_{x_1 \rightarrow 1} \ln \frac{\gamma_1}{\gamma_2} = \ln \gamma_2^\infty \quad (3-83)$$

As the mole fraction of component one approaches zero in solution, its activity coefficient approaches a definite limit. The limiting value is termed the “infinite dilution activity coefficient”. Infinite dilution activity coefficients are of considerable practical and theoretical interest in the design and performance of separation facilities as they operate in the dilute regions. Experimental infinite dilution activity coefficients can be used to predict activity coefficients over the entire range of the composition. Several experimental methods can be used to determine infinite dilution activity coefficients.

- Ebulliometry
- Gas Chromatography
- Differential static methods
- Inert gas stripping
- Raleigh distillation

Raal and Mühlbauer (1998) devote a chapter to these experimental methods. Group contribution methods can also be used to estimate infinite dilution activity coefficients. A review of group contribution methods is given by Fredenslund and Sorensen (1994) and by Gmehling (1998).

3.5 Gas Phase Non-ideality

3.5.1 Chemical Theory

Gas mixtures at low atmospheric pressure behave as an ideal gas. According to Dolezalek (1908), a binary mixture of strongly associating compounds is a multi-component mixture. From Le Chatelier's principle the formation of complexes by weak association or solvation can be shown to be negligible at low pressure. As the pressure rises, large deviations from ideal behaviour are noted. Chemical theory has been shown by many authors to be particularly useful when applied to systems containing one associating substance and inert solvents. In this case the chemical approach has made it possible to obtain an accurate representation of phase equilibria with a number of physically meaningful parameters. Various equilibria may be postulated for a pure gas consisting of component A that associates (e.g. formic acid).



Quantitative analysis of the behaviour of associating mixtures requires equilibrium constants for each of the assumed association equilibria. The equilibrium constant K , for dimerisation reflects the interactions of the two molecules at a time. A relation can be established between the dimerisation equilibrium constant and the second virial coefficient. Similarly the trimerisation equilibrium constant is related to the third virial coefficient and so on. Polymerisation reactions (dimerisation, trimerisation, etc.) result in negative deviations ($Z < 1$) from ideal gas behaviour. Dissociation reactions (important to high temperature equilibrium studies), result in positive deviations ($Z > 1$) from ideal gas behaviour. As stated previously there is strong hydrogen bonding in organic acids, which results in polymerisation. The equilibrium constant K , can be written in terms of the partial pressures rather than fugacities. For the above statement to be true we assume that the mixture is of true species (monomers and dimers) that all behave as an ideal gas.

$$K = \frac{P_{A_2}}{P_A^2} \quad (3-85)$$

$$K = \frac{y_{A_2}}{y_A^2 P} \quad (3-86)$$

where P is the total pressure, y_A is the mole fraction of monomer and y_{A_2} is the mole fraction of the dimer. The equilibrium constant can be calculated from P - V - T data as proposed by Prausnitz et al. (1980). Let v be the volume of one mole of carboxylic acid at total pressure P and temperature T . One mole in this connection means the formula weight of the monomeric acid. Let n_A be the number of moles of dimer; let α be the fraction of molecules which dimerise and n_T be the total number of 'true' moles.

$$n_T = n_A + n_{A_2} \quad (3-87)$$

$$= (1-\alpha) + \frac{\alpha}{2} = 1 - \frac{\alpha}{2} \quad (3-88)$$

We know that:

$$Pv = n_T RT \quad (3-89)$$

One can compute α by substituting and manipulating Equation (3-89).

$$\alpha = 2 - \frac{2Pv}{RT} \quad (3-90)$$

since

$$y_A = \frac{n_A}{n_T} \quad (3-91)$$

$$y_{A_2} = \frac{n_{A_2}}{n_T} \quad (3-92)$$

The equilibrium constant K , is related to α by (Prausnitz et al. [1980]):

$$K = \frac{(\alpha/2)[1-(\alpha/2)]}{(1-\alpha)^2 P} \quad (3-93)$$

If one analyses Equation (3-93), we can see that α must approach zero as P approaches zero. In other words dimerisation decreases as the pressure is lowered. Because of the strong dimerisation in the vapour phase, the fugacity of a pre-saturated carboxylic acid is considerably lower than its saturation (vapour) pressure even when that pressure is small (Prausnitz [1969]). The fugacity coefficient of a carboxylic acid in a gaseous mixture is not close to unity even at low pressures.

Cross dimerisation occurs in a binary mixture of carboxylic acids. Two different low chain carboxylic acids form dimers according to the following equation.



The equilibrium constant for the dimer is given by:

$$K_{AB} = 2\sqrt{K_{A_2} K_{B_2}} \quad (3-95)$$

3.5.2 Hayden and O'Connell (1975) Correlation

The Hayden and O'Connell (1975) correlation was used to calculate the second virial coefficients of equations of state for the carboxylic acids, which were then used to calculate the ratio of the fugacity coefficients, Φ_i , using the virial equation of state Equation (3-116). Hayden and O'Connell (1975) published a well-accepted method for calculating second virial coefficients for a large range of compounds. Their method finds merit in that it can be used for both polar and non-polar chemicals. The correlation requires the critical temperature, T_c , and critical Pressure, P_c , Thompson's mean radius of gyration, Rd , the parachor, P' dipole moment, μ , and if appropriate, a parameter to describe chemical association, η . The contribution to the second virial coefficient is considered to be the sum of three interactions.

$$B_{total} = B_{free} + B_{metastable} + B_{bound} \quad (3-96)$$

where B_{free} is the interaction from free pairs, $B_{metastable}$ is the contribution from molecular interactions that are metastably bound, and B_{bound} is the contribution in strongly non-ideal systems that associate. In their derivation of the correlation, the physics and behaviour of interacting molecules is considered. The derivation is lengthy and the reader is referred to the paper by Hayden and O'Connell (1975) and Appendix A of Prausnitz et al. (1980).

As mentioned earlier, the calculation requires many pure component parameters. The parameters used in this work were obtained from literature sources such as Reid et al. (1988), Prausnitz et al. (1980) and the Dortmund data bank (DDB). The bond addition method of Smyth (1955) was used to calculate the dipole moment for some of the components. The mean radius of gyration was calculated from by group contribution method of Reid et al. (1977) as no values were available in literature. The Rackett (1970) equation was used to calculate the liquid molar volume.

$$V_i = V_{ci} Z_{ci}^{(1-T_r)^{0.2857}} \quad (3-97)$$

where V_{ci} is the critical molar volume of species i and Z_{ci} is the critical compressibility factor. The procedure to calculate the mean radius of gyration Rd is such that you determine the parachor P' using the group contribution method. The parachor is related to the mean radius of gyration by the equation:

$$P' = 50 + 7.6Rd + 13.75Rd^2 \quad (3-98)$$

Solving this quadratic equation for Rd will give two roots of which the positive root is the real value for Rd . No association or solvation parameters could be found in literature. Prausnitz et al. (1980) suggested that if the exact values of the component in question cannot be found, then the values for chemically similar components should be used. The value for propionic acid was used in this work. The input parameters are in Appendix B.

3.5.3 Pitzer-Curl Correlation

The Pitzer-Curl correlation was used to characterise the vapour phase behaviour non-idealities. It is a relatively simple correlation that can yield good results for simple systems. Pitzer and Curl (1957) developed a new correlation for Z , the compressibility factor.

$$Z = Z^0 + \omega Z^1 \quad (3-99)$$

where Z^0 and Z^1 are functions of T_r and P_r and ω is the acentric factor. The use of the Equation (3-99) has a major disadvantage in that the complexity of Z^0 and Z^1 cannot be represented by simple equations. However, analytical approximations have been proposed over limited pressure ranges. The simplest representation is in the form of the virial equation

$$Z = 1 + \frac{BP}{RT} = 1 + \left(\frac{BP_c}{RT_c} \right) \frac{P_r}{T_r} \quad (3-100)$$

Pitzer and coworkers (1957) proposed a correlation for the quantity BP_c/RT_c :

$$\frac{BP_c}{RT_c} = B^0 + \omega B^1 \quad (3-101)$$

The values of B^0 and B^1 are functions of reduced temperature only and can be calculated by:

$$B^0 = 0.083 - \frac{0.422}{T_r^{1.6}} \quad (3-102)$$

$$B^1 = 0.139 - \frac{0.172}{T_r^{4.2}} \quad (3-103)$$

Equation (3-101) is used to calculate the second virial coefficient. Mixing rules have been proposed to calculate the cross coefficients and parameters. Prausnitz et al. (1986) propose:

$$B_{ij} = \frac{RT_{cij}}{P_{cij}} (B^0 + \omega B^1) \quad (3-104)$$

$$T_{cij} = \sqrt{T_{ci} T_{cj}} (1 - k_{ij}) \quad (3-105)$$

$$P_{cij} = \frac{Z_{ci} RT_{cij}}{V_{cij}} \quad (3-106)$$

$$Z_{cij} = \frac{Z_{ci} + Z_{cj}}{2} \quad (3-107)$$

$$V_{cij} = \left(\frac{V_{ci}^{1/3} + V_{cj}^{1/3}}{2} \right)^3 \quad (3-108)$$

$$\omega_{ij} = \frac{\omega_i + \omega_j}{2} \quad (3-109)$$

where k_{ij} is an empirical interaction parameter that is specific for molecular pairing i - j . Generally for chemically similar species k_{ij} is set equal to zero.

3.6 Equations of State

An equation of state (EOS) is a mathematical relationship describing the inter-connection between various macroscopically measurable properties of a system. A great variety of thermodynamic properties can be computed for pure substances and mixtures if the P-V-T relations, i.e., equations of state, are known. In this section a review of equation of state methods for modelling phase equilibria will be discussed focusing on the more relevant ones to this study of carboxylic acids. As discussed in Section (3.2), phases at the same temperature and pressure are in equilibrium when the fugacity of each of the species is the same in all the phases.

$$\hat{f}_i^v = \hat{f}_i^l \quad (i = 1, 2, \dots, N) \quad (3-4)$$

The alternative form of Equation (3-4) is:

$$y_i P \hat{\phi}_i^v = x_i P \hat{\phi}_i^l \quad (3-110)$$

$$y_i \hat{\phi}_i^v = x_i \hat{\phi}_i^l \quad (i = 1, 2, \dots, N) \quad (3-111)$$

where $\hat{\phi}_i^v$ and $\hat{\phi}_i^l$ are the fugacity coefficient expressing the vapour and liquid phase non-idealities respectively. Fugacity coefficients can be readily calculated from equations of state. The derivation for the fugacity coefficient from the Gibbs residual function is lengthy and shall not be discussed here. Malanowski and Anderko (1992) and Smith and Van Ness (1997) present the derivation in detail. The final expression for the fugacity coefficient with respect to Z , the compressibility factor and V , the volume is given by:

$$\ln \hat{\phi}_i = - \int_{\infty}^V \left[\left(\frac{\partial(nZ)}{\partial n_i} \right)_{T,n,V,n_j} - 1 \right] \frac{dV}{V} - \ln Z \quad (3-112)$$

$\ln Z$ and the derivative are evaluated from an equation of state. From a thermodynamic point of view, the equation of state method is more general and comprehensive than the gamma-phi method (Malanowski and Anderko [1992]).

Equations of state were originally used to compute thermodynamic properties for pure components only. Applications to mixtures were virtually limited to non-polar and slightly polar compounds. EOS were not able to characterize the behaviour of strongly polar and hydrogen bonding systems until the 1970's. Multitudes of papers have been published over the last three decades on EOS models applicable to systems containing strongly polar and hydrogen bonding components. Limited success has been achieved in this area, although recently rapid progress is being made to apply suitable EOS to these substances, (Hans et al. [1988]).

3.6.1 Virial Equation of State

Fugacity coefficients (Section 3.2) can be evaluated from the virial equation of state truncated after the second term. Its use however, is only practical where the convergence is rapid and where no more than two or three terms are required to yield reasonably close approximations to the true values in the series. Gases and vapours at low pressures have been successfully correlated using the virial equation of state. The preferred truncated form of the virial equation of state is:

$$Z = \frac{PV}{RT} = 1 + \frac{BP}{RT} \quad (3-113)$$

where Z is the compressibility factor and B is the second virial coefficient, which is a function of temperature and composition for multi-component mixtures. For pure components the second virial coefficient is a function of temperature only. The composition dependence of the second virial coefficient is given by:

$$B = \sum_i \sum_j y_i y_j B_{ij} \quad (3-114)$$

where y_i are the mole fractions in the gas mixture. The indices i and j identify the species in the mixture. The virial coefficient B_{ij} depicts the bimolecular interactions between species i and j . One can therefore note that $B_{ij} = B_{ji}$. The second virial coefficient for a binary mixture may thus be written (Van Ness [1996]):

$$B = y_1 B_{11} + y_2 B_{22} + y_1 y_2 \delta_{12} \quad (3-115)$$

where $\delta_{12} \equiv 2B_{12} - B_{11} - B_{22}$

Equation (3-9) can be written as:

$$\Phi_i = \exp\left[\frac{(B_{ii} - V_i^l)(P - P_i^{sat}) + P y_i^2 \delta_{ij}}{RT}\right] \quad (3-116)$$

There are several correlations that have been proposed for the calculation of the second virial coefficient such as that of Tsonopoulos (1974) and Hayden & O'Connell (1975). In this work we will review the correlation of Hayden & O'Connell (Section 3.5.2) as it is used in the regression of the experimental VLE data measured in this project. Dymond & Smith (1980) have a compilation of some experimentally determined second virial coefficients for pure components and mixtures.

3.6.2 Van der Waals Equation (1873)

The first equation of state that reasonably represented both the gas and liquid phases was proposed by Van der Waals in 1873. Van der Waals based his derivation from Clausius (1873) who argued that the deviations of gases from Boyle's law (1660) were caused by intermolecular attractions and repulsions. In the derivation of the equation, Van der Waals represented the intermolecular attractions with a constant, a , and the repulsions with a constant, b . The Van der Waals equation is a sum of two terms as follows:

$$P = \frac{RT}{V-b} - \frac{a}{V^2} \quad (3-117)$$

It is interesting to note that the van der Waals equation reduces to the ideal gas equation in the infinite volume region. The constants a and b are valid for both the gas and liquid phases. The equation is able to predict the vapour-liquid critical points. However, the equation suffers in that liquid phase P-V-T properties are reproduced much less satisfactorily than those in the gas phase. Berthelot (1899) introduced a temperature dependent a constant $a_T = \frac{a}{T}$. The cubic equations that were to follow from there on resembled that of van der Waals in that they have a repulsive term z_{rep} , and an attractive term z_{attr} .

$$Z = Z_{rep} + Z_{attr} \quad (3-118)$$

Some features and applications of the more recent cubic equations of state have been reviewed by Vidal (1984), Tsonopoulos and Heidman (1986) and Raal and Mühlbauer (1998).

3.6.3 Redlich-Kwong (1949) Equation

Redlich and Kwong (1949) proposed a well-accepted cubic equation of state used for routine engineering calculations of fugacity. In the derivation, Redlich and Kwong (1949) wanted to satisfy the boundary conditions in the low and high-density limit.

$$P = \frac{RT}{V-b} - \frac{a}{T^{1/2}V(V+b)} \quad (3-119)$$

The temperature dependence of the parameter, a , is essential for the reproduction of vapour pressures. Wilson (1964) proposed a general form for the temperature dependence of a , for both the vapour and liquid phases.

$$a = a_c \alpha \quad (3-120)$$

$$\alpha = T_r \left[1 + (1.57 + 1.62\omega)(T_r^{-1}) \right] \quad (3-121)$$

where a_c is the value of a , at the critical point. $T_r = T/T_c$. The Redlich Kwong EOS is adequate for calculation of gas phase properties when the ratio of pressure to the critical pressure is less than about one-half of the temperature at the critical temperature (Malanowski and Anderko [1992]).

In 1972 Soave proposed a simple and accurate function for the α function:

$$\alpha = \left[1 + m T_r^{1/2} \right]^2 \quad (3-122)$$

where m is a quadratic expression for the acentric factor, ω . Soave (1972) obtained Equation (3-122) by forcing the equation to reproduce vapour pressures for non-polar substances at $T_r = 0.7$. Many investigators used Soave's function to develop equations of state of their own, among others Peng and Robinson (1976), Schmidt and Wenzel (1980), Patel and Teja (1987), Adachi et al. (1983) and Watson et al. (1986).

Soave (1984) proposed a new two-parameter equation for the α function:

$$\alpha = 1 + m(1 + T_r) + n(T_r^{-1} - 1) \quad (3-123)$$

Stryjek and Vera (1986) proposed a one parameter equation for the α function.

$$\alpha = \left\{ 1 + \left[k_0(\omega) + k_1(1 + T_r^{1/2})(0.7 - T_r) \right] (1 - T_r^{1/2}) \right\}^2 \quad (3-124)$$

where $k_0 = 0.378893 + 1.4897153\omega - 0.17131848\omega^2 + 0.0196554\omega^3$ and k_1 is an adjustable parameter characteristic of each pure component.

The original Redlich-Kwong EOS is rarely satisfactory for VLE calculation (Smith and Van Ness [1997]). Hence the Redlich-Kwong EOS was not used to regress the carboxylic acids VLE data. The more widely used cubic EOS for VLE calculations are the Soave Redlich Kwong (SRK) and the Peng Robinson (PR) equation.

3.6.4 Peng-Robinson (1976) Equation

Peng and Robinson (1976) proposed a cubic equation of the form:

$$P = \frac{RT}{V-b} - \frac{a(T)}{V(V+b)+b(V-b)} \quad (3-125)$$

The equation improved the representation of the liquid density as compared to that of Soave. The equation is able to accurately calculate vapour pressures and equilibrium ratios especially of non-polar components. Peng and Robinson (1976) wanted to satisfy the following in the equation of state:

1. The parameters should be expressible in terms of the critical properties and the acentric factor.
2. The model should provide reasonable accuracy near the critical point, particularly for the calculations of the compressibility factor and liquid density.
3. The mixing rules should not employ more than a single binary interaction parameter, which should be independent of temperature, pressure and composition.
4. The equation should be applicable to all calculations of all fluid properties in natural gas processes.

The Peng-Robinson equation was chosen to regress the carboxylic acids data because of the above mentioned superiority.

The Peng-Robinson equation can also be written as:

$$P = \frac{RT}{V-b} - \frac{a(T)}{(V+\epsilon b)(V-\sigma b)} \quad (3-126)$$

The parameter, a , is related to the intermolecular forces and is temperature dependent. The parameter b is related to molecular size and is temperature independent. The values for ϵ and σ are given by, $\epsilon = 1 - \sqrt{2}$ and $\sigma = 1 + \sqrt{2}$.

The above equation can be written as:

$$Z^3 - (1-B)Z^2 + (A-3B^2-2B)Z - (AB-B^2-B^3) = 0 \quad (3-127)$$

where Z is the compressibility factor,

$$A = \frac{aP}{R^2T^2} \quad B = \frac{bP}{RT} \quad (3-128)$$

The above cubic equation can be solved for Z yielding one or three roots depending on the number of phases in the systems. For a two-phase system, the largest root is for the compressibility factor of the vapour while the smallest positive root corresponds to that of the liquid (Peng and Robinson [1976]). The temperature dependent parameter a , can be determined by:

$$a(T) = a(T_c) \alpha(T_r, \omega) \quad (3-129)$$

$$a(T_c) = \frac{0.45724R^2T_c^2}{P_c} \quad (3-130)$$

$$\alpha(T_r, \omega) = \left[1 + k(1 - T_r^{1/2}) \right]^2 \quad (3-131)$$

where the parameter k is a constant characteristic of each species given by:
 $k = 0,37464 + 0,154226\omega - 0,26992\omega^2$.

The parameter b is given by: $b(T) = b(T_c)$

$$b(T_c) = \frac{0.07780RT_c}{P_c} \quad (3-132)$$

For a mixture, the parameters a , and b are related to a_i and b_i by mixing rules (Peng and Robinson [1976]). The fugacity coefficient of species i , in a mixture can be determined by:

$$\ln \hat{\phi}_i = \frac{b_i}{b}(Z-1) - \ln(Z-B) - \frac{A}{2\sqrt{2}B} \left(\frac{Z \sum_i x_i a_{ij}}{a} - \frac{b_i}{b} \right) \ln \left(\frac{Z+2.414B}{Z-0.414B} \right) \quad (3-133)$$

Peng and Robinson (1976) proposed the mixing rules:

$$a = \sum_i \sum_j x_i x_j a_{ij} = x_1 x_1 a_{11} + 2x_1 x_2 a_{12} + x_2 x_2 a_{22} \quad (3-134)$$

$$b = \sum_i x_i b_i \quad (3-135)$$

$$a_{ij} = (1 - \delta_{ij}) \sqrt{a_i a_j} \quad \delta_{ij} = \delta_{ji} \quad (3-136)$$

The parameter δ_{ij} is unique for each binary system and is determined by means of regression. Many mixing rules have been proposed over the years and a brief summary is given in Section (3.7).

3.6.5 Equation Of State for Carboxylic Acids (Twu & Coon, [1993])

Twu and co-workers (1993) proposed a cubic equation of state to specifically handle carboxylic acids, taking association into account. The equation however, can only handle a mixture with only one associating substance. Twu et al. (1993) incorporated chemical theory into the cubic equation of state following the approach by Heidemann and Prausnitz (1976). In the equation, a monomer and dimer chemical equilibrium is built into the cubic EOS. The incorporation of chemical theory into the cubic equation of state requires that the chemical equilibrium constant and the monomer parameter be specified. In their derivation Twu and co-workers used a generic two parameter cubic equation:

$$P = \frac{n_T RT}{V - n_T b} - \frac{n_T^2 a(T)}{V^2 + u n_T b V + w n_T^2 b^2} \quad (3-137)$$

n_T is the total number of moles. The constants u and w are integers. It is interesting to note that by taking $n_T = 1$, $u = \epsilon + \sigma$, and $w = \epsilon \sigma$, Equation (3-137) reverts to the Peng-Robinson

equation. The total number of moles n_T is not a constant because, for an associating fluid, it depends on the temperature and density. In this case, the associating carboxylic acid is considered to be made up of monomers and dimers. Twu and co-workers propose the use of the classic quadratic mixing rule for the constants a and b .

$$a = \sum_i \sum_j z_i z_j (a_i a_j)^{1/2} \quad (3-138)$$

$$b = \sum z_i b_i \quad (3-139)$$

z_i is the mole fraction of the species i (monomer and dimer) in the mixture. Heidemann and Prausnitz (1976) assumed for "i-mers"

$$a_i = i^2 a_1 \quad \text{and} \quad b_i = i b_1$$

where 1 and i refer to the monomer and i -mer, respectively. They derived the following mixing rule for a pure fluid, $a = \left(\frac{n_o}{n_T}\right) a_1$ and $b = \left(\frac{n_o}{n_T}\right) b_1$

where n_o is the number of moles that would exist in the absence of association. n_T is the total number of moles of monomer and dimer.

$$\frac{1}{n_r} = \frac{n_o}{n_T} = \sum_i i z_i \quad (3-140)$$

The term, n_r , is the extent of association. By substituting Equation (3-140) into the cubic EOS incorporating association gives:

$$P = n_r \frac{RT}{V - b} - \frac{a(T)}{V^2 + ubV + wb^2} \quad (3-141)$$

$$\text{where } n_r = \frac{n_T}{n_o} \quad \text{and} \quad V = \frac{V}{n_o}$$

It can be seen that the term n_r is the only contribution to association. It is 1.0 when there is no association and approaches 0.5 when there is complete dimerisation. Interestingly, when $n_r = 1.0$, the associating cubic EOS reverts to the Peng-Robinson equation of state. The associating equilibrium constant K is given by Prausnitz et al. (1986):

$$K = \frac{\phi_2}{\phi_1} \frac{z_2}{z_1} \frac{1}{p} \quad (3-142)$$

where ϕ is the fugacity coefficient of the true species (monomer and dimer) and z is the true mole fraction. The equilibrium constant is a function of temperature.

$$K = A + \frac{B}{T} \quad (3-143)$$

where A and B are constants specific to each associating species and are available from DECHEMA.

$$\frac{1}{n_r} = \frac{2(K^* - 1)}{4K^* - 1 - (1 + 8K^*)^{1/2}} \quad (3-144)$$

where $K^* = K \frac{RT}{V - b}$ and is the reduced equilibrium constant.

The fugacity coefficient for the EOS incorporating chemical association is calculated by:

$$\ln \phi = \ln(z_1 n_r) + (Z - n_r) - \ln(Z - b^*) - \frac{a^*}{b^*} \ln\left(1 + \frac{b^*}{Z}\right) \quad (3-145)$$

In the derivation Twu and co-workers (1993) set $u = 1$ and $w = 0$ in Equation (3-137) hence effectively using the Redlich-Kwong EOS. z_1 is the true mole fraction. Z is the compressibility factor without reference to the state of association and is a solution of the non-cubic equation

$$Z^3 - n_r Z^2 + (a^* - n_r b^* - b^{*2})Z - a^* b^* = 0 \quad (3-146)$$

where $a^* = \frac{aP}{R^2 T^2}$ and $b^* = \frac{bP}{RT}$.

The parameters, a , and b , are found from critical points by setting the first and second derivatives of pressure with respect to volume to zero. The parameters that appear in the associating cubic EOS are treated in the same manner as those for common cubic EOS. Adaptation of the equation to handle a binary mixture of carboxylic acids would require some

modification. Attempts were made to modify the Twu et al. (1993) equation to handle a binary mixture of carboxylic acids to no avail in this study.

3.7 Mixing Rules for Equations Of State

Several mixing rules have been proposed over the years by different investigating authors. The superiority of one relative to the other depends much on the physio-chemical properties of the mixture. Most of the mixing rules calculate the mixture parameters a , and b for the EOS according to the one fluid mixing rule Equations (3-134) and (3-135).

$$a = \sum_i^N \sum_j^N x_i x_j a_{ij} \quad (3-147)$$

$$b = \sum_i^N \sum_j^N b_{ij} \quad (3-148)$$

The only difference between them is the combining rule that determines how the cross coefficients a_{ij} and b_{ij} are calculated. Generally all mixing rules offer three adjustable binary interaction parameters, except for the simple quadratic mixing rule, which only offers two adjustable parameters per binary system. In other words, one binary interaction is used to adjust the mixture parameter b . The other parameters are used to adjust the mixture parameter a .

3.7.1 Quadratic Mixing Rule

As mentioned above, the quadratic mixing rule is the only one that offers a maximum of two binary interaction parameters per binary system. All the other mixing rules offer three adjustable binary parameters, where two are used to adjust the parameter a . Interestingly these mixing rules exactly reduce to the quadratic mixing rule if the third parameter, λ , is not used, i.e., set to zero. In the quadratic mixing rule the use of the second adjustable parameter l_{ij} is avoided by setting all $l_{ij} = 0$.

$$a_{ij} = \sqrt{a_i a_j} (1 - k_{ij}) \quad \text{with } k_{ij} = k_{ji} \quad (3-149)$$

$$b_{ij} = \frac{b_i + b_j}{2} (1 - l_{ij}) \quad \text{with } l_{ij} = l_{ji} \quad (3-150)$$

3.7.2 Panagiotopoulos-Reid Mixing Rule

Panagiotopoulos and Reid (1985) were the first to use two binary interaction parameters per binary system in order to fine-tune the parameter a . In most cases the parameter l_{ij} is set equal to

zero because the use of the two parameters k_{ij} and λ_{ij} already allows excellent representation of many highly non-ideal systems.

$$a_{ij} = \sqrt{a_i a_j} \left(1 - k_{ij}^{PR} + \lambda_{ij}^{PR} x_i \right) \quad (3-151)$$

$$b_{ij} = \frac{b_i + b_j}{2} (1 - l_{ij}) \quad (3-124)$$

3.7.3 Stryjek-Vera (1986) Mixing Rule

Stryjek and Vera (1986) came up with their “van Laar type” mixing rule. Stryjek and Vera claim that their mixing rule is better than the “Margules type” mixing rule.

$$a_{ij} = \sqrt{a_i a_j} \left(1 - \frac{k_{ij}^{SV} k_{ji}^{SV}}{x_i k_{ij}^{SV} + x_j k_{ji}^{SV}} \right) \quad (3-152)$$

$$b_{ij} = \frac{b_i + b_j}{2} (1 - l_{ij}) \quad (3-124)$$

3.7.4 Mathias-Klotz-Prausnitz (1991) Mixing Rule

Mathias et al. (1991) proposed a new mixing rule in the form :

$$a_{ij} = \sum_{i=1}^N \sum_{j=1}^N x_i x_j \sqrt{a_i a_j} \left(1 - k_{ij}^{MKP} \right) + \sum_{i=1}^N x_i \left(\sum_{j=1}^N x_j \left(\sqrt{a_i a_j} \lambda_{ij}^{MKP} \right)^{1/3} \right)^3 \quad (3-153)$$

$$b_{ij} = \frac{b_i + b_j}{2} (1 - l_{ij}) \quad (3-124)$$

It is note-worthy that this mixing rule is identical to that of Panagiotopoulos-Reid for binary systems. These mixing rules were not used because the Twu and Coon mixing rule was found superior.

3.8 Gibbs-Duhem Equation

The Gibbs-Duhem equation is an important thermodynamic relation, which shows the dependence of the activity coefficient on the excess properties:

$$\sum x_i d \ln \gamma_i = \frac{V^E}{RT} dP - \frac{H^E}{RT^2} dT \quad (3-154)$$

The Gibbs-Duhem equation finds extensive use in thermodynamic consistency tests discussed in Section 3.9. It is interesting to note that Equation (3-154) reduces to $\sum x_i d \ln \gamma_i = 0$ at constant temperature and pressure.

There are two important applications for Equation (3-154).

- (1) In the absence of complete experimental data or the properties of a mixture, Equation (A-18) may be used to calculate additional properties.
- (2) If experimental data are available for each component over some composition range, it is possible to check the data for thermodynamic consistency. If the data satisfy the Gibbs-Duhem equation, they are thermodynamically consistent and it is likely that they are reliable.

The Gibbs-Duhem equation can also be written as:

$$x_1 \frac{d \ln \gamma_1}{dx_1} = x_2 \frac{d \ln \gamma_2}{dx_1} \quad (\text{const. } T, P) \quad (3-155)$$

3.9 Thermodynamic Consistency Tests

Many research articles are published yearly containing low-pressure VLE data for binary systems. The directly measured variables in binary VLE are P , T , x and y . Experimental VLE measurements are subject to systematic error. Thermodynamic consistency tests become necessary to validate the experimental data and rank its conformance to the Gibbs-Duhem equation (Section 3.8).

3.9.1 Slope Test

Implicit in the Gibbs-Duhem equation is the slope test for thermodynamic consistency. The test compares slopes of curves drawn to fit data points on plots of $\ln \gamma_1$ versus x_1 and $\ln \gamma_2$ versus x_1 . Van Ness (1995) states that the test proved to be tedious and uncertain. The consistent data should conform to the equation:

$$\frac{dG^E}{RT} = \ln \frac{\gamma_1}{\gamma_2} + \epsilon \quad (3-156)$$

where ϵ is assumed to be zero, a generalisation that is true for isothermal data but not so true for isobaric data.

3.9.2 Area Test

The area test is a more practical way of testing for thermodynamic consistency. Redlich and Kister proposed the area test in 1948. It was readily accepted because of its simplicity. Equation (3-11) can be written as:

$$dg^* = \left(\ln \frac{\gamma_1}{\gamma_2} + \epsilon \right) dx_1 + \left(x_1 \frac{d \ln \gamma_1}{dx_1} + x_2 \frac{d \ln \gamma_2}{dx_1} - \epsilon \right) dx_1 \quad (3-157)$$

where $dg^* = \frac{d(G^E/RT)}{dx_1}$. Equation (3-157) can be integrated over the full composition range:

$$\int_{x_1=0}^{x_1=1} dg^* = \int_0^1 \left(\ln \frac{\gamma_1}{\gamma_2} + \epsilon \right) dx_1 + \int_0^1 \left(x_1 \frac{d \ln \gamma_1}{dx_1} + x_2 \frac{d \ln \gamma_2}{dx_1} - \epsilon \right) dx_1 \quad (3-158)$$

The left hand side is zero as $g^* = 0$ at both $x_1 = 0$ and $x_1 = 1$.

$$\int_0^1 \left(\ln \frac{\gamma_1}{\gamma_2} + \epsilon \right) dx_1 + \int_0^1 \left(x_1 \frac{d \ln \gamma_1}{dx_1} + x_2 \frac{d \ln \gamma_2}{dx_1} - \epsilon \right) dx_1 = 0 \quad (3-159)$$

The second integral must equal zero as is required by Equation (3-155) the Gibbs-Duhem equation. Both integrals then equal zero and we can write:

$$\int_0^1 \left(\ln \frac{\gamma_1}{\gamma_2} + \epsilon \right) dx_1 = 0 \quad (3-160)$$

The assumption made in the derivation is that the data are consistent. If one plots the quantity in the parenthesis $\ln \frac{\gamma_1}{\gamma_2}$ versus x_1 , the net area should be zero, i.e., the positive area (above the x

axis) should equal the negative area (below the x axis). The value for ϵ is set equal to zero. Van Ness (1959) states that the area test is merely a necessary but not a sufficient condition for consistency. Van Ness (1995) details all the assumptions and derivations that are made and its inconsistency.

3.9.3 Point/ Residual Test

Van Ness and co-workers (1973) came up with a more stringent test for consistency of VLE data. The four measurable variables of experimental VLE data T , P , x and y present an over specification of variables according to the phase rule of Gibbs. The phase rule of Gibbs provides for two independent intensive variables so that when either the pressure P , or the temperature T , is fixed the composition of the liquid x , and that of the vapour y , cannot be changed without variation in of T and P respectively. Thus when T is fixed, then for any value of x , we can calculate values of y and P . The calculation is done by data regression and is discussed in Chapter 7. In general the vapour phase compositions introduce the most error. The residual (the difference between a derived value and the corresponding experimental value) for the vapour composition can be readily calculated, $\delta y = y_{\text{exp}} - y_{\text{calc}}$. The extent to which the correlated values deviate from the measured values provides an indication of the consistency of the VLE data (Van Ness et al. [1973]). The average absolute deviation $\Delta y_{\text{ad}} = \frac{1}{n(|\delta y|)}$ must be less than 0.01 for the data to be consistent. The point test was done on the carboxylic acids VLE data measured in this project.

3.9.4 Direct Test

Van Ness (1995) developed the direct test. He noted that the residual $\delta \ln \left(\frac{\gamma_1}{\gamma_2} \right)$ offered a unique opportunity for consistency testing.

$$\delta \ln \frac{\gamma_1}{\gamma_2} = x_1 \frac{d \ln \gamma_1^{\text{exp}}}{dx_1} + x_2 \frac{d \ln \gamma_2^{\text{exp}}}{dx_1} - \epsilon \quad (3-161)$$

The derivation of the residual function is obtained by subtracting the Gibbs energy function obtained from experimental data from that of regressed results. The derivation will not be dealt with here. A plot of $\delta \ln \frac{\gamma_1}{\gamma_2}$ versus x_1 shows a residual scatter about the x axis. The extent to

which the residual values scatter about the zero line provides a measure of the departure of the data from thermodynamic consistency. Van Ness developed the criteria to quantify the degree to which the data departs from consistency as seen in Table (3-1). The index of one signifies excellent data and an index of ten, extremely poor data. The direct test was used to verify the consistency of the cyclohexane + ethanol system. This test for consistency could not be carried out on the acids because of the unusual activity coefficients obtained due to association.

Table 3- 1: Direct test index for thermodynamic consistency, Van Ness (1995)

Index	RMS $\delta \ln(\gamma_i/\gamma_2)$	
1	>0	≤ 0.025
2	>0.025	≤ 0.050
3	>0.050	≤ 0.075
4	>0.075	≤ 0.100
5	>0.100	≤ 0.125
6	>0.125	≤ 0.150
7	>0.150	≤ 0.175
8	>0.175	≤ 0.200
9	>0.200	≤ 0.225
10	>0.225	

VAPOUR-LIQUID EQUILIBRIUM EQUIPMENT

4.1 Introduction

This chapter is devoted to the equipment used in this project. A low pressure dynamic VLE still illustrated in Figure 4-1 was used. The still was designed by Raal (Raal and Mühlbauer [1998]). The operation of the still is aided by other peripheral pieces of equipment also discussed in this chapter. The vapour and liquid samples were analysed using a Varian 3300 gas chromatograph fitted with a flame ionisation detector.

4.2 Low Pressure Vapour-Liquid Equilibrium Measurements

The measurement of experimental VLE data can be done using different experimental techniques which have been developed over the years. Hala et al. (1967), Malanowski, (1982) and most recently Raal and Mühlbauer (1998) discuss various experimental techniques for low and high pressure phase equilibria measurements detailing the advantages and disadvantages of some of the techniques. Joseph (2001) and Soni (2003) discuss the history and development of recirculating stills. Low-pressure VLE measurement techniques fall into one of the following categories:

- Dynamic / Circulation methods
- Static VLE methods
- Semi-micro techniques
- Dew-point or bubble point methods

4.2.1 Dynamic Method

The still used in this work falls under dynamic stills. Dynamic stills account for a large portion of VLE data that have been published (Raal and Mühlbauer [1998]). Dynamic VLE measurement methods allow results of high accuracy to be obtained in a rapid and relatively simple manner. Circulation is either of the vapour phase only or circulation of both vapour and liquid. The operating principles common to all dynamic VLE measurement methods include:

1. Continuous separation of vapour phase from liquid phase.
2. Condensation of vapour phase (some methods directly circulate the vapour).
3. Circulation of the condensed vapour.
4. Operate dynamic still under steady state.
5. Operate dynamic still isobarically or isothermally.
6. Measurement of thermodynamic parameters i.e. temperature, pressure, liquid and vapour composition.

The dynamic still used in this work is discussed in Section 4.3.

4.2.2 Static Methods

Static methods make use of an equilibrium cell, which is charged with a liquid mixture and agitated by some mechanical means to achieve vapour-liquid equilibrium. The cell is often placed in a temperature controlled water bath. Only isothermal data can be measured by static methods. One of the major disadvantages of static methods is that the system needs to be completely degassed to remove any small amounts of dissolved gases. The dissolved gases cause erroneous vapour pressures. In the majority of static equilibrium cells, the vapour phase is not sampled for analysis (Raal and Mühlbauer [1998]). The vapour volume hold-up is small at low pressure and cannot be easily sampled and analysed. Raal and Ramjugernath (1999) found that for systems of large relative volatility, vapour phase hold-up must be accounted for. Inoue et al. (1975), tried to address this problem, but many experimentalists, Abbott (1986) among others, did not merit the method. Thermodynamic consistency tests cannot be done on VLE data from static methods unless one measures pressure, temperature, liquid and vapour compositions.

4.2.3 Semi-Micro Techniques

As previously mentioned, VLE measurements are costly. The need for semi-micro techniques arise because some chemicals are difficult to purify to very high levels and thus may be expensive. There are few semi-micro VLE static methods that have been developed. Wichterle

and Hala (1963) designed a semi-micro static VLE still that was moderately accurate. Raal and Mühlbauer (1998) review this equipment and other more recent methods in detail.

4.2.4 Dew Point and Bubble Point Methods

Dew point and bubble point VLE measurements of a mixture can be done when the mixture is either entirely vapour or liquid. A change in temperature, pressure or composition induces condensation or evaporation in a saturated vapour or liquid mixture respectively. The most commonly used method experimentally is the variation of pressure of a mixture of known composition by changing the volume. The dew point and bubble point pressures are determined from the breaks in the P-V curves for each isotherm. Malanowski (1982), and Raal and Mühlbauer (1998) outline this method. Dew point and bubble point measurements are suitable for binary mixtures only. They find more use in high pressure VLE than low pressure VLE. Circulation methods produce results of higher accuracy than dew- or bubble point methods and at much faster rates, a factor that makes dew and bubble point methods very unpopular.

4.3 Raal Dynamic VLE Still

The compact glass dynamic equilibrium still used in this project was designed by Raal (Raal and Mühlbauer [1998]). The still was constructed by glassblower, Mr P. Siegling. The design of the still is based on that of Yerazunis et al. (1964). Joseph (2001) and Harris (2001) describe the still in great detail. However, it is worth noting some of the advantages of this design. Of prime importance is the design of the equilibrium chamber, which contains miniature 3mm stainless steel wire mesh packing increasing interfacial surface area for vapour and liquid contacting allowing fast attainment of equilibrium. The packing in the equilibrium chamber is easily accessible unlike other earlier designs like that of Heertjies (1960) and Yerazunis (1964). This has the advantage that the volume of packing can be adjusted and different more inert packing can be used if desired when handling reactive mixtures. The temperature measuring element, (Pt-100), is embedded in the packing. The liquid and vapour flow over it, thereby enabling it to measure the true equilibrium temperature. The equilibrium chamber is vacuum jacketed to avoid any loss of latent heat to the environment resulting in condensation of the vapour. The cottrell pump is vacuum jacked and enters the equilibrium chamber centrally, thus eliminating temperature gradients.

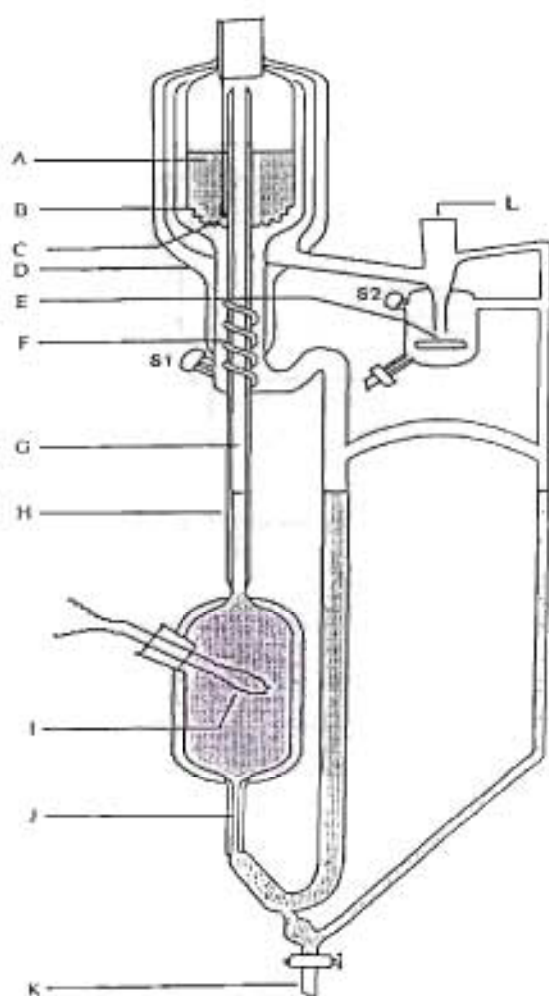


Figure 4-1: Schematic diagram of the VLE Still (Raal)

A: stainless steel wire mesh packing, B: drainage holes, C: PT-100 sensor, D: vacuum jacket, E: magnetic stirrer, F: stainless steel mixing spiral, G: insulated Cottrell pump, H: vacuum jacket, I: internal heater, J: capillary leg, K: drainage valve, L: condenser attachment, S1: liquid sampling septum, S2: vapour sampling septum.

The boiling chamber comprises of two heaters, one internal in the form of a heater cartridge, housed in a glass well, placed in the solution and the other external in the form of nichrome wire wound around the chamber. The internal heater gives very rapid boiling, permits precise control of the circulation rate, and provides nucleation sites for smooth boiling. The still incorporates efficient magnetic stirrers in both the boiling chamber and the condensate receiver. This eliminates any possible concentration and temperature gradients and leads to a high reproducibility of sample concentration. The stirrer in the boiling chamber further provides nucleation sites for boiling in addition to the internal heater. The efficient stirring ensures that the condensed vapour from the condensate receiver (rich in the more volatile component) and

the recirculating liquid are thoroughly mixed before evaporation. This eliminates flashing in the boiling chamber.

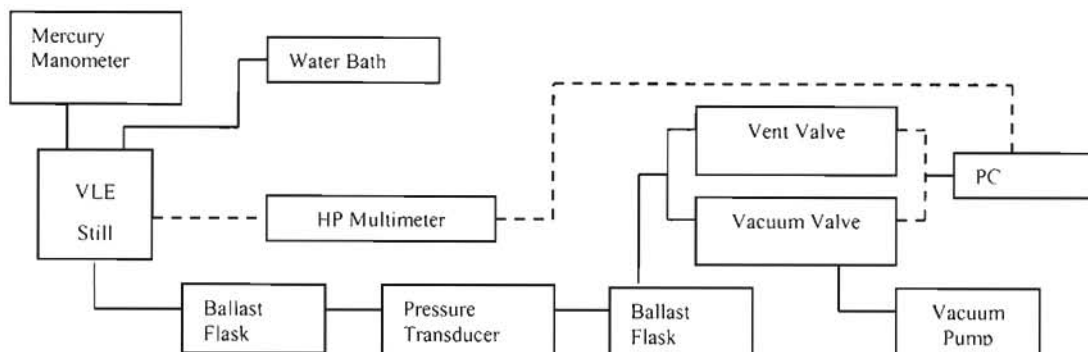


Figure 4-2: Schematic diagram of equipment setup

The operation of the VLE still requires other peripheral apparatus. Figure 4-2 shows a schematic block diagram of the experimental set up. A Photo of the experimental set up can be found in Appendix D. The various experimental apparatus include a VLE still, three pyrex 5L ballast flasks (two of which were joined to provide a 10L ballast flask), a Julabo FT 200 cold finger, a Hewlett-Packard model 34401A multi-meter, a vacuum pump, a Sensotec Super TJE pressure transducer, two solenoid valves, a differential mercury manometer, a Labotech water bath with a glycol-water mixture and pump, three DC power supplies (one providing power for the two magnetic stirrers, one each for the two solenoid valves), two AC voltage regulators for adjustment of the internal and external heater and a computer (with the control scheme for operation of the still). The purpose of the ballast flasks is to reduce pressure fluctuations within the still caused by the vacuum pump. They also trap any condensable vapours should the condenser fail. The mercury manometer is used in the pressure calibration of the still. The excellent computer control scheme was developed and implemented by Joseph (2001).

4.4 Temperature Measurement and Control

The temperature measurement was done in the equilibrium chamber as mentioned in Section 4-2. A Pt-100 sensing element was used with its resistance being displayed by the Hewlett-Packard model 34401A multi-meter. The resistance was converted and read as temperature from the computer interface using the linear correlation $T = m.R+c$, where T represented the temperature in degree Celsius, R was the resistance of the Pt 100 sensor and m and c were the gradient and intercept respectively. The values for m and c were obtained from the temperature calibration as explained in Chapter 5. The accuracy of the measured temperature was estimated

to be within $\pm 0.02^{\circ}\text{C}$, while the accuracy of the temperature control varied between 0.01 and 0.05°C depending on the volatility of the components being studied.

4.5 Pressure Measurement and Control

The pressure of the system was measured using a Sensotec Super TJE pressure transducer. Accuracy of the pressure measurement was ± 0.03 kPa. The pressure control was within ± 0.01 kPa of the set pressure. The pressure calibration of the still is discussed in Chapter 5.

4.6 Sampling and Composition Analysis

The vapour and liquid samples were withdrawn from the respective sample points, S2 and S1 on the still using gas tight plastic and glass syringes. Withdrawal of the samples was possible as long as a higher vacuum could be achieved with the syringe than that in the still. Glass syringes were necessary to withdraw samples at high temperatures ($150^{\circ}\text{C} - 200^{\circ}\text{C}$) and very low pressures (10 kPa). Chemically resistant septa are used to seal the sampling ports. The septum was replaced regularly (once every two days) as it wore out because of the corrosive nature of the carboxylic acids and the high experimental temperatures (up to 170°C).

A gas chromatograph was used to determine the precise equilibrium compositions of the vapour and liquid samples. Gas chromatography is a widely used tool for analysing multi-component organic mixtures. Raal and Mühlbauer (1998) report that more than 250 000 instruments are operated in the United States alone. Packed capillary columns are used to separate the different organic constituents in the mixture, and once separated, quantitative analysis can be achieved with a variety of highly efficient and specialised detectors. A Varian 3300 gas chromatograph with a flame ionisation detector, FID, was used in this project. The detector is only sensitive to species that contain C-H bond and they can detect flows as small as 10^{-11} g/s (Raal and Mühlbauer [1998]). However, before using the gas chromatograph, it needed to be calibrated. The calibration procedure is discussed in Section 5.5.

EXPERIMENTAL PROCEDURE

5.1 Introduction

This chapter details the experimental procedure that was employed in taking the VLE measurements for the carboxylic acids systems.

5.2 Cleaning the VLE Still

Undertaking VLE measurements is a costly and time-consuming exercise. The chemicals used to undertake VLE measurements need to be of the highest purity. The purity of the chemicals needs to be preserved in the whole experimental process. Hence, the still needed to be cleaned before undertaking any measurements. The cleaning was achieved by operating the still with acetone for 30 minutes for several runs at atmospheric pressure. The wash was repeated until no peak other than that of acetone was found after GC analysis of the spent acetone from the wash. When satisfactorily clean, the still was dried by setting the pressure to 5 kPa and allowing the residual acetone to be flashed off.

5.3 Pressure Calibration

A Sensotec Super TJE pressure transducer needed to be calibrated to accurately read the pressure within the system. The calibration was achieved by using a mercury manometer attached to the still and a Vaiscala electronic barometer (model PTB100A). The barometer is NIST (National Institute of Standards and Technology) certified. The pressure in the still was varied progressively through the operating range, 5 – 100 kPa. At each point the mercury manometer reading was taken using a cathetometer, the atmospheric pressure from the barometer and the transducer pressure reading. The height of the mercury manometer represented the pressure difference from atmospheric pressure, hence subtracting the two allowed calculation of the true system pressure, $P_{act} = P_{atm} - |\Delta mmHg|$. A plot of the true pressure against that of the pressure transducer reading gave a linear relationship as shown in Figure B-1, Appendix B.

5.4 Temperature Calibration

The temperature of the system, specifically in the equilibrium chamber, was measured using a Pt-100 temperature sensor. The resistance of the Pt 100 was read from an HP 34401 multimeter. The temperature was read from the GUI (Graphical User Interface) on the computer, which converts the resistance to temperature using a linear equation inputted. The sensor was calibrated “in-situ” by running the still isobarically with a highly pure chemical (> 99.5%). The purity of the chemicals used is shown in Appendix B. The true temperature of the system was correlated using the Antoine equation (Reid et al. [1988]), and plotted against the resistance. The slope and the intercept of the line were entered into the GUI and thus the computer displayed the system temperature. Two temperature calibrations were done on the still, one for high temperature range using n-decane and the other for the low temperature range using cyclohexane. The temperature calibration results are in Appendix B, Figures B-2 and B-3.

5.5 Gas Chromatograph Calibration

A Varian 3300 gas chromatograph fitted with a FID was used to analyse the compositions of the samples. The Varian, gave excellent linear results. The operating conditions used on the Varian 3300 GC are presented in Table 5-1. The detector calibration procedure discussed by Raal and Mühlbauer (1998) was used in this study. Raal and Mühlbauer (1998) state that a gas chromatograph cannot be more accurate than the calibration. Hence, GC calibration is critical to VLE measurement work. The calibration procedure is as follows:

- Known samples of the binary mixture are prepared by gravimetrically weighing samples with the mole fraction ratios x_1/x_2 and x_2/x_1 ranging approximately from 0.1 to 1.5.
- The samples are analysed by the GC which gives the results as peak areas of the different component, A_1 and A_2 .
- Plots of A_1/A_2 versus x_1/x_2 and A_2/A_1 versus x_2/x_1 are generated with the slope (that passes through the origin) giving the response factor.
- The response factor of one of the graphs must equal the reciprocal response factor of the other graph.

In most cases the peak area (A) generated by the integrator is proportional to the number of moles (x) passing through the GC. The following general equation applies:

$$n_i = F_i A_i \quad (5-1)$$

It can be seen that:

$$\frac{n_1}{n_2} = \frac{x_1}{x_2} = \frac{F_1}{F_2} \cdot \frac{A_1}{A_2} \quad (5-2)$$

1 μ L gas chromatograph syringes were used to inject 0.1 – 0.4 μ L of the prepared samples into the GC. The volume injected differed depending on the volatility of the system and care was taken not to overload the detector. The GC calibration results for all the binary systems investigated in this project are reported in Chapter 6.

Table 5-1: Operating conditions for the Varian 3300 gas chromatograph

Gas flow rate (He) 10ml/min						
Detector Temp 25°C						
Attenuation 16						
Range 10						
System	Oven Temp °C (Initial)	Oven Temp °C (Final)	Temperature Ramp °C	Injector Temp °C	Auxilliary Temp °C	Elution Time minutes
Ethanol + Cyclohexane	50	50	-	100	100	6.0
Propionic Acid + Hexanoic Acid	120	150	5.0	200	210	5.3
Isobutyric Acid + Hexanoic Acid	128	150	4.0	200	210	4.5
Valeric Acid + Hexanoic Acid	135	150	5.0	200	210	4.5
Hexanoic Acid + Heptanoic Acid	150	160	4.0	200	210	6.0

5.6 Procedure for Isobaric and Isothermal VLE measurements.

As stated previously, the still can be run either isobarically or isothermally using a computer control scheme. The pressure in the system is maintained below atmospheric pressure by means of a vacuum pump. The computer control scheme regulates the pressure in the still by actuating valves V1 (to the vacuum pump) or V2 (to the atmosphere) as shown in the schematic diagram, Figure 4-2.

5.6.1 Measurement of Isobaric VLE

The procedure is as follows:

1. The computer is switched on. The power supply to the peripheral equipment, solenoid valves, and stirrer motors, HP multimeter, cooling water, pressure transducer and vacuum pump are all switched on.
2. The still is charged with one of the pure components using a plastic syringe through the liquid sampling point. The boiling chamber must be filled to a level approximately 5cm above the top of the chamber.
3. The pressure at which the still is to be run is input into the GUI. At this point the pressure in the still will start to decrease to the set point.
4. The external heater to the boiling chamber is switched on and varied to bring the still to a boil.
5. The internal heater is switched on and varied to obtain smooth boiling and ensure that the liquid is boiling in the "plateau region". This is the region where the temperature remains constant despite slight increase or decrease in the power input. This concept is discussed in detail in Section 5.7.
6. Equilibrium is achieved by ensuring a high circulation rate, which is indicated by the drop rate in the condenser. Equilibrium is obtained in about 45 minutes. However, this can vary depending on the system properties particularly relative volatility and the circulation rate. A good circulation rate is critical to the attainment of equilibrium. This can be checked by the drop rate in the condensate trap, with a drop rate in the range of 120 drops/minute found suitable in these studies.
7. Once equilibrium is reached, the temperature is recorded and the vapour and liquid samples withdrawn. The samples are stored in gas chromatography sample bottles.
8. The vapour and liquid samples are analysed using the GC to get the compositions.
9. A further small amount of liquid is withdrawn from the still and is replaced with the second component thereby changing the composition in the still to generate the next equilibrium points on the phase diagram. Steps 4 onwards are repeated until about half of the phase diagram is complete.
10. The still is drained and cleaned and charged with the second component first and the above steps being followed to generate the other half of the phase equilibria curve. The two curves starting from either end should meet without any discontinuity.

5.6.2 Measurement of Isothermal VLE

The isothermal operation of the still relied on the isobaric operation for heating the still. Isothermal measurements were first discussed as feasible by Rogalski and Malanowski (1980) using their ebulliometric total pressure method. The procedure is such that the pressure is varied to maintain a constant temperature. The procedure for isothermal measurement is that the pressure is set such that the system boiling temperature is as close as possible to the set point temperature. Once this is achieved the computer control scheme is changed from isobaric to isothermal control on the GUI with the set point temperature being input. The control scheme would then vary the pressure to maintain the set temperature.

5.7 Plateau Region

Once the still is charged and heated it is important to find the correct energy input to the reboiler so that the system operates in the plateau region. The concept of the plateau region for boiling liquids in an ebulliometer type still is explained and commented on by Kneisl et al. (1989) and Raal and Mühlbauer (1998). The general concept is that, once the mixture is boiling, an increase in the energy input will increase the temperature of the boiling mixture until the plateau region is reached. In the plateau region small increases in energy input have no effect on the temperature. At a certain point the plateau region is exited and any further increases in energy input results in an increase in temperature. Figure 5-1 illustrates the concept of the plateau region.

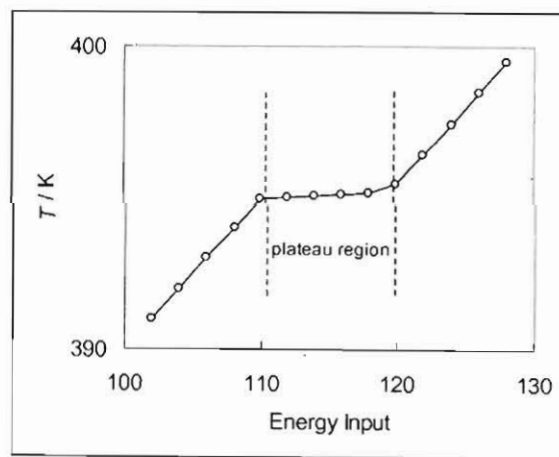


Figure 5-1: The plateau region in the temperature vs. energy input plot for boiling mixtures.

Some chemicals (alkanes) have large, very distinct plateau regions while other chemicals (alcohols) have very small plateau regions, which sometimes appear to be inflection points only (Kneisl et al. [1989]). To get accurate boiling point measurements it is important to always operate in the plateau region.

RESULTS

6.1 Introduction

This chapter presents the results of the GC calibrations and phase diagrams of the VLE measurements undertaken in this project. The chemical purity of the chemicals used are listed. The experimental results are presented in the following order:

- Cyclohexane + Ethanol system
- Propionic acid + Hexanoic Acid
- Isobutyric Acid + Hexanoic Acid
- Valeric Acid + Hexanoic Acid
- Hexanoic Acid + Heptanoic Acid

6.2 Chemical Purity

The chemical purity of the components used in undertaking VLE measurements cannot be emphasised enough. Few areas of chemical engineering research have presented so compelling an experimental challenge as the accurate measurement of multi-component phase equilibria, (Raal and Mühlbauer [1998]). Before undertaking the VLE measurements, the chemical components were checked against manufacturer's claimed purity. The results are presented in Table 6-1.

Table 6-1: Purity of Chemical reagents

Reagent	Supplier	Claimed Purity (mass %)	GC Analysis (Area %)	Refractive Index	
				Lit*.	Exp.
Cyclohexane	Riedel-de Haën	99.5	99.7	1.4265	1.4267
Ethanol	Merck Ltd	99.7	99.7	1.3612	1.3611
Propionic Acid	Fluka Chemicals	99.5	99.6	1.3810	1.3812
Isobutyric Acid	Fluka Chemicals	99.5	99.3	1.3930	1.3931
Valeric Acid	Fluka Chemicals	99.0	99.2	1.4085	1.4082
Hexanoic Acid	Aldrich Chemicals	99.0	98.7	1.4163	1.4150
Heptanoic Acid	Aldrich Chemicals	99.0	99.1	1.4170	1.4172

*Weast and Grasselli (1989) CRC Handbook

6.3 Cyclohexane + Ethanol systems

Isobaric VLE data at 40 kPa and isothermal VLE data at 323.15 K were measured for the binary cyclohexane (1) + ethanol (2) mixture. The system does not constitute part of the new data, but was chosen to test the equipment and the experimental procedure employed. The data were compared with that of Joseph et al. (2001) and were found to be in good agreement, Figures 6-3 to 6-6. The GC calibrations, experimental data, x-y, T-x-y, and P-x-y plots are presented below, Figures 6-1 to 6-2.

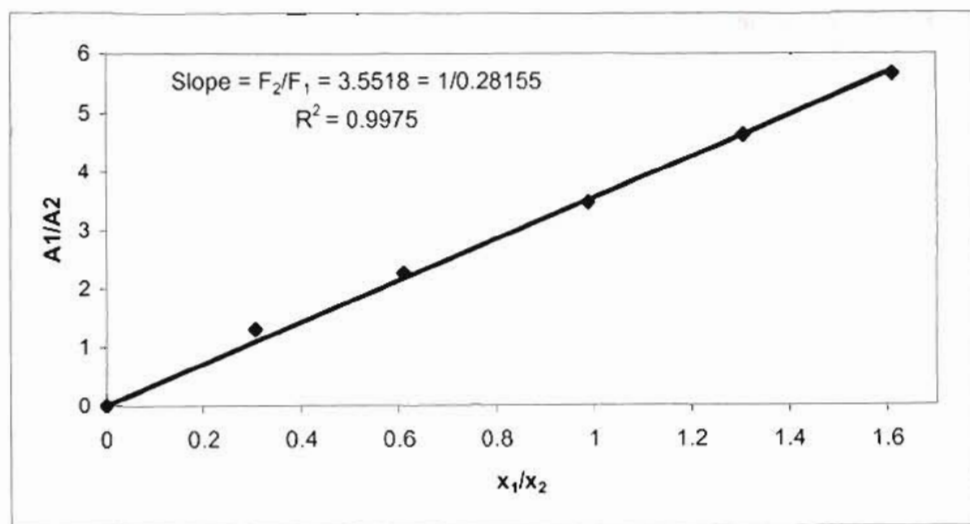


Figure 6-1: GC Calibration for Cyclohexane(1) + Ethanol(2) – Ethanol rich region

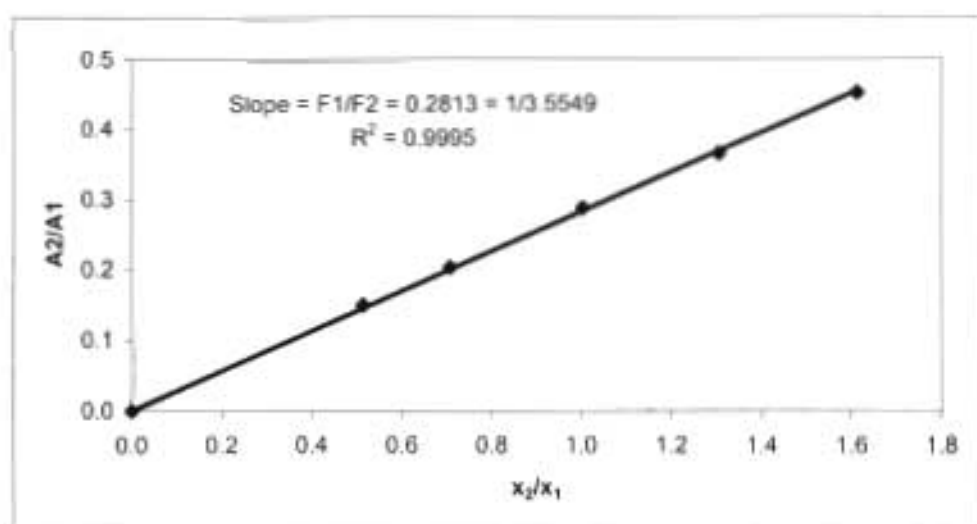


Figure 6-2: GC Calibration for Cyclohexane (1) + Ethanol (2) – Cyclohexane rich region

Table 6-2: Vapour-Liquid Equilibrium Data for Cyclohexane (1) + Ethanol (2) at 40 kPa

T / K	x_1	y_1	T / K	x_1	y_1
325.84	1.000	1.000	315.03	0.320	0.578
316.68	0.957	0.704	316.05	0.216	0.534
314.96	0.844	0.639	317.02	0.161	0.498
314.83	0.810	0.635	319.70	0.095	0.384
314.68	0.669	0.610	321.56	0.063	0.314
314.66	0.637	0.608	323.82	0.042	0.236
314.61	0.553	0.606	326.25	0.019	0.149
314.77	0.450	0.598	329.67	0.000	0.000

Table 6-3: Vapour-Liquid Equilibrium Data for Cyclohexane (1) + Ethanol (2) at 323.15 K

P / kPa	x_1	y_1	P / kPa	x_1	y_1
36.24	1.000	1.000	52.27	0.169	0.492
47.47	0.984	0.792	48.66	0.120	0.440
51.70	0.962	0.707	44.01	0.074	0.363
54.89	0.906	0.652	41.38	0.054	0.302
56.62	0.818	0.626	38.17	0.034	0.232
57.06	0.756	0.609	35.12	0.017	0.154
57.19	0.643	0.600	33.36	0.010	0.110
57.18	0.520	0.588	29.63	0.000	0.000
56.92	0.442	0.575			

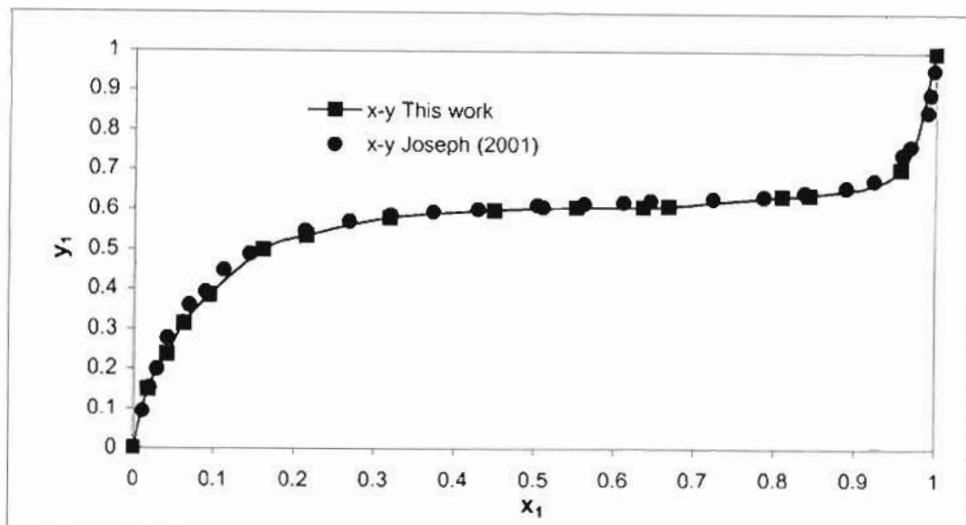


Figure 6-3: x-y Diagram for Cyclohexane (1) + Ethanol (2) System at 40 kPa

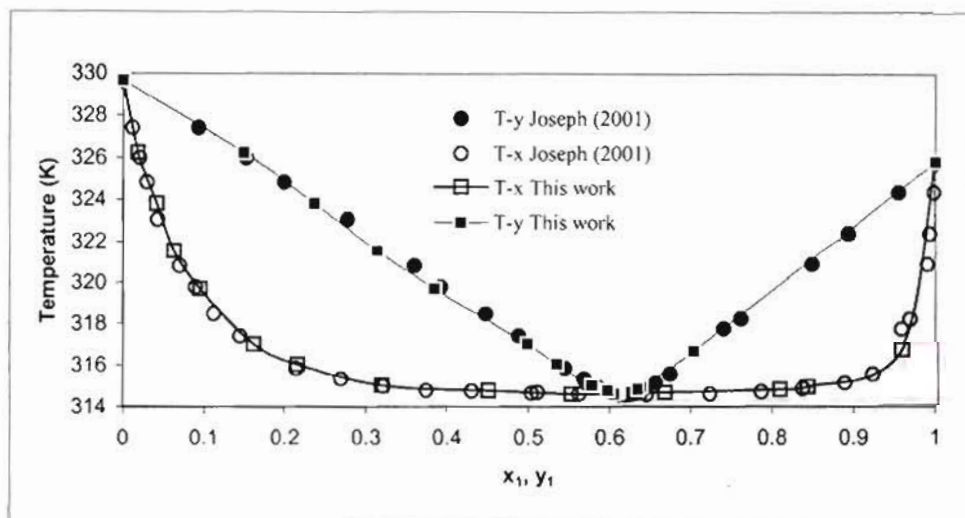


Figure 6-4: T-x-y Phase diagram for Cyclohexane (1) + Ethanol (2) system at 40 kPa.

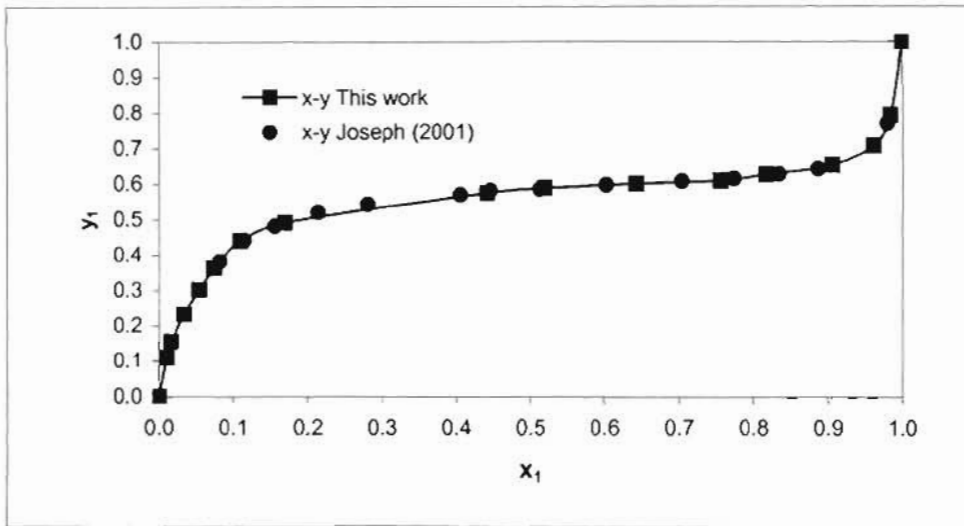


Figure 6-5: x-y Diagram for Cyclohexane (1) + Ethanol (2) System at 323.15 K

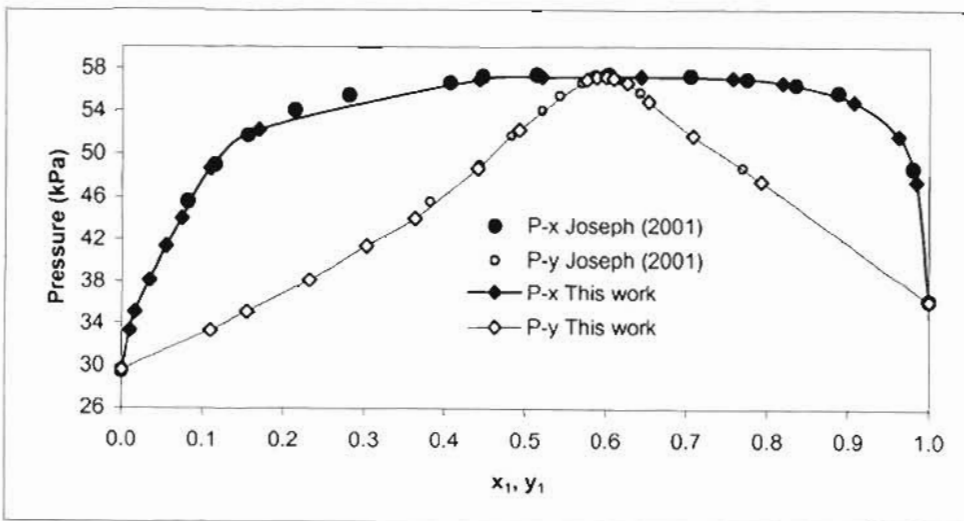


Figure 6-6: P-x-y Phase diagram for Cyclohexane (1) + Ethanol (2) system at 323.15 K.

6.4 Propionic Acid + Hexanoic Acid Systems

The data were measured at 20 kPa, 403.15 K, 408.15 K, and 413.15 K. The composition analysis was done using the Varian 3000 gas chromatograph. The GC calibration, experimental data, x-y, T-x-y and P-x-y phase diagrams are presented below.

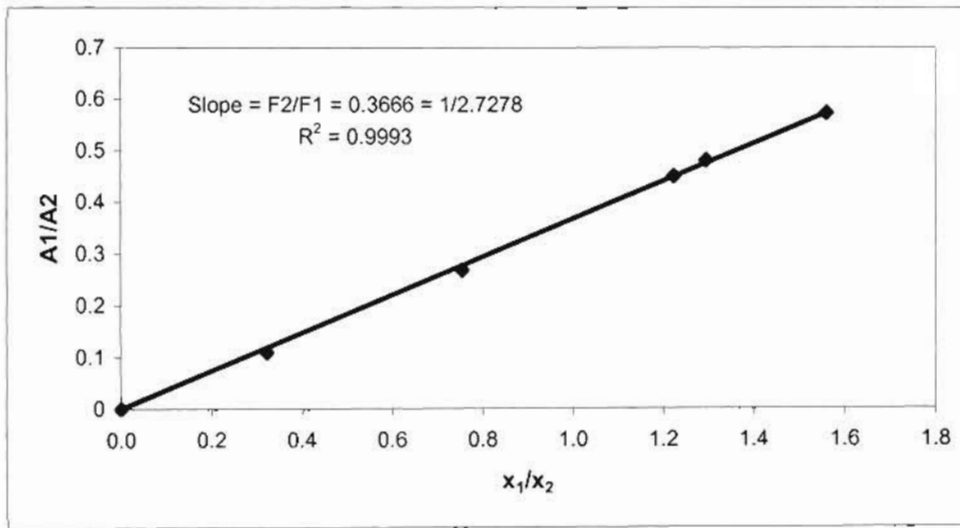


Figure 6-7: GC Calibration for Propionic acid (1) + Hexanoic acid (2) system – Hexanoic acid rich region

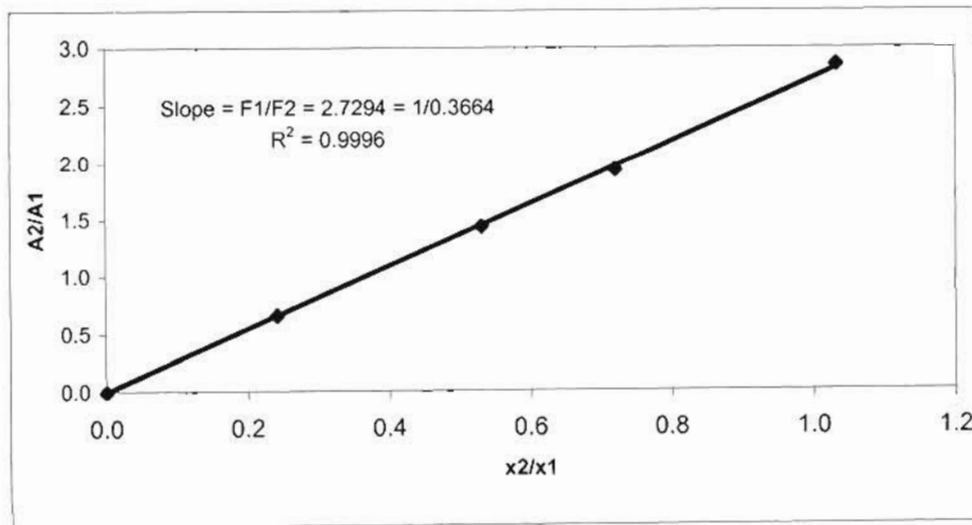


Figure 6-8: GC Calibration for Propionic acid (1) + Hexanoic acid (2) system – Propionic acid rich region

Table 6-4: Vapour-Liquid Equilibrium Data for Propionic Acid (1) + Hexanoic Acid (2) at 20 kPa

T / K	x_1	y_1	T / K	x_1	y_1
430.31	0.000	0.000	387.20	0.558	0.917
426.94	0.018	0.070	377.75	0.809	0.972
421.08	0.072	0.286	376.85	0.827	0.975
411.68	0.172	0.547	373.80	0.912	0.989
405.31	0.248	0.678	372.10	0.963	0.993
393.73	0.415	0.852	368.53	1.000	1.000
392.59	0.437	0.866			

Table 6-5: Vapour-Liquid Equilibrium Data for Propionic Acid (1) + Hexanoic Acid (2) at 403.15 K

P / kPa	x_1	y_1	P / kPa	x_1	y_1
70.88	1.000	1.000	27.69	0.416	0.826
69.02	0.985	0.996	24.58	0.359	0.793
63.19	0.937	0.987	19.95	0.287	0.735
59.06	0.889	0.979	16.01	0.211	0.652
45.85	0.731	0.931	13.17	0.167	0.563
40.33	0.647	0.907	9.84	0.090	0.383
34.01	0.535	0.868	6.55	0.000	0.000

Table 6-6: Vapour-Liquid Equilibrium Data for Propionic Acid (1) + Hexanoic Acid (2) at 408.15 K

P / kPa	x₁	y₁	P / kPa	x₁	y₁
83.59	1.000	1.000	31.51	0.388	0.807
81.51	0.986	0.996	27.26	0.333	0.769
68.42	0.841	0.973	19.36	0.213	0.645
54.91	0.675	0.938	15.15	0.131	0.504
53.99	0.665	0.933	11.19	0.065	0.308
44.94	0.562	0.897	8.25	0.000	0.000

Table 6-7: Vapour-Liquid Equilibrium Data for Propionic Acid (1) + Hexanoic Acid (2) at 413.15 K

P / kPa	x₁	y₁	P / kPa	x₁	y₁
97.06	1.000	1.000	36.15	0.391	0.790
94.52	0.975	0.995	26.75	0.253	0.689
85.19	0.900	0.981	24.31	0.223	0.651
65.77	0.742	0.934	15.58	0.082	0.379
58.24	0.661	0.911	11.99	0.030	0.093
45.53	0.511	0.848	10.13	0.000	0.000
42.45	0.477	0.829			

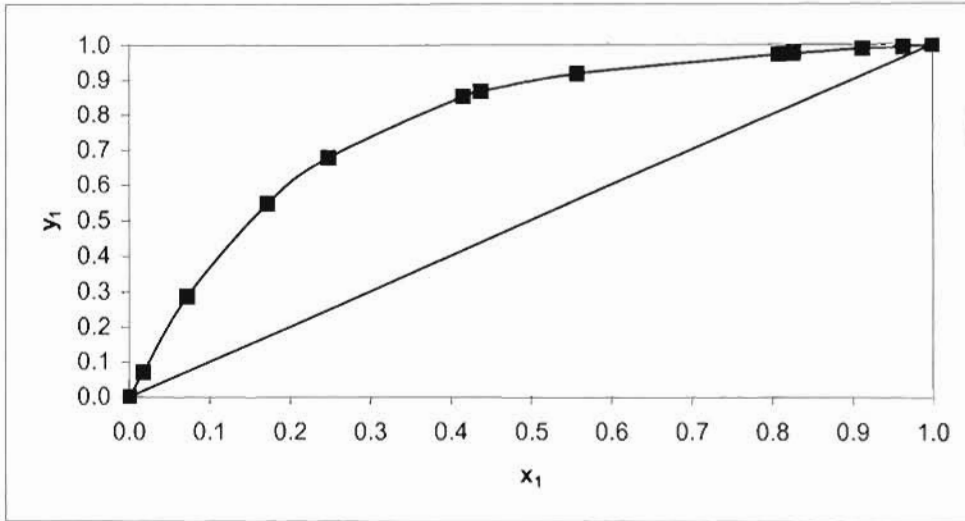


Figure 6-9: x-y Phase diagram for Propionic Acid (1) + Hexanoic Acid (2) at 20 kPa

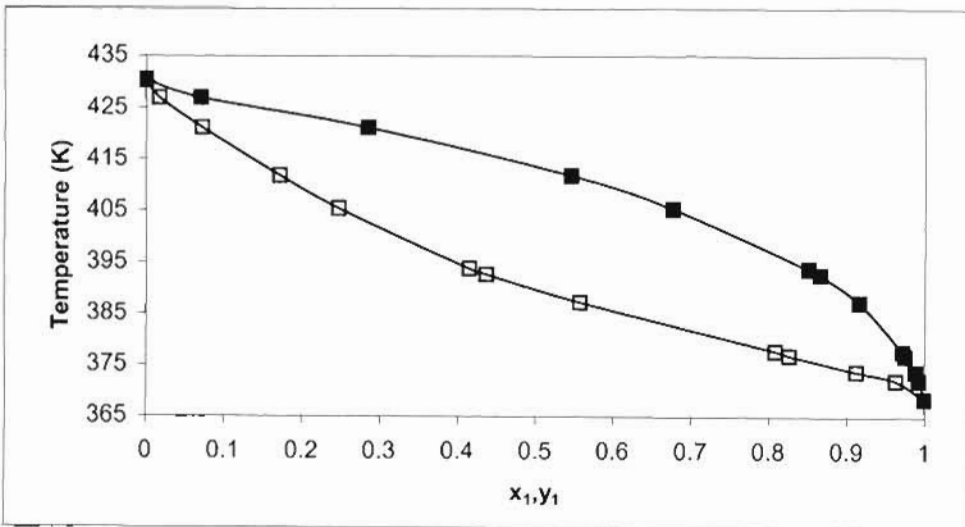


Figure 6-10: T-x-y Phase diagram for Propionic Acid (1) + Hexanoic Acid (2) at 20 kPa

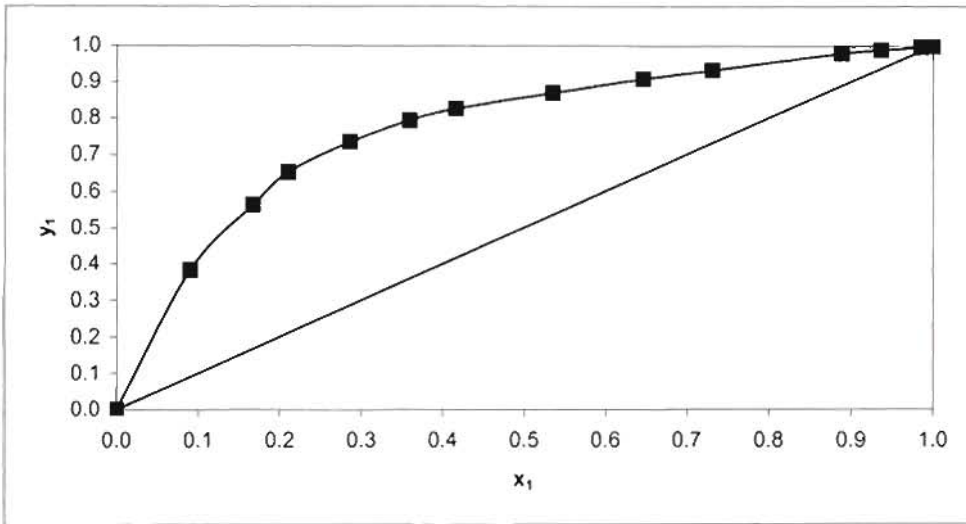


Figure 6-11: x-y Phase diagram for Propionic Acid (1) + Hexanoic Acid (2) at 403.15 K

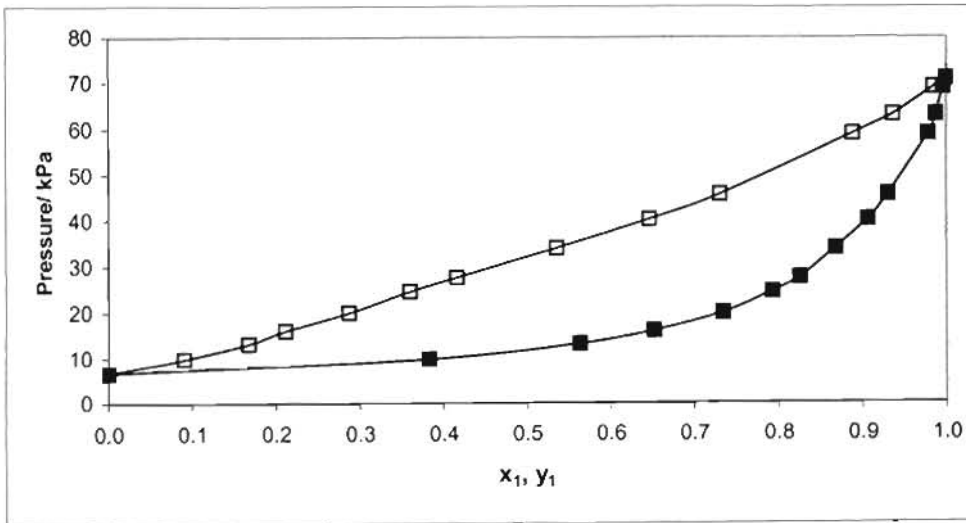


Figure 6-12: P-x-y Phase diagram for Propionic Acid (1) + Hexanoic Acid (2) at 403.15 K

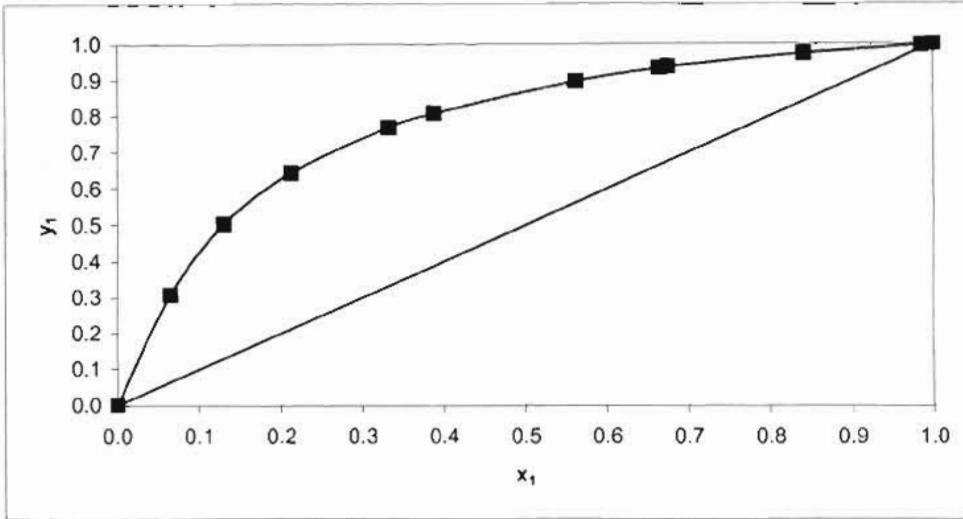


Figure 6-13: x-y Phase diagram for Propionic Acid (1) + Hexanoic Acid (2) at 408.15 K

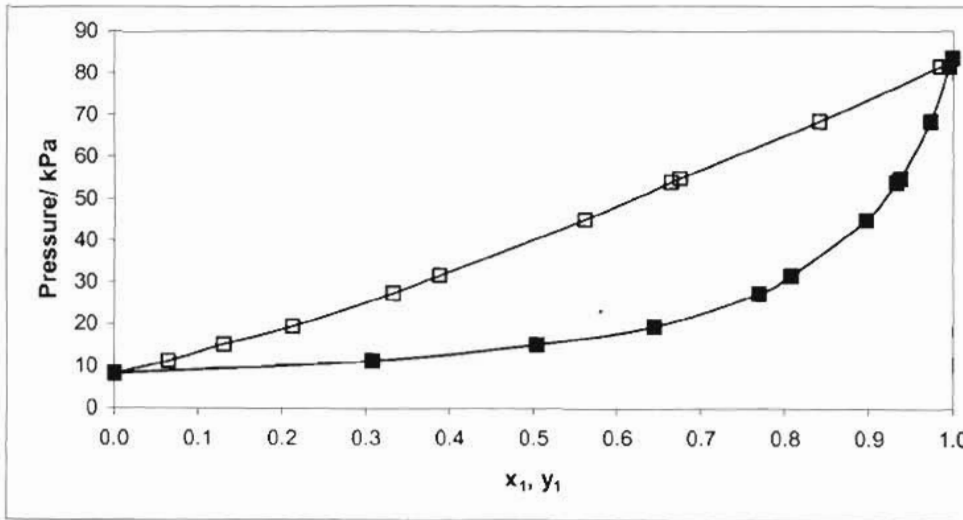


Figure 6-14: P-x-y Phase diagram for Propionic Acid (1) + Hexanoic Acid (2) at 408.15 K

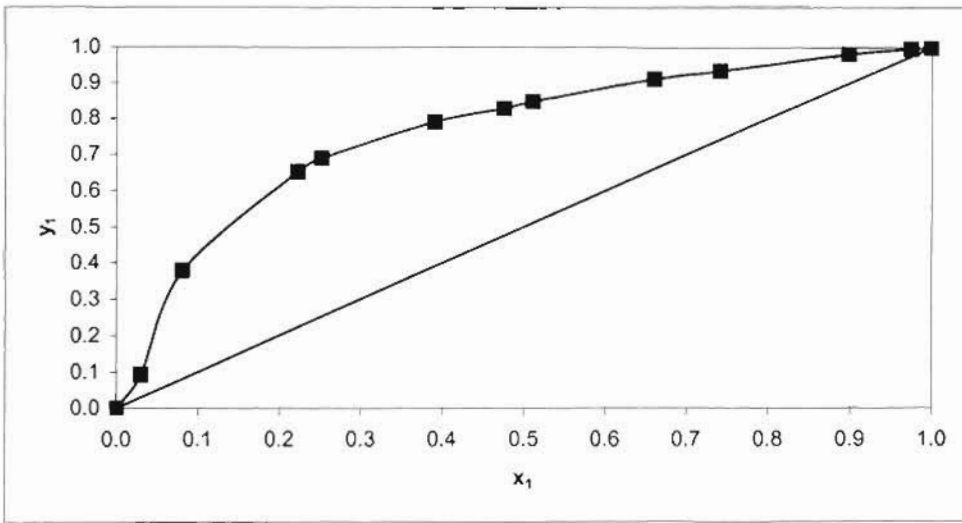


Figure 6-15: x-y Phase diagram for Propionic Acid (1) + Hexanoic Acid (2) at 413.15 K

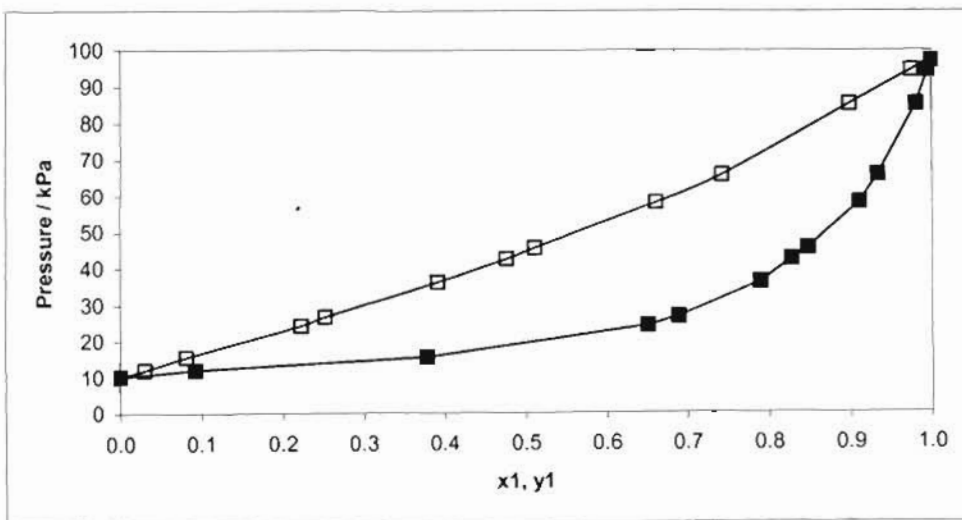


Figure 6-16: P-x-y Phase diagram for Propionic Acid (1) + Hexanoic Acid (2) at 413.15 K

6.5 Isobutyric Acid + Hexanoic Acid Systems

Phase equilibria data for isobutyric acid + Hexanoic acid system were measured at 20 kPa, 408.15 K, and 423.15 K. The experimental data are presented in Table 6-8 to 6-10. The GC calibration, x-y, T-x-y, and P-x-y plots are presented in Figure 6-17 to 6-24.

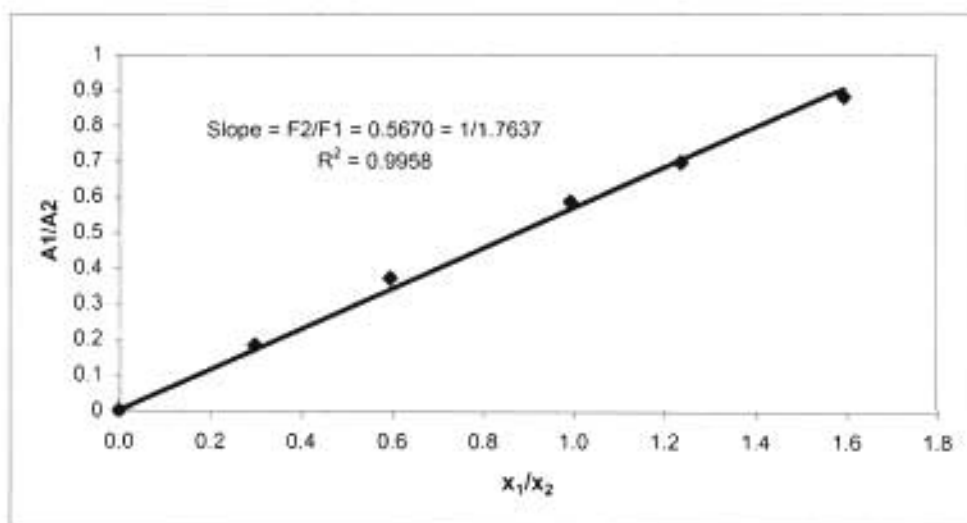


Figure 6-17: GC Calibration for Isobutyric acid (1) + Hexanoic acid (2) system – Hexanoic acid rich region

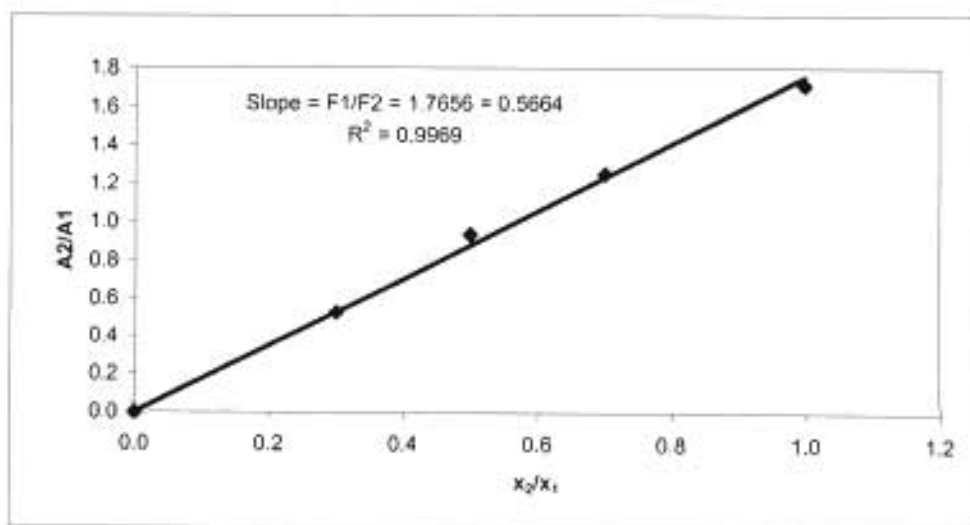


Figure 6-18: GC Calibration for Isobutyric acid (1) + Hexanoic acid (2) system – Isobutyric acid rich region

Table 6-8: Vapour-Liquid Equilibrium Data for Isobutyric Acid (1) + Hexanoic Acid (2) at 20 kPa

T / K	x₁	y₁	T / K	x₁	y₁
380.84	1.000	1.000	409.52	0.322	0.597
382.89	0.945	0.986	413.13	0.252	0.531
389.64	0.744	0.917	419.37	0.150	0.396
393.00	0.637	0.873	423.70	0.081	0.255
396.56	0.558	0.816	427.22	0.033	0.100
405.60	0.390	0.671	430.13	0.000	0.000

Table 6-9: Vapour-Liquid Equilibrium Data for Isobutyric Acid (1) + Hexanoic Acid (2) at 408.15 K

P / kPa	x₁	y₁	P / kPa	x₁	y₁
55.34	1.000	1.000	28.78	0.532	0.768
54.14	0.952	0.984	26.91	0.498	0.745
49.06	0.810	0.940	20.49	0.368	0.631
44.73	0.755	0.907	16.45	0.264	0.547
41.42	0.704	0.880	12.81	0.148	0.416
37.01	0.643	0.843	8.31	0.000	0.000
32.86	0.594	0.811			

Table 6-10: Vapour-Liquid Equilibrium Data for Isobutyric Acid (1) + Hexanoic Acid (2) at 423.15 K

P / kPa	x₁	y₁	P / kPa	x₁	y₁
88.93	1.000	1.000	51.82	0.568	0.777
85.19	0.931	0.975	46.00	0.500	0.726
80.57	0.822	0.944	35.41	0.356	0.613
72.90	0.736	0.886	30.98	0.287	0.555
63.21	0.657	0.841	20.87	0.109	0.308
52.28	0.568	0.781	15.49	0.000	0.000

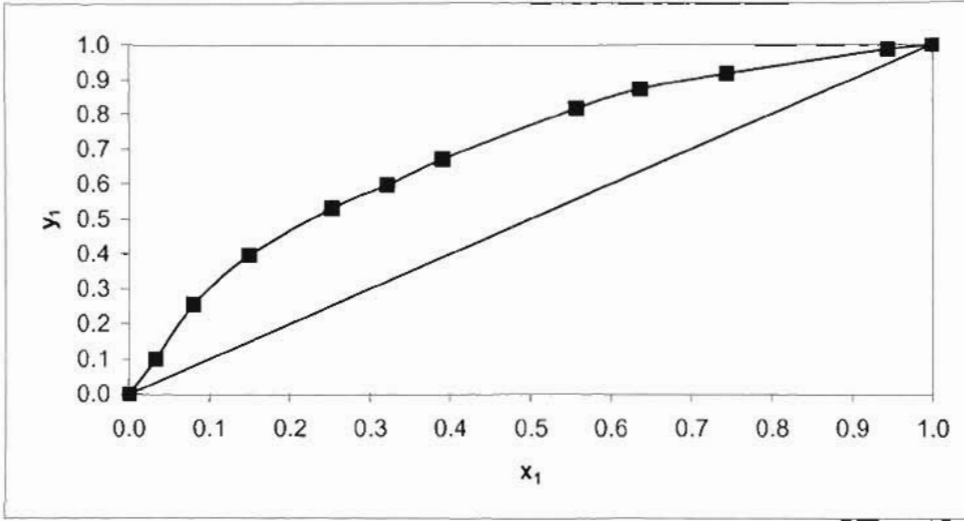


Figure 6-19: x-y Phase diagram for Isobutyric Acid (1) + Hexanoic Acid (2) at 20 kPa

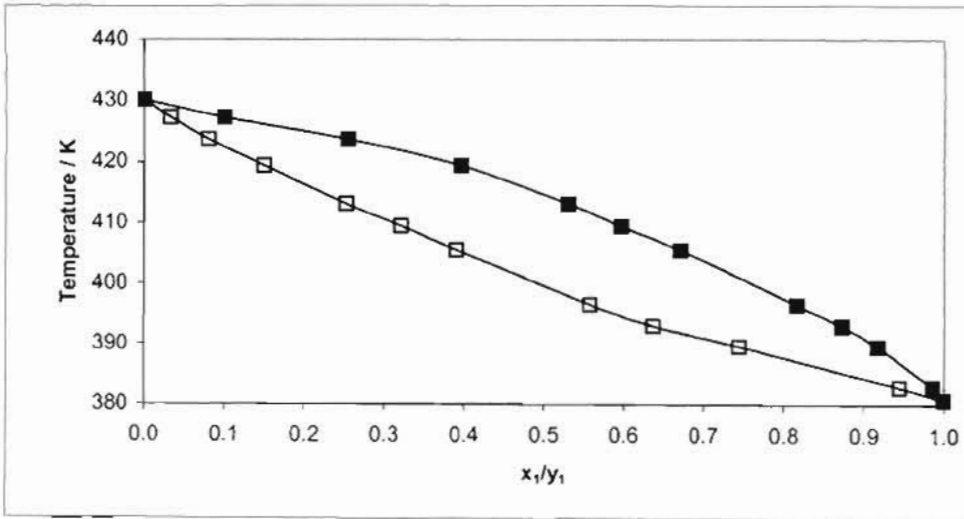


Figure 6-20: T-x-y Phase diagram for Isobutyric Acid (1) + Hexanoic Acid (2) at 20 kPa

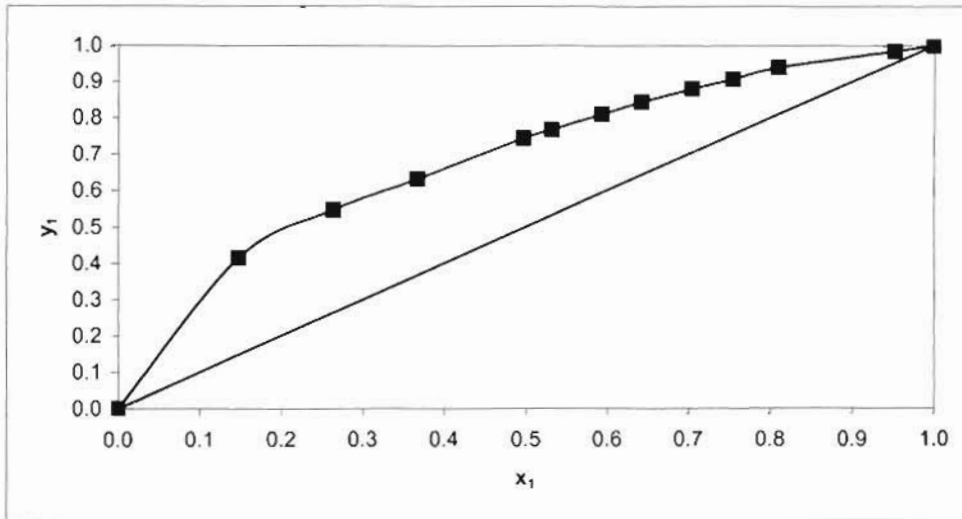


Figure 6-21: x-y Phase diagram for Isobutyric Acid (1) + Hexanoic Acid (2) at 408.15 K

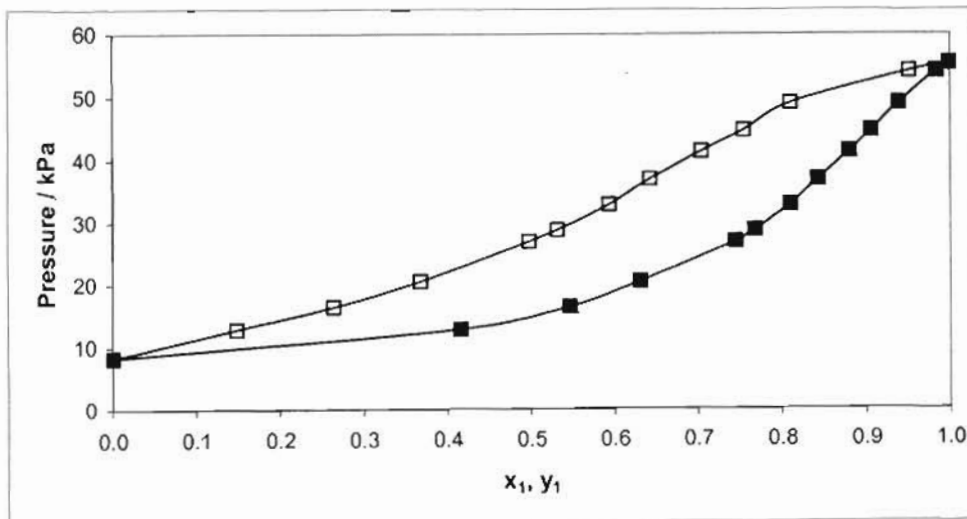


Figure 6-22: P-x-y Phase diagram for Isobutyric Acid (1) + Hexanoic Acid (2) at 408.15 K

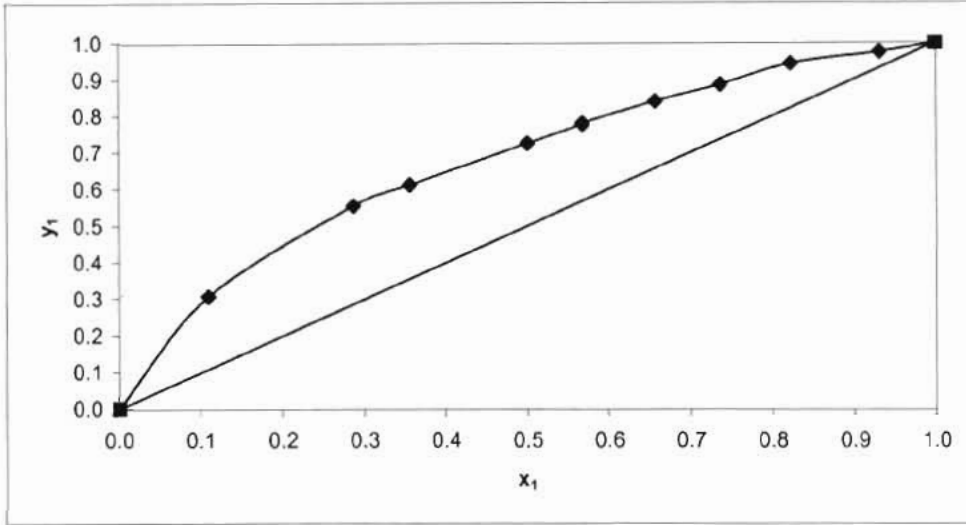


Figure 6-23: x-y Phase diagram for Isobutyric Acid (1) + Hexanoic Acid (2) at 423.15 K

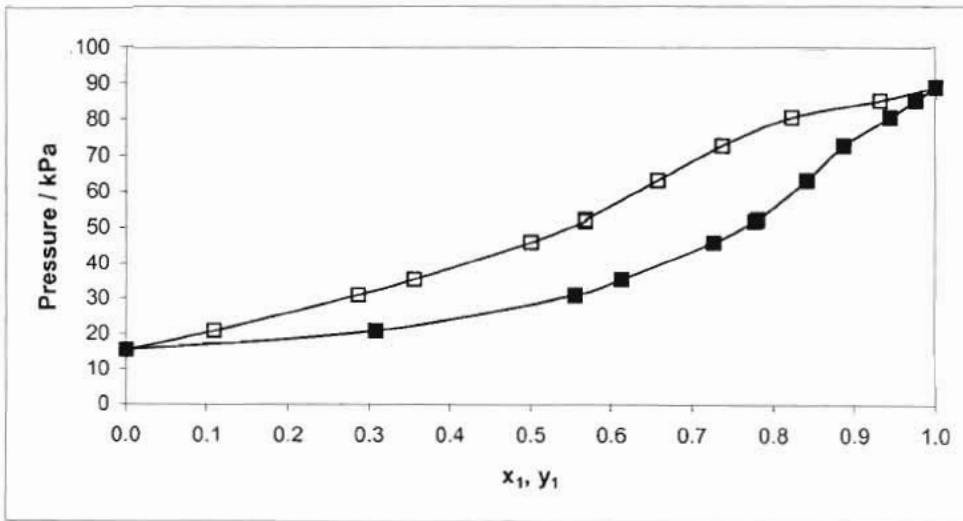


Figure 6-24: P-x-y Phase diagram for Isobutyric Acid (1) + Hexanoic Acid (2) at 423.15 K

6.6 Valeric acid + Hexanoic acid Systems

The Valeric acid + Hexanoic acid system were measured at 15 kPa, 423.15 K and 433.15 K. The experimental data is presented in Tables 6-11 to 6-13. The GC calibration, x-y, T-x-y and P-x-y plots are presented in Figures 6-25 to 6-32.

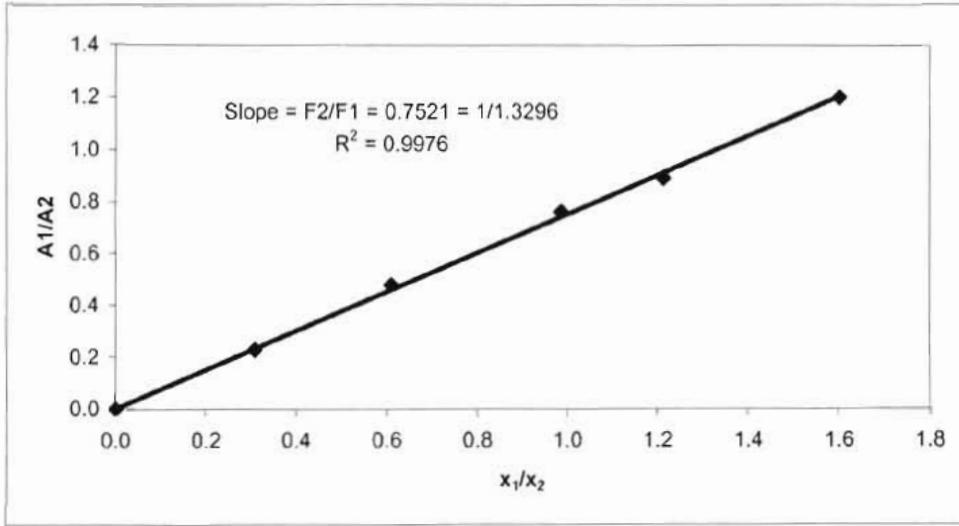


Figure 6-25: GC Calibration for Valeric acid (1) + Hexanoic acid (2) system – Hexanoic acid rich region

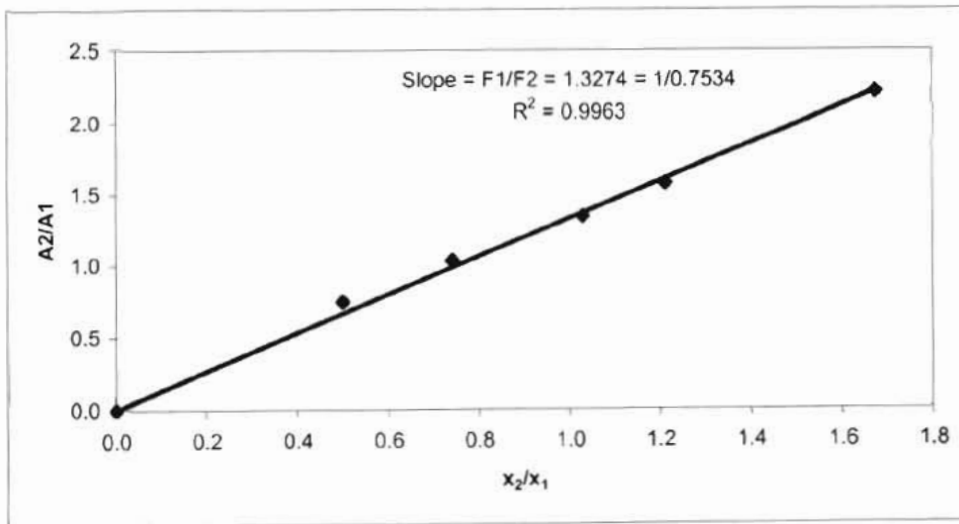


Figure 6-26: GC Calibration for Valeric acid (1) + Hexanoic acid (2) system – Valeric acid rich region

Table 6-11: Vapour-Liquid Equilibrium Data for Valeric Acid (1) + Hexanoic Acid (2) at 15kPa

T / K	x_1	y_1	T / K	x_1	y_1
422.36	0.000	0.000	411.36	0.556	0.685
421.07	0.040	0.068	410.82	0.589	0.713
419.55	0.103	0.169	409.12	0.690	0.792
418.31	0.166	0.263	408.13	0.745	0.841
416.85	0.254	0.371	406.47	0.887	0.930
415.14	0.357	0.473	405.12	0.972	0.983
413.56	0.445	0.570	403.77	1.000	1.000
412.56	0.502	0.620			

Table 6-12: Vapour-Liquid Equilibrium Data for Valeric Acid (1) + Hexanoic Acid (2) at 423.15 K

P / kPa	x_1	y_1	P / kPa	x_1	y_1
15.86	0.000	0.000	23.48	0.567	0.653
16.69	0.070	0.118	24.92	0.639	0.728
17.59	0.141	0.212	25.66	0.682	0.765
18.28	0.202	0.294	26.46	0.733	0.805
19.14	0.275	0.373	28.57	0.848	0.898
20.55	0.384	0.483	29.74	0.908	0.938
21.15	0.422	0.523	30.91	0.968	0.979
22.48	0.507	0.608	31.74	1.000	1.000

Table 6-13: Vapour-Liquid Equilibrium Data for Valeric Acid (1) + Hexanoic Acid (2) at 433.15 K

P / kPa	x_1	y_1	P / kPa	x_1	y_1
45.11	1.000	1.000	32.20	0.476	0.584
44.14	0.940	0.969	31.17	0.414	0.533
42.84	0.903	0.927	28.99	0.277	0.411
41.14	0.847	0.888	27.03	0.184	0.278
38.58	0.756	0.827	25.14	0.109	0.160
37.53	0.709	0.789	23.29	0.031	0.049
35.77	0.639	0.731	22.33	0.000	0.000
34.74	0.591	0.691			

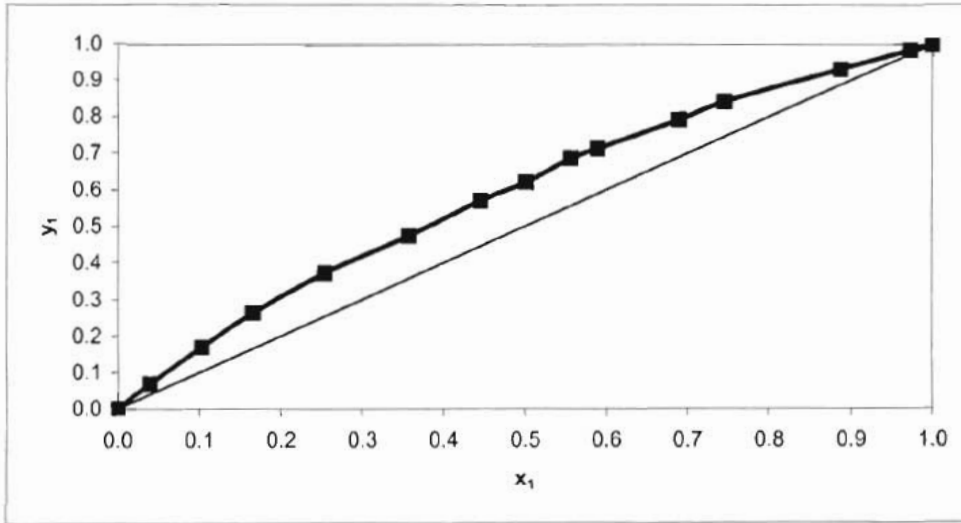


Figure 6-27: x-y Phase diagram for Valeric Acid (1) + Hexanoic Acid (2) at 15 kPa

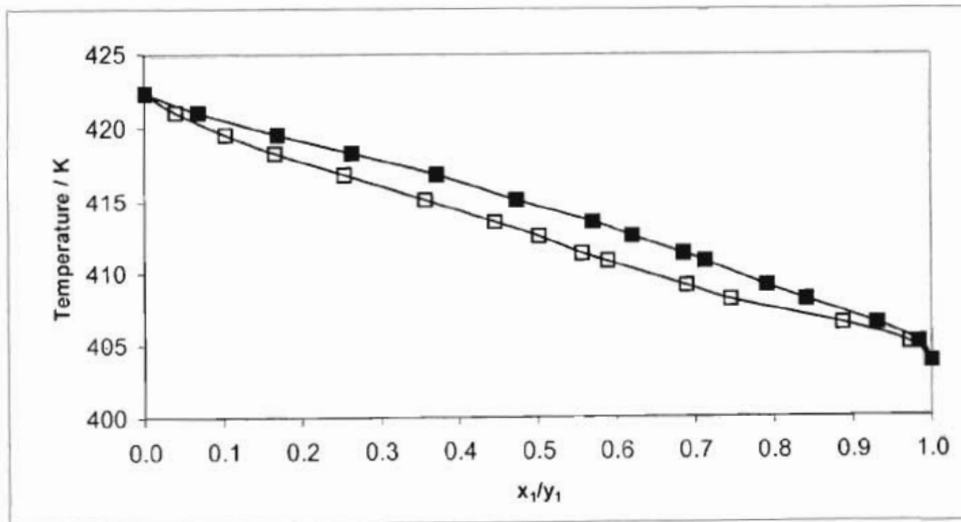


Figure 6-28: T-x-y Phase diagram for Valeric Acid (1) + Hexanoic Acid (2) at 15 kPa

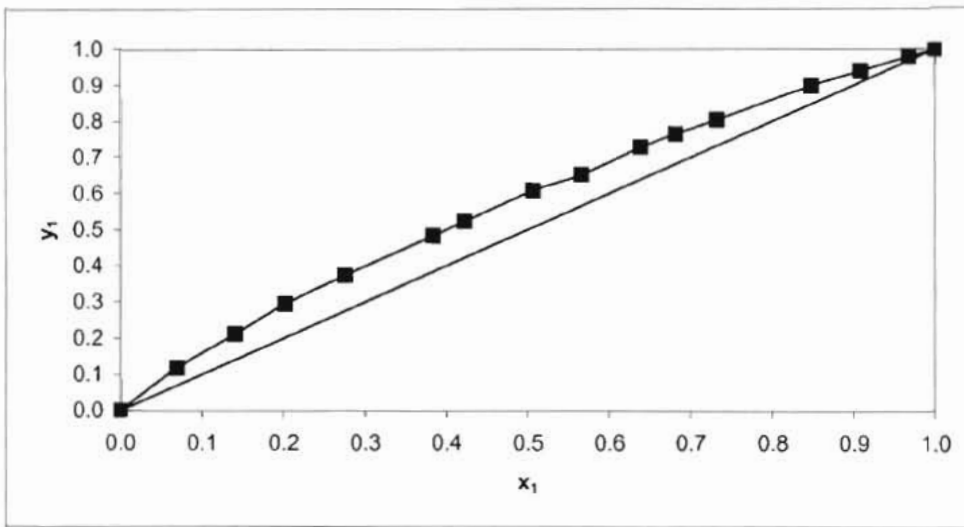


Figure 6-29: x-y Phase diagram for Valeric Acid (1) + Hexanoic Acid (2) at 423.15 K

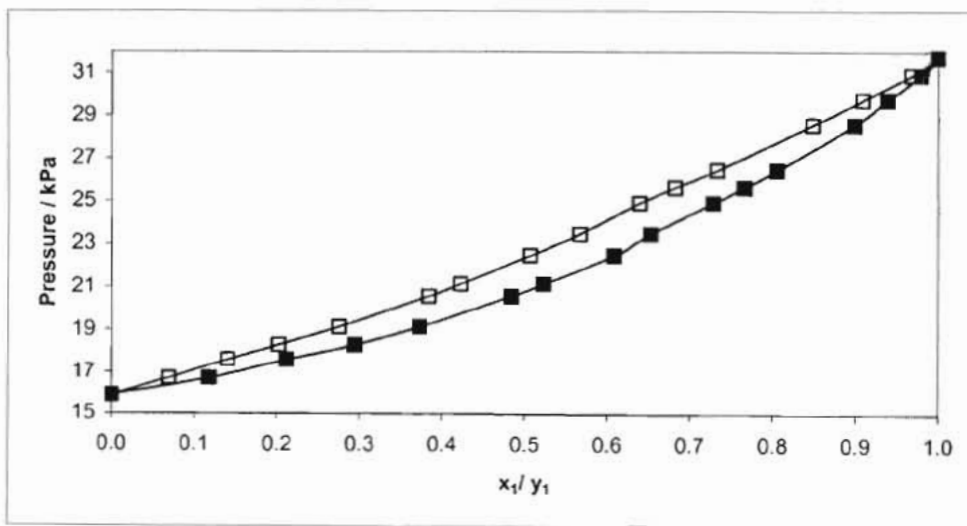


Figure 6-30: P-x-y Phase diagram for Valeric Acid (1) + Hexanoic Acid (2) at 423.15 K

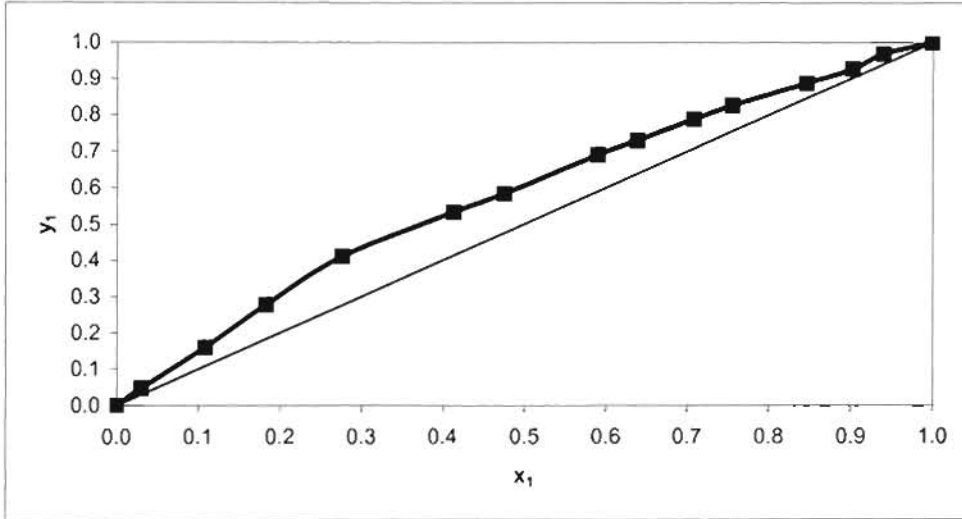


Figure 6-31: x-y Phase diagram for Valeric Acid (1) + Hexanoic Acid (2) at 433.15 K

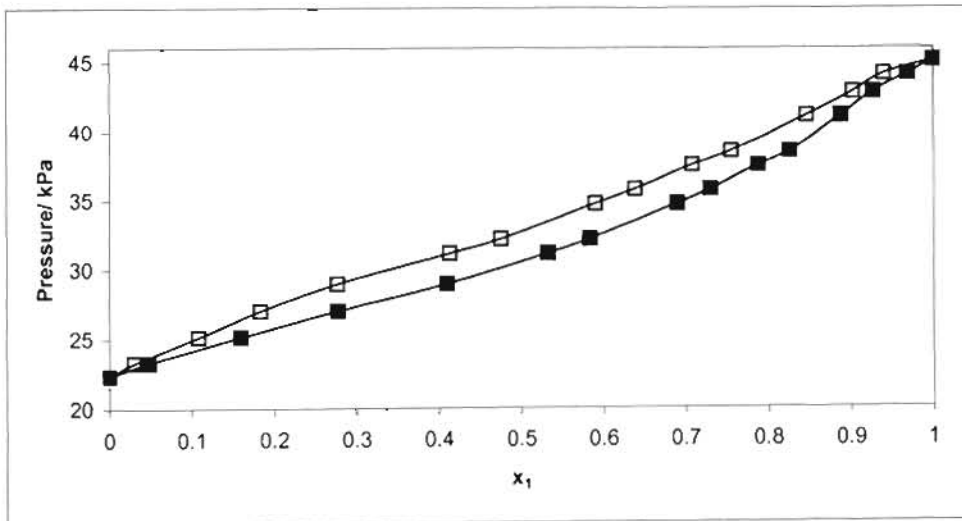


Figure 6-32: P-x-y Phase diagram for Valeric Acid (1) + Hexanoic Acid (2) at 433.15 K

6.7 Hexanoic acid + Heptanoic acid Systems

The experimental data for Hexanoic acid + Heptanoic acid were measured at 10 kPa and 443.15 K. The GC calibration, experimental data, x-y, T-x-y, and P-x-y plots are presented below.

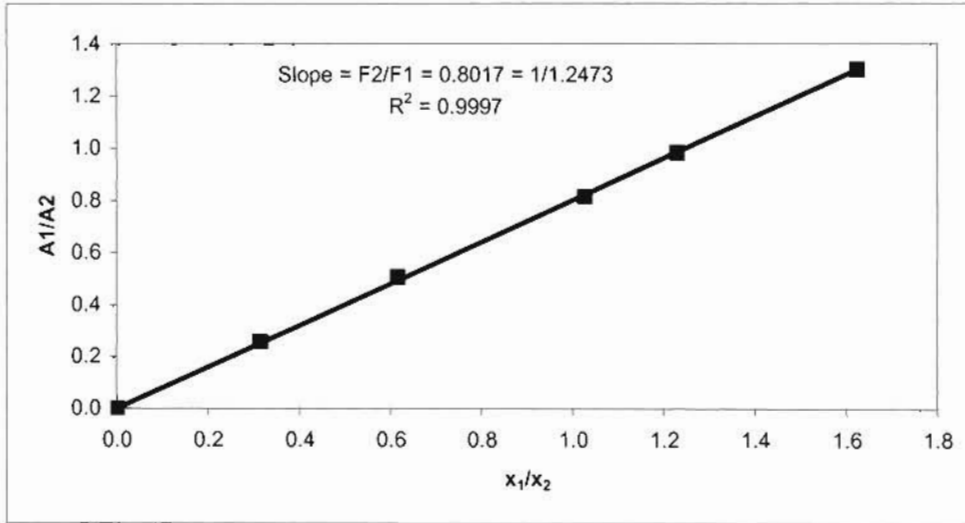


Figure 6-33: GC Calibration for Hexanoic acid (1) + Heptanoic acid (2) system – Heptanoic acid rich region

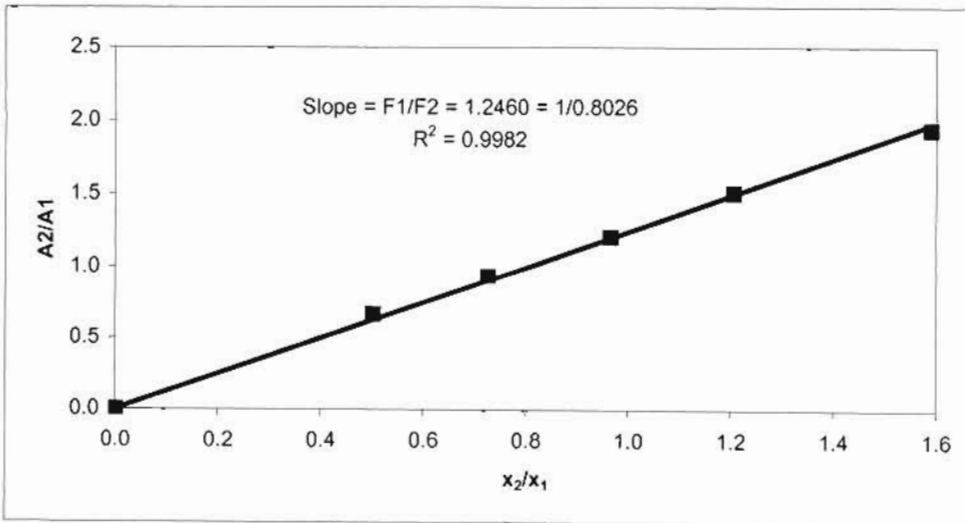


Figure 6-34: GC Calibration for Hexanoic acid (1) + Heptanoic acid (2) system – Hexanoic acid rich region

Table 6-14: Vapour-Liquid Equilibrium Data for Hexanoic Acid (1) + Heptanoic Acid (2) at 10 kPa

T / K	x_1	y_1	T / K	x_1	y_1
427.90	0.000	0.000	419.47	0.493	0.635
426.63	0.051	0.088	418.79	0.545	0.693
425.67	0.104	0.162	416.45	0.742	0.867
425.04	0.135	0.209	415.18	0.875	0.955
424.44	0.164	0.258	414.09	0.971	0.986
422.36	0.302	0.432	412.96	1.000	1.000

Table 6-15: Vapour-Liquid Equilibrium Data for Hexanoic Acid (1) + Heptanoic Acid (2) at 443.15 K

P / kPa	x_1	y_1	P / kPa	x_1	y_1
18.65	0.000	0.000	25.97	0.504	0.604
19.11	0.037	0.074	27.95	0.638	0.722
20.01	0.085	0.153	29.83	0.741	0.806
20.74	0.139	0.212	30.98	0.803	0.864
21.48	0.197	0.286	31.91	0.870	0.905
22.71	0.285	0.394	32.21	0.901	0.915
23.65	0.351	0.465	32.78	1.000	1.000
24.61	0.412	0.514			

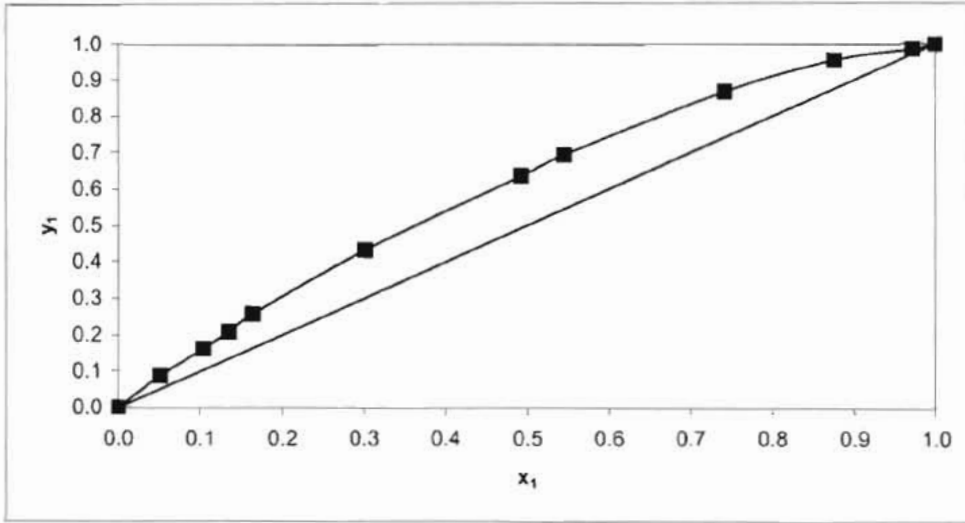


Figure 6-35: x-y Phase diagram for Hexanoic Acid (1) + Heptanoic Acid (2) at 10 kPa

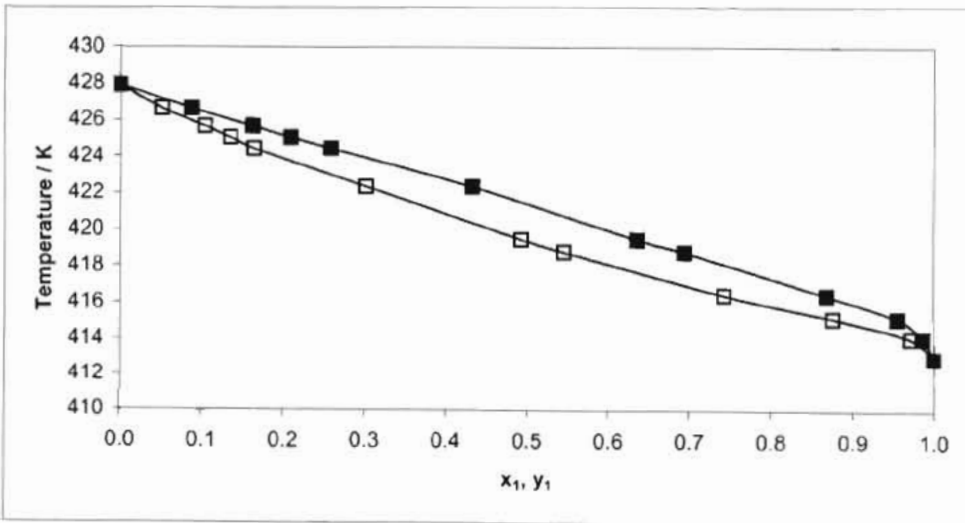


Figure 6-36: T-x-y Phase diagram for Hexanoic Acid (1) + Heptanoic Acid (2) at 10 kPa

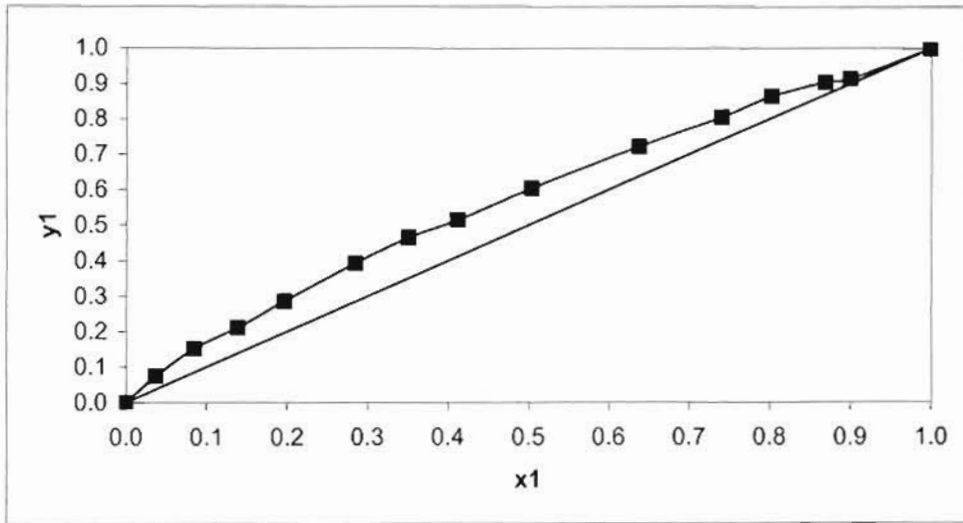


Figure 6-37: x-y Phase diagram for Hexanoic Acid (1) + Heptanoic Acid (2) at 443.15 K

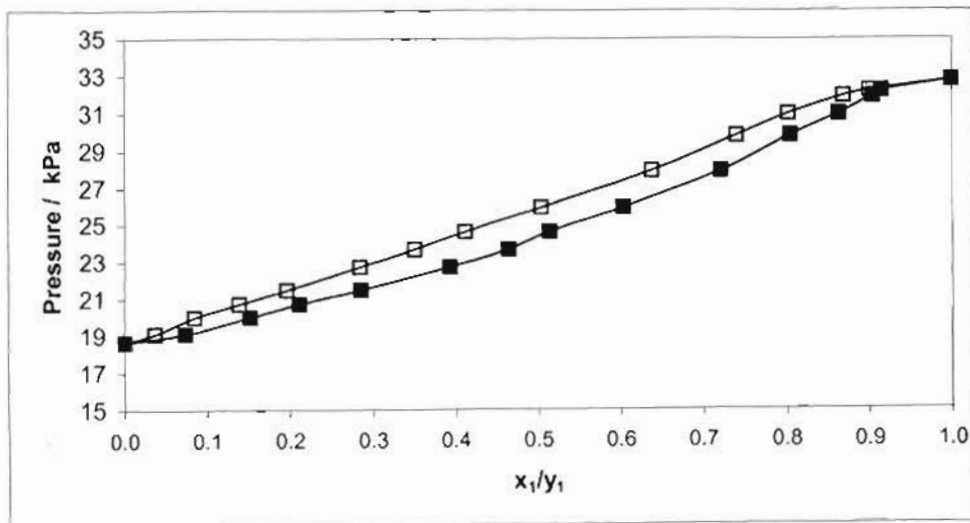


Figure 6-38: P-x-y Phase diagram for Hexanoic Acid (1) + Heptanoic Acid (2) at 443.15 K

DISCUSSION

7.1 Introduction

The theory of low-pressure VLE employed in the reduction and thermodynamic consistency testing of experimental data are reviewed in Chapter Three. This chapter deals with the discussion of the regressed data from both the combined and direct methods.

7.2 Pure Component Properties

Pure component properties are critical in thermodynamic data analysis as certain equations are sensitive to these properties (e.g. acentric factor as explained by Reid et al. (1988)). The critical temperature, critical pressure, critical volume and critical compressibility factors of the components used in this study were obtained from the Dortmund Data Bank. Dipole moments were obtained from the compilation by Reid et al. (1988). No values of the mean radius of gyration for the carboxylic acids were found in open literature. The values were determined using the group contribution method proposed by Reid et al. (1977). The acentric factors for propionic acid and isobutyric acid were obtained from the Korean Data Base. The values for valeric acid, hexanoic acid and heptanoic acid were calculated by the method proposed by Pitzer et al. (1955). The methods used to determine the acentric factor and mean radius of gyration are discussed in Chapter Three. The pure component property values used in the regression of the data are available in Appendix B.

7.3 VLE Data Reduction

VLE data reduction allows large amounts of data to be summarised comprehensively and compactly. It allows accurate interpolation of data and one can extend binary VLE data to predict multi-component VLE data. Predictive VLE methods may be refined from VLE data reduction. Chapter 3 discusses the different VLE data reduction methods pertinent to this work.

For the combined (γ - ϕ) method, the VLE data were correlated using three liquid-phase activity coefficient models namely, Wilson, NRTL and Uniquac equations. The vapour phase non-ideality was accounted for by two methods. The Pitzer-Curl correlation (Pitzer and Curl [1957]) was used to calculate the second virial coefficients of the carboxylic acids, (Appendix B, Tables B-5 to B-8), which were then used to calculate the fugacity coefficients of the carboxylic acids. The Hayden and O'Connell correlation (Hayden and O'Connell [1975]) incorporating chemical theory to gas phase non-ideality was used to calculate the fugacity coefficients.

The Peng-Robinson equation of state (Peng and Robinson [1976]) in conjunction with the Twu and Coon mixing rule (Twu et al. [1996]) was used in the direct method. Bubblepoint pressure and bubblepoint temperature iterations were used for the VLE data regression. Figures of the iteration algorithms are in Appendix A, Section A.4.

The regression programs were written in MATLAB. The Marquardt optimisation function (Marquardt [1963]) was used for regressing the VLE data for the cyclohexane + ethanol system. The built-in MATLAB optimisation function *fminsearch* was utilised in the data reduction of the carboxylic acids. The objective function in the regression programs was either pressure or temperature for the isotherms and isobars respectively.

7.4 Cyclohexane (1) + ethanol (2) system

The data for the chosen test system is presented in Chapter 6. The system has been used many times in the laboratory, (Joseph [2001], Soni [2004] and Clifford [2004]), as it exhibits non-ideal behaviour and high relative volatilities in the dilute regions. The system was used to check the equipment functionality and the experimental technique being employed to measure the VLE data. The data obtained for the test system was checked with reliable literature data of Joseph (2001). It is clear from Figures 6-3 to 6-6 that the data matches that of literature exceedingly well.

All the models used to regress the test system fitted the data well. From Table 7-1, it is evident that the Wilson model provides the best fit for the data while the Uniquac is the least accurate. From these results it was possible to conclude that the equipment worked well and the experimental technique was accurate. The phase diagrams for the 40 kPa isobar are in Appendix C. A comparison of the experimental activity coefficient and those calculated by each of the models is given in Figure 7-3. The Wilson and NRTL equations proved to be the best fit for the activity coefficients. The calculated Uniquac activity coefficients differ slightly from the experimental ones in the dilute region. One would expect the Uniquac equation to correlate the cyclohexane + ethanol data best because of its complexity. Walas (1985) proposes α_{12} values between -1 and 0.5 with the arbitrary value of 0.4 being recommended for organic mixtures. The α_{12} parameter regressed at the two different conditions is very similar (0.486 at 323.15 K and 0.480 at 40 kPa). The observed results agree with those of other experimentalist.

Table 7-1: Model parameters and deviations between calculated and experimental vapour phase, pressure and temperature for cyclohexane (1) + ethanol (2) system

Equation	323.15 K	40 kPa
Wilson		
$\lambda_{12} - \lambda_{11}$ (J/mol)	1503.419	1904.435
$\lambda_{12} - \lambda_{22}$ (J/mol)	9501.031	8719.511
Average Δy_1	0.009	0.0089
Average del P or del T (kPa/K)	0.25	0.19
RMS $\delta \ln(\gamma_1/\gamma_2)$	0.0391	0.0361
NRTL		
$g_{12} - g_{11}$ (J/mol)	7190.941	6289.519
$g_{12} - g_{22}$ (J/mol)	4441.042	4318.419
α	0.486	0.480
Average Δy_1	0.011	0.007
Average del P (kPa)	0.39	0.20
RMS $\delta \ln(\gamma_1/\gamma_2)$	0.0423	0.0481
UNIQUAC		
$u_{12} - u_{11}$ (J/mol)	4306.101	1754.543
$u_{12} - u_{22}$ (J/mol)	-461.2054	-429.519
Average Δy_1	0.024	0.011
Average del P (kPa)	0.64	0.31
RMS $\delta \ln(\gamma_1/\gamma_2)$	0.0934	0.0891

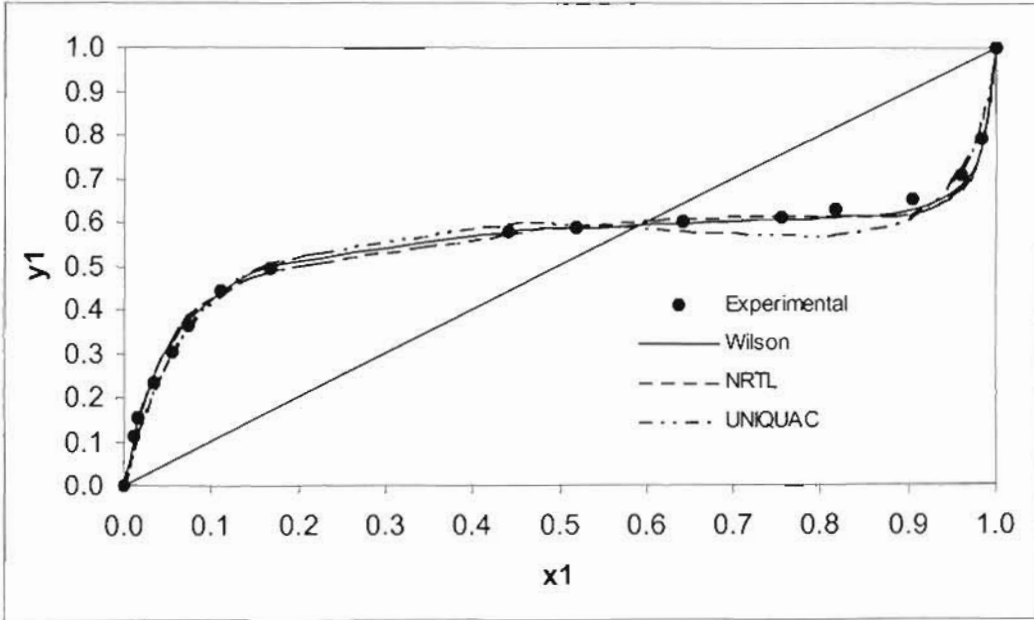


Figure 7-1: Fit of Wilson, NRTL and Uniquac model to x-y diagram of cyclohexane (1) + ethanol (2) system at 323.15 K

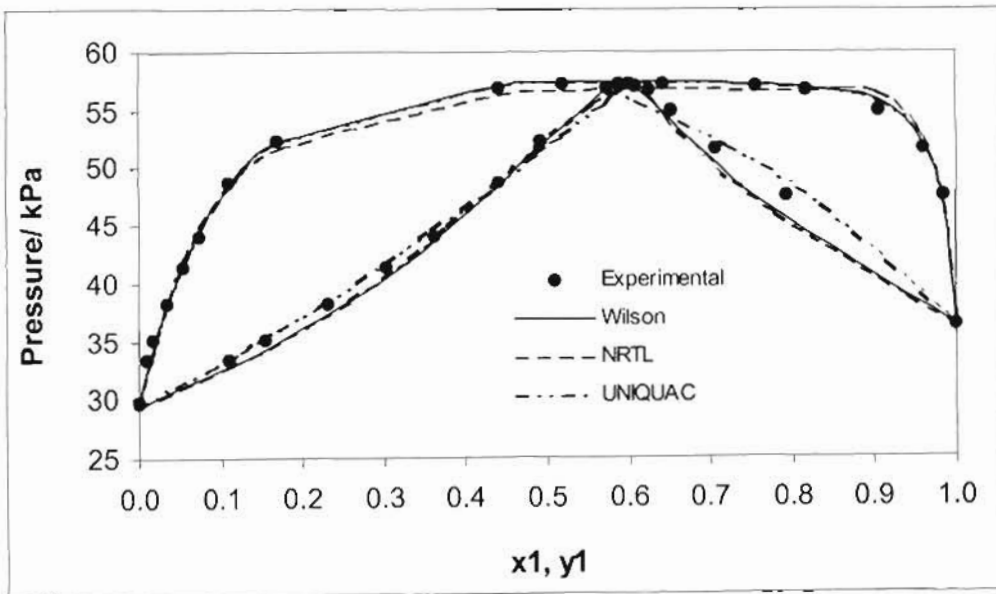


Figure 7-2: Fit of Wilson, NRTL and Uniquac model to P-x-y diagram of cyclohexane (1) + ethanol (2) system at 323.15 K

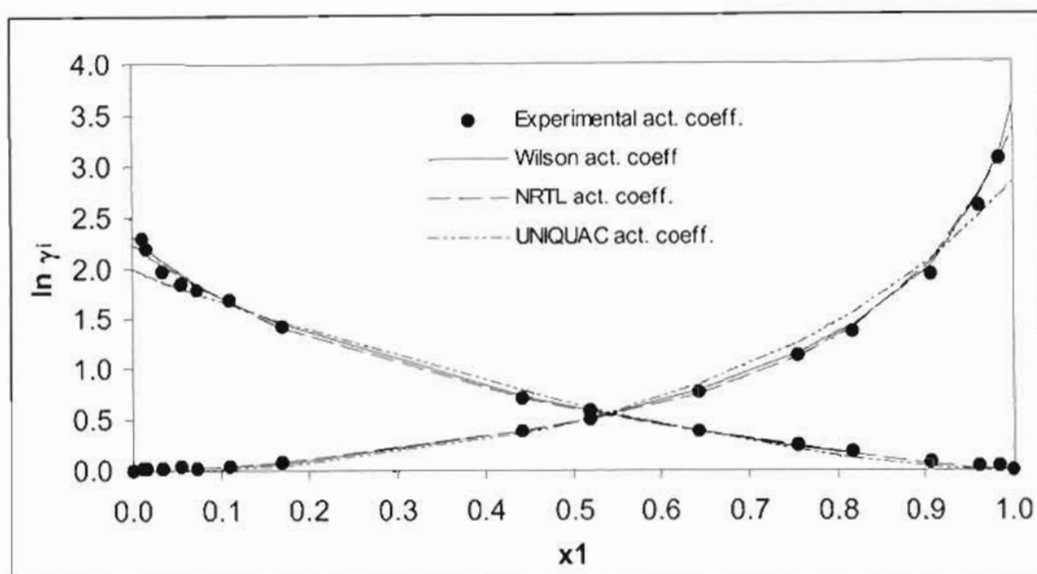


Figure 7-3: Comparison between the experimental activity coefficients and those calculated from the Wilson, NRTL and Uniquac model for the cyclohexane (1) + ethanol (2) system at 323.15 K

7.5 Carboxylic Acid Systems

The experimental results of the binary carboxylic acid systems measured are presented in Chapter 6. In total 12 sets of VLE data were measured. In Chapter Two a detailed discussion of carboxylic acid dimerisation is presented. A binary mixture of carboxylic acids is “macroscopically” a five-component system consisting of 2 monomers, 2 homodimers and 1 heterodimer (Malijevska et al. [1984]). Prausnitz et al. (1980), Kato et al. (1989), and Klekers et al. (1968) state that carboxylic acids dimerise even at low pressures. The extent of dimerisation depends on the temperature and pressure of the system (Klekers et al. [1968]). Below atmospheric pressure higher polymers do not appear to be present in the vapour phase to any significant extent (Pimental et al. [1960]). Prausnitz et al. (1980) also states that dimerisation decreases as pressure falls as a direct consequence of Le Chatelier’s principle.

A number of observations can be drawn from examination of the experimental data shown in Figures 6-9 to 6-38. All the P-x-y or T-x-y phase diagrams exhibit an “S” sigmoidal shape. The isobutyric acid + hexanoic acid system has the most prominent “S” shape. Alpert et al. (1949) Klekers et al. (1968), Kato et al. (1990), Sewnarain (2001) and Clifford (2004) observed similar “S” shaped phase diagrams for the binary carboxylic acid systems they measured. The phase envelopes narrow in the dilute regions. Tamir et al. (1975) states that dimerisation effectively

narrows the phase diagrams of associating substances. The measured binary systems by Tamir et al. (1975), Kato et al. (1990) and Sewnarain (2001) exhibit the narrowing effect very well. Both the "S" shape and narrowing effect is more pronounced in the high-pressure regions of the isothermal phase diagrams. This agrees with the observation by Klekers et al. (1968), Malijevaska et al. (1984) and as stated by Prausnitz et al. (1980).

From the experimental data for all the systems measured, it is observed that the phase envelopes broaden as the temperature rises. The phase envelopes maintain the same shape though for a particular system. The x-y curves get closer to the 45° line with increase in temperature. Comparing the four binary systems, it is readily noticeable that all the phase envelopes become narrow as the difference on the carbon number between the compounds in the binary system decreases (Figures 7-6 to 7-68). As the difference in carbon number decreases, the difference in the volatilities/ of the pure components decreases. The x-y curves become flatter and closer to the 45° line as the volatility decreases. These differences are most likely a result of the varying chain lengths of the carboxylic acids. This observation is consistent with that of Kato et al. [1990] who measured data for formic acid + acetic acid and formic acid + propionic acid.

7.5.1 Alpha Functions

Many methods have been proposed for calculating the alpha function for cubic equations of state in the direct method of VLE data regression. The alpha function is used to calculate the a parameter in the cubic equation of state, in this case the Peng-Robinson (1976) equation. Most of the alpha functions proposed by different authors make use of the acentric factor in the calculation procedure. The acentric factor is a parameter that characterises the non-sphericity of a molecule. The acentric factors for carboxylic acids are large as compared to those of other organic molecules. This is expected from the definition of acentric factor. Reid et al. (1988) states that the acentric factor is used to measure the complexity of a molecule with respect to geometry and polarity. The use of the Peng-Robinson (1976) alpha function (Equation 3-131) proved to be rather inaccurate: Stryjek and Vera (1986) concluded from their studies that the Peng-Robinson (1976) method introduced large errors at all temperatures for compounds with large acentric factors like carboxylic acids. Stryjek and Vera went on to propose their modified form for the alpha function. Twu and Coon (1991) developed a correlation for alpha that superseded that of Stryjek and Vera (1986) and hence it was used in this project. The Twu and Coon (1991) function has three parameters, L' , M' and N' . The L' , M' and N' parameters are obtained by regression of the pure component vapour pressures using an applicable equation of state. The objective function used in the regression of these parameters is pure component vapour pressure. The L' , M' and N' parameters for propionic acid, isobutyric acid, valeric acid,

hexanoic acid and heptanoic acid are presented in Appendix B. The NRTL equation was used with the mixing rule for the Twu and Coon alpha function.

7.5.2 Activity Coefficients

The experimental activity coefficients calculated are inconsistent with the normal trends expected for binary systems. Figure 7-4 shows the calculated activity coefficients for the propionic acid + hexanoic acid system. Experimental activity coefficients are calculated from Equation 3-8, after making γ_i the subject of the formula.

$$\gamma_i = \frac{y_i \Phi_i P_{ex}}{x_i P_i^{sat}} \quad (3-8)$$

The fugacity coefficient term, Φ_i , is calculated from second virial coefficients as discussed in Section 3.3. In most of the systems the activity coefficients were very close to unity and would not intersect. Alpert et al. (1949), Tamir and Wisniak (1975), Miyamoto et al. (2001) and Clifford (2004) observed similar behaviour. Alpert (1949) measured VLE data for formic acid + acetic acid at 760.00 mmHg. He observed γ_1 values increasing from 0.85 to 0.98 and γ_2 values increasing from 1.07 to 1.46. The curves were close to unity and did not intersect. Miyamoto et al. (2001) measured eleven carboxylic acid systems and reports experimental activity coefficients close to unity. The unusual curves of the experimental activity coefficients are as a result of the strong association that occurs in carboxylic acids. The hydrogen bonding causes dimerisation in both the liquid and the vapour phases. Applying chemical theory to the liquid phase may account for this effect. Prausnitz et al. (1999) proposes activity coefficients models for a binary mixture of an associating component with one that does not associate. No activity coefficient models incorporating chemical theory were found in literature for a binary mixture of associating components. Professors Raal and Ramjugernath (University of Kwa-Zulu Natal, Thermodynamics Research Unit) are currently working on developing activity coefficient models incorporating chemical theory for a binary mixture of carboxylic acids. Thermodynamic consistency tests could therefore not be done using the Van Ness (1995) direct test based on residual activity coefficient values.

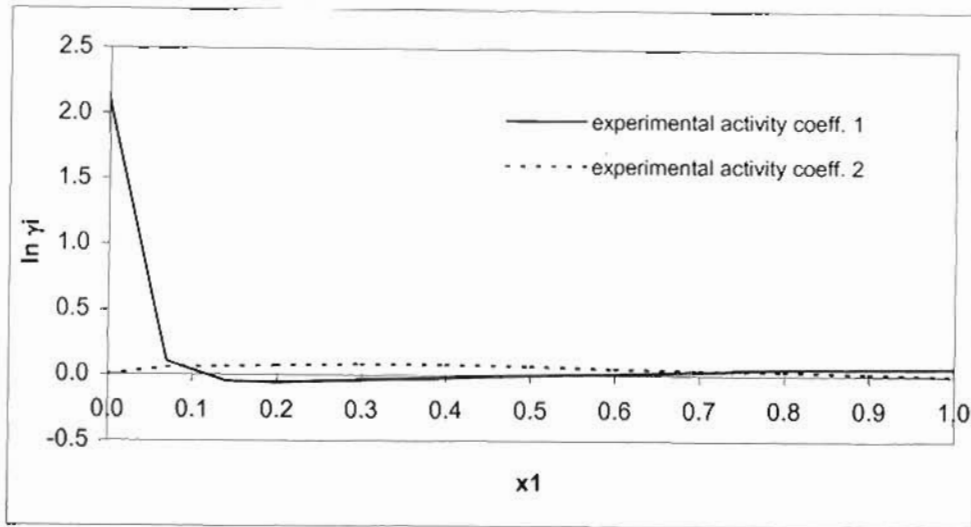


Figure 7-4: Liquid-phase activity coefficients calculated from measured data for propionic acid (1) + hexanoic acid (2) system at 408.15 K

7.6 Propionic Acid + Hexanoic Acid Systems

Table 7-2 shows the best-fit models for the propionic acid + hexanoic acid system. The results of the VLE data reduction for the system are given in Tables 7-3 to 7-5. The propionic acid + hexanoic acid system looks remarkably ideal apart from the narrow ends. The “S” shape is not as pronounced in all the phase diagrams of the propionic acid + hexanoic acid systems. The fact noteworthy is that there is a large difference between the number of carbon atoms in propionic acid (C_3) and hexanoic acid (C_6). The association effect appears not to be as strong as in the other systems. All the models slightly over predict the vapour composition in the x_2 dilute regions. This is consistent with Le Chatelier’s principle as the pressure is high, increasing dimerisation in the vapour phase. The Peng-Robinson equation of state (Peng and Robinson [1976]) modelled the data well. The point tests results for the Peng-Robinson EOS for the 408.15K isotherm is 0.011. Applying chemical theory to account for vapour phase non-ideality remarkably improves the results as indicated by the point test for thermodynamic consistency as compared to that of the Pitzer-Curl correlation (Pitzer and Curl [1957]). For example the Δy improved from 0.033 to 0.022 for the 408.15K isotherm with the Wilson’s equations (Tables 7-4 and 7-5). This is because chemical theory takes into account the dimerisation that occurs in carboxylic acid mixtures. This is indicative that chemical theory is key to understanding the phase behaviour of carboxylic acids. The Wilson equation gave the best fit followed by the NRTL equation. One would expect the NRTL to give better results than the Wilson, because it is a three-parameter model whilst the later is a two-parameter model. The α parameters observed

are rather high (1.01 to 2.78) compared with the range recommended ($-1 < \alpha < 0.5$). The α parameter is a measure of the non-randomness of a solution. The high values observed suggest complex molecular interactions in the solution. As stated previously, carboxylic acids dimerise by forming strong hydrogen bonds in both liquid and vapour phases. The Uniquac equation surprisingly, irrespective of its complexity did not do as well as the other models to fit the data.

Table 7-2: Best fit models for the propionic acid + hexanoic acid system

System	403.15 K	408.15 K	413.15 K	20 kPa
Best Fit	Peng-Robinson	Peng-Robinson	Wilson (CT)	Peng-Robinson

CT = chemical theory PC = Pitzer-Curl

Table 7-3: Model parameters and deviations between calculated and experimental vapour phase and pressure/ temperature using the Peng-Robinson EOS and the Twu & Coon mixing rule for the Propionic acid + Hexanoic acid system.

Equation	403.15 K	408.15 K	413.15 K	20 kPa
Peng-Robinson				
$G_{12} - g_{11}$ (J/mol)	-15.56	-299.01	-3948.20	8753
$G_{12} - g_{22}$ (J/mol)	-5925.48	-2857.02	329.33	6139.76
α	0.1045	0.3358	0.2784	1.2279
k_{ij}	-0.0364	-0.0325	-0.0375	-0.04993
l_{ij}	-0.0114	-0.0069	0.0068	-0.0056
Average Δy_i	0.016	0.011	0.027	0.028
del P or del T (kPa/K)	1.32	1.10	1.49	0.76

Table 7-4: Model parameters and deviations between calculated and experimental vapour phase and pressure/ temperature using the Pitzer-Curl correlation for the Propionic acid + Hexanoic acid system.

Equation	403.15 K	408.15 K	413.15 K	20 kPa
NRTL				
$g_{12} - g_{11}$ (J/mol)	128.85	506.32	332.60	4213.10
$g_{12} - g_{22}$ (J/mol)	-812.72	-1863.30	-1154.30	-575.68
α	1.0113	1.3176	2.785	1.943
Average Δy_1	0.0445	0.0337	0.0386	0.0379
del P or del T (kPa/K)	0.43	0.53	0.66	0.38
UNIQUAC				
$u_{12} - u_{11}$ (J/mol)	932.10	452.60	211.62	-
$u_{12} - u_{22}$ (J/mol)	-1989.80	-1429.04	-1994.30	-
Average Δy_1	0.038	0.032	0.035	-
del P or del T (kPa/K)	1.48	0.49	2.13	-
Wilson				
$\lambda_{12} - \lambda_{11}$ (J/mol)	1796.02	-342.62	-2316.54	-
$\lambda_{12} - \lambda_{22}$ (J/mol)	-1796.51	-1120.40	2059.41	-
Average Δy_1	0.038	0.033	0.0329	-
del P or del T (kPa/K)	1.37	0.5082	1.89	-

Table 7-5: Model parameters and deviations between calculated and experimental vapour phase and pressure/ temperature using chemical theory for the Propionic acid + Hexanoic acid system.

Equation	403.15 K	408.15 K	413.15 K
UNIQUAC			
$u_{12} - u_{11}$ (J/mol)	1554.50	1334.51	1661.76
$u_{12} - u_{22}$ (J/mol)	-2318.81	-1334.50	-1661.76
Average Δy_1	0.042	0.034	0.037
del P/ (kPa)	1.43	0.06	2.15
Wilson			
$\lambda_{12} - \lambda_{11}$ (J/mol)	-72.93	2300.61	-1849.50
$\lambda_{12} - \lambda_{22}$ (J/mol)	-1961.80	-4152.63	1849.50
Average Δy_1	0.021	0.022	0.026
del P (kPa)	1.43	0.79	1.43

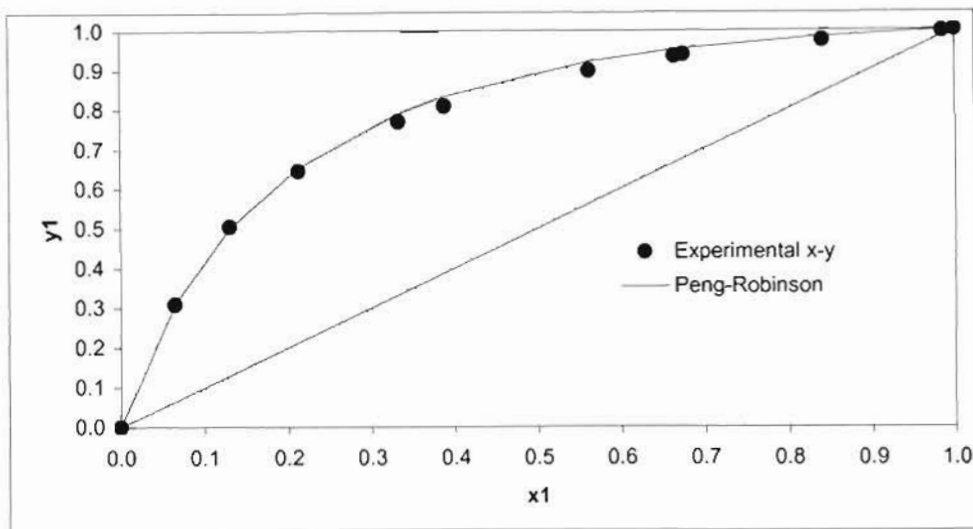


Figure 7-5: Fit of Peng-Robinson EOS to x-y data using the Twu-Coon mixing rule for the propionic acid (1) + Hexanoic acid (2) system at 403.15 K

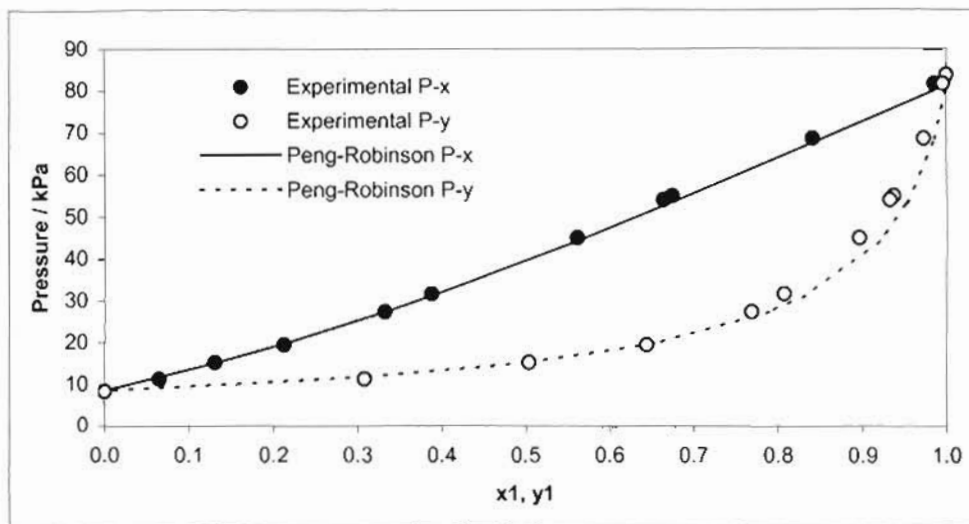


Figure 7-6: Fit of Peng-Robinson EOS to P-x-y data using the Twu-Coon mixing rule for the propionic acid (1) + Hexanoic acid (2) system at 403.15 K

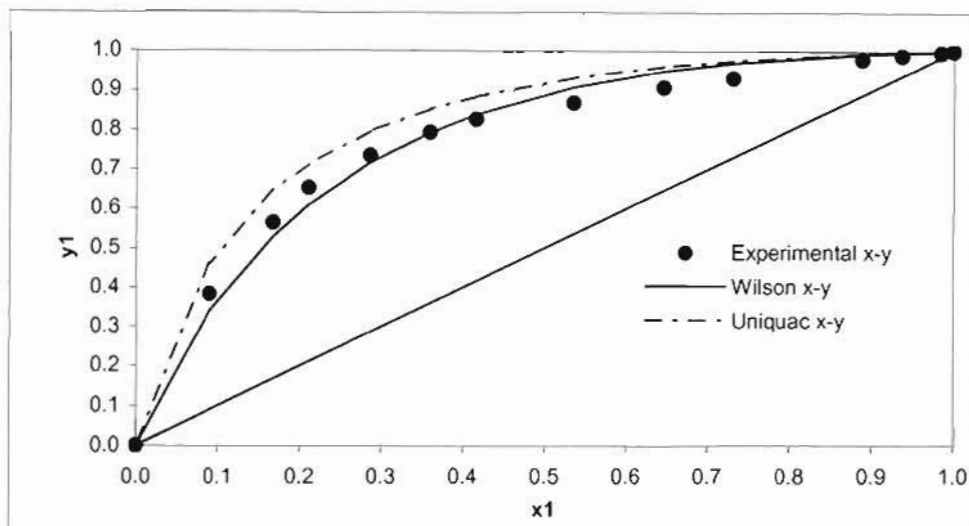


Figure 7-7: Fit of Wilson and Uniquac model to x-y data using chemical theory for the propionic acid (1) + Hexanoic acid (2) system at 403.15 K

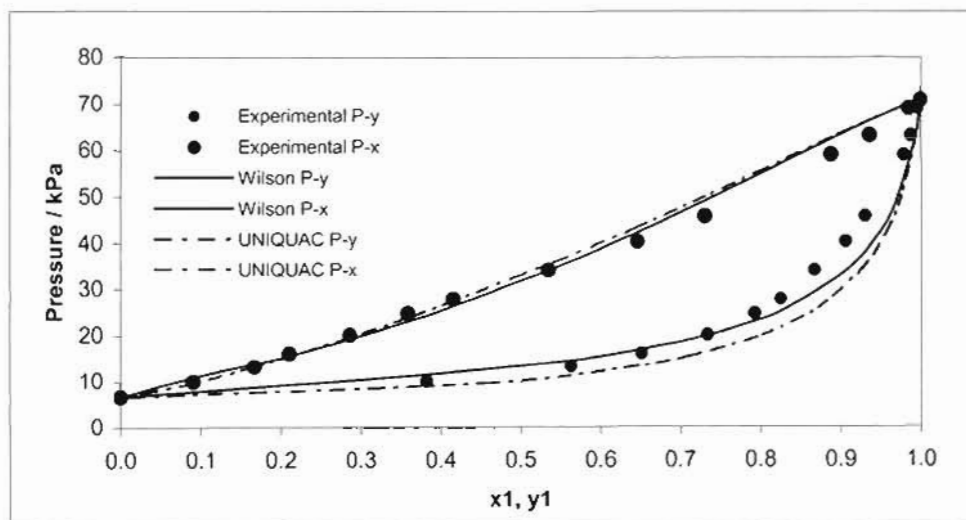


Figure 7-8: Fit of Wilson and Uniquac model to P-x-y data using chemical theory for the propionic acid (1) + Hexanoic acid (2) system at 403.15 K

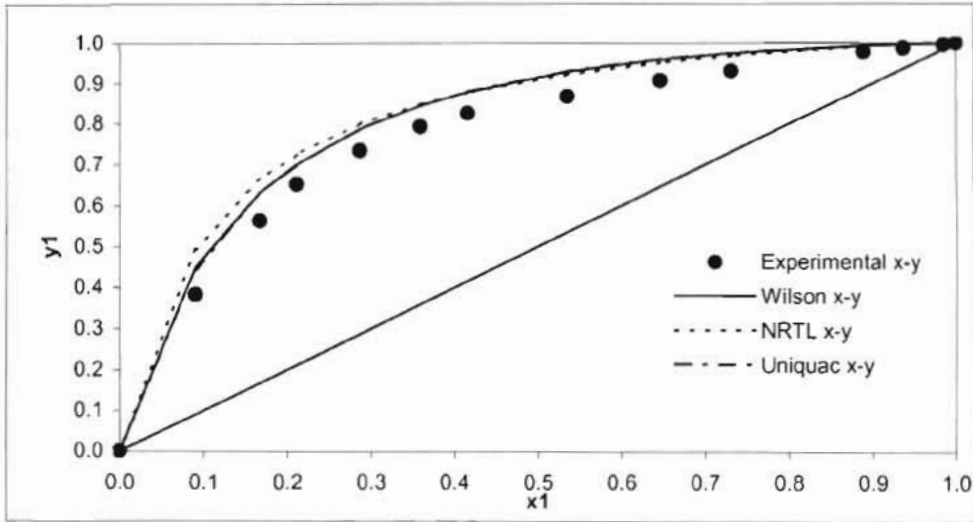


Figure 7-9: Fit of Wilson, Uniquac and NRTL model to x-y data using the Pitzer-Curl correlation for the propionic acid (1) + Hexanoic acid (2) system at 403.15 K

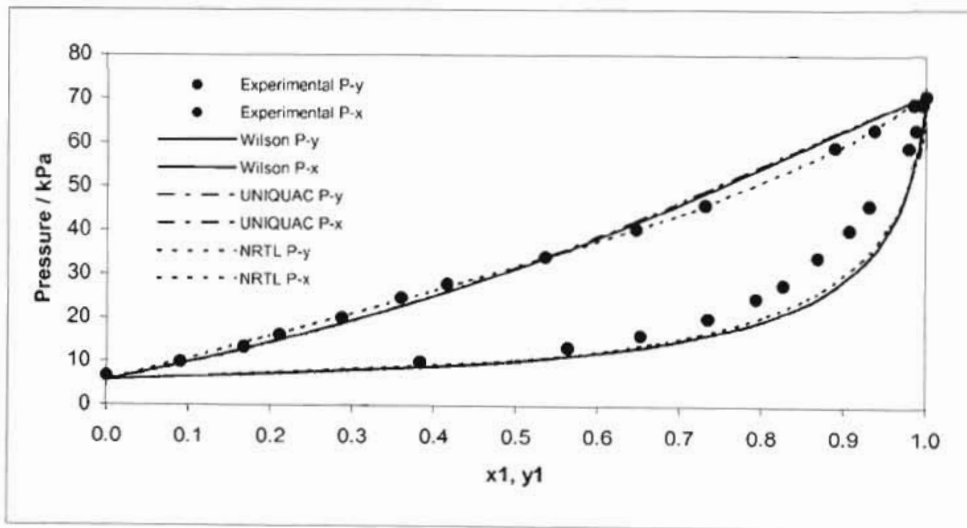


Figure 7-10: Fit of Wilson, Uniquac and NRTL model to P-x-y data using the Pitzer-Curl correlation for the propionic acid (1) + Hexanoic acid (2) system at 403.15 K

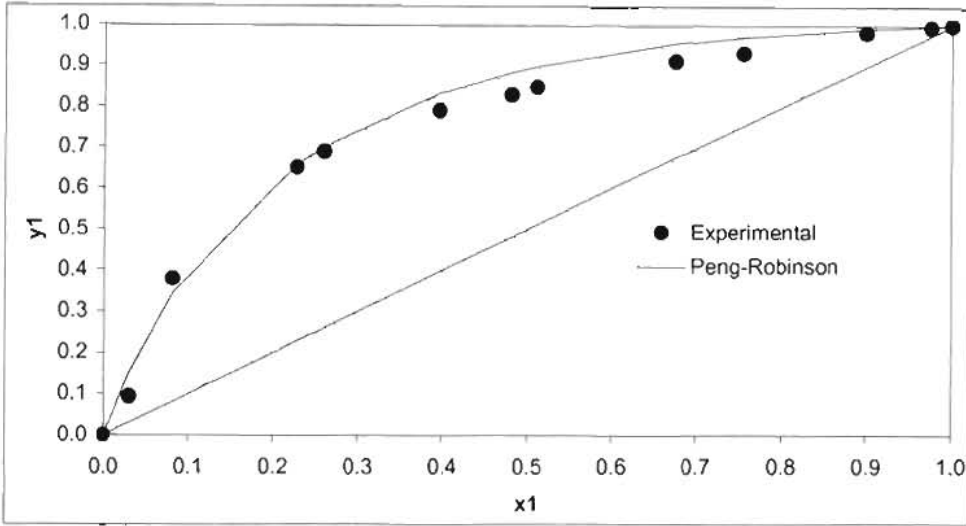


Figure 7-11: Fit of Peng-Robinson EOS to x-y data using the Twu-Coon mixing rule for the propionic acid (1) + Hexanoic acid (2) system at 408.15 K

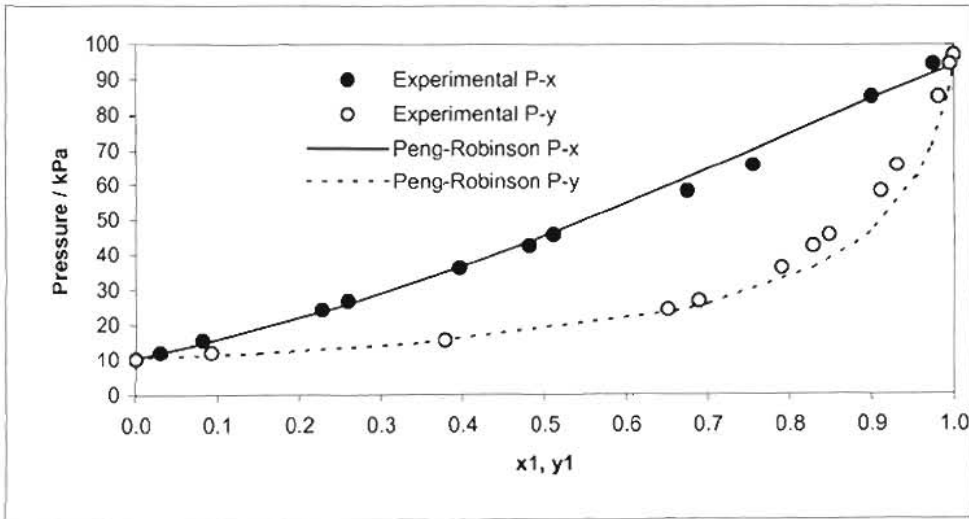


Figure 7-12: Fit of Peng-Robinson EOS to P-x-y data using the Twu-Coon mixing rule for the propionic acid (1) + Hexanoic acid (2) system at 408.15 K

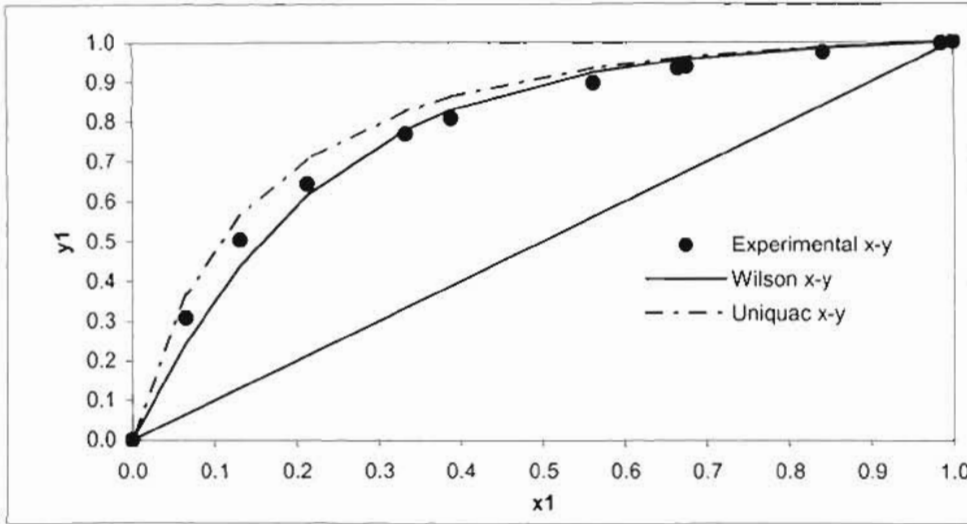


Figure 7-13: Fit of Wilson and Uniquac model to x-y data using chemical theory for the propionic acid (1) + Hexanoic acid (2) system at 408.15 K

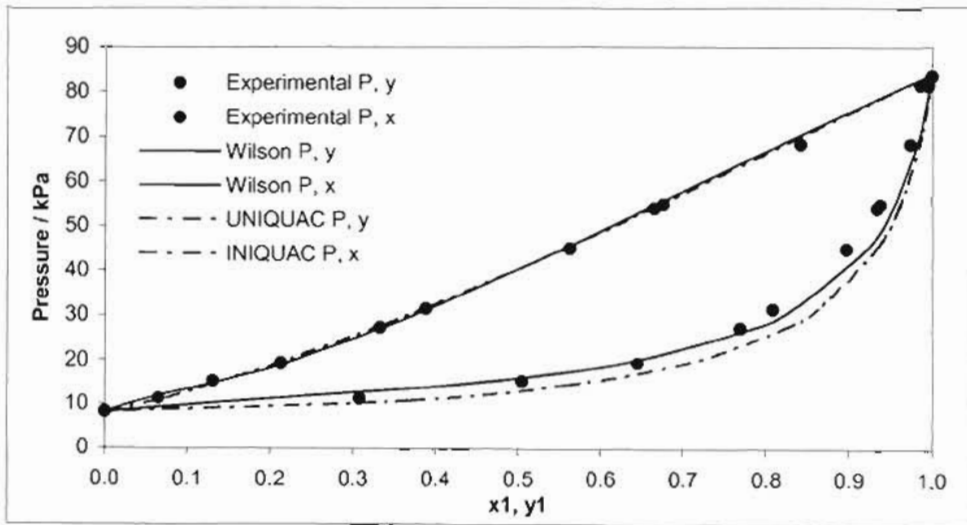


Figure 7-14: Fit of Wilson and Uniquac model to P-x-y data using chemical theory for the propionic acid (1) + Hexanoic acid (2) system at 408.15 K

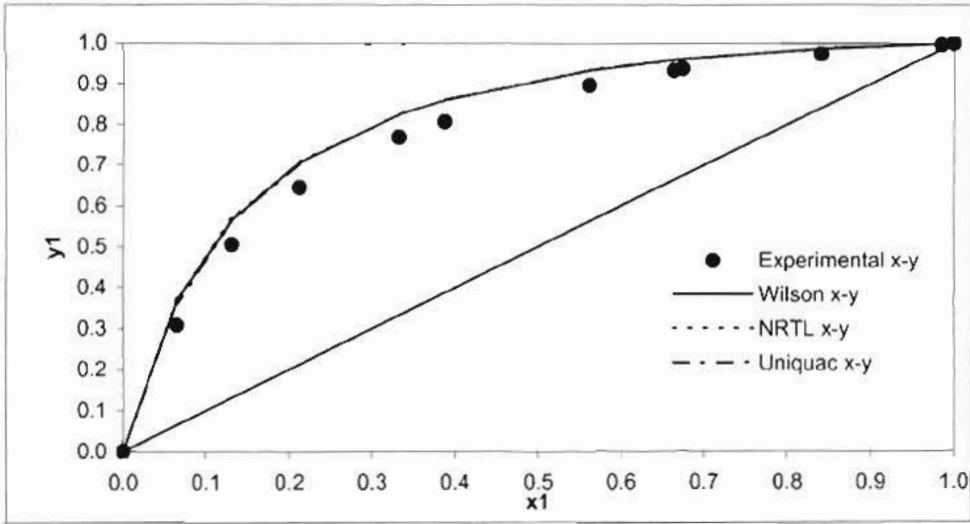


Figure 7-15: Fit of Wilson, Uniquac and NRTL model to x-y data using the Pitzer-Curl correlation for the propionic acid (1) + Hexanoic acid (2) system at 408.15 K

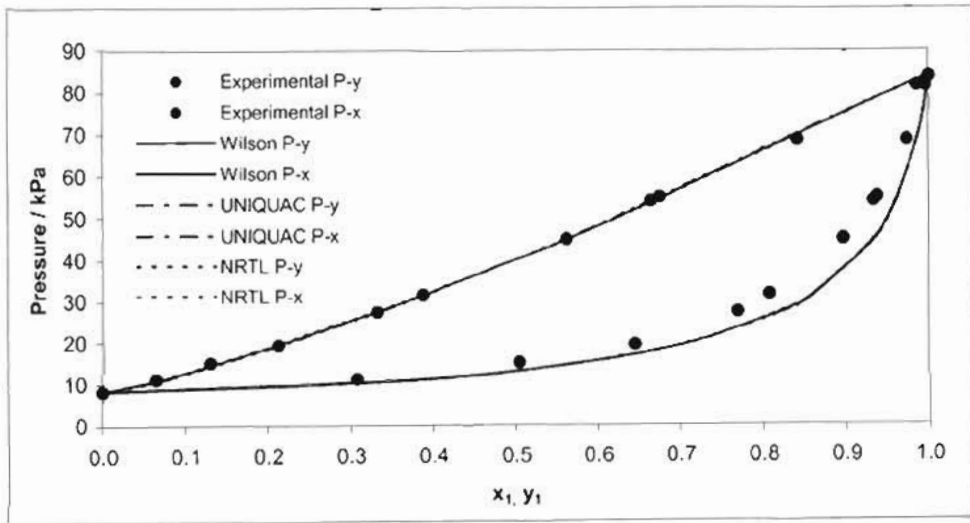


Figure 7-16: Fit of Wilson, Uniquac and NRTL model to P-x-y data using the Pitzer-Curl correlation for the propionic acid (1) + Hexanoic acid (2) system at 408.15 K

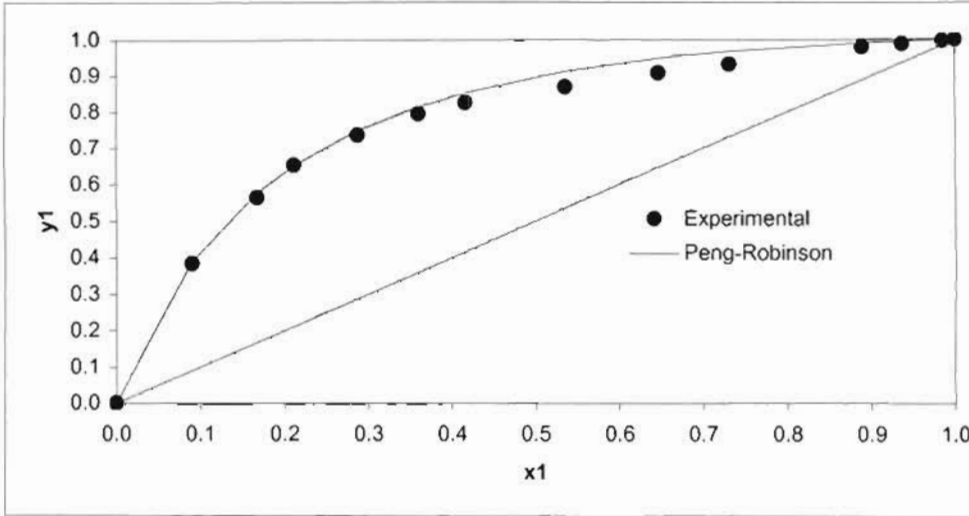


Figure 7-17: Fit of Peng-Robinson EOS to x-y data using the Twu-Coon mixing rule for the propionic acid (1) + Hexanoic acid (2) system at 413.15 K

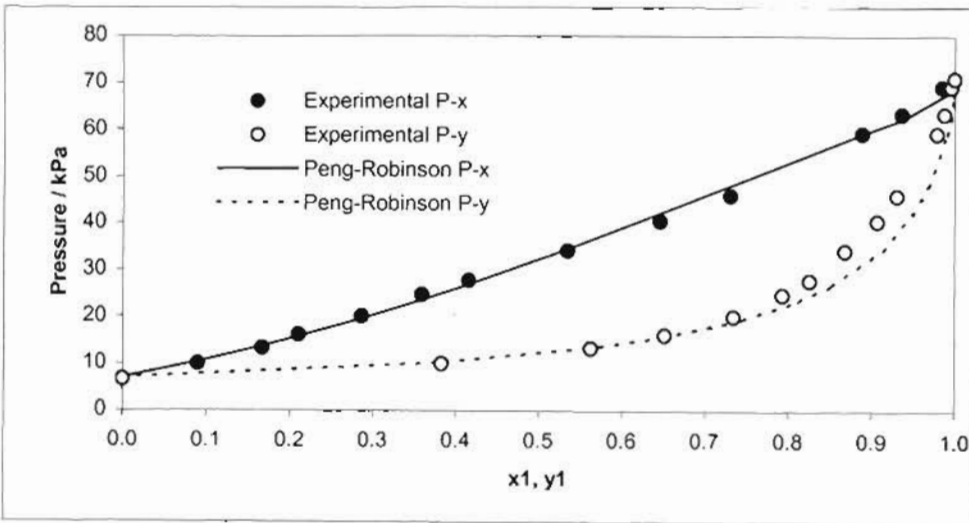


Figure 7-18: Fit of Peng-Robinson EOS to P-x-y data using the Twu-Coon mixing rule for the propionic acid (1) + Hexanoic acid (2) system at 413.15 K

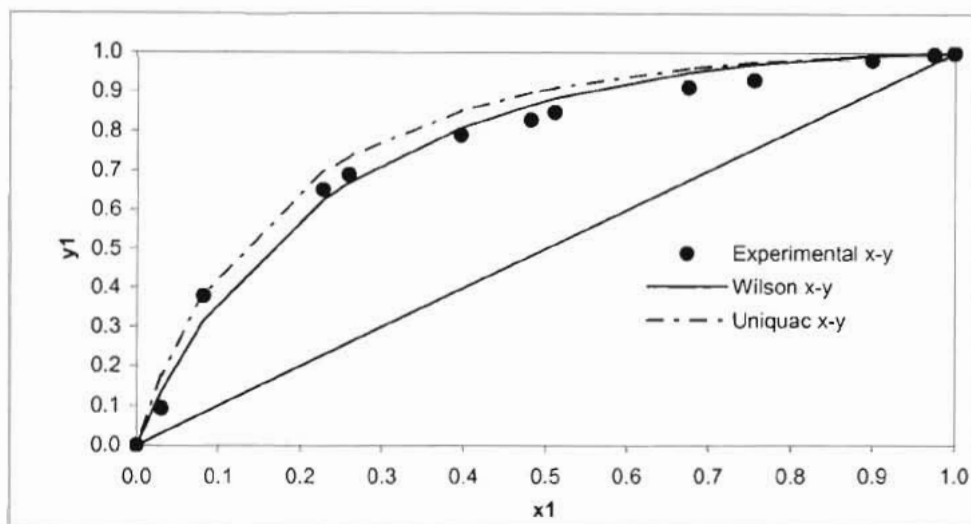


Figure 7-19: Fit of Wilson and Uniquac model to x-y data using chemical theory for the propionic acid (1) + Hexanoic acid (2) system at 413.15 K

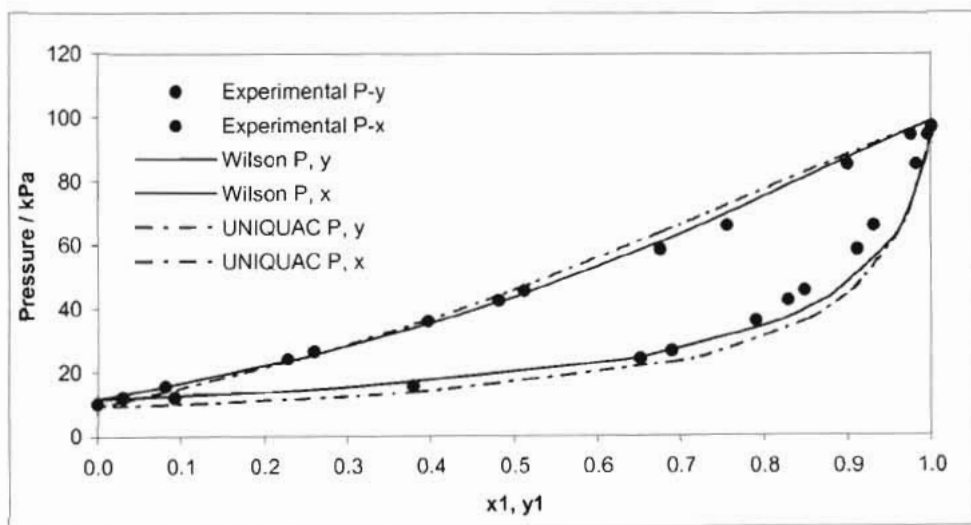


Figure 7-20: Fit of Wilson and Uniquac model to P-x-y data using chemical theory for the propionic acid (1) + Hexanoic acid (2) system at 413.15 K

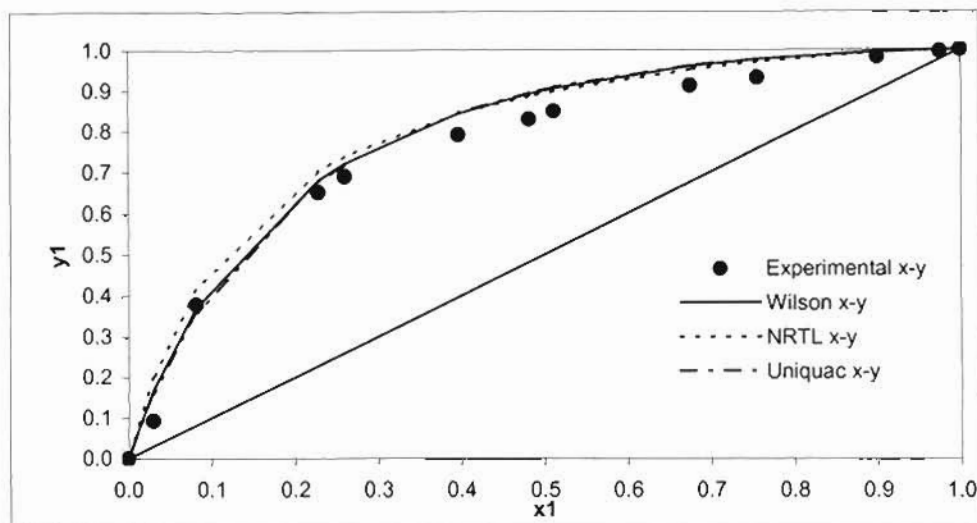


Figure 7-21: Fit of Wilson, Uniquac and NRTL model to x-y data using the Pitzer-Curl correlation for the propionic acid (1) + Hexanoic acid (2) system at 413.15 K

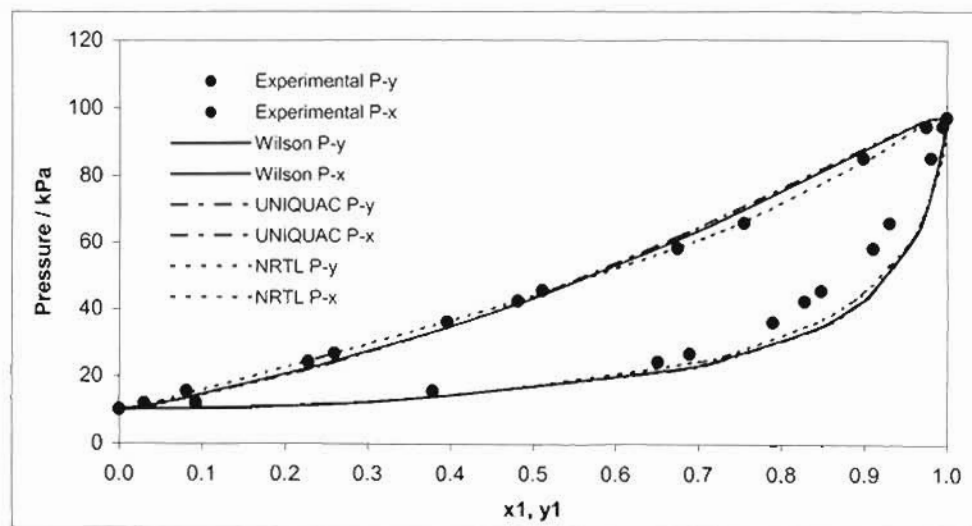


Figure 7-22: Fit of Wilson, Uniquac and NRTL model to P-x-y data using the Pitzer-Curl correlation for the propionic acid (1) + Hexanoic acid (2) system at 413.15 K

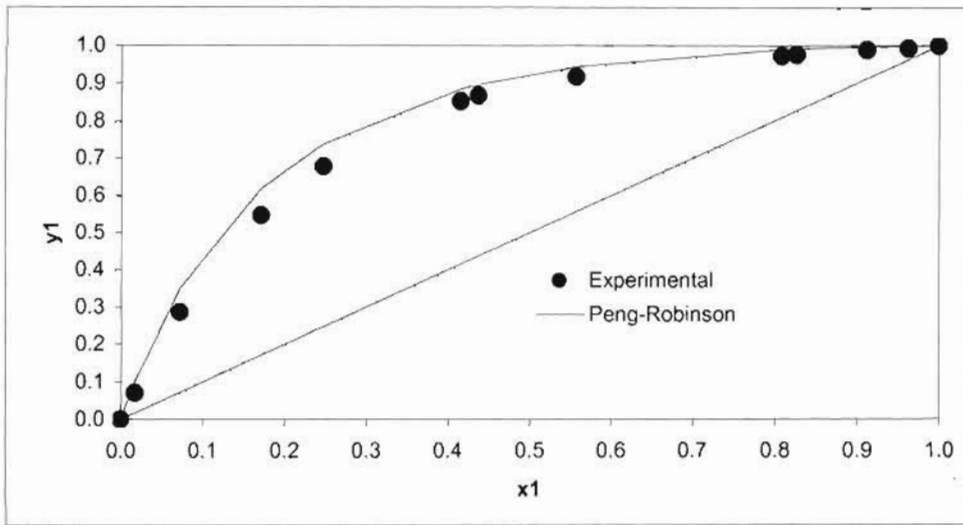


Figure 7-23: Fit of Peng-Robinson EOS to x-y data using the Twu-Coon mixing rule for the propionic acid (1) + Hexanoic acid (2) system at 20 kPa

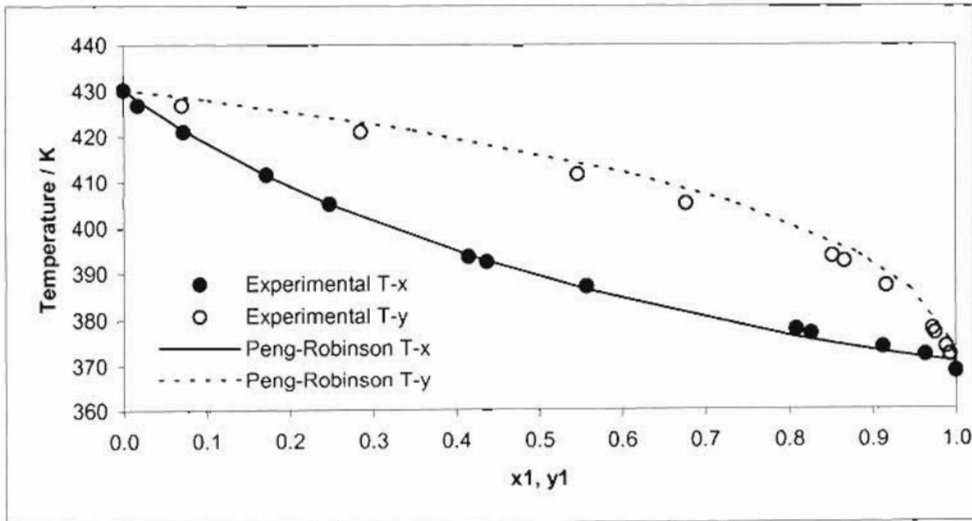


Figure 7-24: Fit of Peng-Robinson EOS to T-x-y data using the Twu-Coon mixing rule for the propionic acid (1) + Hexanoic acid (2) system at 20 kPa

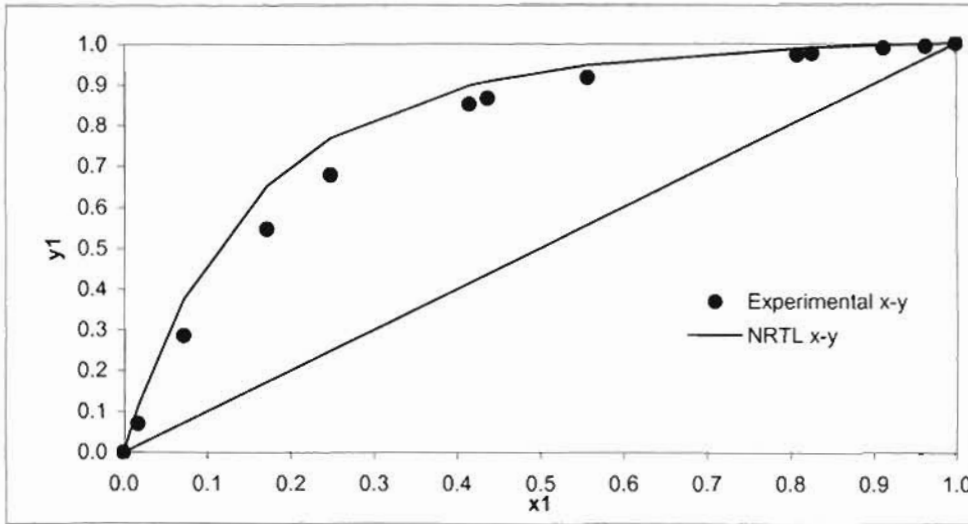


Figure 7-25: Fit of NRTL model to x-y data using the Pitzer-Curl correlation for the propionic acid (1) + Hexanoic acid (2) system at 20 kPa

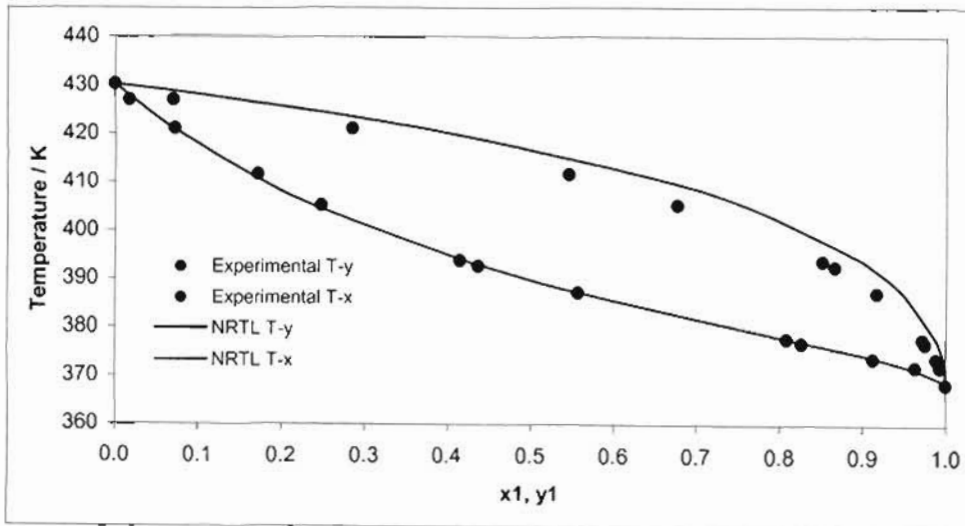


Figure 7-26: Fit of NRTL model to T-x-y data using the Pitzer-Curl correlation for the propionic acid (1) + Hexanoic acid (2) system at 20 kPa

7.7 Isobutyric Acid + Hexanoic Acid system

The model parameters for the isobutyric acid + hexanoic acid system are presented in Tables 7-7 to 7-9. All the models over predicted the vapour phase composition for the more volatile component. The isobutyric acid + hexanoic acid system has the most pronounced “S” shape. This suggests strong complex hydrogen bonding in both the liquid and vapour phases. It is interesting to note that isobutyric acid is a branched chain organic molecule. It is possible that the branching gives the molecule a unique associating behaviour.

The Peng-Robinson equation fitted the data better than all the other models. The point test results for thermodynamic consistency for all the systems were rather high. This is mainly due to the pronounced “S” shape of the phase diagrams, which the models failed to predict accurately. The point test results for the Peng-Robinson equation ranged between 0.050 and 0.062 over the three conditions measured. The Wilson equation combined with chemical theory to account for vapour phase non-ideality had Δy values between 0.061 and 0.063. The Wilson equation combined with the Pitzer-Curl correlation had Δy values 0.66 and 0.83. Applying chemical theory to the vapour phase association improves the results. The effect of molecules forming dimers needs to be accounted for. The α parameter values for system were high ranging from 0.132 to 1.98 over the three different conditions the system was measured. This clearly shows the non-ideal behaviour of carboxylic acid mixtures. The ΔP values were rather high ranging between 0.86 and 1.83 kPa for the isotherms. The ΔT value ranged from 0.42 and 0.51 K for the isobars.

Table 7-6: Best fit models for the isobutyric acid + hexanoic acid system

System	408.15 K	423.15 K	20 kPa
Best Fit	Peng-Robinson	Wilson (CT)	Peng-Robinson

CT = chemical theory PC = Pitzer-Curl

Table 7-7: Model parameters and deviations between calculated and experimental vapour phase and pressure/ temperature using the Peng-Robinson EOS and the Twu & Coon mixing rule for the Isobutyric acid + Hexanoic acid system.

Equation	408.15 K	423.15 K	20 kPa
Peng-Robinson			
$g_{12} - g_{11}$ (J/mol)	-2909.86	1514.69	-1818.50
$g_{12} - g_{22}$ (J/mol)	-356.58	-1368.64	-6421.29
α	0.9813	-0.4040	-1.7971
k_{ij}	-0.0305	-0.0304	-0.0194
l_{ij}	0.0018	0.0022	0.0028
Average Δy_1	0.056	0.062	0.050
del P or del T (kPa/K)	1.47	1.64	0.42

Table 7-8: Model parameters and deviations between calculated and experimental vapour phase and pressure/ temperature using the Pitzer-Curl correlation for the Isobutyric acid + Hexanoic acid system.

Equation	408.15 K	423.15 K	20 kPa
NRTL			
$g_{12} - g_{11}$ (J/mol)	-1308.70	-1585.01	8067.20
$g_{12} - g_{22}$ (J/mol)	470.48	632.67	-7047.10
α	1.9815	1.2367	0.132
Average Δy_1	0.082	0.071	0.066
del P or del T (kPa/K)	1.58	1.83	0.51
UNIQUAC			
$u_{12} - u_{11}$ (J/mol)	4083.90	1553.60	-
$u_{12} - u_{22}$ (J/mol)	-1311.46	-3121.52	-
Average Δy_1	0.082	0.071	-
del P or del T (kPa/K)	1.58	1.84	-
Wilson			
$\lambda_{12} - \lambda_{11}$ (J/mol)	4100.41	3573.3	-
$\lambda_{12} - \lambda_{22}$ (J/mol)	-1201.98	4007.20	-
Average Δy_1	0.083	0.073	-
del P or del T (kPa/K)	1.58	1.81	-

Table 7-9: Model parameters and deviations between calculated and experimental vapour phase and pressure/ temperature using chemical theory for the Isobutyric acid + Hexanoic acid system.

Equation	408.15 K	423.15 K
UNIQUAC		
$u_{12} - u_{11}$ (J/mol)	16436.01	5830.14
$u_{12} - u_{22}$ (J/mol)	-3371.64	3315.55
Average Δy_1	0.081	0.071
del P/ (kPa)	0.866	1.24
Wilson		
$\lambda_{12} - \lambda_{11}$ (J/mol)	2881.24	2399.40
$\lambda_{12} - \lambda_{22}$ (J/mol)	-4239.93	-3770.60
Average Δy_1	0.063	0.061
del P/ (kPa/K)	1.45	1.68

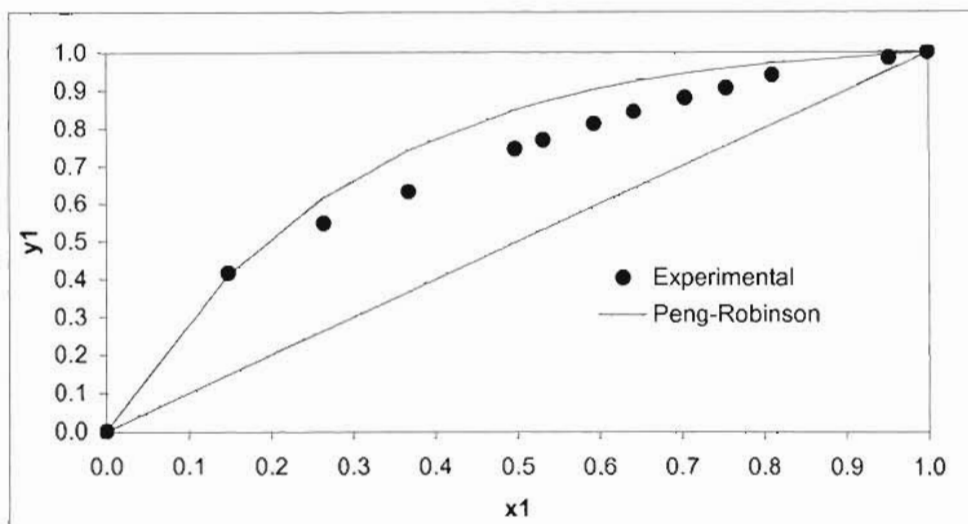


Figure 7-27: Fit of Peng-Robinson EOS to x-y data using the Twu-Coon mixing rule for the Isobutyric acid (1) + Hexanoic acid (2) system at 408.15 K

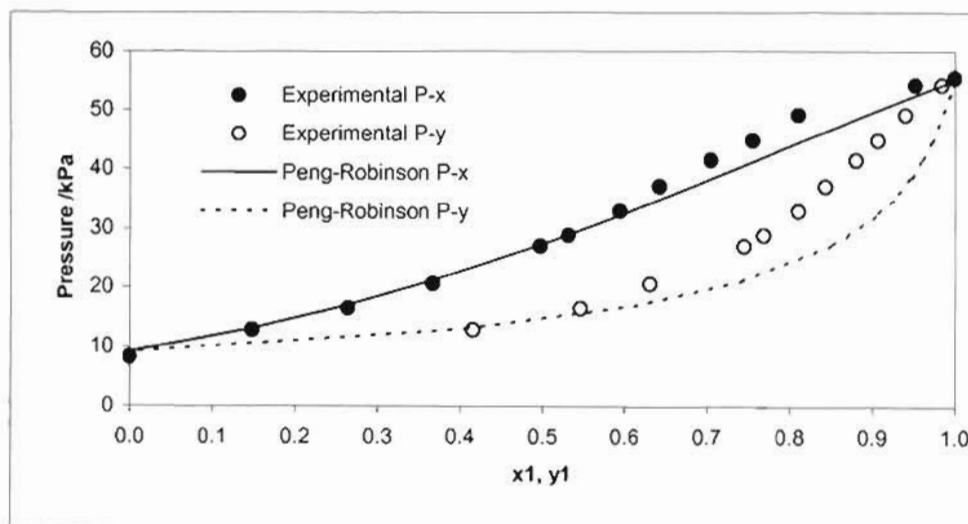


Figure 7-28: Fit of Peng-Robinson EOS to P-x-y data using the Twu-Coon mixing rule for the Isobutyric acid (1) + Hexanoic acid (2) system at 408.15 K

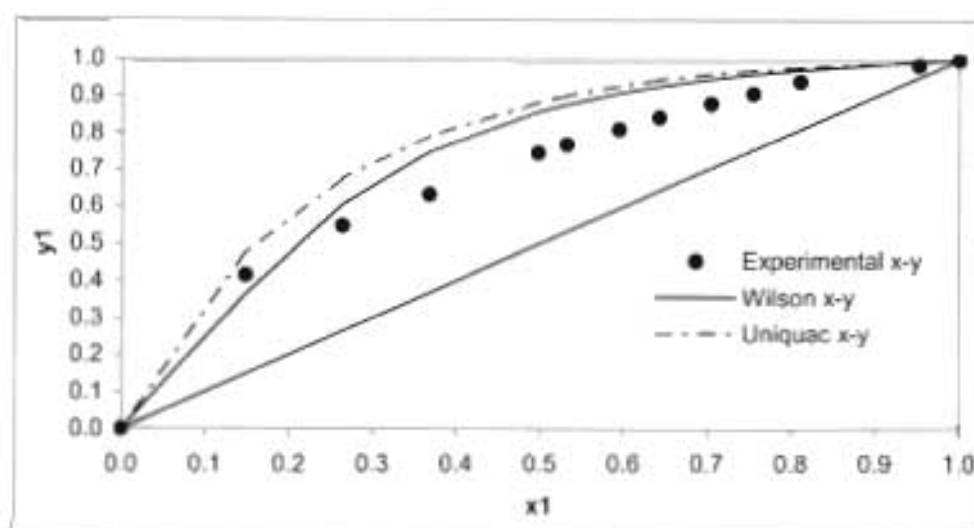


Figure 7-29: Fit of Wilson and Uniquac model to x-y data using chemical theory for the Isobutyric acid (1) + Hexanoic acid (2) system at 408.15 K

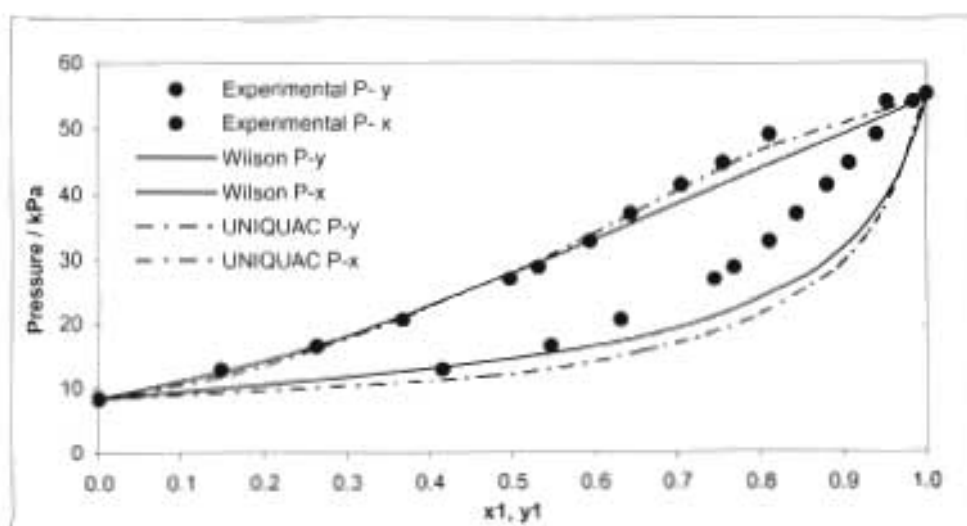


Figure 7-30: Fit of Wilson and Uniquac model to P-x-y data using chemical theory for the Isobutyric acid (1) + Hexanoic acid (2) system at 408.15 K

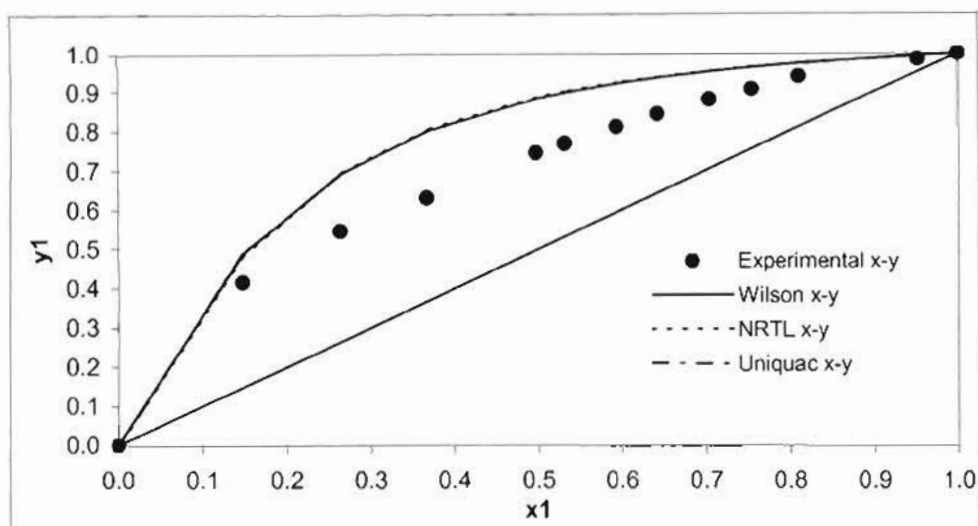


Figure 7-31: Fit of Wilson, Uniquac and NRTL model to x-y data using the Pitzer-Curl correlation for the Isobutyric acid (1) + Hexanoic acid (2) system at 408.15 K

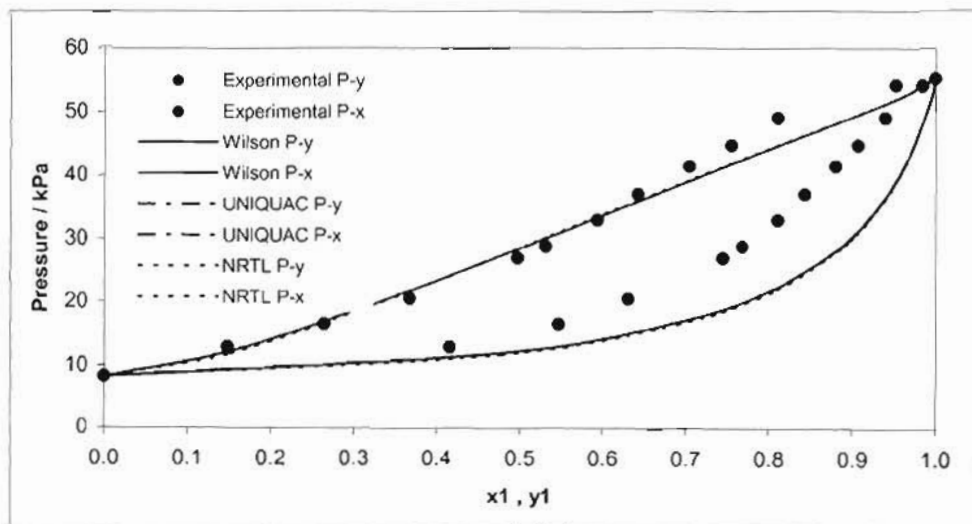


Figure 7-32: Fit of Wilson, Uniquac and NRTL model to P-x-y data using the Pitzer-Curl correlation for the Isobutyric acid (1) + Hexanoic acid (2) system at 408.15 K

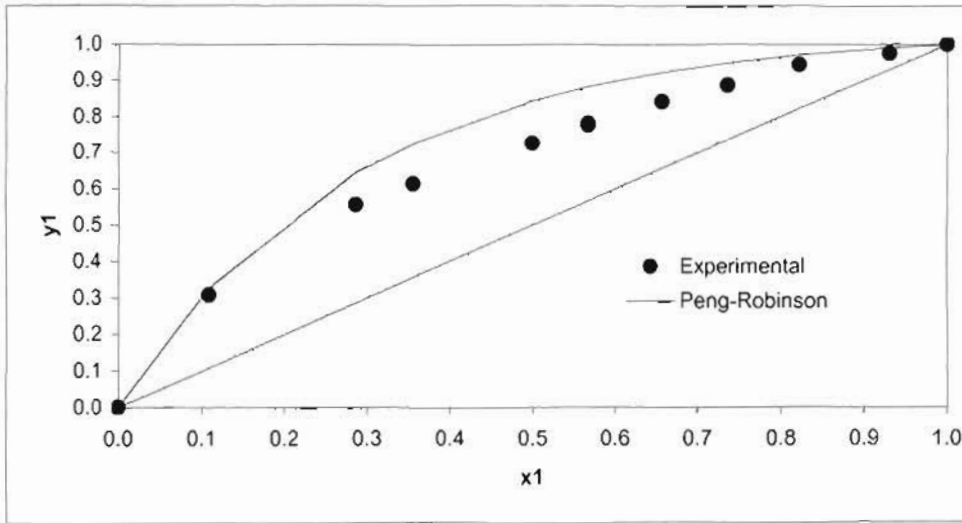


Figure 7-33: Fit of Peng-Robinson EOS to x-y data using the Twu-Coon mixing rule for the Isobutyric acid (1) + Hexanoic acid (2) system at 423.15 K

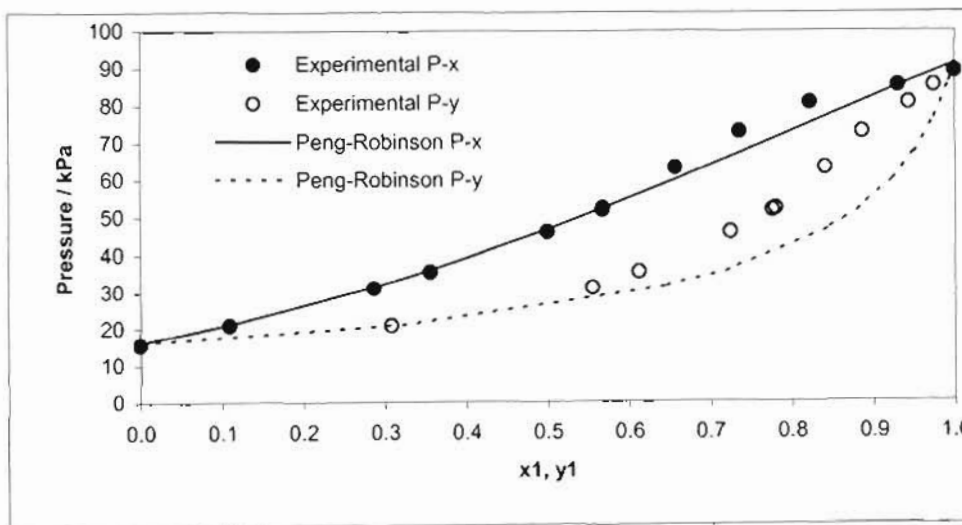


Figure 7-34: Fit of Peng-Robinson EOS to P-x-y data using the Twu-Coon mixing rule for the Isobutyric acid (1) + Hexanoic acid (2) system at 423.15 K

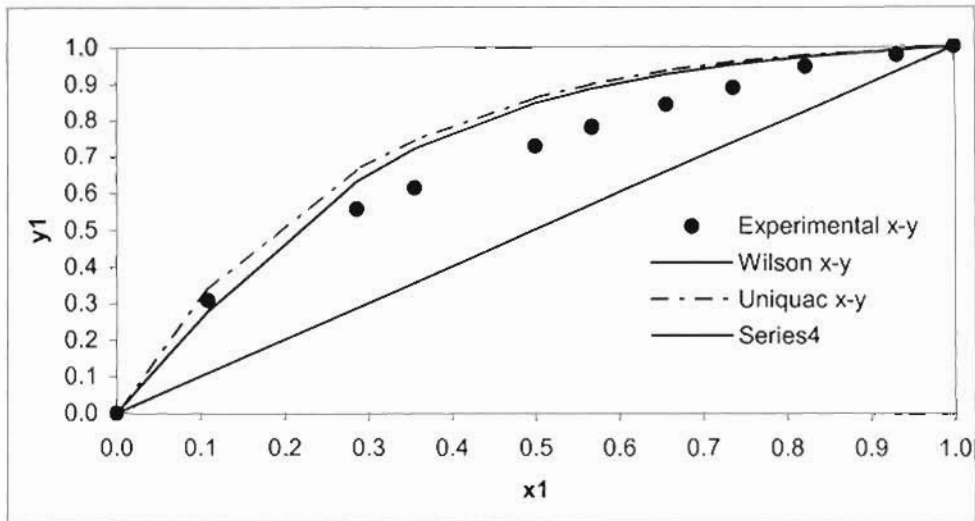


Figure 7-35: Fit of Wilson and Uniquac model to x-y data using chemical theory for the Isobutyric acid (1) + Hexanoic acid (2) system at 423.15 K

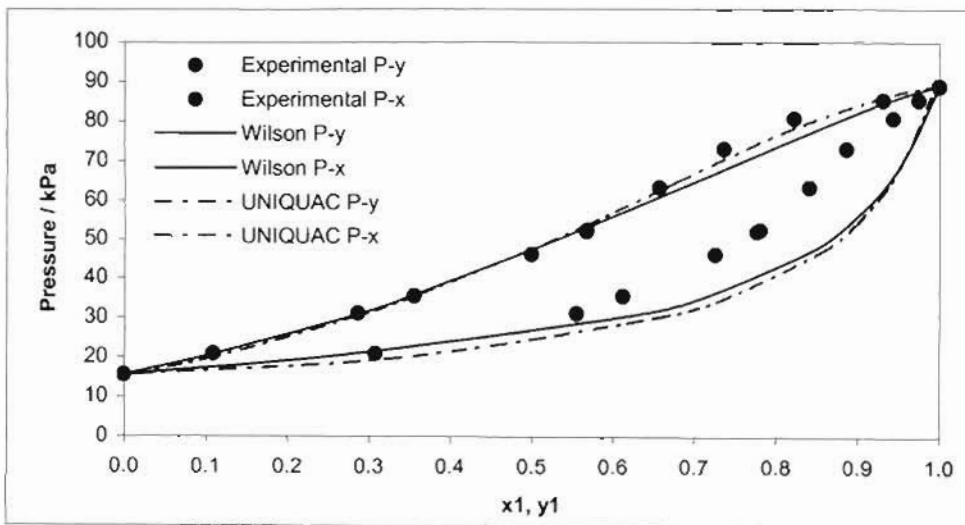


Figure 7-36: Fit of Wilson and Uniquac model to P-x-y data using chemical theory for the Isobutyric acid (1) + Hexanoic acid (2) system at 423.15 K

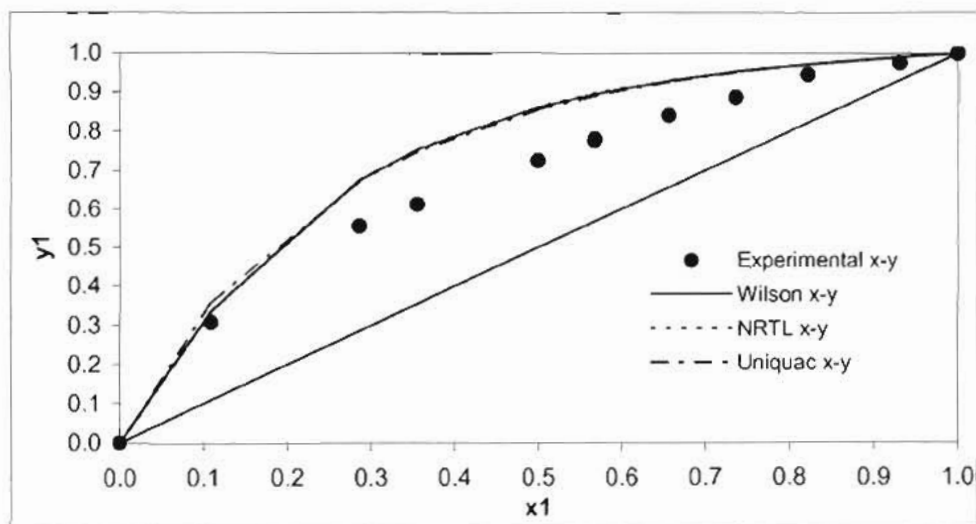


Figure 7-37: Fit of Wilson, Uniquac and NRTL model to x-y data using the Pitzer-Curl correlation for the Isobutyric acid (1) + Hexanoic acid (2) system at 423.15 K

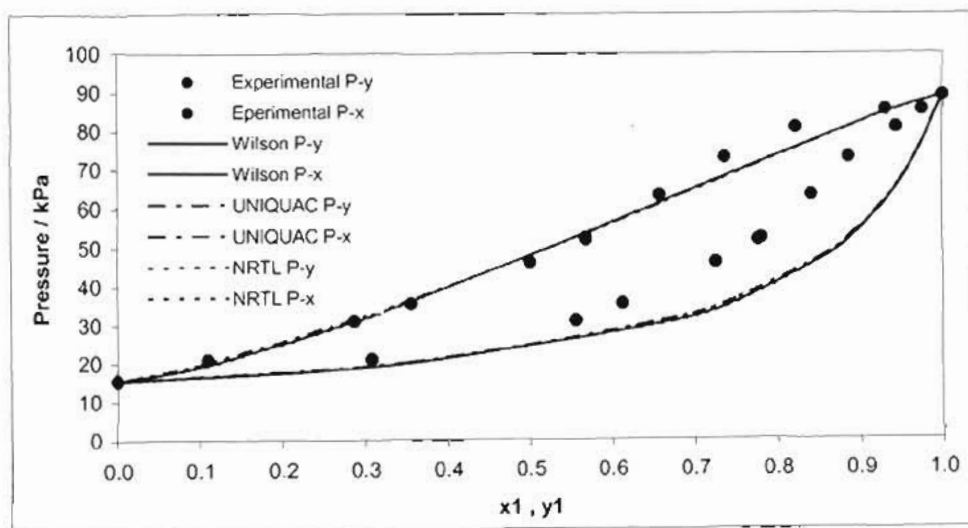


Figure 7-38: Fit of Wilson, Uniquac and NRTL model to P-x-y data using the Pitzer-Curl correlation for the Isobutyric acid (1) + Hexanoic acid (2) system at 423.15 K

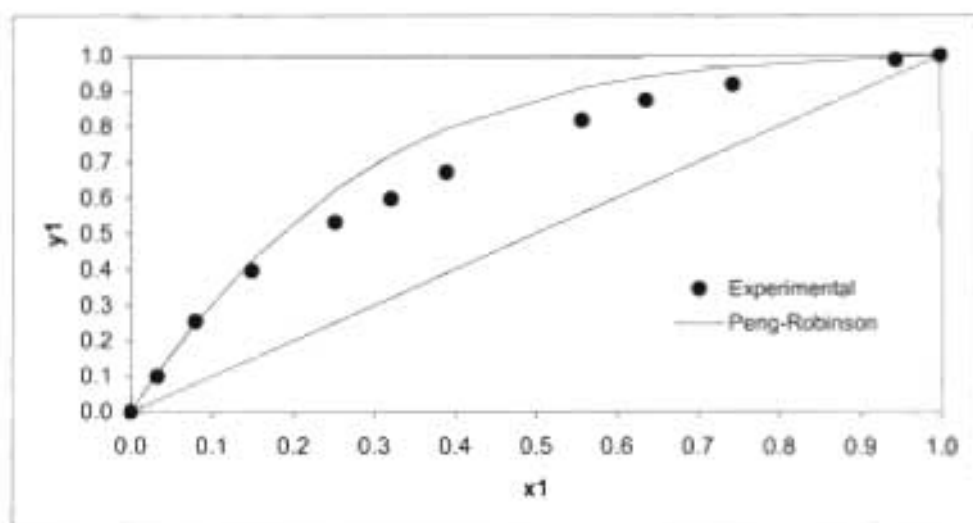


Figure 7-39: Fit of Peng-Robinson EOS to x - y data using the Twu-Coon mixing rule for the Isobutyric acid (1) + Hexanoic acid (2) system at 20 kPa

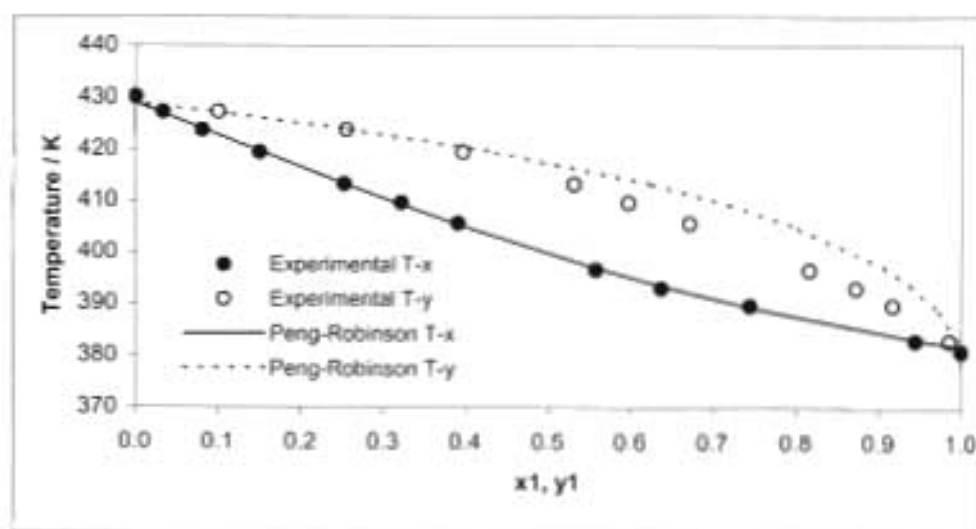


Figure 7-40: Fit of Peng-Robinson EOS to T - x - y data using the Twu-Coon mixing rule for the Isobutyric acid (1) + Hexanoic acid (2) system at 20 kPa

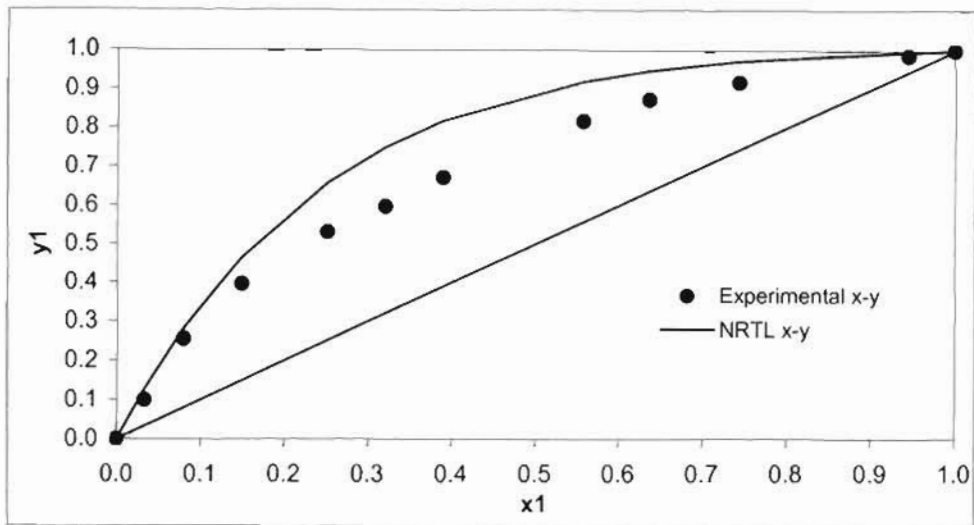


Figure 7-41: Fit of NRTL model to x-y data using the Pitzer-Curl correlation for the Isobutyric acid (1) + Hexanoic acid (2) system at 20 kPa

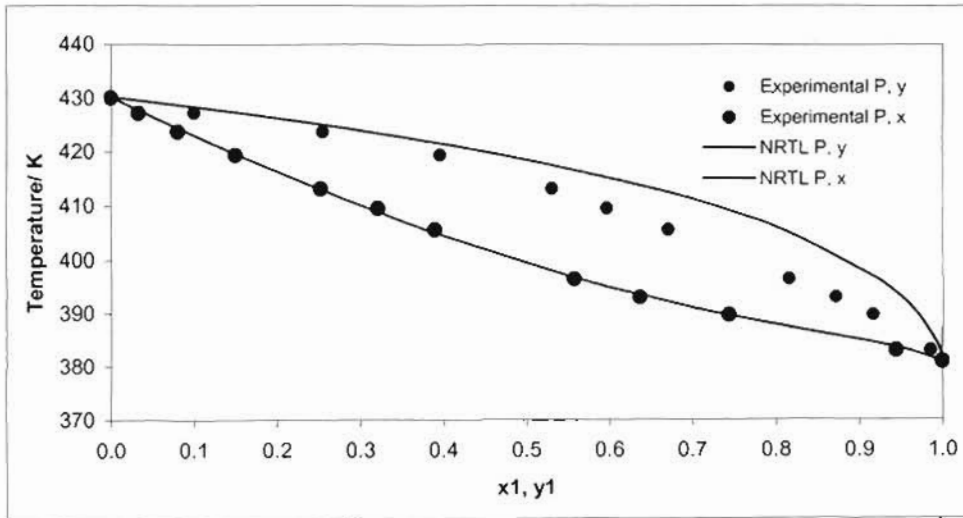


Figure 7-42: Fit of NRTL model to T-x-y data using the Pitzer-Curl correlation for the Isobutyric acid (1) + Hexanoic acid (2) system at 20 kPa

7.8 Valeric acid + Hexanoic Acid System

The best-fit models are presented in Table 7-10. The model parameters for the three systems are presented in Tables 7-11 to 7-13.

The phase diagrams for this system are exceptionally narrow. As discussed in Section 7.5 this is consistent with results of Kato et al. (1990), Klekors and Scheller (1968), Tamir and Wisniak (1975) and Sewnarain et al. (2002). The "S" shape is prominent and the phase envelopes are acutely narrow in the dilute regions. All the models fitted the valeric acid + hexanoic acid system well in general. This is evident from the deviations between experimental and calculated vapour compositions. The pressure deviations are considerably better than those of the isobutyric acid + hexanoic acid system. The results obtained from the Peng-Robinson equation of state were good. The direct method proved to be comparable with the combined method (considered superior for low pressure VLE). As observed for the propionic acid system and the isobutyric acid system, chemical theory account for vapour phase non-ideality resulted in a marked improvement in the vapour phase deviation (refer to Table 7-13). The NRTL non-randomness parameter, α , lay out of the conventional limits (-1 to 0.5). Values between 1.4 and 2.2 were observed. This is a result of the model attempting to incorporate the "S" shape and narrowing effect of the phase envelopes. Consistency test on the data gave Δy values in the range 0.019 to 0.034 with the best results being that of the Wilson equation in combination with chemical theory.

Table 7-10: Best fit models for the valeric acid + hexanoic acid system

System	423.15 K	433.15 K	15 kPa
Best Fit	Wilson (CT)	Wilson (CT)	Peng-Robinson

CT = chemical theory PC = Pitzer-Curl

Table 7-11: Model parameters and deviations between calculated and experimental vapour phase and pressure/ temperature using the Peng-Robinson EOS and the Twu & Coon mixing rule for the Valeric acid + Hexanoic acid system.

Equation	423.15 K	433.15 K	15 kPa
Peng-Robinson			
$g_{12} - g_{11}$ (J/mol)	275.57	952.18	-6059.89
$g_{12} - g_{22}$ (J/mol)	807.75	4295.57	15092.98
α	0.6563	-0.3363	0.5086
k_{ij}	-0.0162	-0.0130	-0.0144
l_{ij}	-0.0003	0.0003	-0.0023
Δy_1	0.034	0.028	0.0263
del P or del T (kPa/K)	0.11	0.41	0.33

Table 7-12: Model parameters and deviations between calculated and experimental vapour phase and pressure/ temperature using the Pitzer-Curl correlation for the Valeric acid + Hexanoic acid system.

Equation	423.15 K	433.15 K	15 kPa
NRTL			
$g_{12} - g_{11}$ (J/mol)	-482.46	-714.10	-711.70
$g_{12} - g_{22}$ (J/mol)	7837.09	1992.04	4668.78
α	1.4791	2.2205	1.4700
Δy_1	0.033	0.024	0.035
del P or del T (kPa/K)	0.32	0.40	0.25
UNIQUAC			
$u_{12} - u_{11}$ (J/mol)	-2285.81	-2034.72	-
$u_{12} - u_{22}$ (J/mol)	3511.21	2915.01	-
Δy_1	0.039	0.024	-
del P or del T (kPa/K)	0.39	0.39	-
Wilson			
$\lambda_{12} - \lambda_{11}$ (J/mol)	344.45	584.67	-
$\lambda_{12} - \lambda_{22}$ (J/mol)	-1431.41	-584.67	-
Δy_1	0.042	0.025	-
del P or del T (kPa/K)	0.41	0.50	-

Table 7-13: Model parameters and deviations between calculated and experimental vapour phase and pressure/ temperature using chemical theory for the Valeric acid + Hexanoic acid system.

Equation	423.15 K	433.15 K
UNIQUAC		
$u_{12} - u_{11}$ (J/mol)	-2477.83	-2141.42
$u_{12} - u_{22}$ (J/mol)	3992.39	3136.25
Average Δy_1	0.037	0.024
del P/ (kPa)	0.39	0.40
Wilson		
$\lambda_{12} - \lambda_{11}$ (J/mol)	3487.05	2856.89
$\lambda_{12} - \lambda_{22}$ (J/mol)	-1346.09	-2856.89
Average Δy_1	0.028	0.019
del P or del T (kPa/K)	0.39	0.63

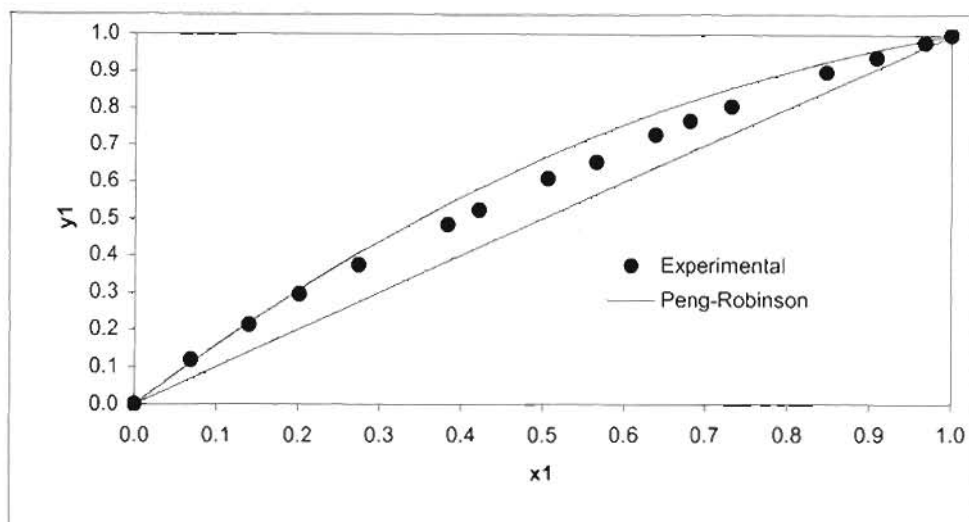


Figure 7-43: Fit of Peng-Robinson EOS to x-y data using the Twu-Coon mixing rule for the Valeric acid (1) + Hexanoic acid (2) system at 423.15 K

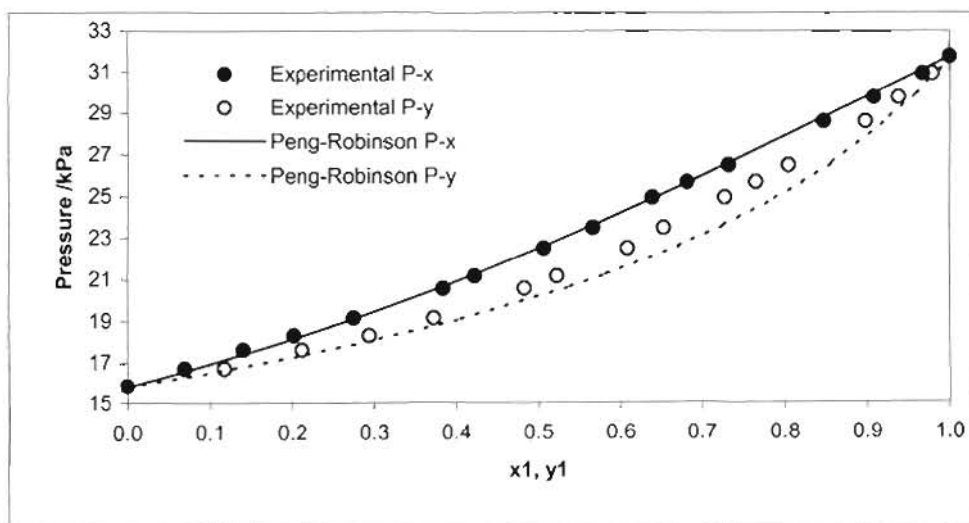


Figure 7-44: Fit of Peng-Robinson EOS to P-x-y data using the Twu-Coon mixing rule for the Valeric acid (1) + Hexanoic acid (2) system at 423.15 K

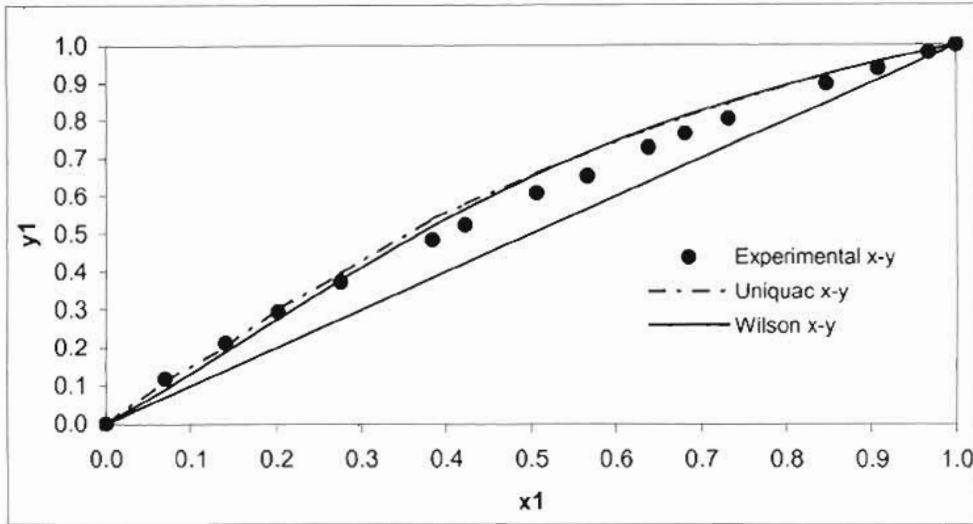


Figure 7-45: Fit of Wilson and Uniquac model to x-y data using chemical theory for the Valeric acid (1) + Hexanoic acid (2) system at 423.15 K

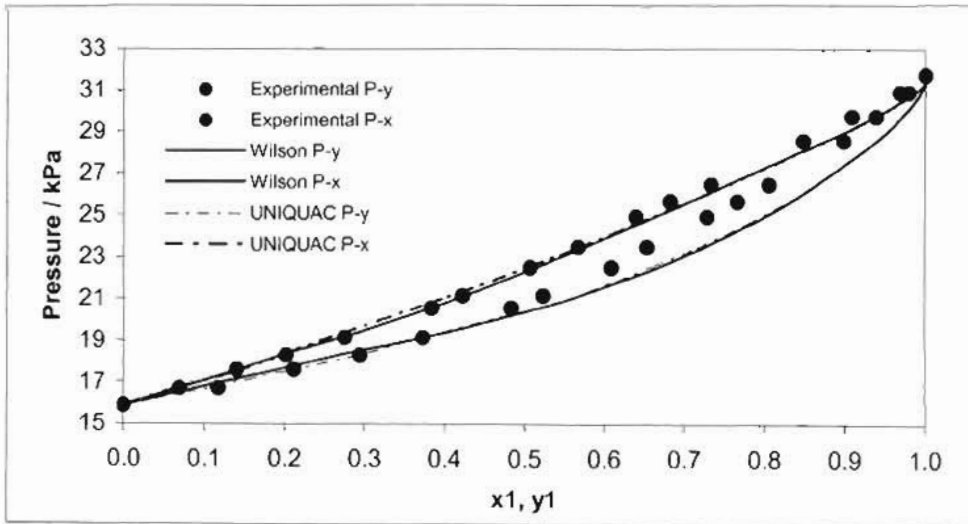


Figure 7-46: Fit of Wilson and Uniquac model to P-x-y data using chemical theory for the Valeric acid (1) + Hexanoic acid (2) system at 423.15 K

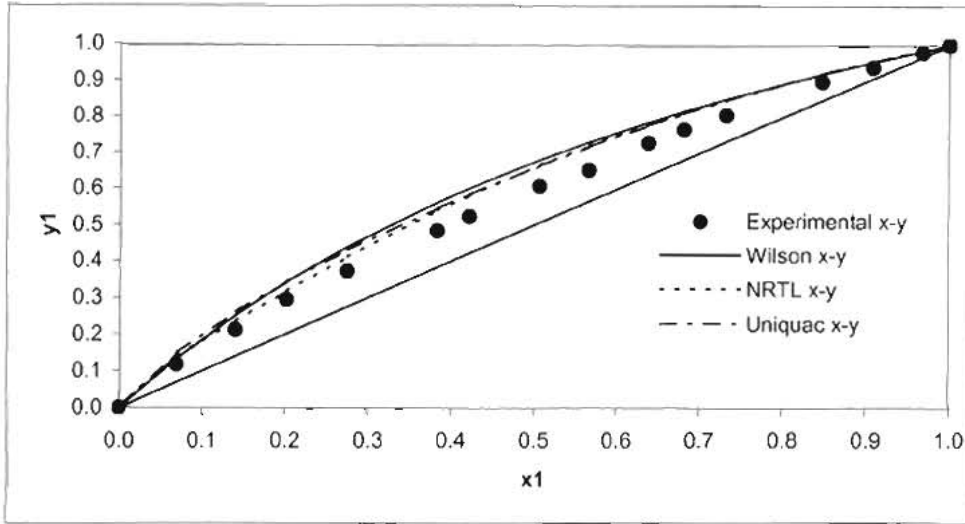


Figure 7-47: Fit of Wilson, Uniquac and NRTL model to x-y data using the Pitzer-Curl correlation for the Valeric acid (1) + Hexanoic acid (2) system at 423.15 K

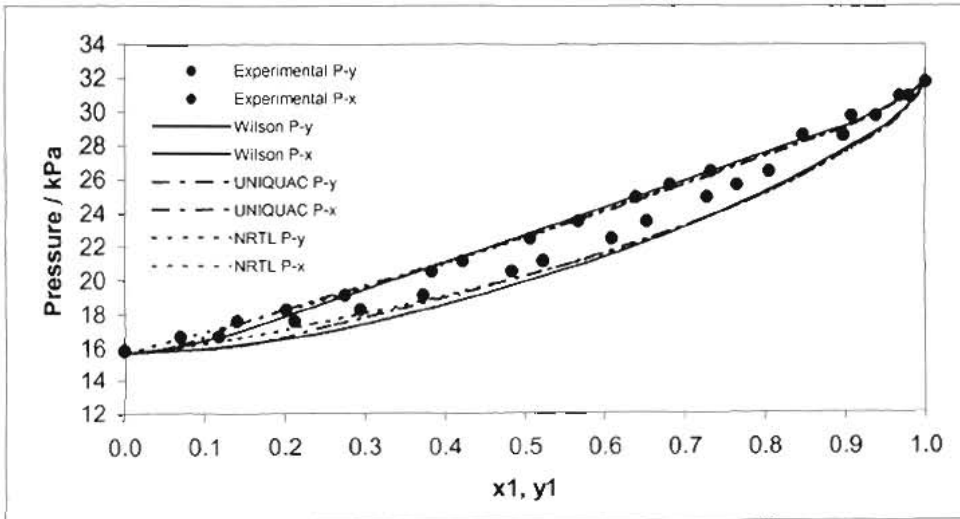


Figure 7-48: Fit of Wilson, Uniquac and NRTL model to P-x-y data using the Pitzer-Curl correlation for the Valeric acid (1) + Hexanoic acid (2) system at 423.15 K

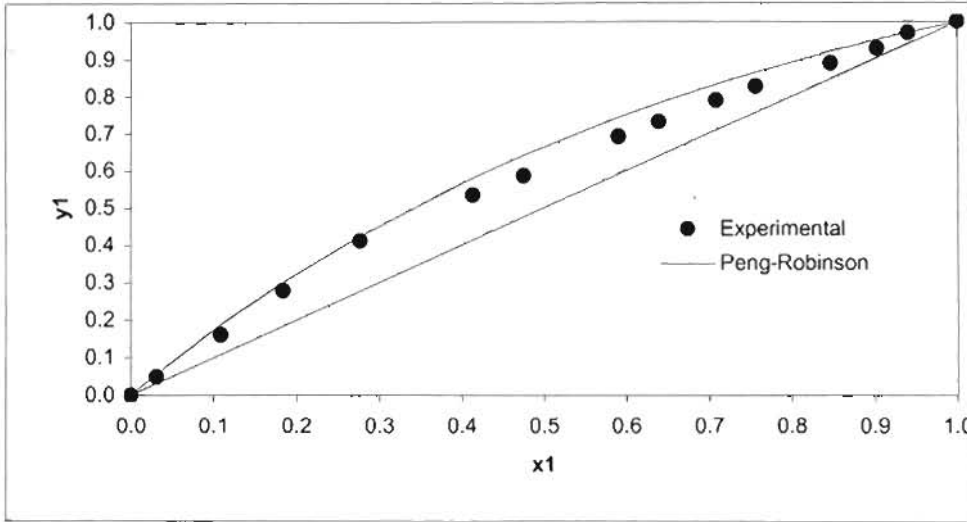


Figure 7-49: Fit of Peng-Robinson EOS to x - y data using the Twu-Coon mixing rule for the Valeric acid (1) + Hexanoic acid (2) system at 433.15 K

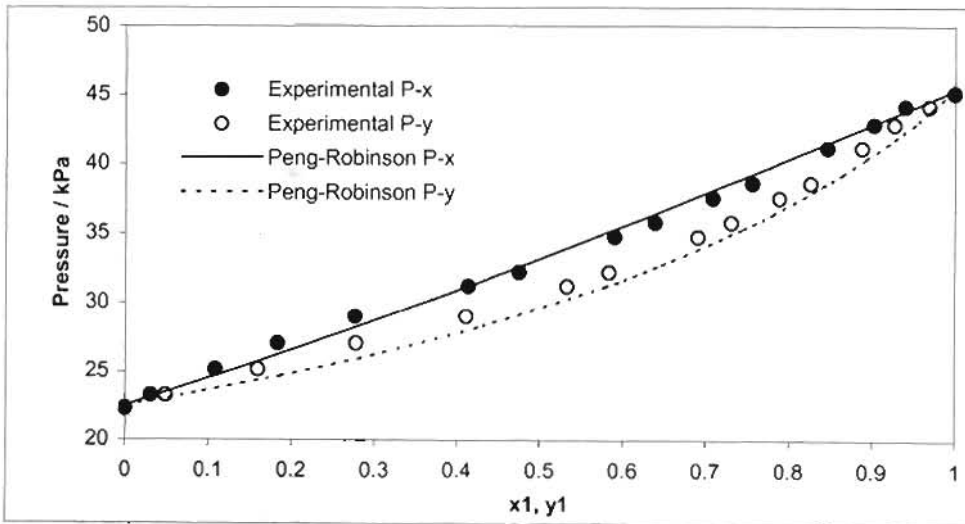


Figure 7-50: Fit of Peng-Robinson EOS to P - x - y data using the Twu-Coon mixing rule for the Valeric acid (1) + Hexanoic acid (2) system at 433.15 K

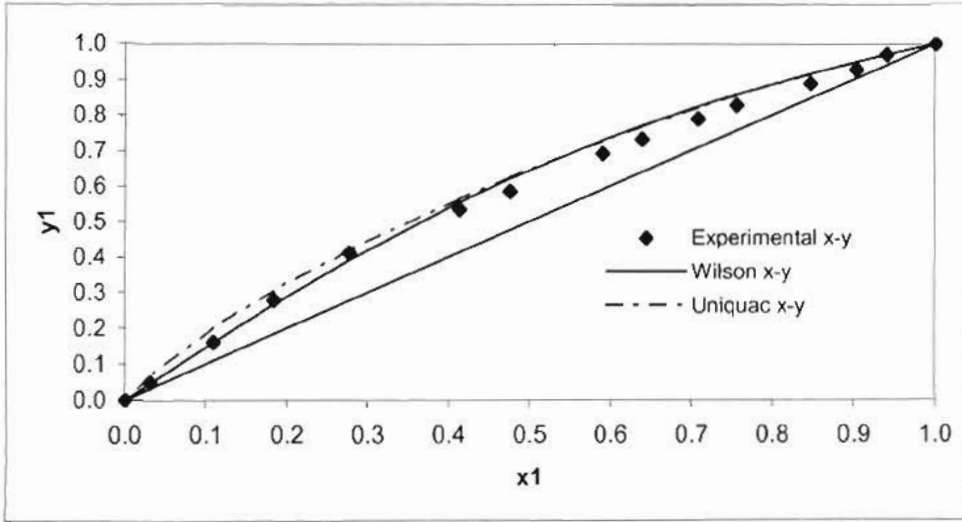


Figure 7-51: Fit of Wilson and Uniquac model to x-y data using chemical theory for the Valeric acid (1) + Hexanoic acid (2) system at 433.15 K

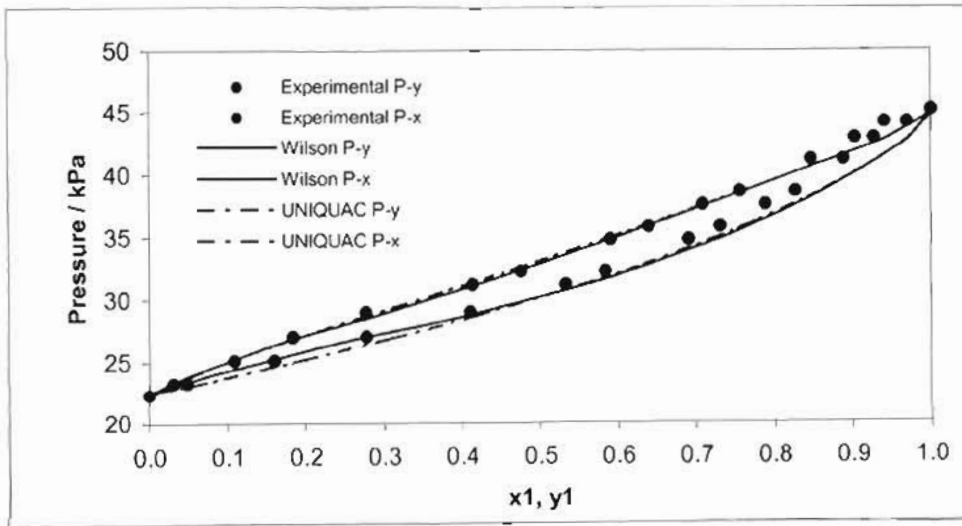


Figure 7-52: Fit of Wilson and Uniquac model to P-x-y data using chemical theory for the Valeric acid (1) + Hexanoic acid (2) system at 433.15 K

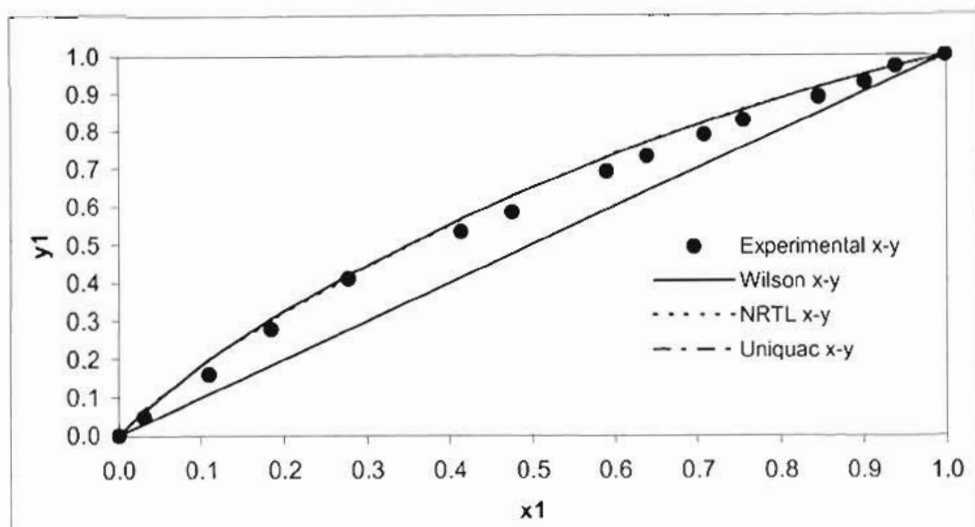


Figure 7-53: Fit of Wilson, Uniquac and NRTL model to x-y data using the Pitzer-Curl correlation for the Valeric acid (1) + Hexanoic acid (2) system at 433.15 K

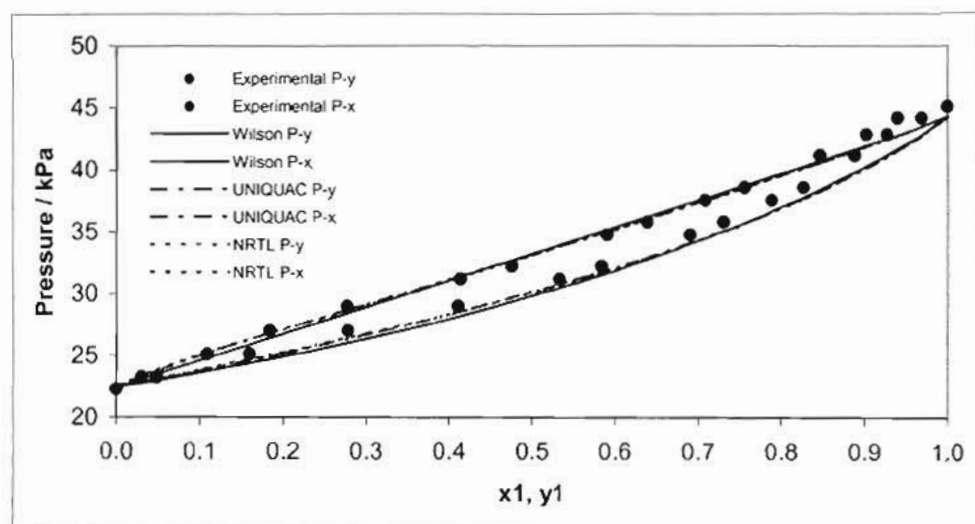


Figure 7-54: Fit of Wilson, Uniquac and NRTL model to P-x-y data using the Pitzer-Curl correlation for the Valeric acid (1) + Hexanoic acid (2) system at 433.15 K

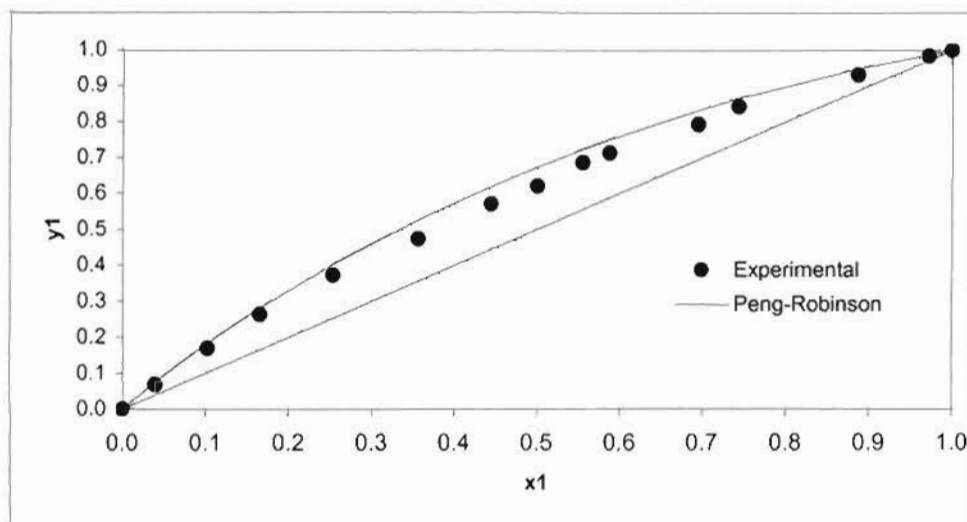


Figure 7-55: Fit of Peng-Robinson EOS to x - y data using the Twu-Coon mixing rule for the Valeric acid (1) + Hexanoic acid (2) system at 15 kPa

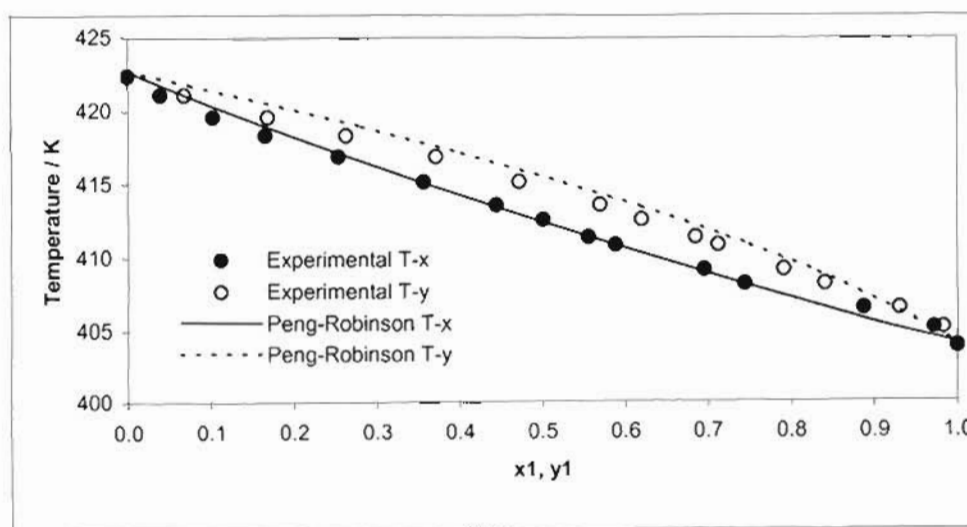


Figure 7-56: Fit of Peng-Robinson EOS to T - x - y data using the Twu-Coon mixing rule for the Valeric acid (1) + Hexanoic acid (2) system at 15 kPa

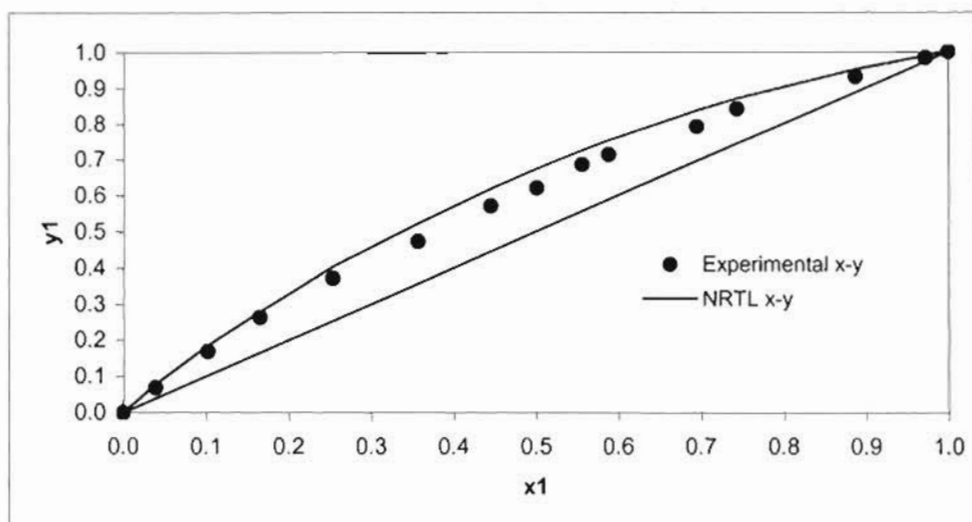


Figure 7-57: Fit of NRTL model to x-y data using the Pitzer-Curl correlation for the Valeric acid (1) + Hexanoic acid (2) system at 15 kPa

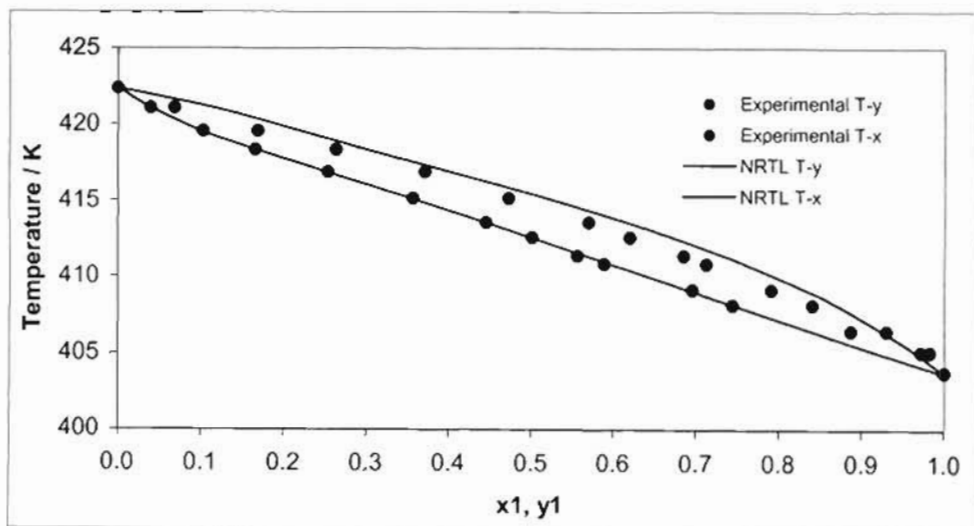


Figure 7-58: Fit of NRTL model to T-x-y data using the Pitzer-Curl correlation for the Valeric acid (1) + Hexanoic acid (2) system at 15 kPa

7.9 Hexanoic Acid + Heptanoic Acid System

The best-fit models are presented in Tables 7-14. Table 7-15 to 7-17 presents the model parameters for the systems.

All the models fitted the data well. The largest Δy is 0.029 being that of the Uniquac equation in combination with the Pitzer-Curl correlation. The Pitzer-Curl correlation (Pitzer and Curl [1957]) accounting for vapour phase imperfections proves to be the least accurate in modelling the data. This is not surprising as it is a relatively simple correlation. The smallest Δy is 0.008 being that of the 10 kPa system using the Peng-Robinson equation of state. Generally all the models fail to accurately predict the “S” shape especially in the dilute regions. The vapour phase compositions differ increasingly as the pressure rises for the isotherms. As was found in all the other systems, use of chemical theory in accounting for the vapour phase imperfections resulted in a marked improvement in the vapour phase deviations. The Peng-Robinson equation fitted the data better than the models. In all the cases the direct method was compared to the combined method. The success of the combined method to predict accurate VLE data for carboxylic acids lies in incorporating chemical theory to both the liquid and vapour phases. The non-randomness parameter in the NRTL equation was out of the usual limits of -1 to 0.5 . This is attributed to the highly non-ideal behaviour of carboxylic acid mixtures.

Table 7-14: Best fit models for the hexanoic acid + heptanoic acid system

System	443.15 K	10 kPa
Best Fit	Peng-Robinson	Peng-Robinson

CT = chemical theory PC = Pitzer-Curl

Table 7-15: Model parameters and deviations between calculated and experimental vapour phase and pressure/ temperature using the Peng-Robinson EOS and the Twu & Coon mixing rule for the Hexanoic acid + Heptanoic acid system.

Equation	443.15 K	10 kPa
Peng-Robinson		
$g_{12} - g_{11}$ (J/mol)	-5855.68	3267.86
$g_{12} - g_{22}$ (J/mol)	-387.69	2059.43
α	3.8183	-0.0830
k_{ij}	0.0082	-0.0118
l_{ij}	-0.0014	-0.0042
Average Δy_1	0.021	0.008
del P or del T (kPa/K)	0.21	0.18

Table 7-16: Model parameters and deviations between calculated and experimental vapour phase and pressure/ temperature using the Pitzer-Curl correlation for the Hexanoic acid + Heptanoic acid system.

Equation	443.15 K	10 kPa
NRTL		
$g_{12} - g_{11}$ (J/mol)	936.73	800.54
$g_{12} - g_{22}$ (J/mol)	834.47	6972.11
α	1.7100	1.6419
Average Δy_1	0.024	0.029
del P or del T (kPa/K)	0.19	0.47
UNIQUAC		
$u_{12} - u_{11}$ (J/mol)	505.92	-
$u_{12} - u_{22}$ (J/mol)	-243.42	-
Average Δy_1	0.025	-
del P or del T (kPa/K)	0.28	-
Wilson		
$\lambda_{12} - \lambda_{11}$ (J/mol)	4436.19	-
$\lambda_{12} - \lambda_{22}$ (J/mol)	-2702.34	-
Average Δy_1	0.023	-
del P or del T (kPa/K)	0.25	-

Table 7-17: Model parameters and deviations between calculated and experimental vapour phase and pressure/ temperature using chemical theory for the Hexanoic acid + Heptanoic acid system.

Equation	433.15 K
UNIQUAC	
$u_{12} - u_{11}$ (J/mol)	-1926.84
$u_{12} - u_{22}$ (J/mol)	2816.78
Average Δy_1	0.023
del / (kPa)	0.34
Wilson	
$\lambda_{12} - \lambda_{11}$ (J/mol)	3653.00
$\lambda_{12} - \lambda_{22}$ (J/mol)	-4346.19
Average Δy_1	0.029
del P or del T (kPa/K)	1.02

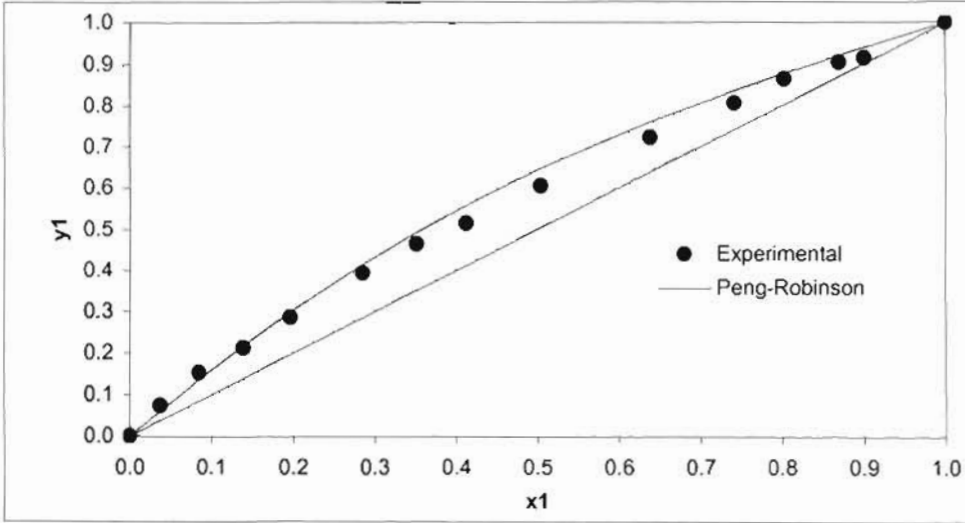


Figure 7-59: Fit of Peng-Robinson EOS to x-y data using the Twu-Coon mixing rule for the Hexanoic acid (1) + Heptanoic acid (2) system at 443.15 K

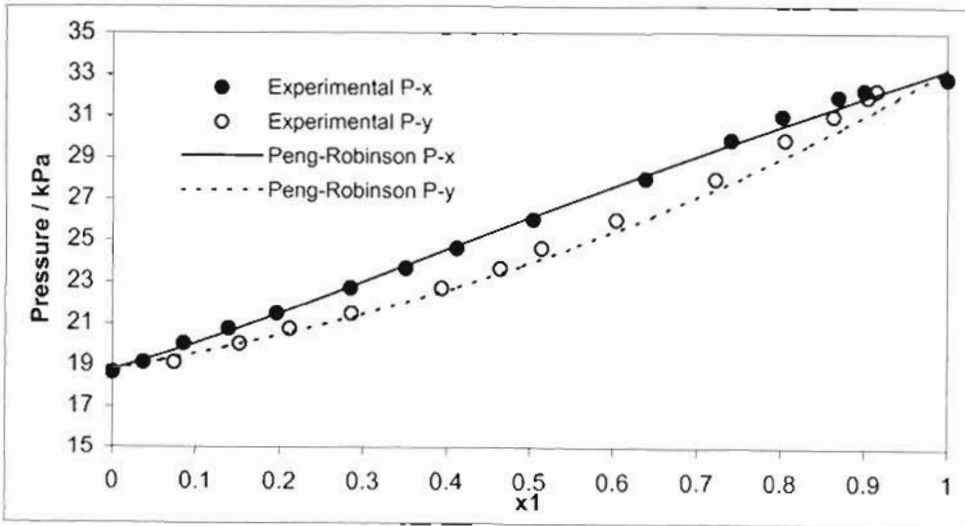


Figure 7-60: Fit of Peng-Robinson EOS to P-x-y data using the Twu-Coon mixing rule for the Hexanoic acid (1) + Heptanoic acid (2) system at 443.15 K

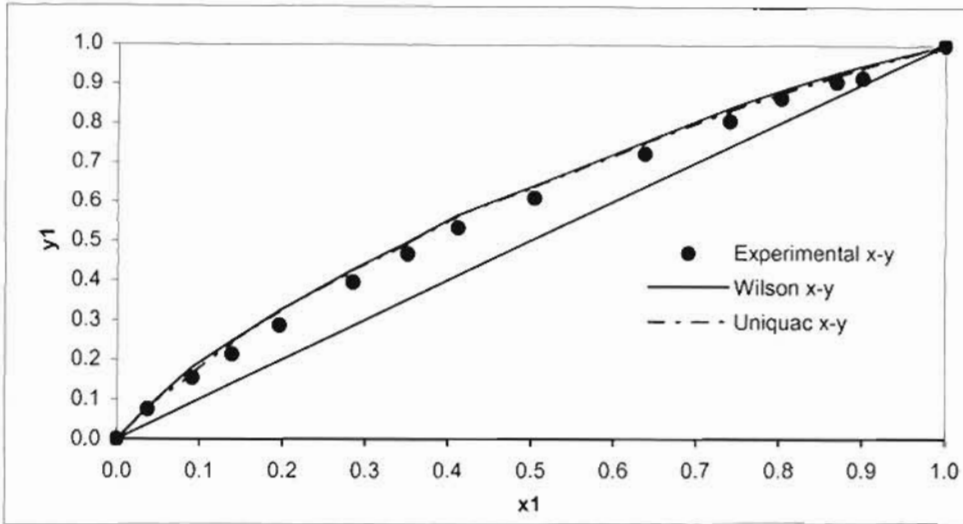


Figure 7-61: Fit of Wilson and Uniquac model to x-y data using chemical theory for the Hexanoic acid (1) + Heptanoic acid (2) system at 443.15 K

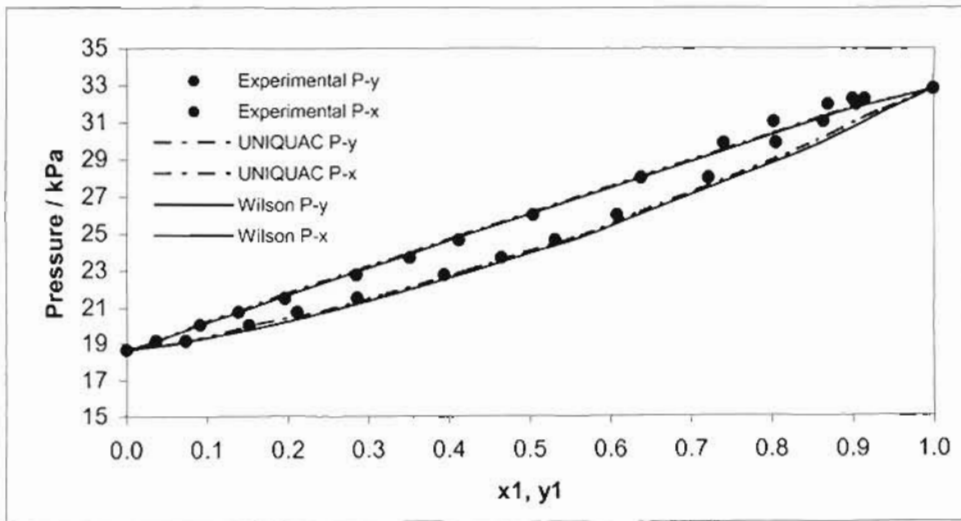


Figure 7-62: Fit of Wilson and Uniquac model to P-x-y data using chemical theory for Hexanoic acid (1) + Heptanoic acid (2) system at 443.15 K

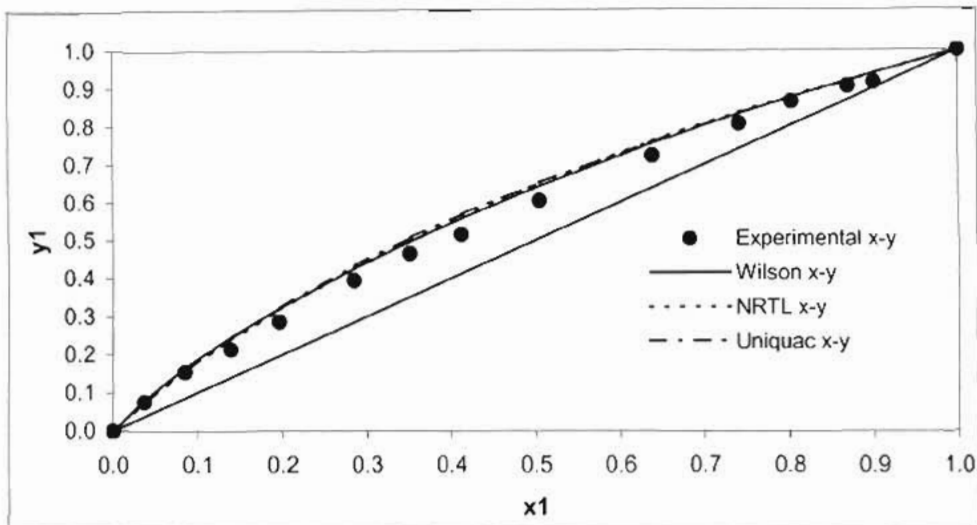


Figure 7-63: Fit of Wilson, Uniquac and NRTL model to x-y data using the Pitzer-Curl correlation for Hexanoic acid (1) + Heptanoic acid (2) system at 443.15 K

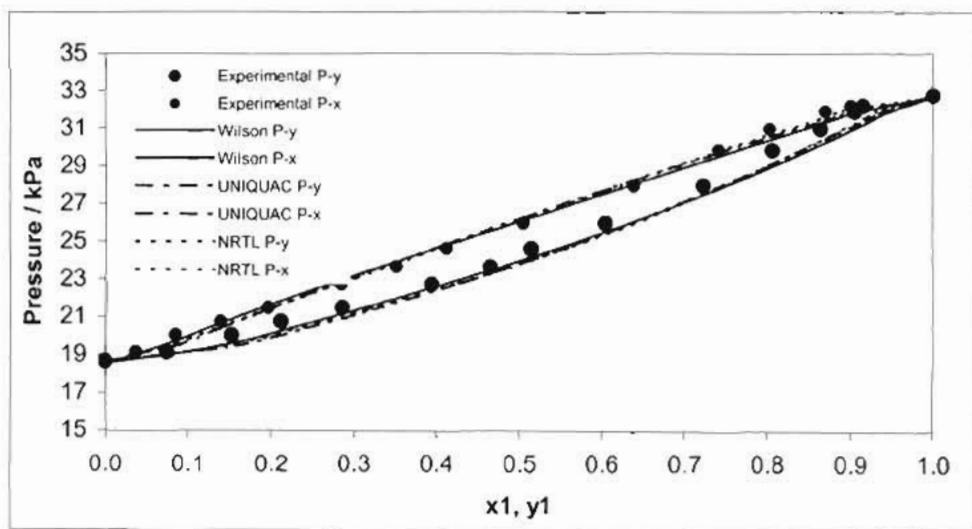


Figure 7-64: Fit of Wilson, Uniquac and NRTL model to P-x-y data using the Pitzer-Curl correlation for Hexanoic acid (1) + Heptanoic acid (2) system at 443.15 K

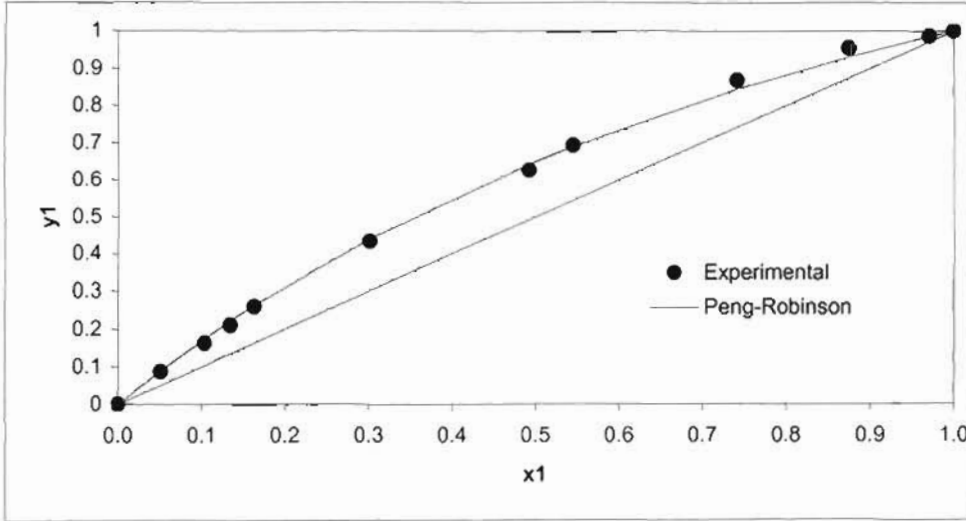


Figure 7-65: Fit of Peng-Robinson EOS to x-y data using the Twu-Coon mixing rule for the Hexanoic acid (1) + Heptanoic acid (2) system at 10 kPa

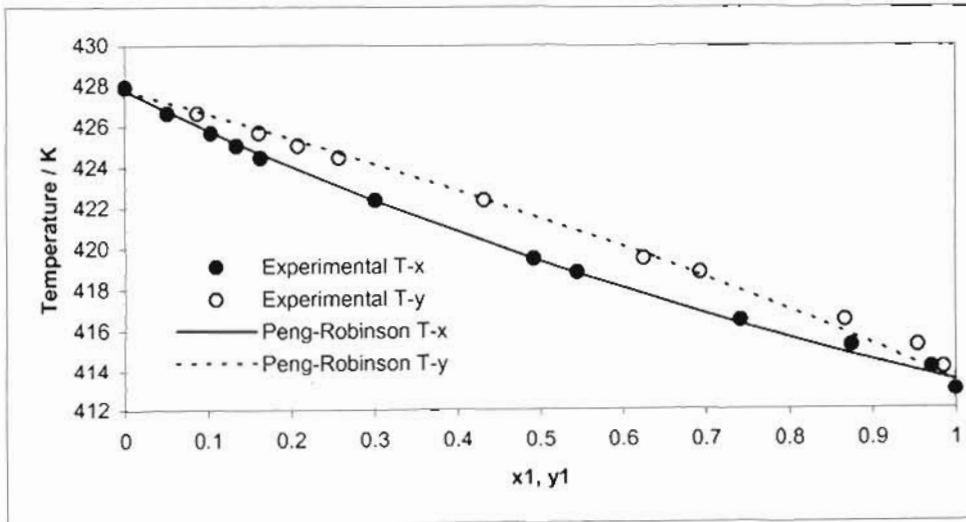


Figure 7-66: Fit of Peng-Robinson EOS to T-x-y data using the Twu-Coon mixing rule for the Hexanoic acid (1) + Heptanoic acid (2) system at 10 kPa

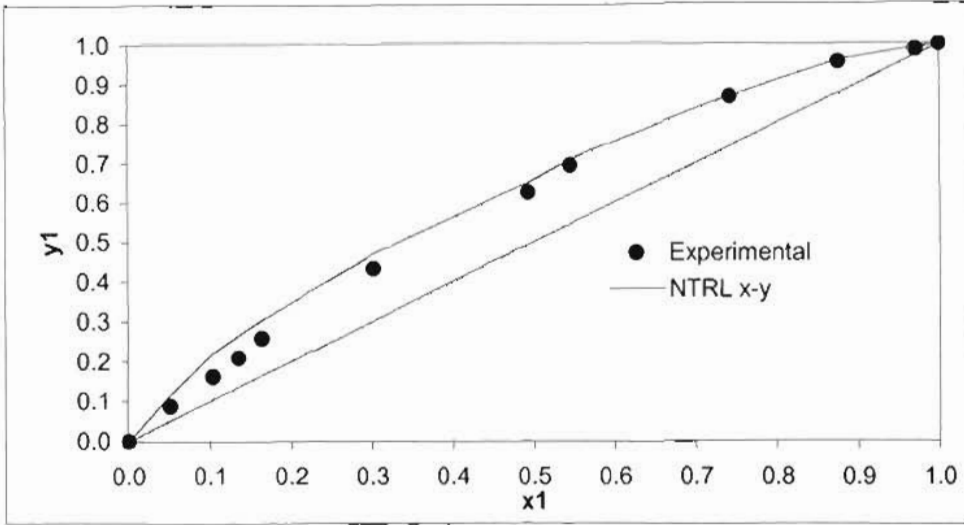


Figure 7-67: Fit of NRTL model to x-y data using the Pitzer-Curl correlation for Hexanoic acid (1) + Heptanoic acid (2) system at 10 kPa.

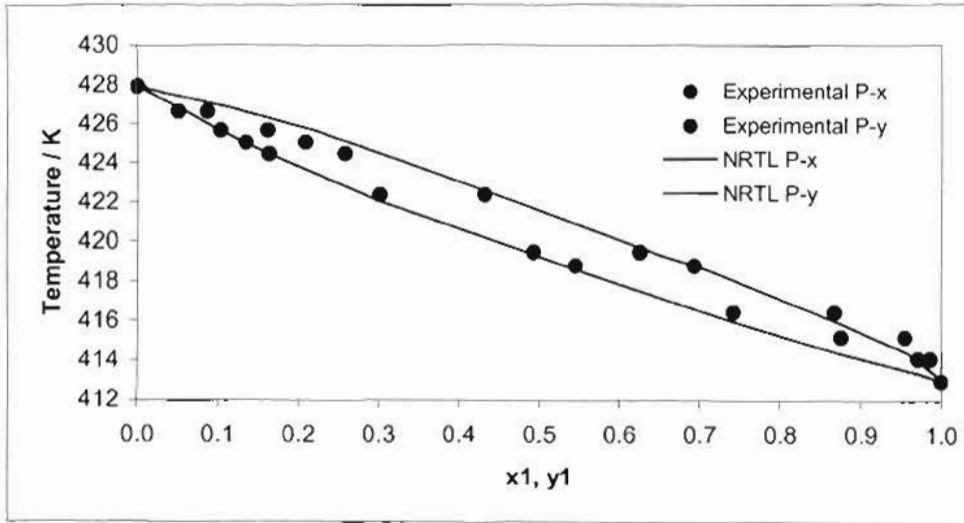


Figure 7-68: Fit of NRTL model to T-x-y data using the Pitzer-Curl correlation for Hexanoic acid (1) + Heptanoic acid (2) system at 10 kPa.

CONCLUSIONS

This project was a continuation of research initiated by Sewnarain (2002) and Clifford (2004) at the University of KwaZulu-Natal. The aim of this project was to measure new vapour-liquid equilibrium (VLE) data for binary carboxylic acid + carboxylic acid systems unavailable in open literature. A literature survey was done to determine which binary carboxylic acid systems required VLE measurements. New previously unmeasured vapour-liquid equilibrium data were measured for the following binary carboxylic acid systems:

- Propionic acid + Hexanoic acid at 20 kPa, 403.15 K, 408.15 K and 413.15 K.
- Isobutyric acid + Hexanoic acids at 20 kPa, 413.15 K and 423.15 K.
- Valeric acid + Hexanoic acid at 15 kPa, 423.15 K and 433.15 K.
- Hexanoic acid + Heptanoic acid at 10 kPa and 443.15 K.

A dynamic VLE still designed by Raal, (Raal and Mühlbauer [1998]) was used to undertake the VLE measurements. A full description of the VLE still is presented in Chapter 4. Prior to making the measurements, the functionality of the equipment and the experimental procedure were verified by making VLE measurements for the highly non-ideal cyclohexane + ethanol system. The data were in excellent agreement with that found in literature and passed both the direct test (VanNess [1995]) and point test (VanNess et al. [1973]) for thermodynamic consistency. In total fourteen sets of VLE data were measured. Twelve of the sets represent previously unmeasured data of binary carboxylic acid mixtures. All the data were correlated using thermodynamic models discussed in Chapter 3.

Reduction of VLE data

Two methods were used to regress the data: namely the “gamma – phi” method and the “phi – phi” method. For the “gamma – phi” method the vapour phase non-ideality was taken into account using the virial equation of state (Section 3.6.1). The second virial coefficients were calculated using the method of Pitzer and Curl (1957) and the Hayden and O’Connell (1975) approach with chemical theory. Three local composition based activity coefficient models: Wilson [1964], NRTL (Renon and Prausnitz [1968]), and Uniquac (Abrams and Prausnitz (1975) were used in the “gamma – phi” method. The second regression technique, “phi – phi” method, was done using the Peng and Robinson (1976) equation of state in combination with the Twu and Coon (1996) mixing rule. All the models (in general) fitted the experimental data well. The vapour phase composition deviations were lowest for the direct (ϕ - ϕ) method. The Peng-Robinson equation produced most of the best fits for the data followed by the Wilson (1964) equation in combination with chemical theory as embodied in the Hayden and O’Connell (1975) correlation accounting for vapour phase non-ideality. The isobutyric acid + hexanoic acid system had the largest deviations between the calculated and experimental values because of the very pronounced “S” shape. The efforts to accurately describe the phase behaviour of carboxylic acids are on going. Peng et al. (2004) are working on developing an equation of state incorporating chemical theory. Raal and Clifford (University of Kwa-Zulu Natal) are working on developing activity coefficient models incorporating chemical theory for carboxylic acid mixtures.

The experimental activity coefficients were generally close to unity but did not follow the expected trends. In some of the cases they did not intersect. This is attributed to the strong association of carboxylic acid mixtures. The vapour phase non-ideality was not well accounted for by both the Hayden and O’Connell (1975) approach with chemical theory and the Pitzer Curl (1957) correlation.

Thermodynamic Consistency Tests

Both the point test and the direct test for thermodynamic consistency were performed on the cyclohexane + ethanol system. The cyclohexane + ethanol system passed both tests. This confirmed the proper equipment operation and calculation procedure. Only the point test (VanNess et al. [1973]) for thermodynamic consistency could be performed on the carboxylic acids data. The superior direct test (VanNess [1995]) could not be performed on the data, as the experimental activity coefficients could not be obtained due to complex vapour phase

behaviour. In all the cases incorporating chemical theory to account for vapour phase non-ideality improved the results.

RECOMMENDATIONS

The models investigated in this work did not accurately predict the narrow ended “S” shaped envelopes of binary carboxylic acids phase diagrams. As discussed in Chapter 7, many experimentalists have found difficulty in accurately modelling the phase behaviour of carboxylic acid mixtures. The equation of state for carboxylic acids by Twu and Coon (1991) can be used to correlate pure component properties of carboxylic acids. Considerable effort was made in the course of this study to implement the equation of state to correlate a binary mixture of carboxylic acids. However, this did not yield good results. Different mixing rules were investigated, (Peng and Robinson [1975], Stryjek-Vera [1986] and Twu and Coon [1996]) in the direct method for data reduction. Only the Twu and Coon (1996) mixing rule modelled the data well. This study has shown that the available procedures for describing vapour phase behaviour are inappropriate and there exists room for improvement.

Recommendations are:

1. The need to accurately describe the phase behaviour of binary carboxylic acid systems is still currently being investigated by many experimentalists. Peng et al. (2004) presented their progress on developing an equation of state that incorporates chemical theory to predict the phase behaviour of strongly associating binary mixtures like carboxylic acids at the ICCT conference, Beijing 2004. Different models for strongly associating components should be investigated. Nan et al. (2003) proposed a correlation for the simultaneous calculation of excess enthalpy and vapour-liquid equilibria for carboxylic acid + carboxylic acid system.

2. Alternative methods for calculating the activity coefficient that incorporate chemical theory into modelling of binary carboxylic acids systems should be investigated. No activity coefficient correlations incorporating chemical theory for a binary carboxylic acid + carboxylic acid were found in literature. Prausnitz et al. (1999) proposed activity coefficient correlations for a binary mixture with only one associating component. Raal and Ramjugernath (University of Kwa-Zulu Natal) are currently working on developing activity coefficient models incorporating chemical theory for a binary mixture of carboxylic acids.
3. Activity coefficients at infinite dilution should be experimentally determined by ebulliometry techniques. Raal developed ebulliometers to measure infinite dilution activity coefficients (Raal and Mühlbauer (1998)).

REFERENCES

- Anderson, T. F, Prausnitz, J. M, (1978), "Application of the UNIQUAC Equation to Calculation of Multicomponent Phase Equilibria. 1: Vapour-Liquid Equilibria; 2: Liquid-Liquid Equilibria", *Industrial and Engineering Chemistry. Process Design and Development*, Vol. 17, pp 552-567.
- Alpert, N, and Elving, P. J, (1949), "Vapour-Liquid Equilibria in Binary Systems Ethylene Dichloride – Toluene and Formic acid – Acetic acid", *Industrial and Engineering Chemistry*, Vol. 41, pp 2864 – 2867.
- Atkins, P, Paula, J, (2001) "Physical chemistry" Oxford University Press, UK
- Cholinski, J, Szafranski, A and Wyrzykowska-Stankiewicz, D, (1986), "Computer Aided Second Virial Coefficient Data for Organic Individual Compounds and Binary Systems", *PWN-Polish Scientific Publishers, Warsaw*.
- Conti, J, J, Othmer, D, F, Gilmont, R, (1960), "Systems containing Formic Acid, Acetic Acid, Water, and Chloroform", *Journal of Chemical and Engineering Data*, Vol 5, No. 3, p 301-307.
- C.R.C. Handbook of Chemistry and Physics*, 84th Edition; (1984); Editor: Weast, R.C.; C.R.C. Press Inc.: Baton Rouge.
- Dortmund Data Bank Software purchased 1998.
- Durham, F P, (1965), "Thermodynamics" Englewood Cliffs, N. J. Prentice-Hall.
- Dymond, J H and Smith, E B, (1980), "The Virial Coefficients of Gases and Gaseous Mixtures", Clarendon Press, Oxford.
- Ellis, S R M and Jonah, D A, (1962), "Prediction of Activity Coefficients at Infinite Dilution", *Chemical Engineering Science*, Vol. 17, pp. 971-976.

- Fredunslund, A, Gmehling, J and Rasmussen, P, (1977), "Vapour-Liquid Equilibria using UNIFAC", *Elsevier*, Amsterdam.
- Fredenslund, A, Sorensen, J, M, (1994), Group Contribution methods Estimation Methods in Models for Thermodynamic and Phase Equilibria Calculations. New York, Marcel Dekker.
- Gautreaux, M F and Coates, J, (1955), "Activity Coefficients at Infinite Dilution", *American Institute of Chemical Engineers. Journal*, Vol. 1, pp. 496-500.
- Gess, M A, Danner, R P and Nagvekar, M, (1991), "Thermodynamics Analysis of Vapour-Liquid Equilibria: Recommended Models and a Standard Data Base", Design Institute for Physical Property Data, American Institute of Chemical Engineers.
- Gmehling, J Liu, D. D, and Prausnitz J. M, (1979), "High-Pressure Vapour-Liquid Equilibria for Mixtures Containing one or more Polar Components", *Chemical Engineering Science*, Vol. 34, pp 951-958.
- Gmehling, J and Onken, U, (1977), "Vapour-Liquid Equilibrium Data Collection", DECHEMA Chemistry Data Series, Frankfurt/Main.
- Gmehling, J, (1998), Prediction of vapour-liquid equilibria for asymmetric systems at low and high pressures with the PSRK model, "*Fluid Phase Equilibria*", Vol 143, p 77 –82.
- Hartwick, R P and Howat, C S, (1995), "Infinite Dilution Activity Coefficients of Acetone in Water. A New Experimental Method and Verification", *Journal of Chemical and Engineering Data*, Vol. 40, pp. 738-745.
- Hayden, J G and O'Connell, J P, (1975), "A Generalized Method for Predicting Second Virial Coefficients", *Industrial and Engineering Chemistry., Process Design and Development*, Vol. 14, pp. 209-216.
- Heidemann, R A and Prausnitz, J M, (1976), "A van der Waals-type Equation of State for Fluids with Associating Molecules", *Proc. Natl. Acad. Sci.*, Vol. 73, pp. 1773-1776.
- Herington, E F G, (1947), "A Thermodynamic Consistency Test for the Internal Consistency of Experimental Data of Volatility Ratios", *Nature*, Vol. 160, pp. 610-611.

- Huron, M J and Vidal, J, (1977), "New Mixing Rules in Simple Equations of State for Representing Vapour-Liquid Equilibria in Strongly Non-Ideal Mixtures", *Fluid Phase Equilibria*, Vol. 3, pp. 255-271.
- Inoue, M, Azumi, K, and Suzuki, N, (1975), A new vapour pressure assembly for static vapour-liquid equilibrium. *Industrial Engineering Chemistry Fundamentals* Vol 14, 312.
- Joseph, M A, Raal, J D and Ramjugernath, D, (2001), "Phase Equilibrium Properties of Binary Systems with Diacetyl from a Computer Controlled Vapour-Liquid Equilibrium Still", *Fluid Phase Equilibria*, Vol. 182, pp. 157-176.
- Joseph, M A, Raal, J D and Ramjugernath, D, (2002), "Computer-aided Measurement of Vapour-Liquid Equilibria in a Dynamic Still at Sub-Atmospheric Pressures", *Developments in Chemical Engineering Mineral Processes*, Vol. 10, pp. 615-637.
- Kato, M, Yoshikawa, H and Yamaguchi, M, (1990), "Vapour-Liquid Equilibrium Measurements of Three Binary Systems Made of Formic Acid, Acetic Acid and Propionic Acid by the Dew-Point Temperature Method", *Fluid Phase Equilibria*, Vol. 54, pp. 47-56.
- Klekers, A J and Scheller, W A, (1968), "Isothermal Vapour-Liquid Equilibrium Data for the System Formic Acid – Valeric Acid at 50 °, 75 °, and 100 °C", *Journal of Chemical Engineering Data*, Vol. 13, pp. 480-482.
- Kreglewski, A, (1969), "Second Virial Coefficients of Real Gases", *Journal of Physical Chemistry*, Vol. 73, pp. 608-615.
- Maher, P J and Smith, B D, (1979), "Infinite Dilution Activity Coefficient Values from Total Pressure VLE Data. Effect of Equation of State Used", *Journal of Chemical and Engineering Data*, Vol. 24, pp. 16-22.
- Malanowski, S, Anderko, A, (1992), "Modelling Phase Equilibria" John Wiley & Sons, New York.
- Malanowski, S.; (1982); "Experimental Methods for Vapour-Liquid Equilibria. Part I. Circulation Methods"; *Fluid Phase Equilibria*, **8**, 197.

- Malijska, I, Sysova, M, Vlckova, D (1986), "Vapour Liquid Equilibrium in strongly associated systems", *Collection Czechoslovak Chem.*, vol 51. No 194-205.
- Marquadt, D W, (1963), "An Algorithm for Least-Squares Estimation of Non-Linear Parameters", *Journal. Society of Industrial and Applied Mathematics*, Vol. 11, pp. 431-441.
- McClellan, A L, (1963-1974), "Tables of Experimental Dipole Moments", W. H. Freeman, San Francisco.
- Minkin, V I, Osipov O A, and Zhdanov Y A, "Dipole moments in organic chemistry", *Trans. from the Russian B. J Hazard*, Plenum, New York. (1970).
- Miyamoto, S, Nakamura, S, Iwai, Y and Arai, Y, (2001), "Measurement of Isothermal Vapour-Liquid Equilibria for Monocarboxylic Acid + Monocarboxylic Acid Binary Systems with a Flow-Type Apparatus", *Journal of Chemical Engineering Data*, Vol. 46, pp. 405-409.
- Morachevsky, A G and Zharov, V T, (1963), *Zhurnal Prikladnoi Khimii*, Vol. 36, pp 2771 as reported by Gmehling, J and Onken, U, (1977), "Vapour Liquid Equilibrium Data Collection, Organic Hydroxy Compounds:Alcohols", Vol. 1, Part 2a, 429, DECHEMA, Frankfurt/Main.
- Nan, Y Q, and Hao, L S, (2003), "Simultaneous Calculations of Excess Enthalpy and Vapour-Liquid Equilibria for Binary Carboxylic Acid + Carboxylic Acid Systems", *Industrial and Engineering Chemistry Research*, Vol 42, pp 2262-2268.
- O'Connell, J P and Prausnitz, J M, (1967), "Empirical Correlation of Second Virial Coefficients for Vapour-Liquid Equilibrium Calculations", *Industrial and Engineering Chemistry, Process Design and Development*, Vol. 6, pp. 245-250.
- Orbey, H and Sandler, S I, (1996), "A Comparison of Various Cubic Equation of State Mixing Rules for the Simultaneous Description of Excess Enthalpies and Vapour-Liquid Equilibria", *Fluid Phase Equilibria*, Vol. 121, pp. 67-83.
- Panayiotou, C and Sanchez, I C, (1991), "Hydrogen Bonding in Fluids: Equation of State Approach", *Journal of Physical Chemistry*, Vol. 95, pp. 10090-10097

- Patai, S (1969), "The Chemistry of Carboxylic Acids and Esters", John Wiley & Sons, New York.
- Peng, D. Y. and Robinson, D. B. (1976) "A New Two Constant Equation of State", *Industrial and Engineering Chemistry Fundamentals*, Vol. 15, pp 59-64.
- Peng, D. Y. and Pang, J (2004) "Incorporating Association Models with the Peng-Robinson Equation of State" *IUPAC International Conference on Chemical Thermodynamics*, Beijing, China
- Perry, R H and Green, D W, (1997), "Perry's Chemical Engineers' Handbook", McGraw-Hill Book Company, Singapore.
- Pitzer, K S, Lippmann, D Z, Curl, R F, Huggins, C M and Petersen, D E, (1955), "The Volumetric and Thermodynamic Properties of Fluids. II. Compressibility Factor, Vapour Pressure and Entropy of Vapourization", *Journal of the American Chemical Society*, Vol. 77, pp. 3433.
- Pitzer, K S and Curl, R F, (1957), "Empirical Equation for the Second Virial Coefficient", *Journal of the American Chemical Society*, Vol. 79, pp. 2369-2370.
- Prausnitz, J M, Anderson, T F, Grens, E A, Eckert, C A, Hsieh, R, O'Connell, J P, (1980), "Computer Calculations for Multicomponent Vapour-Liquid and Liquid-Liquid Equilibria", Prentice-Hall, Englewood Cliffs, NJ.
- Prausnitz, J M, Lichtenthaler, R N, Gomes de Azevedo, E, (1986), "Molecular Thermodynamics of Fluid Phase Equilibria", Prentice-Hall, Englewood Cliffs, NJ.
- Prausnitz, J M, Lichtenthaler, R N and Gomes de Azevedo, E G, (1999), "Molecular Thermodynamics of Fluid-Phase Equilibria", 3rd edition, Prentice-Hall, Upper Saddle River, New Jersey.
- Raal, J D, (2000), "Characterization of Differential Ebulliometers for Measuring Activity Coefficients", *American Institute of Chemical Engineers. Journal*, Vol. 46, pp. 210-220.

- Raal, J D and Mühlbauer, A L, (1998), "Phase Equilibria: Measurement and Computation", Taylor and Francis, Bristol, PA.
- Raal, J D and Naidoo, P, (1990), "Excess Enthalpy Measurements Using a Novel Highly Refined Microflow Calorimeter and the Prediction of Vapour Liquid Equilibria From Such Data", *Fluid Phase Equilibria*, Vol. 57, pp 147-160.
- Rackett, H G, (1970), "Equation of State for Saturated Liquids", *Journal of Chemical and Engineering Data*, Vol. 15, pp. 514-517.
- Redlich, O and Kister, A T, (1948), "Algebraic Representation of Thermodynamic Properties and the Classification of Solutions", *Industrial Engineering Chemistry*, Vol. 40, pp. 345-348.
- Redlich, O and Kwong, J, (1949), "On the Thermodynamics of Solutions. V. An Equation of State. Fugacities of Gaseous Solutions" *Chemical Reviews*, Vol. 44, pp. 233-244.
- Reid, C R, Prausnitz, J M and Polling, B E, (1977), "The Properties of Gases and Liquids", 3rd edition, McGraw-Hill Book Company, Singapore.
- Reid, C R, Prausnitz, J M and Polling, B E, (1988), "The Properties of Gases and Liquids", 4th edition, McGraw-Hill Book Company, Singapore.
- Renon, H and Prausnitz, J M, (1968), "Local Compositions in Thermodynamic Excess Functions for Liquid Mixtures", *American Institute of Chemical Engineers. Journal*, Vol. 14, pp. 135-144.
- Roberts, J D, (1965), "Basic Principles of Organic Chemistry", W.A Benjamin Inc, New York.
- Sandler, S I, Orbey, H and Lee, B, (1994), "Models for Thermodynamic and Phase Equilibria Calculations", Marcel Dekker, New York.
- Sewnarain, R, Raal, J D and Ramjugernath, D, (2002), "Isobaric Vapour-Liquid Equilibria for the Systems Propionic Acid + Butyric Acid, Isobutyric Acid + Butyric Acid, Butyric Acid + Isovaleric Acid, and Butyric Acid + Hexanoic Acid at 14 kPa", *Journal of Chemical Engineering Data*, Vol. 47, pp. 603-607.

- Smith, J M, Van Ness, H C and Abbott, M M, (1996), "Introduction to Chemical Engineering Thermodynamics", 5th edition, McGraw-Hill International Editions, New York.
- Smyth, C P, (1955), "Dipole Moment and Molecular Structure", McGraw-Hill, New York.
- Soave, G, (1972), "Equilibrium Constants from a Modified Redlich-Kwong Equation of State", *Chemical Engineering Science*, Vol. 27, pp, 1197-1203.
- Stryjek, R and Vera, J H, (1986), "PRSV: An Improved Peng-Robinson Equation of State for Pure Compounds and Mixtures", *The Canadian Journal of Chemical Engineering*, Vol. 64, pp. 323-333.
- Tamir, A, Dragoescu, C, Apelblat, A and Wisniak, J, (1983), "Heats of Vaporisation and Vapour-Liquid Equilibria in Associated Solutions Containing Formic acid, Acetic acid, Propionic Acid and Carbon Tetrachloride", *Fluid Phase Equilibria*, Vol. 10, pp. 9-42.
- Tamir, A and Wisniak, J, (1975), "Vapour-Liquid Equilibria in Associating Solutions", *Chemical Engineering Science*, Vol. 30, pp. 335-342.
- Tsonopoulos, C, (1974), "An Empirical Correlation of Second Virial Coefficients", *American Institute of Chemical Engineers Journal*, Vol. 20, pp. 263-272.
- Tsuboka, T and Katayama, T, (1975), *Journal of Chemical Engineering Japan*, Vol. 8, pp. 181.
- Twu, C H, (1988), "A Modified Redlich-Kwong Equation of State for Highly Polar, Supercritical Systems", International Symposium on Thermodynamics in Chemical Engineering and Industry, pp. 148-169.
- Twu, C H, Bluck, D, Cunningham, J R and Coon, J E, (1991), "A Cubic Equation of State with a New Alpha Function and a New Mixing Rule", *Fluid Phase Equilibria*, Vol. 69, pp. 33-50.
- Twu, C H, Coon, J E and Cunningham, J R, (1993), "An Equation of State for Carboxylic Acids", *Fluid Phase Equilibria*, Vol. 82, pp. 379-388.
- van Leeuwen, M E, (1994b), "Derivation of Stockmayer Potential Parameters for Polar Fluids", *Fluid Phase Equilibria*, Vol. 99, pp. 1-18.

- Van Ness, H C, Byer, S M and Gibbs, R E, (1973), "Vapour-Liquid Equilibrium: Part I. An Appraisal of Data Reduction Methods", *American Institute of Chemical Engineers Journal*, Vol. 19, pp. 238-244.
- Van Ness, H C, (1995), "Thermodynamics in the Treatment of Vapour/Liquid Equilibrium (VLE) Data", *Pure and Applied Chemistry*, Vol. 67, No. 6, pp. 859-872.
- Van Ness, H C and Abbott, M M, (1982), "Classical Thermodynamics of Non-electrolyte Solutions: With Applications to Phase Equilibria", McGraw-Hill, New York.
- Walas, S M, (1985), "Phase Equilibrium in Chemical Engineering", Butterworth, Boston.
- Wilson, G M, (1964), "Vapour-Liquid Equilibrium. XI: A New Expression for the Excess Free Energy of Mixing", *Journal of the American Chemical Society*, Vol. 86, pp. 127-130.
- Winnick, J; (1997); *Chemical Engineering Thermodynamics*; Chapter 11 & 13; John Wiley and Sons, Inc.; USA.
- Wisniak, J and Tamir, A, (1978), "Mixing and Excess Thermodynamic Properties", Elsevier Scientific Publishing Company, Netherlands.
- Wong, D S H and Sandler, S I, (1977), "A Theoretically Correct Mixing Rule for Cubic Equations of State", *American Institute of Chemical Engineers. Journal*, Vol. 38, No.5, pp. 671-680.
- Yan-Qing Nan, Li-Sheng Hao, (2003) "Simultaneous Calculation of Excess Enthalpy and Vapour-Liquid Equilibria for Binary Carboxylic Acid + Carboxylic Acid Systems", *Industrial & engineering Chemistry Research*, Vol 42, No. 10, p 2262 – 2268.
- Yerazunis, S, Plowright, J D and Smola, F M, (1964), " Vapour-Liquid Equilibrium Determination by a New Apparatus", *American Institute of Chemical Engineers. Journal*, Vol. 10, pp. 660-665.

Appendix A

Table A-1 : Carboxylic Acids Binary Vapour-Liquid Equilibrium Data Currently Available

Formic Acid								
50 mm Hg 100 mm Hg 200 mm Hg 760 mm Hg 30 °C 40 °C	Acetic Acid							
750.06 mm Hg 760 mmHg 30 °C	750.06 mm Hg 760 mm Hg 30 °C 40 °C	Propionic Acid						
760 mm Hg	760 mm Hg	14 kPa 760 mm Hg	Butyric Acid					
		760 mm Hg	14 kPa	Isobutyric Acid				
50 °C 75 °C 100 °C	760 mm Hg	20 kPa 760 mm Hg 120 °C 130 °C 140 °C	760 mm Hg	20 kPa 120 °C 130 °C 140 °C	Valeric Acid			
			14 kPa			Isovaleric Acid		
		*	14 kPa	*	*		Hexanoic Acid	
							*	Heptanoic Acid

* Areas Covered by this project

Table A-2: Common names, IUPAC names, Melting point, Boiling point and Solubility of Carboxylic acids, Patai (1979)

Carboxylic Acid	Common Name, Acid	IUPAC Name, Acid	Melting point °C	Boiling point °C	Solubility g/100g H ₂ O @20°C
HCOOH	Formic	Methanoic	8	101	∞
CH ₃ COOH	Acetic	Ethanoic	17	118	∞
CH ₃ CH ₂ COOH	Propionic	Propanoic	-22	141	∞
H ₂ C=CHCOOH	Acrylic	Propenoic	-	-	∞
CH ₃ (CH ₂) ₂ COOH	Butyric	Butanoic	-6	164	∞
CH ₃ (CH ₂) ₃ COOH	Valeric	Pentanoic	-34	187	3.7
CH ₃ (CH ₂) ₄ COOH	Caproic	Hexanoic	-3	205	1.0
CH ₃ (CH ₂) ₅ COOH	Heptylic	Heptanoic	-10	223	Slightly Soluble
CH ₃ (CH ₂) ₆ COOH	Caprylic	Octanoic	16	239	0.7
CH ₃ (CH ₂) ₇ COOH	Pelargonic	Nonanoic	15	255	Insoluble
CH ₃ (CH ₂) ₈ COOH	Capric	Decanoic	31	269	0.2
CH ₃ (CH ₂) ₁₆ COOH	Stearic	Octadecanoic	70	183 @1Torr	Insoluble

A.1 Chemical Properties of Carboxylic Acids

In this section we shall be concerned with the chemistry of carboxylic acids. Although the carbonyl functional group, COOH, is a combination of a hydroxyl and a carbonyl group, the combination is such a close one that neither group behaves independently of the other. The properties of the hydroxyl and carbonyl groups of carboxylic acids are not expected to be typical of the alcohols, aldehydes, or ketones. However, there is sufficient similarity and analogous behaviour.

A.1.1 Acidity

The carboxyl group of carboxylic acids produces an acid reaction with water through ionisation of the carboxyl hydrogen as shown in Figure A-1 below and can be represented by the chemical reaction equation (A-1).

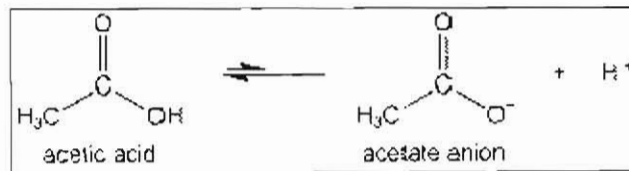
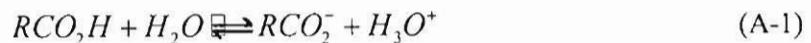


Figure A-1: Ionisation of acetic acid in water



Carboxylic acids are weak acids so that ionisation is far from complete compared with mineral acids such as hydrochloric, perchloric, nitric and sulphuric acids. The acidity constant K_A , is approximately 10^{-5} and is given by equation (A-2).

$$K_A = \frac{[RCO_2^-][H_3O^+]}{[RCO_2H]} \sim 10^{-5} \quad (A-2)$$

The acidity of the carboxyl group stems from the polar nature of the carbonyl group, the polarity of which can be ascribed to contributions of the $C=O$ and $C-O$ bond structures.

A.1.2 Carboxylic Acid Reactions

Most of the reactions of carboxylic acids can be classified as belonging to one of the following four types. The detailed discussion on the reactions will not be dealt with here. The reader is referred to the text by Patai (1979) wholly devoted to the chemistry of carboxylic acids.

A.1.2.1 Reactions involving cleavage of the $O-H$ bond

The hydrogen on the carboxylic acids is split off, e.g., acid dissociation and solvolytic reactions.

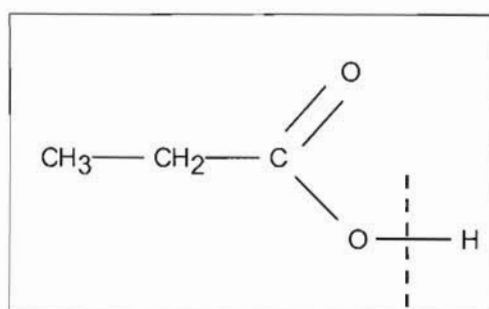


Figure A-2: Cleavage of the $O-H$ bond.

A.1.2.2 Reaction at the carbonyl carbon

This involves the attack by a nucleophile, $:\text{N}$, on the carbonyl carbon with subsequent cleavage of a C—O bond, e.g., esterification, acid chloride formation and reduction by hydrides.

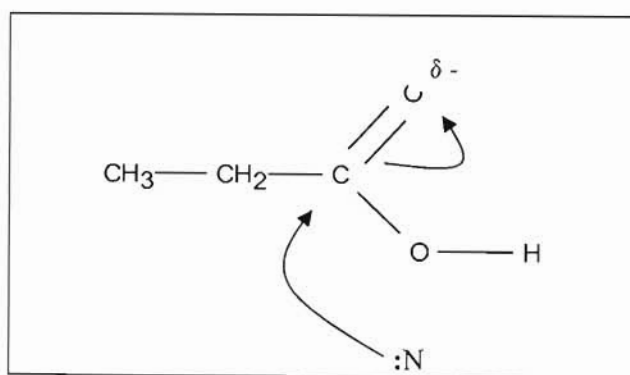


Figure A-3: Reaction at the carbonyl carbon

A.1.2.3 Decarboxylation

Decarboxylation is the removal of the carboxyl group from a chemical compound (usually replacing it with hydrogen), Roberts (1965), e.g., Kolbe electrolysis and Hunsdieker reactions.

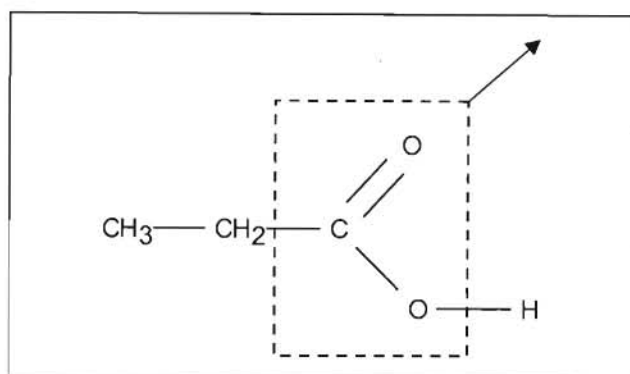


Figure A-4: Decarboxylation reaction

A.1.2.4 Reaction of the α carbon

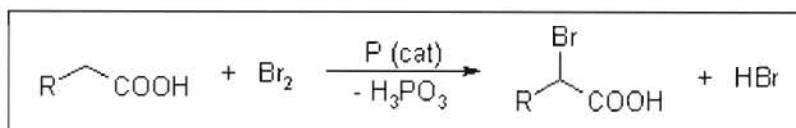


Figure A-5: Reaction of the α carbon

This involves the halogenation of carboxylic acids in the presence of catalytic phosphorus, e.g., Hell-Volhard-Zelinsky reactions and reactions of α substituted carboxylic acids, Patai (1979).

A.2 Phase Equilibria

The concept of phase equilibria is best interpreted through the Gibbs energies as mentioned in Chapter 3. If we consider any closed system, the temperature and pressure of the system are related to the Gibbs energy by Equation (A-3):

$$d(nG) = (nV)dP - (nS)dT \quad (\text{A-3})$$

Applying Equation (A-3) to a single-phase fluid that does not undergo chemical reaction. One can deduce that:

$$\left[\frac{\partial(nG)}{\partial P} \right]_{T,n} = nV \quad (\text{A-4})$$

and

$$\left[\frac{\partial(nG)}{\partial T} \right]_{P,n} = -nS \quad (\text{A-5})$$

where n is the number of moles of all chemical species and they are held constant. The above derivation can be extended to an open system that can interchange matter with the surroundings. The Gibbs energy then becomes a function of n_i , the number of moles of a particular species i that are present in the system.

$$nG = g(P, T, n_1, n_2, \dots, n_i, \dots) \quad (\text{A-6})$$

The total differential of nG is over all the summations of the species present:

$$d(nG) = (nV)dP - (nS)dT + \sum_i \left[\frac{\partial(nG)}{\partial n_i} \right]_{P,T,n_j} dn_i \quad (\text{A-7})$$

the subscript n_j indicates that all the mole numbers are held constant except the i th component.

The term $\left[\frac{\partial(nG)}{\partial n_i} \right]_{P,T,n_j}$ is referred to as the chemical potential of species i and is given the

symbol μ . Equation (A-7) may thus be re-written as:

$$d(nG) = (nV)dP - (nS)dT + \sum_i \mu_i dn_i \quad (\text{A-8})$$

Equation (A-8) in phase equilibria is known as the fundamental property relation.

The above derivation can be extended to a system with two phases. For a closed system with two phases, the Gibbs energies for the individual phases can be written as:

$$d(nG)^\alpha = (nV)^\alpha dP - (nS)^\alpha dT + \sum_i \mu_i^\alpha dn_i^\alpha \quad (\text{A-9})$$

$$d(nG)^\beta = (nV)^\beta dP - (nS)^\beta dT + \sum_i \mu_i^\beta dn_i^\beta \quad (\text{A-10})$$

where the superscripts α and β identify the different phases and μ is the chemical potential. Each total system property (e.g. nG) is found by summing up the individual single properties in all the phases. This can be represented mathematically by the following relation:

$$nM = (nM)^\alpha + (nM)^\beta \quad (\text{A-11})$$

The change in the total Gibbs energy of the two-phase closed system is the sum of two Equations, (A-9) and (A-10):

$$d(nG) = (nV)dP - (nS)dT + \sum_i \mu_i^\alpha dn_i^\alpha + \sum_i \mu_i^\beta dn_i^\beta \quad (\text{A-12})$$

Comparing Equations (A-8) and (A-12) in conditions of equilibrium gives:

$$\sum_i \mu_i^\alpha dn_i^\alpha + \sum_i \mu_i^\beta dn_i^\beta = 0 \quad (\text{A-13})$$

From the law of conservation of mass we know that:

$$dn_i^\alpha = -dn_i^\beta \quad (\text{A-14})$$

therefore

$$\sum_i (\mu_i^\alpha - \mu_i^\beta) dn_i^\alpha = 0 \quad (\text{A-15})$$

dn_i^α is independent and can take on any value. If one analyses Equation (A-15) one can see that the only way the left hand side of this equation can be zero is for each term in the parenthesis separately to be zero. One can therefore conclude that:

$$\mu_i^\alpha = \mu_i^\beta \quad (i = 1, 2, \dots, N) \quad (\text{A-16})$$

where N is the number of species present in the system. In other words the chemical potential of species i in phase α should be equal to the chemical potential of i in phase β for the system to be

in equilibrium. This concept can be generalised to systems that have more than two phases; the results for π phases is:

$$\mu_i^\alpha = \mu_i^\beta = \dots = \mu_i^\pi \quad (i = 1, 2, \dots, N) \quad (\text{A-17})$$

A.3 Evaluation of Infinite Dilution Activity Coefficient

The interpolation or extrapolation of infinite dilution activity coefficient has been ruled incorrect and inaccurate by many authors. Hartwick and Howart (1995) show that extrapolation of the binary activity coefficient curves to the end points seldom gives accurate values for γ_i^∞ . Raal and Mühlbauer (1998) state that extrapolation by any correlation of γ_i^∞ is unacceptable. The Smith and Maher (1979) method is a well-accepted correlation for calculating infinite dilution activity coefficients from isothermal data.

$$\gamma_i^\infty = \varepsilon_i^\infty \frac{P_j^{sat}}{P_i^{sat}} \left[1 + \beta_j \frac{1}{P_j^{sat}} \left(\frac{\partial P}{\partial x_1} \right)_{x_1=0}^\infty \right]^{x_i \rightarrow 0} \quad (\text{A-18})$$

where

$$\varepsilon_i^\infty = \exp \left[\frac{(B_{ii} - V_i^l)(P_j^{sat} - P_i^{sat}) + \delta_{ij} P_j^{sat}}{RT} \right] \quad (\text{A-19})$$

$$\beta_j = 1 + P_j^{sat} \left[\frac{B_{ij} - V_j^l}{RT} \right] \quad (\text{A-20})$$

where $\delta_{ij} = 2B_{ij} - B_{ii} - B_{jj}$

The parameters B_{ii} and B_{ij} are the second virial coefficients of the pure components. B_{ij} is the virial coefficient for the i-j interaction. They can be obtained from such correlations as the Hayden and O'Connell (Section 3.4.2). P_i^{sat} is the saturated vapour pressure of species i and V_i^l the corresponding liquid molar volume. P_i^{sat} is calculated by the Antoine equation and V_i^l is calculated from the Rackett equation.

$$P_D = P - \left[P_2^{sat} + (P_1^{sat} - P_2^{sat})x_1 \right] \quad (\text{A-21})$$

$$\left(\frac{P_D}{x_1 x_2} \right)_{x_1=0} = \left(\frac{\partial P}{\partial x_1} \right)_{x_1=0} - P_1^{sat} + P_2^{sat} \quad (\text{A-22})$$

The term on the left-hand side of Equation (A-22) is determined by the extrapolation of a plot of $P_D/x_1 x_2$ vs x_1 to $x_1 = 0$. If the curve is not linear, Maher and Smith (1979) suggest a plot of $x_1 x_2 / P_D$ against x_1 . Thus the partial derivative and hence γ_1^∞ can be determined. A similar procedure is used to determine γ_2^∞ . P_D is the deviation pressure, which refers to the degree to which a system deviates from ideality defined in Equation (A-21).

A.4 Low Pressure VLE Data Regression

The measured VLE data was regressed using the following iterative bubble point pressure and temperature calculations.

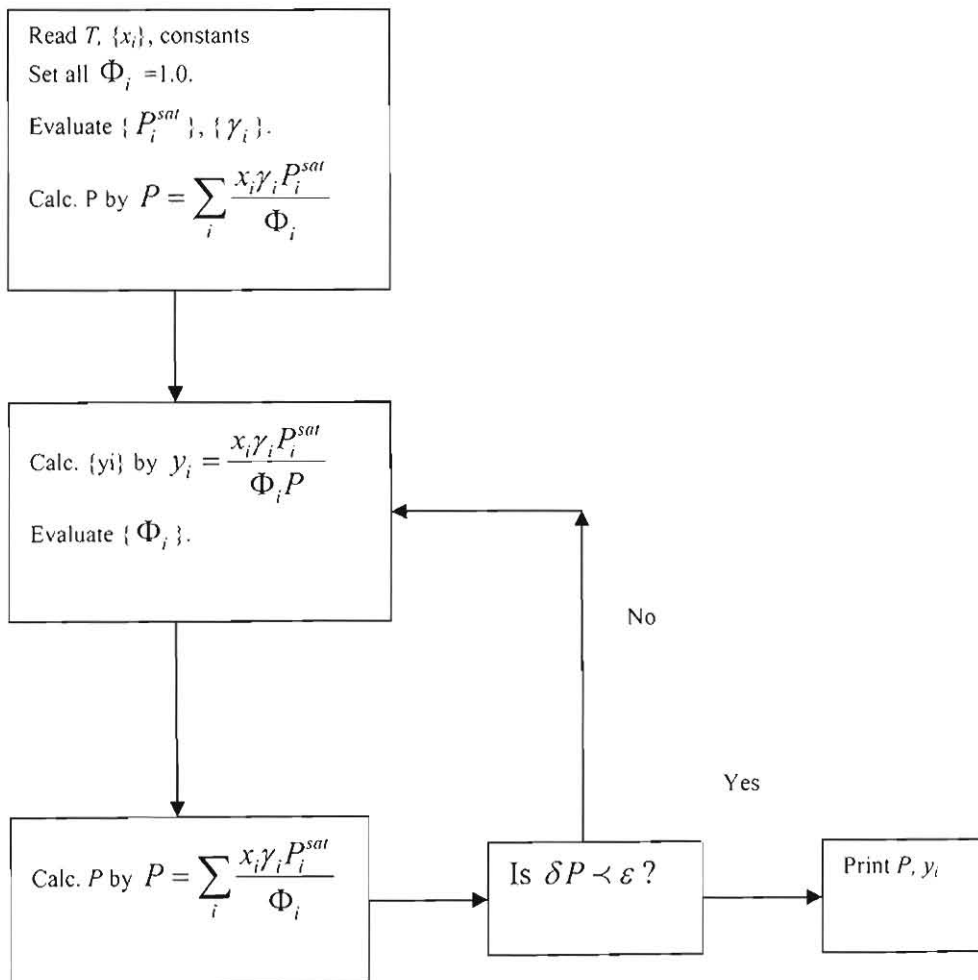


Figure A-10: Block diagram for the bubble point pressure calculation (Combined method) Smith & van Ness (1996)

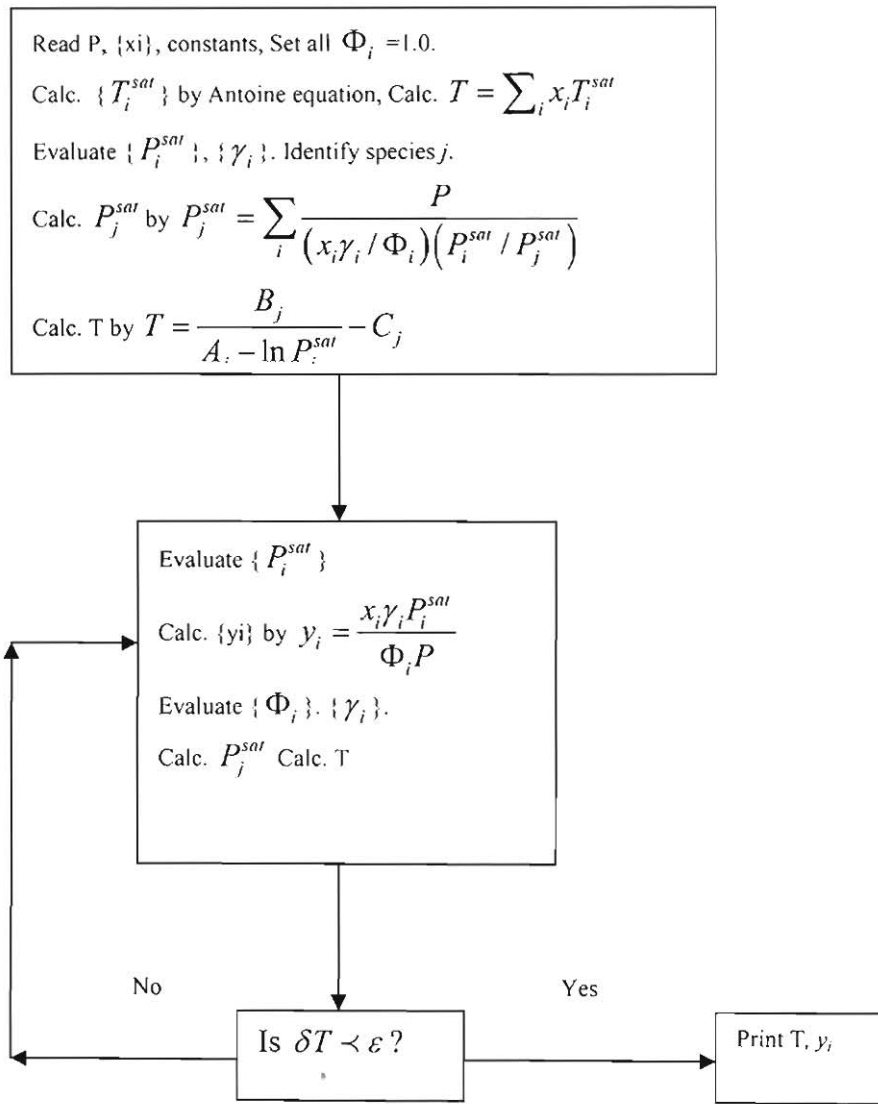
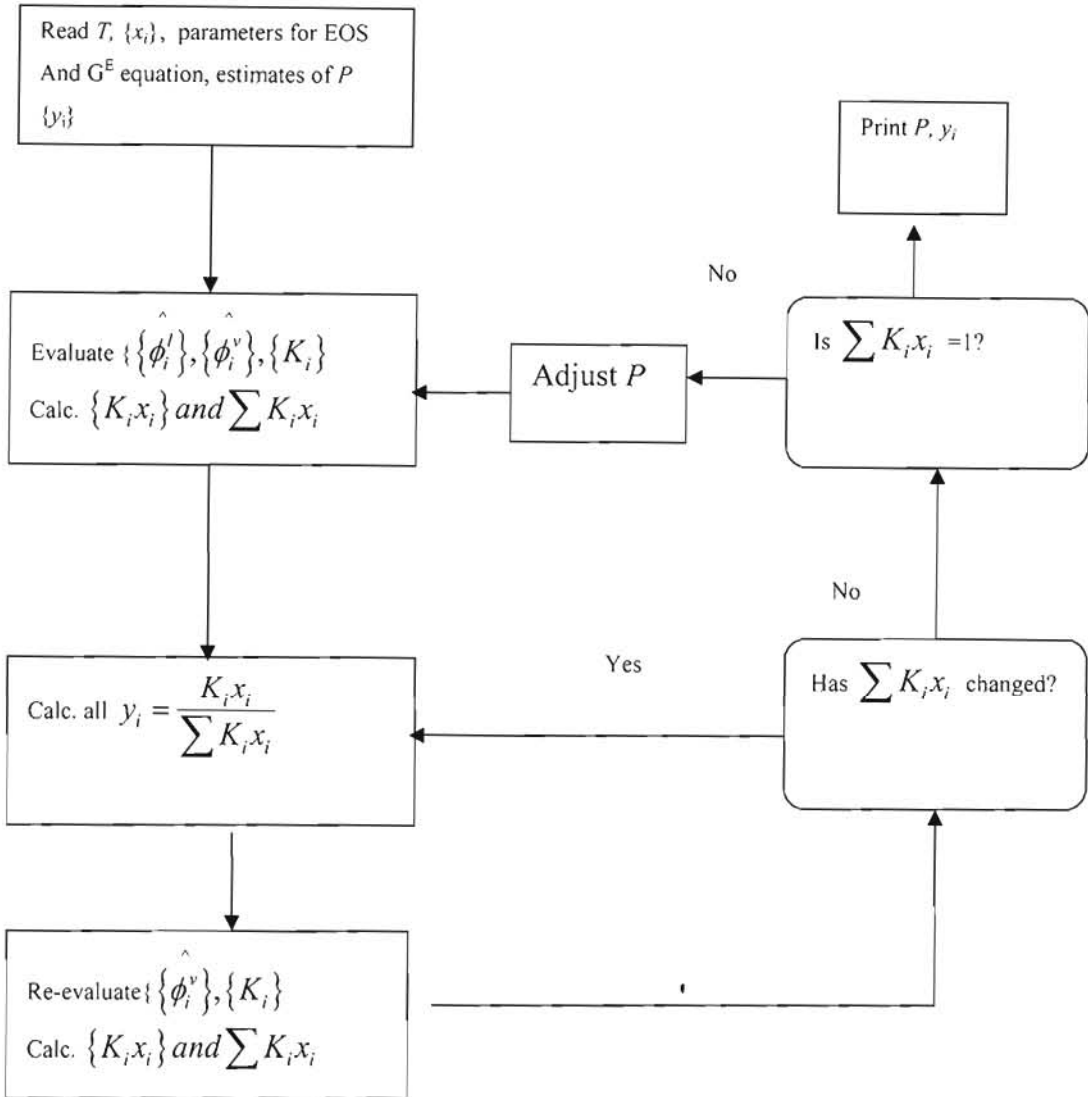


Figure A-11: Block diagram for the bubble point temperature calculation (Combined method) Smith & van Ness (1996)



where $y_i = K_i x_i$ and $K_i = \frac{\hat{\phi}_i^l}{\hat{\phi}_i^v}$

Figure A-12: Block diagram for bubblepoint pressure calculation (Direct method) Smith & van Ness (1996)

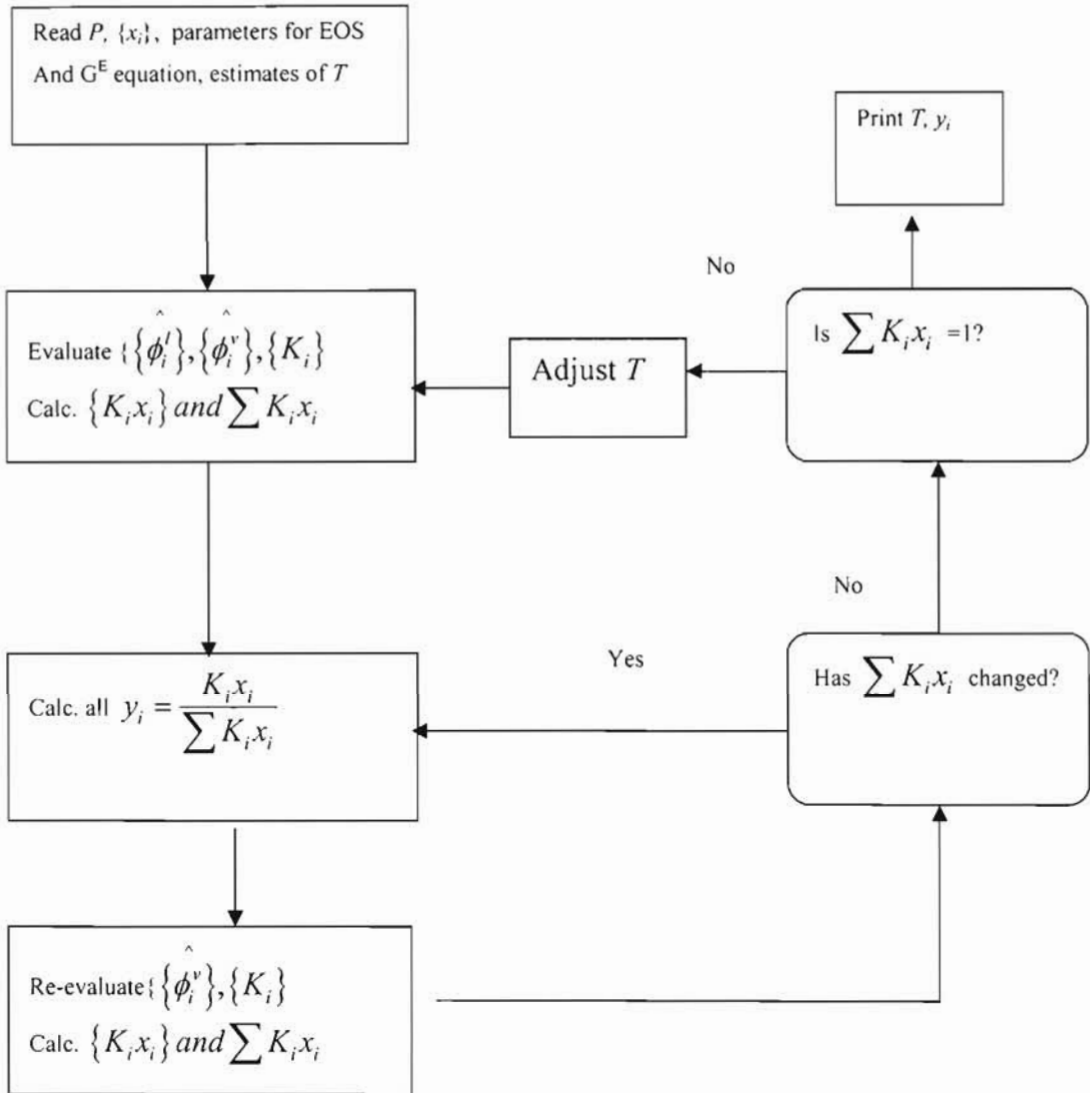


Figure A-13: Block diagram for bubblepoint temperature calculation (Direct method)
Smith & van Ness (1996)

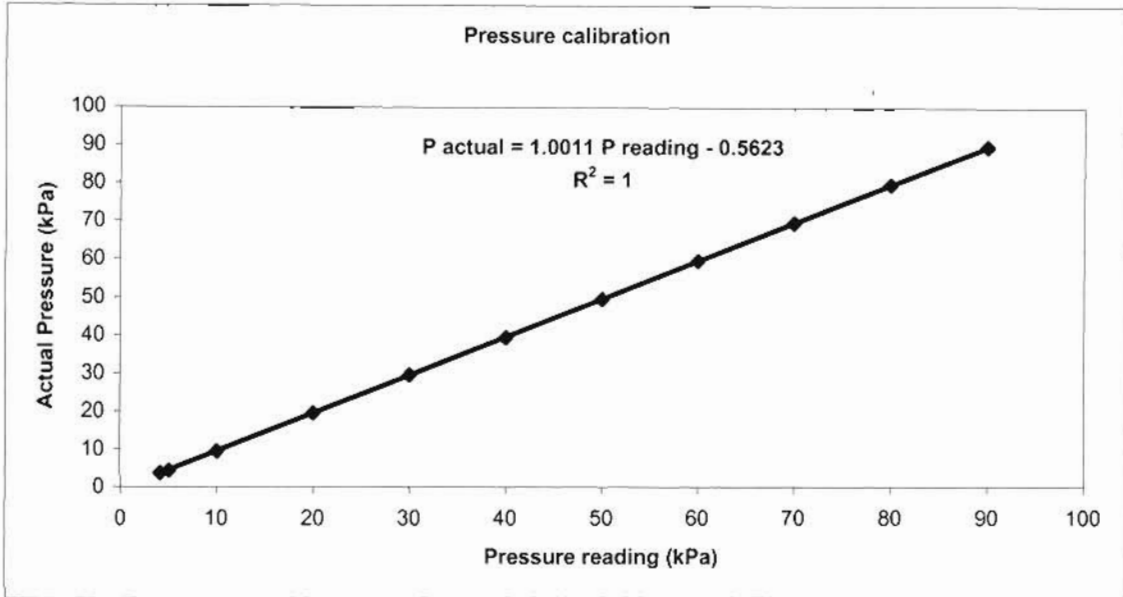


Figure B-1: Pressure Transducer calibration

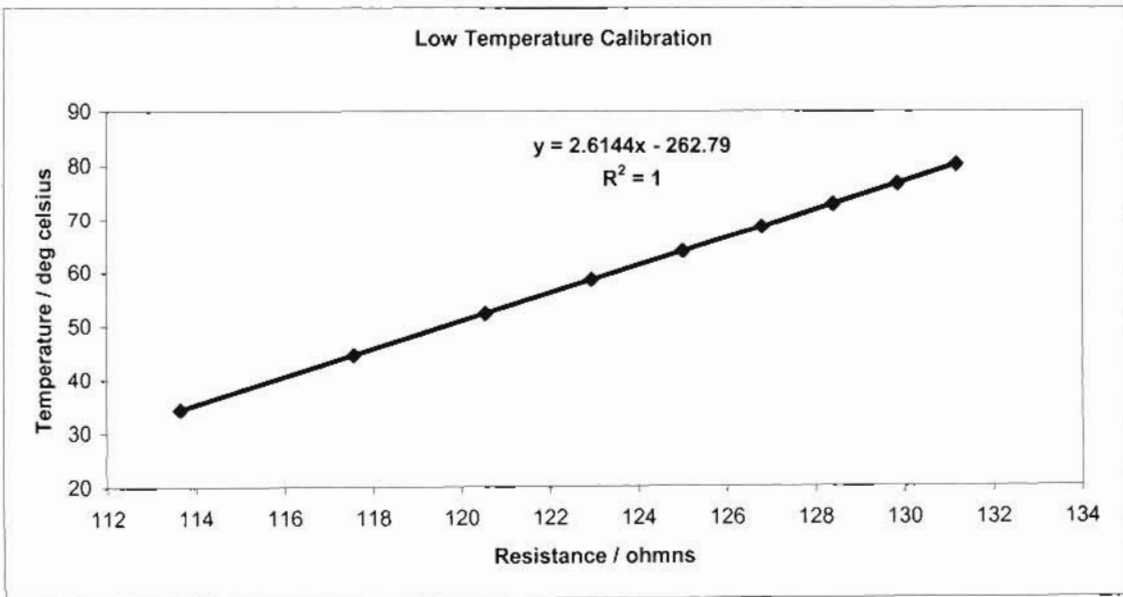


Figure B-2: Low Temperature Calibration of Pt-100 Bulb.

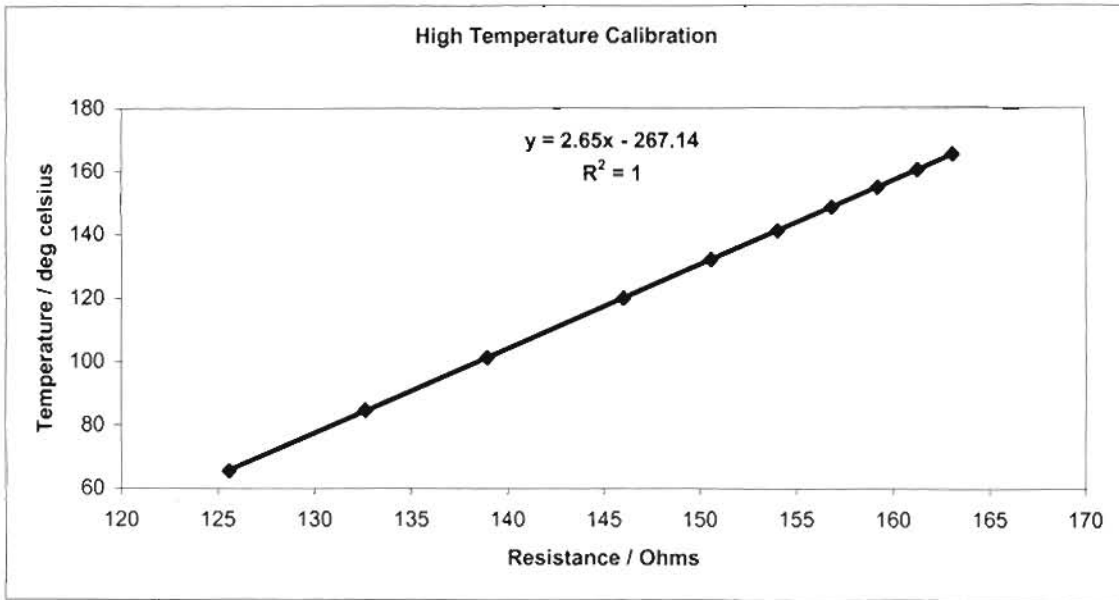


Figure B- 3: High Temperature Calibration of Pt-100 Bulb.

B.1 Carboxylic Acids Dimerisation Equilibrium Constants

$$\ln K_{eq} = A_{11} + \frac{B_{11}}{T} \text{ mmHg}$$

T is in Kelvin.

Table B-1: Carboxylic Acids Dimerisation Equilibrium Constants

Acid	A_{11}	B_{11}
Formic acid	-24.7367	7098.9
Acetic acid	-23.9952	7290.0
Propionic acid	-24.9669	7635.4
Butyric acid	-23.2561	6999.9
Isobutyric acid	-23.2561	6999.9
Valeric acid	-23.0374	6891.6
Hexanoic acid	-22.7749	6776.5
Heptanoic acid	-22.5815	6776.5
Octanoic acid	-22.2499	6543.9

Table B- 2: Carboxylic Acids L, M And N Parameters For The Twu-Coon Mixing Rule.

Acid	L'	M'	N'
Propionic acid	0.2636	0.7412	2.3367
Isobutyric acid	0.2926	0.7176	2.3244
Valeric acid	0.7040	0.9226	2.0869
Hexanoic acid	0.1896	0.6914	2.7057
Heptanoic acid	0.1663	0.6576	2.6119

B.2 Acentric Factor

Very little pure component data is available in literature for carboxylic acids. This calls for one to estimate the pure component data using correlations. The value of the acentric factor was estimated by

$$\omega = -\log P_v - 1.000 \text{ at } T_r = 0.7$$

$$P_v = f(P_r)$$

where P_v is the reduced vapour pressure $P_r = \frac{P}{P_c}$ at $T_r = \frac{T}{T_c} = 0.7$

The acentric factor represents the acentricity or nonsphericity of a molecule Reid (1987). Monoatomic gases therefore have an acentric factor of zero. Generally, the smaller the molecule the smaller the value of the acentric factor and visa versa. The acentric factor also rises with the polarity of the molecule. The parameter is a measure of the complexity of a molecule with respect to both geometry and polarity.

B.3 Mean Radius of Gyration

The radius of gyration used in the correlation was calculated from the parachor. The parachor is estimated from additive group contributions methods. The structural contributions for calculating the parachor can be found in the text by Reid (1987).

Table B- 3: Pure Component Properties for Cyclohexane and Ethanol.

Property	Cyclohexane	Ethanol
T_c / K	553.5	513.9
P_c / atm	41.42	62.21
$V_c / \text{cm}^3/\text{mol}$	308.0	167.1
Z_c	0.2730	0.2400
ω	0.2120	0.6450
Dipole moment /debye	0.30	1.70
$R_d / \text{\AA}$	3.261	2.250
Solvation parameter	0.0	1.4

Table B- 4: Pure Component Properties for Carboxylic Acids.

Property	Propionic acid	Isobutyric acid	Valeric acid	Hexanoic acid	Heptanoic acid
T_c / K	604.0	605.0	639.9	663.0	679.00
P_c / atm	44.70	36.50	35.82	31.60	28.40
$V_c / \text{cm}^3/\text{mol}$	230.0	292.0	340.0	416.0	466.0
Z_c	0.2003	0.2148	0.2253	0.2252	0.2344
ω	0.5184	0.6100	0.6160	0.6701	0.7297
→Dipole moment /debye	1.76	1.34	1.81	1.19	1.21
→ $R_d / \text{\AA}$	2.6821	3.1151	3.5408	3.9045	4.2391
r	2.8768	3.7779	4.2256	5.3002	5.5744
q	2.6120	3.4600	3.6920	4.2320	4.7720
→ Solvation parameter	4.5	4.5	4.5	4.5	4.5

Table B-5: Second Virial Coefficients for the Propionic acid + Hexanoic acid system

Temperature/ K	$B_{11} \text{ cm}^3/\text{mol}$	$B_{22} \text{ cm}^3/\text{mol}$	$B_{12} \text{ cm}^3/\text{mol}$
403.15	-1017.97	-1998.76	-2717.24
408.15	-994.20	-1952.32	-2544.40
413.15	-971.10	-1907.20	-2531.01

Table B-6: Second Virial Coefficients for the Isobutyric acid + Hexanoic acid system

Temperature/ K	B_{11} cm ³ /mol	B_{22} cm ³ /mol	B_{12} cm ³ /mol
413.15	-1229.79	-1777.90	-2428.60
423.15	-1172.33	-1820.81	-2316.46

Table B- 7: Second Virial Coefficients for the Valeric acid + Hexanoic acid system

Temperature/ K	B_{11} cm ³ /mol	B_{22} cm ³ /mol	B_{12} cm ³ /mol
423.15	-1415.49	-1820.81	-2123.78
433.15	-1352.80	-1739.21	-2062.20

Table B- 8: Second Virial Coefficients for the Hexanoic acid + Heptanoic acid system

Temperature/ K	B_{11} cm ³ /mol	B_{22} cm ³ /mol	B_{12} cm ³ /mol
443.15	-1662.02	-2031.93	-2612.87

C.1 Regression Results for Cyclohexane + Ethanol at 40 kPa

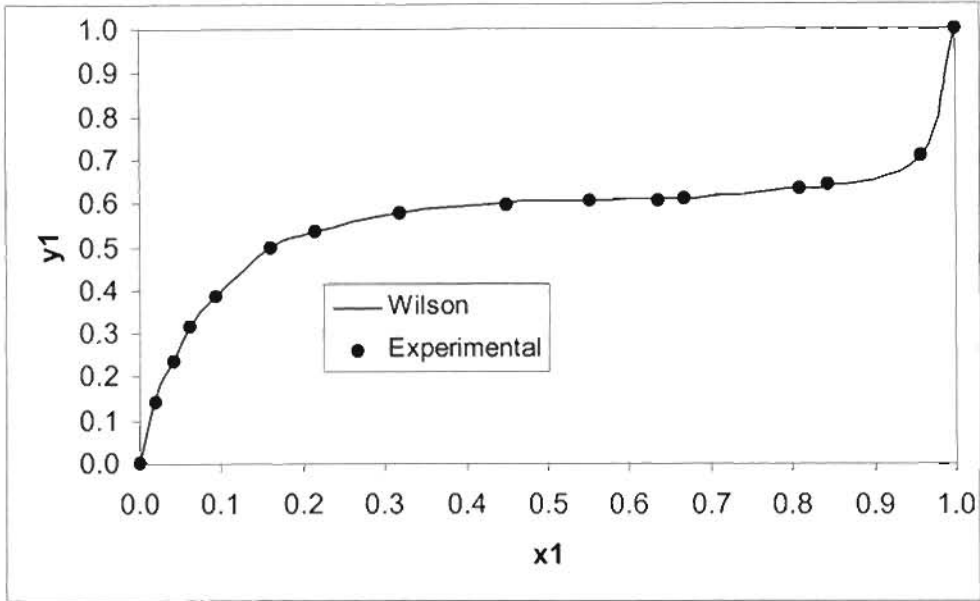


Figure C-1: Fit of Wilson model to x-y diagram of cyclohexane (1) + ethanol (2) system at 40 kPa

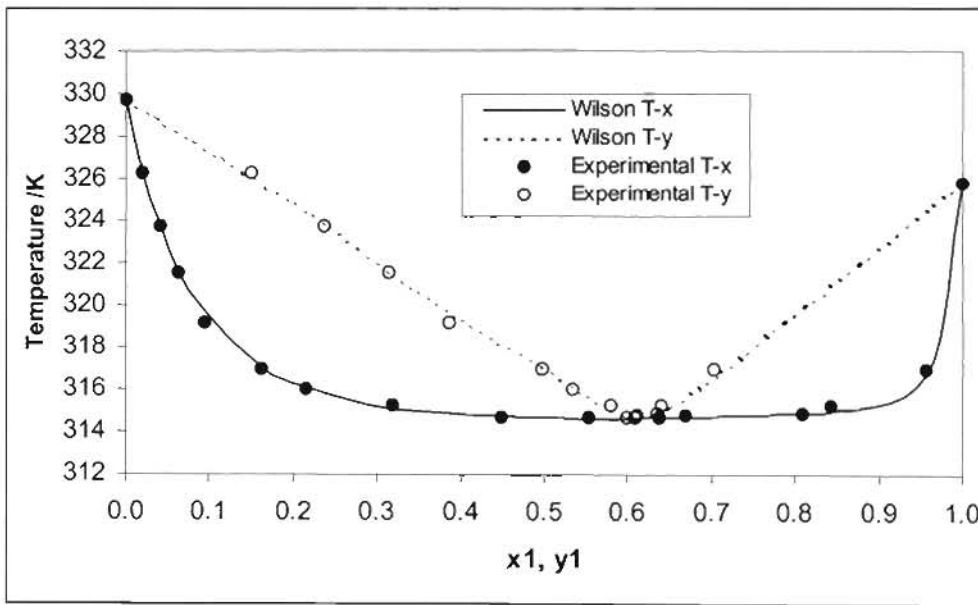


Figure C-2: Fit of Wilson model to P-x-y diagram of cyclohexane (1) + ethanol (2) system at 40 kPa

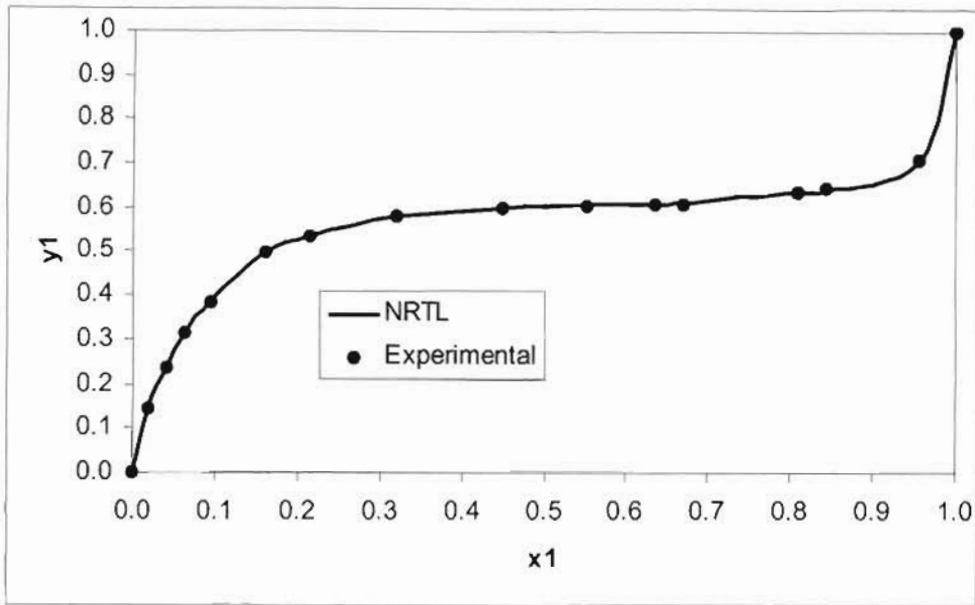


Figure C-3: Fit of NRTL model to x-y diagram of cyclohexane (1) + ethanol (2) system at 40 kPa

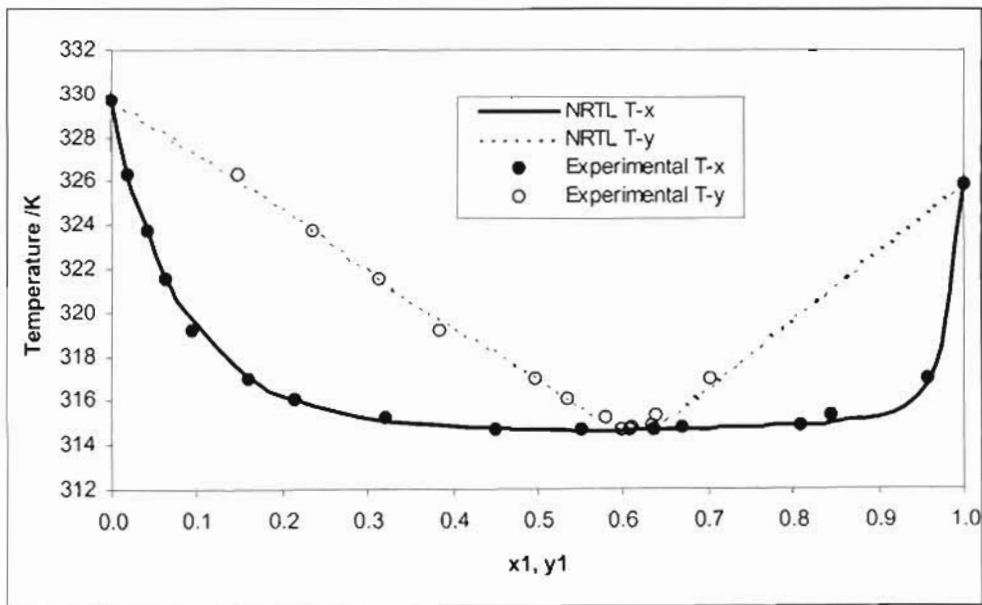


Figure C-4: Fit of NRTL model to P-x-y diagram of cyclohexane (1) + ethanol (2) system at 40 kPa

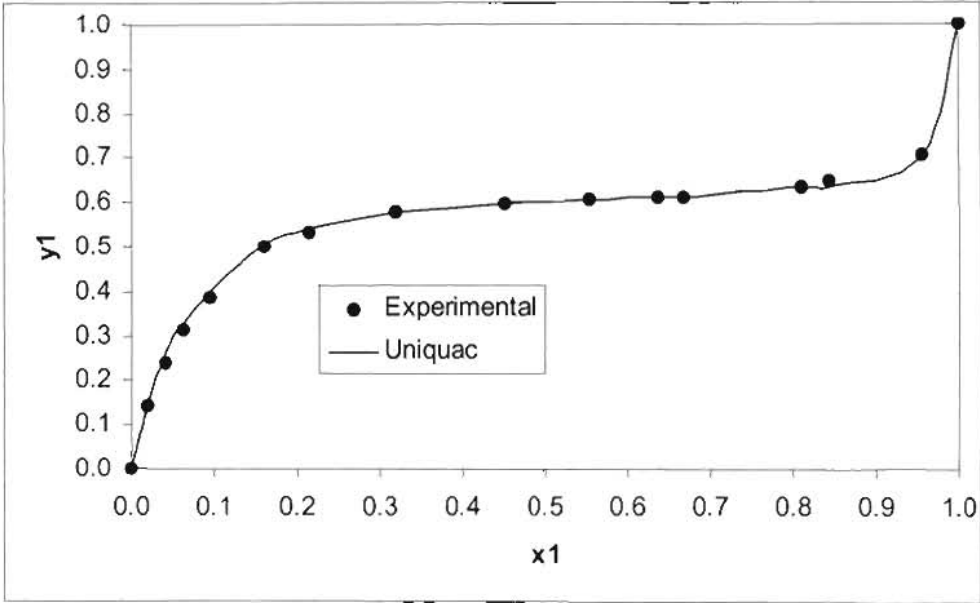


Figure C-5: Fit of UNIQUAC model to x-y diagram of cyclohexane (1) + ethanol (2) system at 40 kPa

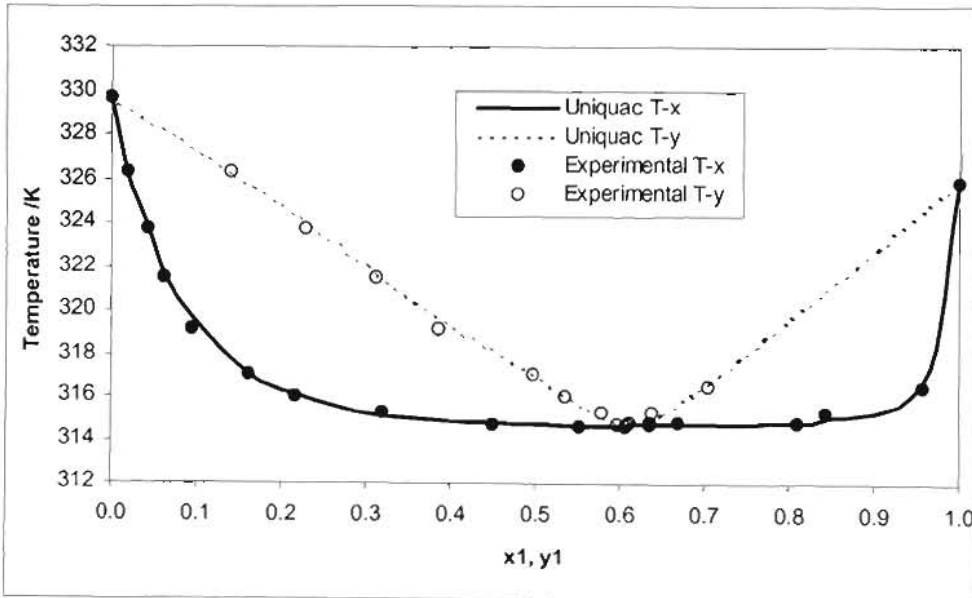


Figure C-6: Fit of UNIQUAC model to P-x-y diagram of cyclohexane (1) + ethanol (2) system at 40 kPa

C.2 Thermodynamic Consistency Results for Cyclohexane (1) + Ethanol (2) System 323.15

K

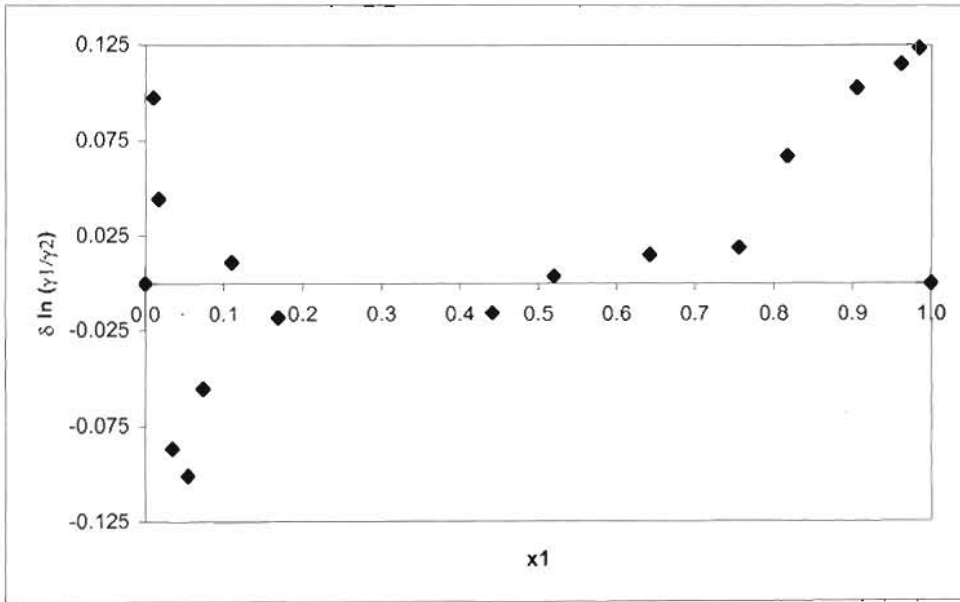


Figure C-7: Graph showing the deviation of the activity coefficients calculated using the Wilson model from the experimental activity coefficients for the cyclohexane (1) + ethanol (2) system at 323.15 K

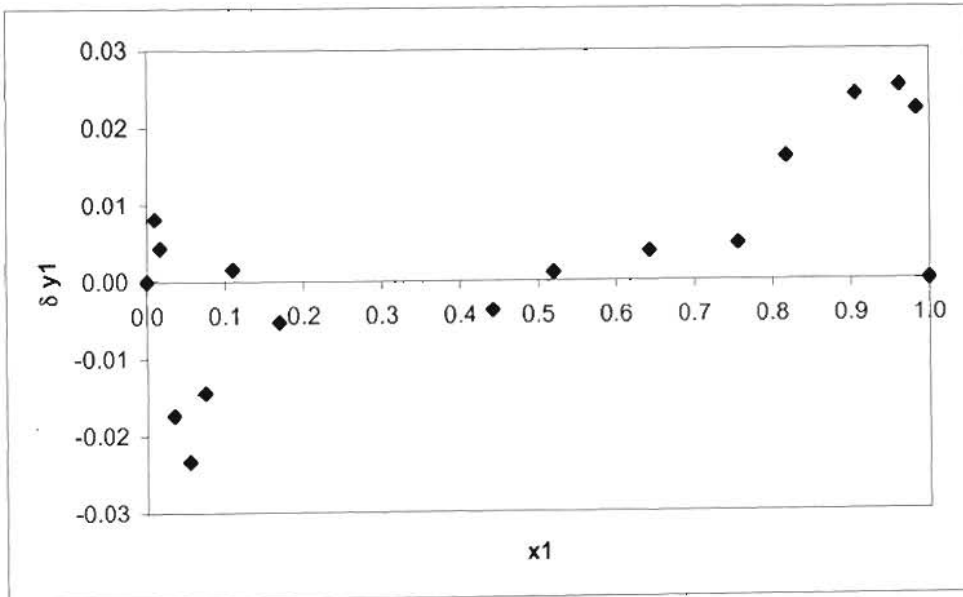


Figure C-8: Graph showing the deviation of the vapour compositions calculated using the Wilson model from the experimental activity coefficients for the cyclohexane (1) + ethanol (2) system at 323.15 K

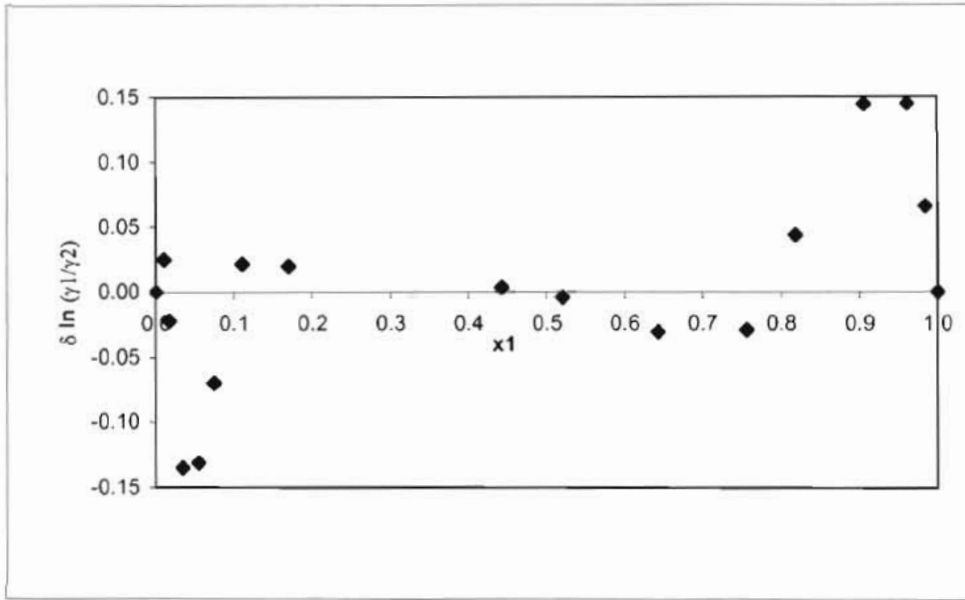


Figure C-9: Graph showing the deviation of the activity coefficients calculated using the NRTL model from the experimental activity coefficients for the cyclohexane (1) + ethanol (2) system at 323.15 K

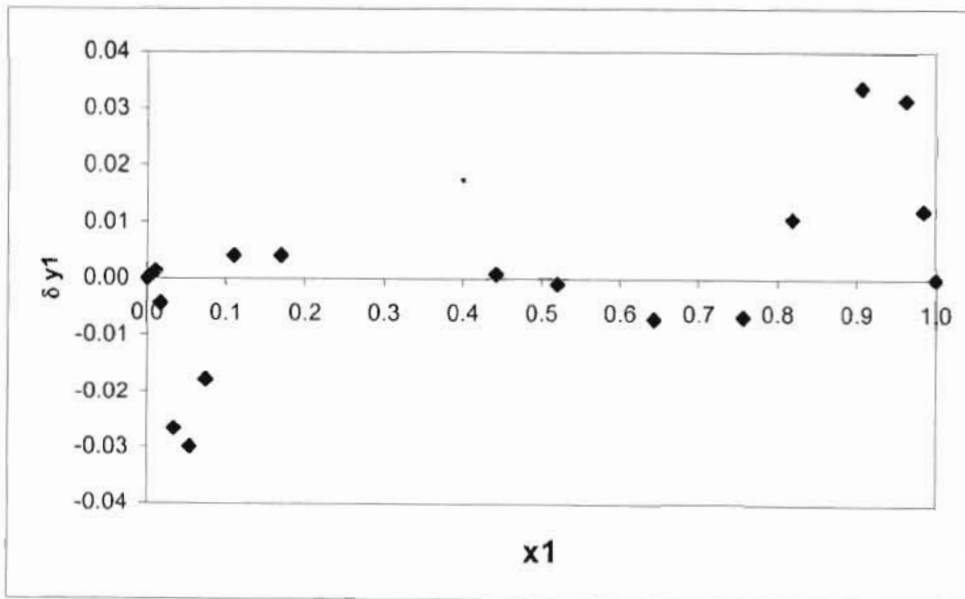


Figure C-10: Graph showing the deviation of the vapour compositions calculated using the NRTL model from the experimental activity coefficients for the cyclohexane (1) + ethanol (2) system at 323.15 K

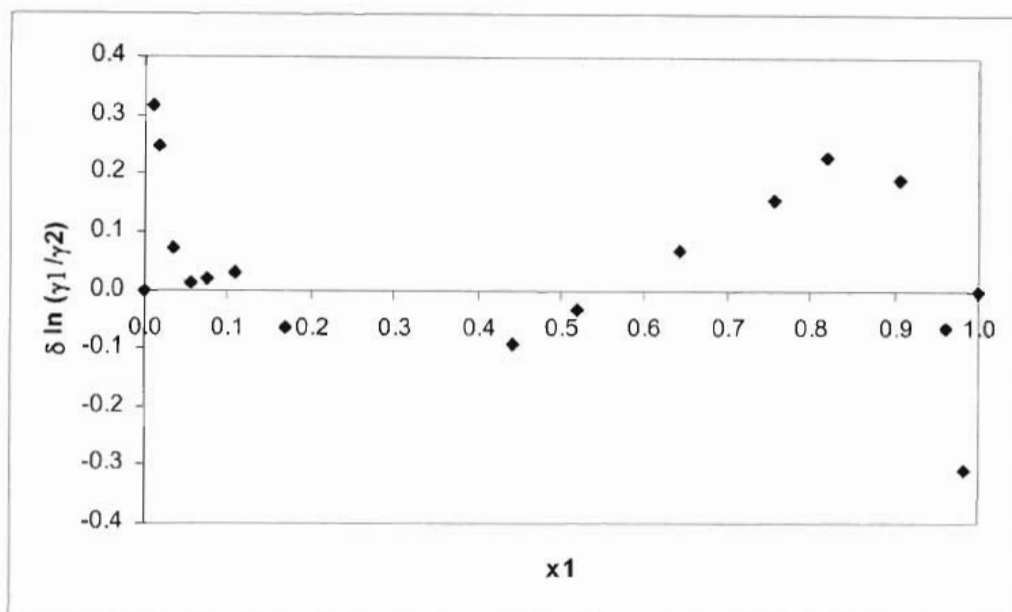


Figure C-11: Graph showing the deviation of the activity coefficients calculated using the UNIQUAC model from the experimental activity coefficients for the cyclohexane (1) + ethanol (2) system at 323.15 K

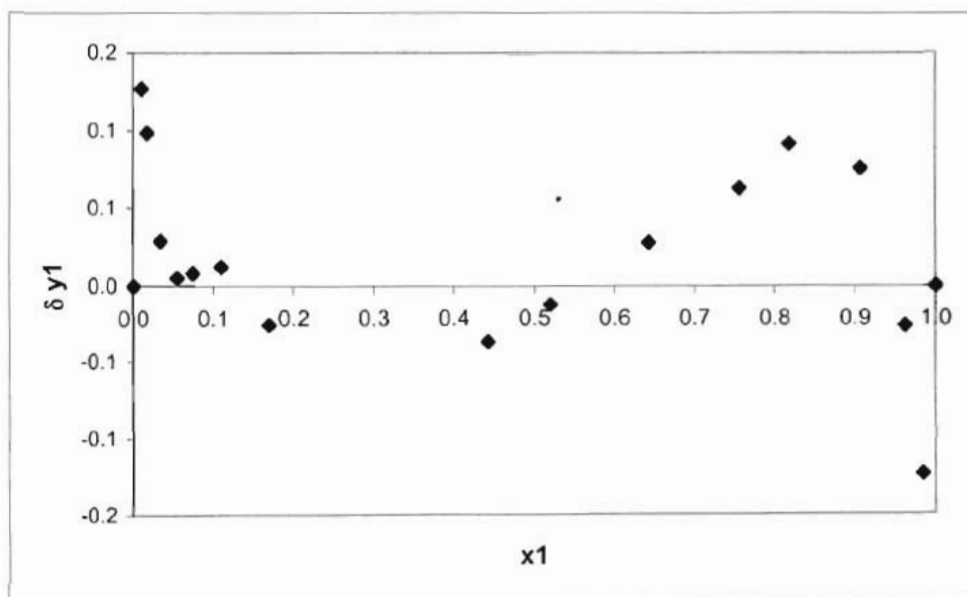


Figure C-12: Graph showing the deviation of the vapour compositions calculated using the UNIQUAC model from the experimental activity coefficients for the cyclohexane (1) + ethanol (2) system at 323.15 K

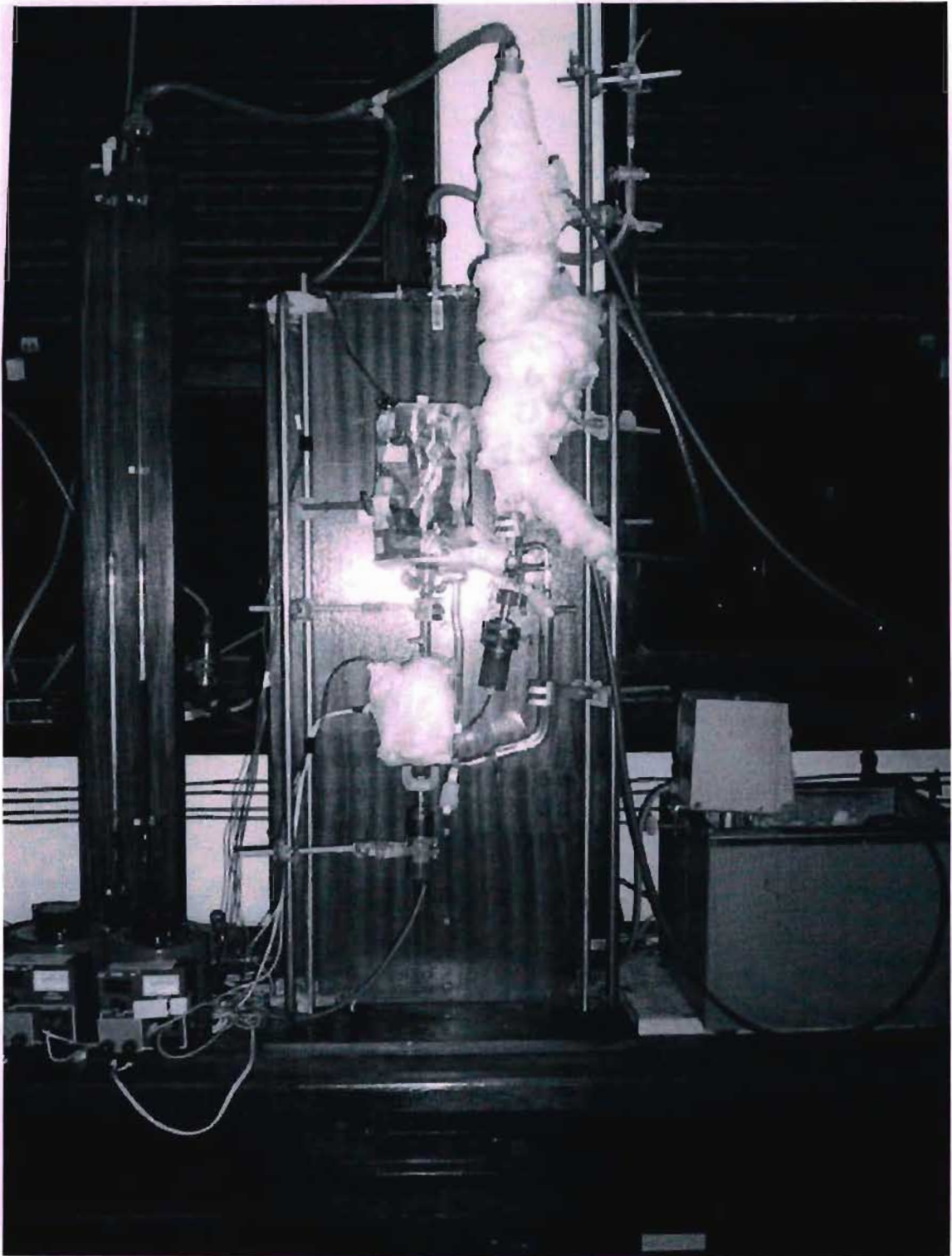


Figure D-1: Photograph of the experimental used in this project.